On the roles and sub-cellular localisations of lipids in neurodegenerative disorders

Simon Wheeler

Thesis submitted in partial fulfilment of the requirements for the degree of Doctor of Philosophy

De Montfort University, September 2019

Contents

Abstract

Niemann-Pick type C disease (NPCD) is a ruinous condition that mostly affects children. Although stemming from a single genetic error its pathology involves dysfunction of multiple organs especially liver, spleen and brain. Life expectancy is dramatically reduced.

NPCD is usually caused by a mutation in NPC1 a protein located in the lysosome, the cell's recycling centre, and believed to export cholesterol from there for use elsewhere in the cell. Consequently NPCD patients accumulate cholesterol in their lysosomes. Extensive research has found that mutation of this single protein restricted to one organelle has effects that encompass almost every aspect of cellular function. This is rather surprising so chapter 1 attempts to piece together what we know to give as coherent and complete an account as possible of the cellular pathology of this disease including insights gathered from the various treatment approaches tried to date.

Using a combined docking-molecular dynamics approach Chapter 2 supports the idea, previously advanced from in vitro experiments, that NPC1 and its partner NPC2 may also bind sphingosine, the simplest sphingolipid. This chapter also uses docking to understand some previously observed, but not fully explained, aspects of lysosomal dysfunction in NPCD including reduced big potassium channel activity, annexin mislocalisation and impaired SNARE recycling. These errors are traced ultimately to cholesterol accumulation but pathological roles are found for other lipids which also accumulate in this disease

Chapter 3 finds that lysosomal pH is increased in fibroblasts from NPC1-deficient patient fibroblasts; inhibtion of glucocerbrosidase 2 (GBA2), the only clinically approved NPCD treatment, corrects this error. The same treatment is not effective in other Niemann-Pick variants. Only limited and preliminary success was encounted when GBA2 inhibition was examined as a potential treatment for related diseases.

Chapter 4 finds that the mitochondrial defect in NPCD is not responsive to GBA2 inhibition nor to manipulation of sphingolipids more widely. Attempts at correcting this error by manipulating mitochondrial cholesterol, widely believed to be elevated to levels toxic to this organelle, were not clearly effective.

Chapter 5 draws the various threads of this thesis together and combines them with very recent work published elsewhere to sketch an integrated cellular pathology of NPCD.

Acknowledgements

Firstly my thanks to Dan Sillence who has guided my studies, allowed me to explore things, asked me questions, encouraged me when I needed to persevere and pointed out when I was wrong.

Isaac Newton famously said he had seen further than other men by standing on the shoulders of giants. Less well known is the saying of Leonardo da Vinci that only a poor student does not surpass his master. What these two renaissance geniuses were both getting at, I think, is the idea that human endeavour is always building on what has gone before. And so it is with a sense of my small place in the huge enterprise we call science that I thank those predecessors and colleagues whose work is cited in the references - I have relied on their ideas and used their techniques, and if my work helps others in similar ways I will have partially repaid my debt. Others do not require citing but cannot fail to be acknowledged: this thesis is written 10pt Timeless from fontsquirrel.com, BioRender.com was used for some biological schematics; calculations were run on an HP Z440 PC with an Intel Zeon processor and an NVIDIA Quadro M4000 GPU.

At DMU I have been helped in various ways by Paul Ainsworth, Meenakshi Bhardwaj, Alexandra Davis, Angela Ferguson, Neil Horley, Aamir Hussain, Lukasz Lagojda, Jinit Masania, Eva Masiero, Glen McCann, Zain Mohammed, Nicoleta Moisoi, Dave Reeder, Lukasz Stolarczyk, Nikol Sullo, Zahoor ul-Haq, Tyra Zetterstron and Lan Zhu. Further afield I have received gifts of cells, data, drugs and advice variously from Prof Dagmar Wachten (CAESAR, Bonn), Dr Per Haberkant (EMBL, Heidelberg), Dr João Ribeiro (Illinois at Urbana-Champaign), Dr Stephen Muench (Leeds), Prof Hans Aerts and Dr Maria Ferraz (Leiden), Prof Nigel Hooper, Dr Kate Kellett and Miss Kate Fisher (Manchester), Prof Volker Gerke (Münster), Prof Cliff Lingwood (Sick Kids, Toronto) and Prof Fran Platt (Oxford). In particular Dr Ralf Schmid (Leicester) got me started on protein modelling and molecular docking and has remained an invaluable source of advice.

I would like to thank De Montfort university for funding me through my studies. To spend three years finding out about the world is a privilege. To be paid for doing so, whilst aiming at alleviating disease in that world, only enhances the privilege.

3 months into working as a pharmacist, and knowing that I found it rather dull, my wife Celia uttered the fateful words, 'I don't mind if you want to do something else.' Regardless of circumstances her love and support have been unwavering ever since. I would also like to thank our children Iona, Caleb and Bethan for all those complicated board games that gave me things to think about which weren't cells, proteins or lipids. A special thank you to Bethan for all her help with full stops.

I cannot finish without paying tribute to the role of my Christian faith in my studies. Jesus announces himself as God's pre-existent, creative Word and declares that without him nothing was made that has been made (Gospel according to John, chapter 1 verses 1-3). From such thoughts I have daily drawn inspiration.

Publications arising from this thesis

Lipid-protein interactions in Niemann-Pick type C disease: insights from molecular modelling
Simon Wheeler, Ralf Schmid, Dan J Sillence
International Journal of Molecular Sciences **20** (3) *2019*, 717

Cytosolic glucosylceramide regulates endolysosomal function in Niemann-Pick type C disease
Simon Wheeler, Per Haberkant, Meenakshi Bhardwaj, Paige Tongue, Maria J Ferraz, David Halter, Hein Sprong, Ralf Schmid, Johannes M F G Aerts, Nikol Sullo, Dan J Sillence
Neurobiology of Disease **127**, *2019*, 242-252

Niemann-Pick type C disease: cellular pathology and pharmacotherapy
Simon Wheeler, Dan J Sillence
Journal of Neurochemistry, manuscript accepted

Abbreviations

*	activated
21-AcP	21-Acetoxy Pregnenolone
$\Delta\Psi$	mitochondrial inner membrane potential
Aß	Amyloid beta
$A_{2A}R$	$Adenosine_{2A}$ Receptor
ABC	ATP Binding Cassette
aCerase	acid Ceramidase
AD	Alzheimer's Disease
ADP	Adenosine DiPhosphate
AMP-DNJ	AdamantylMethoxyPentyl-DeoxyNoJirimicin
Anx	Annexin
APP	Amyloid Precursor Protein
aSMase	acid SphingoMyelinase
ATP	Adenosine TriPhosphate
BLAST	Basic Linear Alignment Search Tool
BMP	Bis(Monoacylglycero)Phosphate
BODIPY	BOron DI-PYrolyl
BSA	Bovine Serum Albumin
cath	cathepsin
CBE	Conduritol-β-epoxide
CCCP	Carbonyl Cyanide m-ChloroPhenyl hydrazone
CD	CycloDextrin
cdk	Cyclin Dependent Kinase
Cer	Ceramide
CERT	CERamide Transfer protein
CFTR	Cystic Fibrosis Transmembrane conductance Regulator
CHARMM	Chemistry at HARvard Molecular Mechanics
CHO	Chinese Hamster Ovary

CLEAR	Co-ordinated Lysosomal Expression And Regulation
CLIC	CLathrin Independent Carrier
CLN	Ceroid Lipofuscinosis, Neuronal
CRAC	Cholesterol Recognition Amino acid Consensus
CSF	CerebroSpinal Fluid
Cyp	Cytochrome P450
Cyt	Cytochrome
dhSph	dihydroSphingosine
DMEM	Dulbecco's Modified Eagle Medium
(D)-PDMP	(D)-Phenyl-2-Decanoylamino-3-Morpholino-1-Propanol
DRM	Detergent Resistant Membrane
DS	Down Syndrome
EGFR	Endothelin Growth Factor Receptor
EL	EndoLysosome
ELISA	Enzyme-Linked ImmunoabSorbent Assay
EM	Electron Microscopy
ER	Endoplasmic Reticulum
ERK	Extracellular-signal Regulated Kinase
ESC	Embryonic Stem Cell
FAPP2	Fosphatidylinositol-four-phosphate AdaPter Protein 2
FAD	Flavin Adenine Dinucleotide
fc	final concentration
FRET	Förster Resonance Energy Transfer
Gal	Galactose, galactosyl
GFP	Green Fluorescent Protein
GBA1	Glucocerebrosidase 1
GBA2	Glucocerebrosidase 2
GCS	GlcCer Synthase
GlcCer	GLuCosylCERamide

GLTP	GlycoLipid Transfer Protein
GPCR	G-Protein Coupled Receptor
GSL	GlycoSphingoLipid
GTP	Guanosine TriPhosphate
HDAC	Histone DeACetylase
HEK	Human Embyronic Kidney
HF	Human Fibroblast
HOPS	HOmotypic vacuole and fusion Protein Sorting
Hsp	Heat shock protein
IP_3	Inositol triPhosphate
iPSC	induced Pluripotent Stem Cell
Lac	Lactose, lactosyl
LAL	Lysosomal Acid Lipase
LBPA	LysoBisPhosphatidic Acid
LDL	Low Density Lipoprotein
LEL	Late EndoLysosome
L_o	Liquid Ordered phase
LIMP-2	Lysosomal Integral Membrane Protein-2
(L)-PDMP	(L)-Phenyl-2-Decanoylamino-3-Morpholino-1-Propanol
LSD	Lysosomal Storage Disorder
LXR	Liver X Receptor
MAPK	Mitogen Activated Protein Kinase
MCS	Membrane Contact Site
MD	Molecular Dynamics
MENTAL	Mln64 N-TerminAL
MES	Morpholino-Ethane-Sulfonic acid
ML-IV	MucoLipidosis type IV
MPSIIIa	MucoPolySaccharidosis type IIIa
mTORC1	mammalian Target Of Rapamycin Complex 1

MVB	Multi-Vesicular Body
NAD	Nicotinamide Adenine Dinucleotide
NB-DNJ	N-ButylDeoxyNoJirimycin
nCerase	neutral Ceramidasee
NMR	Nuclear Magnetic Resonance
NPCD	Niemann-Pick type C Disease
NTD	N-Terminal Domain
OPM	Orientation of Proteins in Membranes
ORP	Oxysterol binding protein Related Protein
PBS	Phosphate Buffered Saline
PD	Parkinson's Disease
PDB	Protein Data Bank
PI	PhosophatidylInositide
$PI(3,5)P_2$	PhosphatidylInositol-3,5-diphosphate
$PI(4,5)P_2$	PhosphatidylInositol-4,5-diphosphate
PKA	Protein Kinase A
PKC	Protein Kinase C
PLA_2	PhosphoLipase A_2
PPMP	D-*threo*-1-Phenyl-2-Palmitoylamino-3-Morpholino-1-Propanol
PS	PhosphatidylSerine
RCK	Regulatory of Conductance for potassium
RFP	Red Fluorescent Protein
RIPA	Radio ImmunoPrecipitAtion
RMSD	Root Mean Square Difference
RMSF	Root Mean Square Fluctuation
ROS	Reactive Oxygen Species
ROSIE	Rosetta Online Server that Includes Everyone
RPMI	Roswell Park Memorial Institute
RyaR	Ryanodine Receptor

S1P	Sphingosine-1-Phosphate
SCAP	SREBP Cleavage Activation Protein
SERCA	Sarco-/Endoplasmic Reticulum Calcium ATPase
SL	SphingoLipid
SM	SphingoMyelin
SNAP	Soluble NSF-Attachment Protein
SNARE	SNAp REceptor
Sph	Sphingosine
SphK	Sphingosine Kinase
SPT	Serine Palmitoyl Transferase
SREBP	Sterol Response Element Binding Protein
SSD	Sterol Sensing Domain
StAR	Steroidogenic Acute Regulatory protein
START	STeroidogenic Acute Regulatory Transport
Stx	Syntaxin
TFEB	Transcription Factor EB
TMH	TransMembrane Helix
TNFα	Tumour Necrosis Factor α
TPC	Two Pore Channel
TSPO	TranSlocator PrOtein
TRPML	Transient Recetor Potential MucoLipin
VAMP	Vesicle Associated Membrane Protein
vATPase	Vacuolar ATPase
VDAC	Voltage Dependent Anion Channel
VGCC	Voltage Gated Calcium Channel
YFP	Yellow Fluorescent Protein

1

Introduction

Whilst this thesis will range widely over neurodegenerative diseases of children and adults the focus will be on Niemann-Pick type C disease (NPCD) which will serve as an exemplar of the complexity of these conditions. First described in 1914 and affecting approximately 1 in 150,000 live births,[1] NPCD is characterised by diverse symptoms affecting liver, spleen, motor control and brain; premature death invariably results.[2,3] Its molecular origins were traced, as late as 1997, to a protein of late endosomes and lysosomes which was named NPC1.[4,5]

NPC1

Behold, I show you a mystery.

Paul the apostle
First letter to the Corinthians

Despite years of research the functions of NPC1 still resist simple definition. It has been proposed as an exporter of lipophilic molecules[6] and amines,[7] and to bind sphingolipids[8] and mycolic acids.[9] However the emphasis has been on this protein as a cholesterol exporter following the recognition that it possess a sterol sensing domain (SSD).[4] Mutations in the SSD were found to impede cholesterol export from the lysosome[10] and to reduce labelling of the protein by a fluorescent cholesterol analogue.[11] The developing view of the pathogenesis of NPCD was complicated somewhat by the discovery that a second lysosomal protein, termed NPC2, was also involved in the disease.[12] However this molecule was swiftly established as capable of binding cholesterol[13,14] and subsequent studies confirmed this.[15,16] The idea that NPC1 and -2 act together was put forward[17,18] and has been confirmed and refined by later work. Thus within the lysosome NPC2 collects cholesterol[19] and conveys it to NPC1 in the limiting membrane. This account has been refined and developed though it retains its difficulties to which we shall return in subsequent chapters. Beyond controversy (eg[4]) is that mutant NPC1 or -2 lead to accumulation (often termed storage) of cholesterol in late endosomes and lysosomes of NPCD patients. This condition thus constitutes a member of the class of lysosomal storage disorders (LSDs) but is unusual in that category as most such diseases derive from failure of catabolism rather than from failure of export. Cholesterol in the lysosome is mostly derived from low density lipoprotein (LDL) via the process of endocytosis.

NPC1 serves to export cholesterol from lysosomes; mutation leads to cholesterol storage

Endocytosis

Endocytosis is a constitutive process by which cells internalise nutrients and turn over their outer membranes. There are at least three varieties known to modern biology (Figure 1). The best studied depends on the protein clathrin which accumulates in regions of the plasma membrane and forms pits (Figure 1, ❶). These pits contain certain receptors such as that for LDL and the iron-binding protein transferrin. Clathrin induces a curvature in the membrane that eventually becomes so pronounced that the pit is almost separated from the membrane; the protein dynamin completes the separation and an approximately spherical, clathrin-coated vesicle forms. The coat is soon shed and the resulting vesicle proceeds to carry its cargo into the cell. A less well understood mechanism uses the protein caveolin to induce membrane curvature and form structures known as caveolae (Figure 1, ❷); the insulin receptor is internalised in this way.[20] Once a caveola has been pinched off it too forms a vesicle. Similarly the protein galectin-3 can form structurally distinct vesicles known as clathrin-independent carriers (CLICs, Figure 1, ❸).[21] This process depends on glycosphingolipids,[21] a class of compound we will meet much more extensively later in this chapter. Once the vesicles are generated by whichever mechanism they eventually fuse with bodies known as early endosomes (Figure 1, ❹). From here some material is recycled to the cell surface while other is progressed along the endocytic pathway to late endosomes (Figure 1, ❺). The regulation of this process is not fully understood but involves both rab proteins and phosphoinositide lipids.[22,23] Late endosomes are also known as multi-vesicular bodies (MVBs) as they feature intra-luminal membranes which is where the original endocytic cargo resides (Figure 1, ❻).

Further processing requires the late endosome to fuse with a lysosome. This in turn necessitates them being close in space meaning both organelles must be mobile. The small GTPase rab7 attached to the membrane of each organelle contacts motor proteins that attach to the cytoskeleton[24–26] and allow the requisite movement. (As rab7 is present on both late endosomes and lysosomes it is not possible to distinguish the two sets of organelles precisely so the term ‘late endolysosome’ (LEL) will be used here to include both). Merging of endocytic vesicles may also require annexin A2 (AnxA2),[27,28] possibly through its ability to mediate membrane fusion events.[29] The definite requirements are the initial formation of a tether between rab7 and a cognate effector, probably the HOPS complex[30] (Figure 1, ❼), release of calcium ions[31] (Figure 1, ❽) and finally formation of a SNARE complex (Figure 1, ❾) from

.

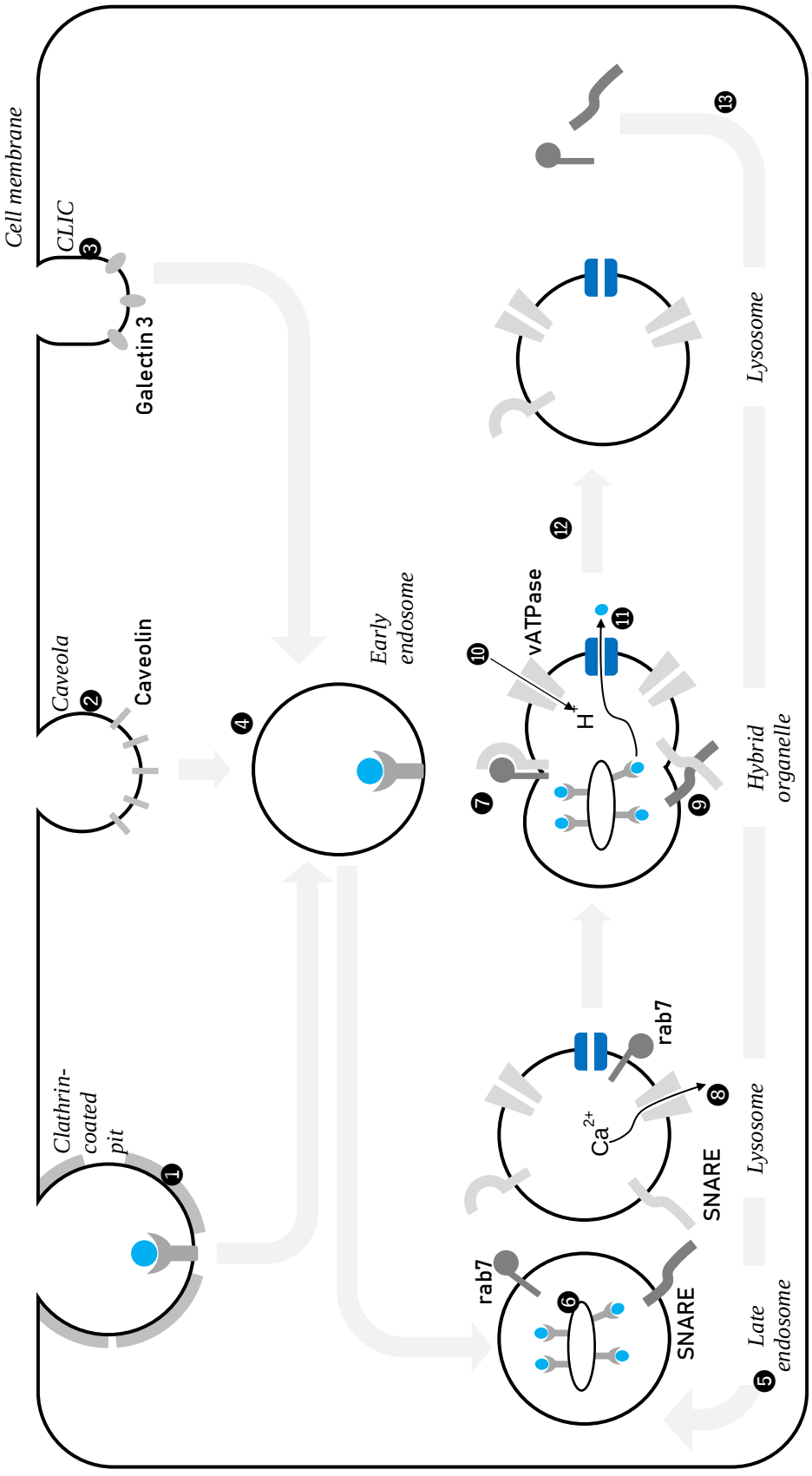

Figure 1 Schematic of endocytosis For details see text

proteins on the surface of each partner. For endocytosis these SNAREs are syntaxin 7 (Stx7) and VAMP8.[32–34]

Once the hybrid organelle has formed from an endosome and a lysosome catabolism of the contents is performed by an array of enzymes; the pH optima of many of these enzymes are low[35] thus an acidic environment is necessary. Acidity is achieved by the activity of the vacuolar ATPase pump (vATPase, Figure 1, ❿)[36] inhibition of which is reported by some studies to lead to widespread failure of endocytosis.[37,38] Metabolites generated in the LEL are exported (Figure 1, ⓫) by a variety of proteins including NPC1, the lysosome reforms (Figure 1, ⓬) while the rab and SNARE proteins are removed from the membrane to be reused (Figure 1, ⓭).

In addition to the failure to export cholesterol from the LEL a variety of experiments have detected multiple transport defects in Niemann-Pick cells[39–45] including a slowing of the entire endocytic process.[40,43] How can an accumulation of a single metabolite have such wide-ranging effects? As we have already seen (Figure 1) endocytosis relies on an extensive, complex set of protein machines to function. There is a growing appreciation of the interaction of lipids, especially cholesterol (eg[46,47]), with proteins and that this interaction has functional consequences. Could the origins of the endocytic defect in NPCD result from protein dysfunction induced by cholesterol accumulation?

Accumulating cholesterol interacts with proteins needed for endocytosis; these interactions have functional consequences.

Successive investigations have indeed found it to be so. Thus under conditions of high cholesterol content such as pertain in NPCD the endolysosomal protein ORP1L undergoes conformational change.[24,48] Through a complex of proteins, including rab7, this associates the motor protein dynein with the organelle. Dynein is responsible for movement to the minus-end of microtubules, which is to say toward the cell interior. In NPCD the endolysosomal cholesterol content is permanently high so dynein remains associated and the organelles become immobilised[24–26,49,50] away from the cell periphery[24,26,51] and therefore unable to fuse with early endosomes This mechanism also keeps them away from the ER. This is important as the ER is believed to replenish[52] endolysosomal calcium stores which have been used up in vesicle fusion (Figure 1, ❽) but are needed if the lysosome is to fuse with and therefore process the next wave of incoming vesicles. Indeed lysosomal calcium was found to be low in NPCD cells[53–55] while blocking the IP_3 receptor, a channel plausibly implicated in endolysosomal calcium refilling, led to a proliferation of endocytic vesicles,[56] a characteristic of lysosomal storage diseases (see chapter 3).

Cholesterol accumulation also makes a more direct contribution the endocytic defect. Annexins A2[27,57] and A6[58,59] both associate with cholesterol-rich areas of membrane and so in NPCD mislocalise to late, rather than early, endosomes;[60,61] this defect is recapitulated in cells treated with a small molecule blocker of NPC1.[27] Whilst the function(s) of annexins in endocytosis have only been partially elucidated[27–29] their tendency to associate with cholesterol-rich membranes renders likely some role in the NPCD endocytic defect. Other proteins found in membrane subfractions with high cholesterol content include rab7,[62] syntaxin7[62,63] and VAMP8.[64] As shown above (Figure 1, ⓭) the successful continuation of the endocytic cycle requires their removal from membranes for re-use. This removal is retarded for all these proteins when they are present in cholesterol-rich membranes,[26,50,65] such as those present in NPCD endolysosomes, and so endocytosis as a whole is slowed down.[26,50] (A similar defect affects NPCD synapses.[66]) Consistently this transport defect can be rescued by over-expression of rab7.[41] (Experiments involving rab7 should be interpreted with caution as this protein has a plethora of functions,[67] many of which such as cathepsin D maturation,[68] autophagy[69,70] and lysosome-mitochondrion contacts[71] are likely to be relevant to NPCD. Controlling adequately for all these factors is necessarily challenging.)

It is, however, questionable whether the vATPase proton pump through which these organelles acquire the requisite acidic pH is similarly affected by cholesterol. The pH of lysosomes in NPCD cells has been reported as elevated,[43,72] though other studies find it normal.[54,73,74] This issue will be revisited in chapter 3. Acidification will generate an electrical potential[52,75,76] and there is debate whether ion fluxes mediated by other ion channels in the endolysosomal membrane are necessary to balance this. The debate has been wide-ranging[77–79] and will not be entered here, though the association of calcium,[80] chloride[81–83] and potassium[84,85] channels with neurodegeneration may well be significant. Indeed even the absence PIKfyve, the protein responsible for synthesising the ligand for some calcium channels, results in neurodegenerative disease[86] perhaps through impaired acidification and consequent inhibition of autophagy.[87]

Autophagy

Autophagy is the process by which cells degrade worn out organelles and toxic proteins. It begins with the formation of a double-membraned organelle termed the phagophore which seals to become an autophagosome.[88] This fuses with a lysosome to become an autolysosome wherein the necessary degradation occurs and metabolites are exported.

Given the resemblance of this process to endocytosis we might expect similar requirements to pertain, particularly to the organelle fusion step. Indeed correct acidification,[89–91] rab7,[69,70,92] Ca^{2+} efflux through the TRPML1 channel,[93] Stx17[94] (though not -7[95]) and VAMP7[96] or -8[95] have all been reported as necessary. The additional dependence on the correct proportion of membrane cholesterol[90,92] raises the expectation that autophagy will be slowed in NPCD, just as endocytosis is, and that this deficiency may have similar molecular origins. Such an error would be expected to appear as a proliferation of autophagosomes (visualised as positive for marker protein LC3-II) as they fail to fuse with lysosomes. This has indeed been repeatedly reported in NPCD (eg[97–99]).

Autophagy is also dysfunctional in NPCD; though not certainly for the same reasons as endocytosis

Nonetheless alternative accounts, only partially consistent, are available. Work in NPC neurones (derived from embryonic stem cells, ESCs) found the autophagic pathway not stalled but rather over-active,[100] a result echoed in NPC fibroblasts.[74,98] On this model the proliferation of autophagic vesicles (eg[98,99]) derives from reduced clearance of autolysosomes and not from impaired fusion of their precursors. In turn clearance may be slowed by reduced activity of lysosomal proteases the cathepsins which was attributed, after elimination of more conventional causes, to direct enzyme inhibition by stored lipids.[74]

From cholesterol storage to protein misregulation

It is becoming increasingly apparent that lysosomes, rather than being merely waste processing units, are fully integrated into the life of the cell.[101] Accordingly failure of lysosomal metabolite export will have effects that cannot be contained to the organelles directly affected but will impact the whole cell. In the case of cholesterol the onward destination from the lysosome has not been fully elucidated - there seem to be multiple cholesterol transport pathways operating simultaneously[102–105] and other proteins seem to have roles that have yet to be discovered.[106,107] However it is generally agreed that NPCD results in a cholesterol deficit at both the ER[108,109] and the Golgi[110] with consequences for protein regulation (Figure 2 where the suffix * denotes a protein in its activated state).

Reduced levels of cholesterol at the Golgi[110] (Figure 2, ❶) affect the sterol homeostatic protein SREBP and its regulator SCAP. Under normal conditions cholesterol binds to SCAP inducing conformational change and keeping it associated with SREBP (Figure 2, ❷). Under conditions of low Golgi cholesterol, such as found in NPCD, SCAP dissociates from SREBP which is therefore broken down by Golgi proteases. A SREBP fragment then migrates to the nucleus (Figure

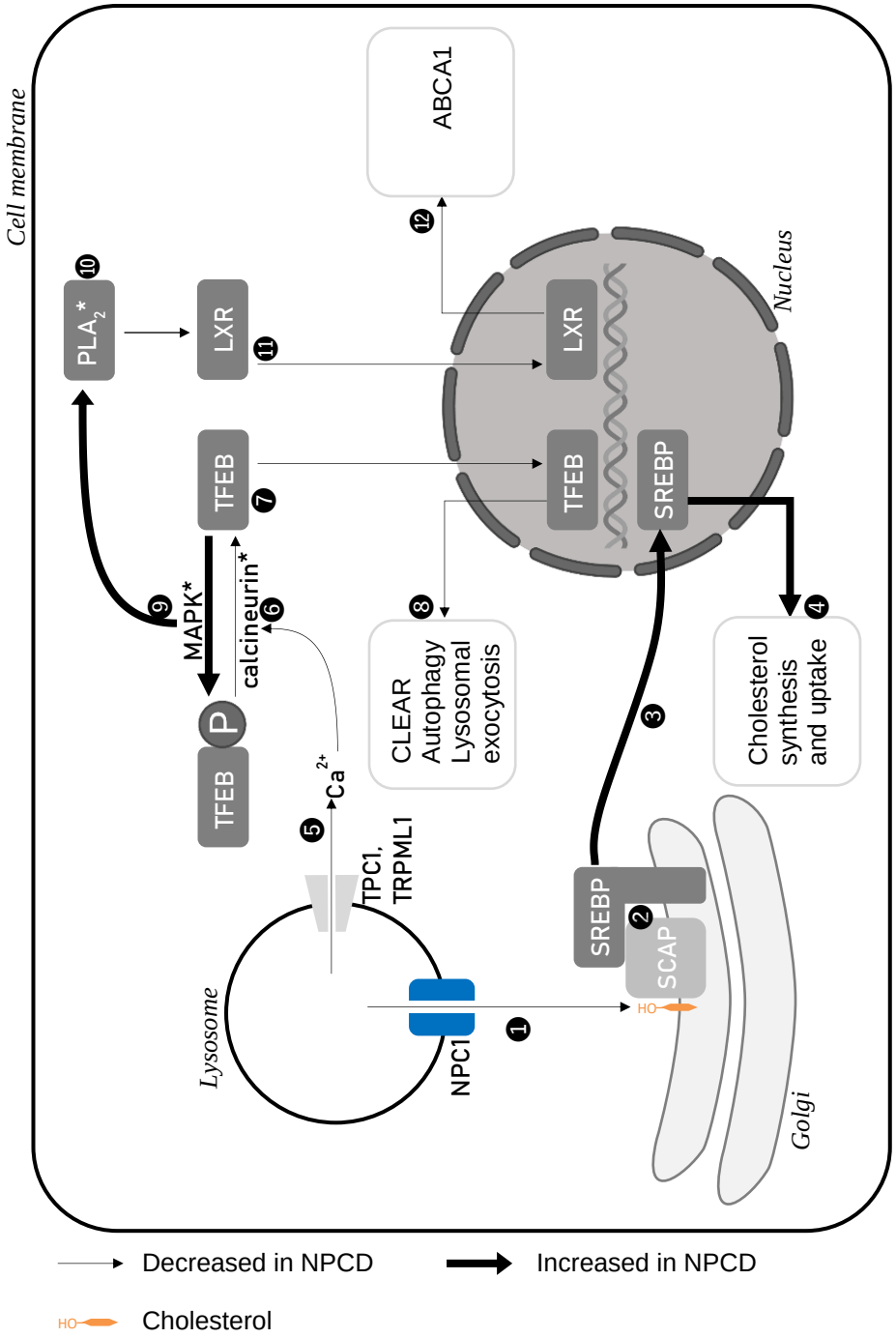

Figure 2 From cholesterol storage to protein misregulation Cholesterol storage in NPCD sets off chains of events that lead ultimately to the over-expression of certain proteins and the under-expression of others. For details see text

2, ❸)[111] where it acts as a transcription factor and upregulates the enzymes involved in cholesterol synthesis and uptake[111] (Figure 2, ❹). Thus NPCD produces a cellular excess of cholesterol but the defect in its lysosomal export fools the cell into believing that it is experiencing a cholesterol deficit. The cell responds accordingly

by making more cholesterol and attempting to gather more from the extracellular medium.[112,113]

Cholesterol storage leads to counter-intuitive misregulation of genes involved in cholesterol handling. It also down regulates lysosomal activation genes.

For reasons that have yet to be fully explained (but were alluded to briefly above[24,56]) NPCD lysosomes have lower Ca^{2+} content than normal[53–55] and thus calcium efflux is impaired[114,115] (Figure 2, ❺). This in turn leads to a reduced activity of the cytosolic phosphatase calcineurin[116] (Figure 2, ❻) which hydrolyses transcription factor EB (TFEB)[117] rendering it active (Figure 2, ❼). Thus there is less active TFEB to translocate to the nucleus.[114] TFEB upregulates the CLEAR network[118,119] of genes necessary for lysosomal function and also enhances autophagy[120] and lysosomal exocytosis[121] (Figure 2, ❽) which lead to cellular off-load of toxic substances and their metabolites. Thus the consequences of reduced lysosomal calcium in NPCD is a reduction in all these processes at the transcriptional level as well as through the vesicle fusion defect discussed above. This is reinforced by the over-activation of mitogen activated protein kinase (MAPK) in NPCD,[122,123] which occurs for reasons to be discussed later, as one report makes this enzyme responsible for phosphorylating TFEB keeping it inactive[124] (Figure 2, ❾). (A variant account[125] makes the nutrient sensing complex mTORC1 the kinase for TFEB though the impact of cholesterol storage on mTOR status is still debated.[98,125,126]) MAPK is also known to phosphorylate and thereby activate PLA_2 (Figure 2, ❿)[127,128] which in turn reduces the action of the transcription factor liver X receptor (LXR, Figure 2, ⓫) and reduces expression of one of its target genes the cell surface cholesterol exporter ABCA1 (Figure 2, ⓬).[129,130] Thus cholesterol is retained in the cell and, again, the net result of storage of excess cholesterol is to make the cell behave as though it was suffering a cholesterol deficit.

From cholesterol storage to cell death

As significant as these processes are, we may question whether the errors are serious enough in NPCD to account for the progressive cell death seen in patient neurones. This can be explained by a complex series of events shown in Figure 3 (the * suffix represents a protein in its activated state).

Along with cholesterol NPCD endolysosomes accumulate other lipids including sphingomyelin (SM).[43,61] These can permeabilise the lysosomal limiting membrane (Figure 3, ❶);[131–133] the glycocalyx which lines the membrane and protects it from the harsh degradative environment of the lysosomal interior is also altered in NPCD.[134] Such perforations allow molecules usually localised to the lysosomal interior to escape into the cytosol; among these are the cathepsin proteases (Figure

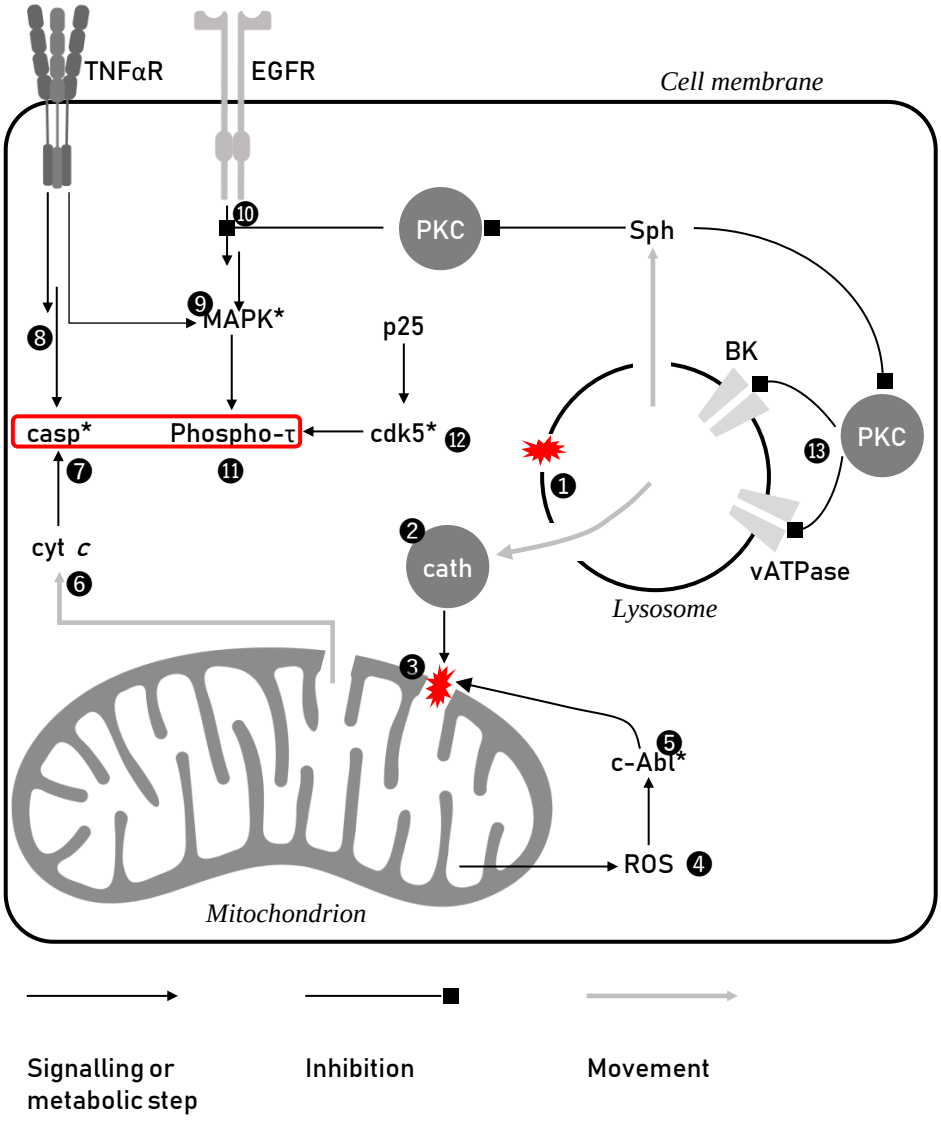

Figure 3 From cholesterol storage to cell death Dysfunction in NPCD cells activates events that ultimately result in cell death. For details see text.

3, ❷) which have been shown to damage mitochondria (Figure 3, ❸).[133,135] Mitochondrial damage can also result indirectly from a cellular state known as oxidative stress. Oxidative stress is a harmful increase in reactive oxygen species (ROS, hydrogen peroxide, and the superoxide and hydroxide radicals) caused in turn by their increased generation (often resulting from mitochondrial leak, Figure 3, ❹) or decreased detoxification pathways (such as catalase in peroxisomes). Increased ROS have been observed in NPCD cells[136–138] (with patient biochemistry also being affected[139,140]) which leads by an unknown mechanism to the activation of the kinase c-Abl (Figure 3, ❺)[137,141,142] and thereby to mitochondrial damage.[143] Whether initiated either by cytosolic cathepsins or by activated c-Abl, mitochondrial damage leads to release of respiratory chain protein cytochrome c (cyt *c*) from mitochondria (Figure 3, ❻).[133,135,143] This triggers the intrinsic apoptotic pathway[144] resulting in

the activation of the caspase proteolytic cascade (Figure 3, ❼)[145] which ultimately dismantles key cellular components including the nuclear envelope and leads to cell death. The extrinsic apoptotic pathway, triggered by binding of TNFα at its receptor (Figure 3, ❽), is also up-regulated in NPCD.[146] Accordingly both a c-Abl inhibitor[147] and an anti-TNFα antibody[148] have demonstrated symptomatic improvement in NPCD mice.

A second pathway leads to cell death: in NPCD MAPK is found activated[122,123] (Figure 3, ❾). The reasons for this are unclear, though MAPK can be activated by binding of TNFα to its receptor[149] and this pathway is up-regulated in NPCD [146] MAPK activation by this means has not yet been explicitly demonstrated for this disease. More commonly MAPK is regarded as being on the EGFR pathway where protein kinase C (PKC) normally serves as a brake[150,151] (Figure 3, ❿). Sphingosine (Sph), another lipid that accumulates in NPCD,[54] may[152,153] or may not[154,155] inhibit PKC (IC_{50} at least 1μM) so if enough Sph escapes the lysosome to effect inhibition, itself an open question, then the brake on the EGFR pathway may be removed leading to activated MAPK. Alternatively localisation may play a role. In rat brain synapse PKC has been found associated with cholesterol and AnxA6.[156] If the AnxA6 is diverted to lysosomes, as it is in NPCD,[61] then the PKC may also be removed from proximity to the cell membrane and so to EGFR. One of the targets of aberrantly activated MAPK is the cytoskeletal protein tau (τ) and so in NPCD this activation leads to hyperphosphorylated tau (Figure 3, ⓫)[122,123] possibly consistent with the finding of increased tau in the CSF of NPCD patients.[157] This forms fibrillary tangles similar to those found in Alzheimer's disease;[158] neuronal cell death results. In NPCD cells hyperphosphorylation was reduced *in vitro* on treatment with a MAPK inhibitor.[123] An alternative pathway to hyperphosphorylated tau starts with the observation that the protein p25, also known as Cdk5R1 and a proteolytic fragment of p35, is increased in NPCD. p25 serves as an activator of cyclin dependent kinase 5 (cdk5, Figure 3, ⓬) which then hyperphosphorylates tau;[159] cdk5 inhibition led to reduced phosphorylation and symptomatic improvements in a mouse model of NPCD.[160]

Cholesterol storage appears to activate diverse cell death pathways; details are not completely worked out.

None of the preceding paragraph can be regarded as uncontroversial. When MAPK inhibition was translated from *in vitro* to a mouse model enzyme activity was indeed reduced, but tau phosphorylation was increased and no clinical improvement could be observed.[161] However, selectivity in kinase inhibition is notoriously hard to achieve and the MAPK inhibitor used in both studies[123,161] hits a range of enzymes;[162] it is therefore difficult to be clear on the origins of the observed effects. Similarly neither of the cdk inhibitors used[160] is selective for cdk5 (data from the ChEMBl

database[163]). The genetic knockout of p35, the cdk5 activating protein, would be expected to give more targeted effects but did not result in the expected clinical improvements in NPC mice.[164]

Nonetheless PKC activation has been reported by two groups to result in improvements in NPCD cell culture models[165,166] which was attributed to a pathway involving rab9 and the cytoskeletal protein vimentin (see also[167,168]); the possible involvement of tau was not examined. None of the studies cited in this section investigates the idea that PKC has a potential role in the regulation of vATPase[169] and the lysosomal potassium channel BK (Figure 3, ⓭),[170] proteins we will meet again in subsequent chapters.

Mitochondria

Mitochondria are dsyfunction in NPCD cells; cholesterol poisoning is likely but unproved.

Mitochondrial damage (Figure 3, ❻) raises the expectation of metabolic dysfunction in NPCD and indeed reduced mitochondrial potential,[55,171] reduced oxygen consumption,[138,172] reduced ATP production[171] and increased levels of lactate[138] have all been reported alongside increased ROS.[136–138] Most workers attribute this respiratory impairment not to loss of cyt *c*, or structurally aberrant mitochondria more generally, but to excess mitochondrial cholesterol poisoning the organelle. This hypothesis is superficially appealing and also consistent with mitochondrial dysfunction induced by cholesterol over-feeding in hepatic[173] and pancreatic[174] cells. However it is also problematic as mechanisms for cholesterol-induced mitochondrial toxicity have been postulated but not yet proved.[172,175] Additionally mitochondria play a role in cellular cholesterol homeostasis for they house Cyp27A1 an enzyme responsible for converting cholesterol to 27-hydroxycholesterol, a ligand of the liver X receptor (LXR).[176] Agonism of this receptor in turn signals increased expression of the cell surface cholesterol exporter ABCA1. Thus high levels of cholesterol at the mitochondrion, postulated to account of respiratory dysfunction in NPCD, function as a signal that the cell has excess cholesterol and will lead to export of this lipid via increased expression of ABCA1. In fact ABCA1 expression is reduced in NPCD[129,130] (though other studies disagree[113,177]) and, as we shall see later, LXR agonists have enjoyed some success as therapies. (The role, if any, of SREBP in regulating ABCA1 is unclear with contradictory results having been reported.[178,179]) Different pieces of evidence therefore lead to the construction of different arguments for different conclusions regarding the question of cholesterol over-load at the NPCD mitochondrion. The issue could perhaps be settled if cholesterol in control and disease mitochondria could be quantitated, but this requires isolation of clean and complete mitochondrial samples, a problem noted for its difficulty.[180] The NPCD studies that work with isolated mitochondria and assess the purity of this cellular

fraction do uniformly report increased mitochondrial cholesterol.[138,171,181,182] However in all cases they also find mitochondrial marker proteins in other fractions so while these results are highly suggestive they cannot be regarded as conclusive. Intriguingly, work with isolated mitochondria from healthy cells[171,183] reported a decrease in respiration on cholesterol lowering which, taken together with the NPCD work, may suggest that mitochondria have a narrow range of tolerable cholesterol levels.

The idea that excess cholesterol poisons mitochondria in NPCD also asks how excess cholesterol in the LELs might find its way to mitochondria when it never arrives at its more expected destinations in the ER or Golgi.[108,184] It has been hypothesised that lysosomal luminal protein NPC2 transports cholesterol to the LEL outer membrane in a manner independent of NPC1[185] and from there it is collected by steroidogenic acute regulatory protein D3 (StARD3, also known as MLN64)[181,186] and/or StARD1[187] and inserted into the mitochondrial membrane. This pathway, and how it might be manipulated for benefit in NPCD, will be investigated in much greater detail in chapter 4.

Thus starting from a simple failure of metabolite export, NPCD progresses via multiple pathways to affect numerous important cellular functions and results ultimately in cell death. This multi-faceted pathology poses an obvious question to those who would treat the disease: which aspect do you target? Perhaps surprisingly, many of the treatment options that have been explored depend upon the sphingolipids which co-accumulate with cholesterol in the NPCD lysosome. Thus it is important to understand their metabolism - for a recent review see.[188]

Sphingolipid metabolism

Sphingolipid synthesis *in vivo* begins with the condensation of serine with a long-chain acyl-CoA, usually palmitoyl, mediated by serine palmitoyl transferase (Figure 4A, ❶). The reduction of the ketone group thereby generated gives dihydrosphingosine (dhSph, also known as sphinganine), acylation of the nitrogen with a second long-chain acyl-CoA mediated by ceramide synthase (Figure 4A, ❷) gives dihydroceramide before oxidation to give a carbon-carbon double bond yields ceramide. These steps happen in the ER (Figure 4B, ❶, ❷).[189] Ceramide

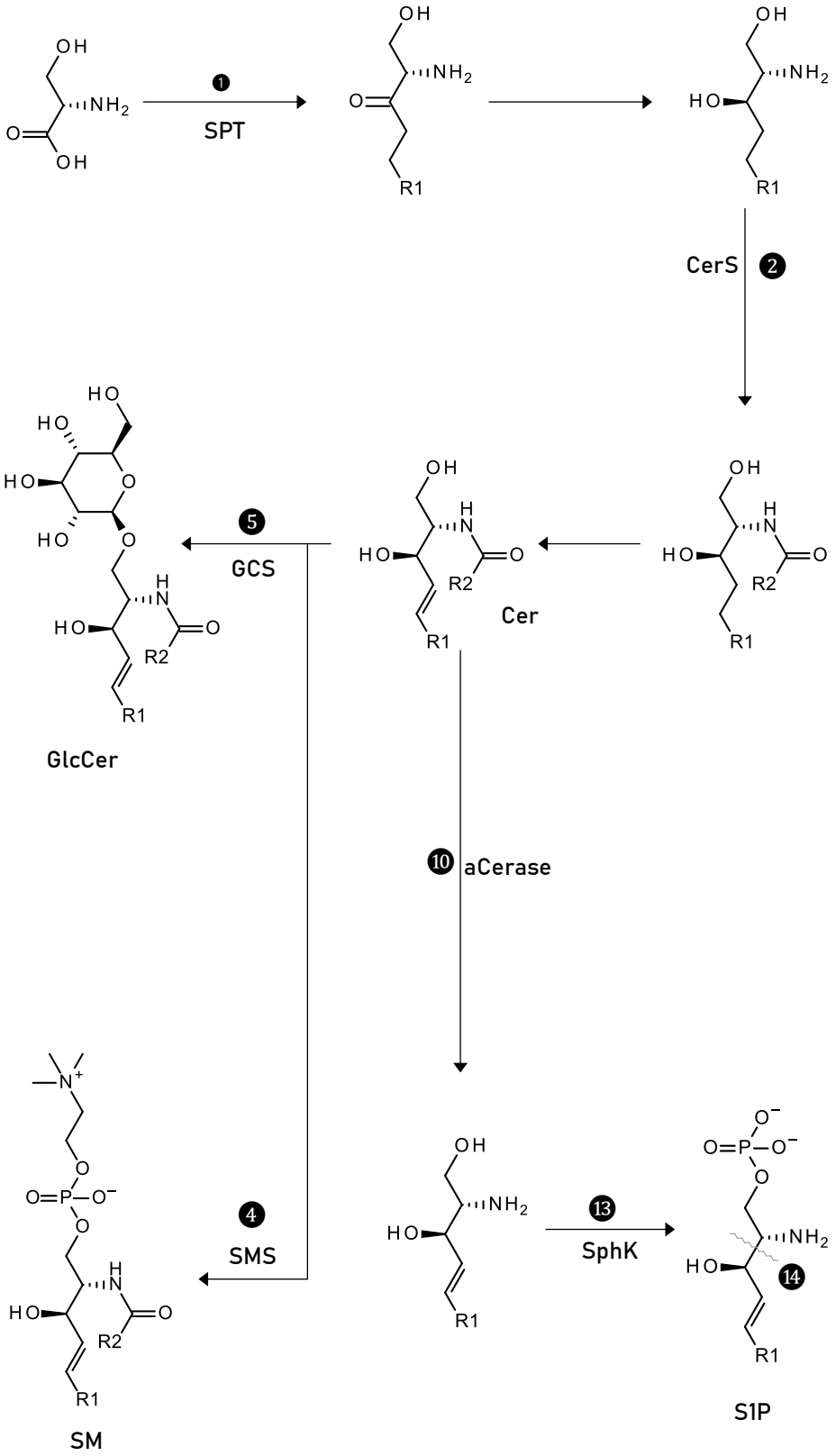

Figure 4A Simplified biochemistry of sphingolipid metabolism The numbered steps are the same as those in Figure 4B which shows subcellular localisation

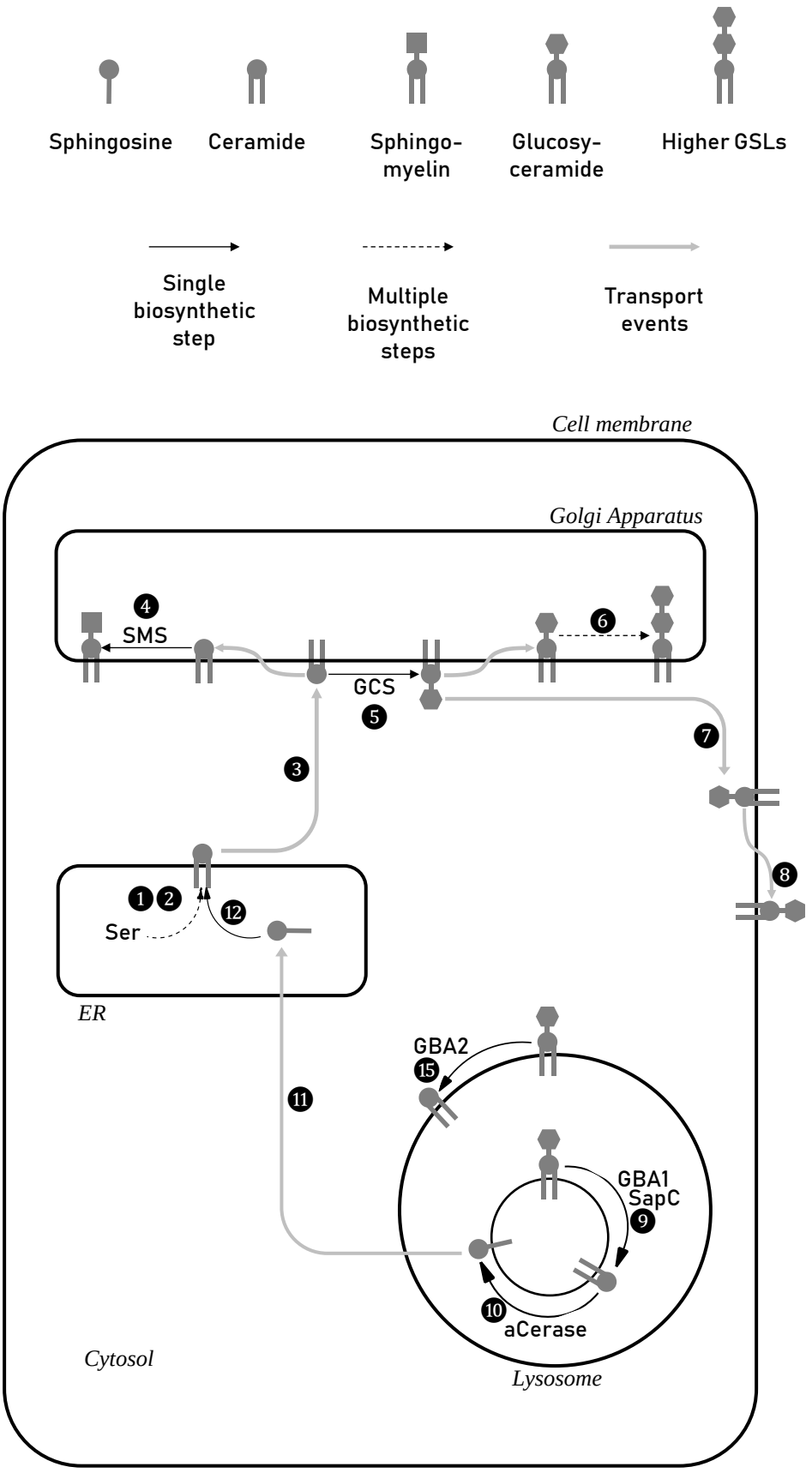

Figure 4B Simplified schematic of sphingolipid metabolism The numbered steps are the same as those in Figure 4A which shows chemical structures

is then transported to the Golgi in a vesicular manner and also by ceramide transfer protein (CERT, also known as StARD11, Figure 4B, ❸).[190] Translocation to the luminal face of the Golgi membrane allows addition of a zwitterionic head group to give sphingomyelin (SM, Figure 4A,B, ❹). Ceramide remaining on the cytoplasmic face can be glycosylated to give glucosylceramide (GlcCer) by the requisite synthase GCS (Figure 4A,B, ❺).[191,192] GlcCer is thus the simplest glycosphingolipid (GSL). GlcCer can then be transferred to the opposite face of the Golgi membrane, likely by an indirect mechanism,[193] where elaboration to higher GSLs such as gangliosides occurs (Figure 4B, ❻). GlcCer is also transported to the cell membrane (Figure 4B, ❼) by a non-vesicular route[194] mediated by glycolipid transfer protein (GLTP) and phosphatidylinositol-four-phosphate adapter protein 2 (FAPP2, also known as PLEKHA8) where it eventually emerges on the cell surface (Figure 4B, ❽).[194] This renders it susceptible to endocytosis and metabolism. Thus on an internal lysosomal membrane GlcCer is hydrolysed to ceramide by glucocerbrosidase (GBA1)[195] with saposin C as an essential co-factor (Figure 4B, ❾).[196] Ceramide is further catabolised by acid ceramidase (Figure 4A,B, ❿) to sphingosine (Sph) which is returned to the ER by an unknown mechanism (Figure 4B, ⓫) and processed to regenerate ceramide (Figure 4B, ⓬). Sphingosine in the cytosol is generally phosphorylated by sphingosine kinase (SphK, Figure 4A, ⓭) to give sphingosine-1-phosphate (S1P) before irreversible carbon-carbon bond cleavage by S1P lyase (Figure 4A, ⓮, zig-zag line marks the bond broken) removes the molecule from the sphingolipid pathway completely. A minor sub-population of GlcCer on the cytosolic face of membranes can be hydrolysed by specific enzyme GBA2 (Figure 4B, ⓯). These metabolic pathways have several consequences for the life of the cell.

Most obviously the localisation of sphingolipid metabolic enzymes means the two sides of the lipid bilayers which form cell and organelle membranes are inequivalent.[197] Ceramide is glycosylated only on the cytosolic face of the Golgi membrane, and subsequent processes preserve the asymmetry this induces. For example GLTP and FAPP2 transport GlcCer to the cell membrane (Figure 4B, ❼)[194] where they are believed to interact with existing lipids[198] to insert GlcCer. This insertion necessarily occurs only on the cytosolic (inner) leaflet. Equally endocytosis does not disturb membrane asymmetry: note that the receptor on the cell surface (Figure 1, ❶) progresses exclusively to the luminal face of the endosome (Figure 1, ❹). This spatial property can, however, be removed by proteins that translocate ('flip') lipids from one membrane leaflet to the other. All these features will become important later in this chapter and again in chapter 3.

Treatment

Expression

Histone deacetylases (HDACs) are a family of enzymes involved in regulating gene transcription and are over-expressed in NPCD[199] possibly as a result of c-Abl activation (Figure 3, ❺).[200] Consequently inhibition of HDACs leads to increased expression of NPC1,[201,202] enough of which can then be transported to the lysosome where sufficient function is preserved to export stored cholesterol and normalise levels of this lipid.[199,203] From testing various small molecule inhibitors with different selectivity profiles HDAC1 and -2 were tentatively identified as the key enzymes to target.[201] Experiments in mice have thus far failed to confirm the *in vitro* promise of such compounds.[204]

After translation to protein newly synthesised NPC1 is transported from the ER to the lysosome chaperoned by Hsp70;[205] mutant protein misfolds and is targeted for degradation.[206] Supplying a small molecule scaffold of the correct shape can cause mutant protein to fold correctly and thereby escape proteolysis. While the structural requirements of such an agent have been defined,[207] and correct protein localisation demonstrated,[208] studies have not progressed to disease modification.

A recent approach seeks to correct protein misfolding by manipulating ER calcium.[209] While this has been successful in a mouse model of another LSD[210] its potential in NPCD is currently unclear given that pathology depends on calcium in various ways.

Cholesterol

Trapping excess cholesterol in the lysosome fools the NPCD cell that it is experiencing a cholesterol deficit. We may expect therefore that therapies aimed at cholesterol reduction at the whole-body level will be ineffective. Indeed when various combinations of lipid-lowering agents were tried in patients, levels of plasma and hepatic cholesterol fell, but no impact on disease was reported.[211] In NPCD mice nifedipine (a Ca^{2+}-channel blocker, postulated also to induce cholesterol efflux) and probucol (an inhibitor of cell surface cholesterol exporter ABCA1) led to reductions in hepatic cholesterol but no effect on disabling neurological symptoms.[212] (Given the later finding that ABCA1 is downregulated in NPCD (Figure 2)[129,130] this is not surprising.) Lipid lowering agent clofibrate failed to reduce cholesterol levels in disease fibroblasts,[213] though given the pleiotropic effects of this class of drugs this finding might have been expected. Statins have recently been revisited and found ineffective in iPSC-derived neurones,[214] though showing some promise in oligodendrocyte culture.[215]

A subtler approach to cholesterol reduction is an agonist of the liver X receptor (LXR) which leads to an increase in ABCA1 levels in turn causing cholesterol offload in NPC1-deficient cells.[216,217] This increased the lifespan of NPCD mice though offered only a very slight improvement in neurological symptoms.[218]

Cyclodextrins (CDs) are large hydrophilic molecules containing a hydrophobic cleft and are thus suitable for solubilising lipophilic molecules including cholesterol. A range of studies has demonstrated the effectiveness of CDs in treating NPCD, though not, as might first be expected, by extracting cholesterol from membranes.[219] Rather CDs are endocytosed[219,220] where they sequester excess cholesterol in the LEL and return it to circulation – cholesterol is thus exocytosed,[219,221] reduced at the lysosome[220] and increased at the ER;[222] cholesterol synthesis is reduced.[223] (An alternative narrative makes cholesterol normalisation dependent on corrected autophagy.[224] While an explanation of the reasons behind this is not offered it is noteworthy that the sphingolipid field has produced similar findings on the interdependence of the two processes.[225,226]) Mitochondrial dysfunction is also normalised by cyclodextrin treatment,[171] though these experiments were conducted on isolated mitochondria which questions whether this approach would be successful in whole cells. CDs have been successfully used in mouse models of NPCD[223,227,228] though a major drawback is their inability to cross the blood-brain barrier.[229] Use in patients thus requires intrathecal administration; this technique underpinned the initial success[230,231] of a small clinical trial (NCT01747135), though a phase IIb/III clinical trial (NCT02534844) failed to demonstrate statistically significant improvement in patients.[a]

Surprisingly, treating NPCD by reducing cholesterol has led to mixed results

LEL calcium

As we have already seen NPCD cells have a deficit in endolysosomal Ca^{2+}, as demonstrated by multiple studies[53–55] (though there has been some disagreement[115]). This might explain the defects in endocytosis and autophagy, both of which depend on Ca^{2+}-efflux from the lysosome. Thus inhibiting Ca^{2+}-uptake by the ER might increase cytosolic Ca^{2+}, allow lysosomal stores to refill and so restore LEL function. Accordingly curcumin, an inhibitor of the SERCA calcium pump, restored aberrant endocytosis *in vitro* and improved lifespan in NPCD mice.[54] While neurological defects in the murine model were unaffected by curcumin monothereapy,[232,233] the benefits of other treatments were amplified.[232]

Calcium is also a key intermediary in the pathway of adenosine$_{2A}$ receptor ($A_{2A}R$) agonists the only extra-cellular target successfully investigated to date. The success

[a] See https://mallinckrodt.gcs-web.com/static-files/e0712994-a013-4658-b8be-0a3bc4da0c5b, accessed 21st August 2019.

of this approach in correcting both lysosomal and mitochondrial defects in a whole cell model[55,234] marks it as unique. Pharmacological experiments suggest a downstream effect of $A_{2A}R$ agonism is PKA activation[234] consistent with the classical pathway of this GPCR (though earlier work in fibroblasts invoked the ERK class of MAP kinases instead[55]). The pathway between PKA activation and Ca^{2+}-mobilization is not explored, nor is the idea that PKA can activate CFTR and induce lysosomal re-acidification.[235,236] The finding that $A_{2A}R$ agonism can lead to cholesterol efflux via increased ABCA1 expression[237] is likewise neglected. $A_{2A}R$ agonists in NPCD mice give small improvements in neurological symptoms and lifespan.[238]

Vitamin E component δ-tocopherol has also been reported to repair the lysosomal calcium deficit in NPCD, though the endocytic defect was unaffected.[53] Two reports claim the almost identical compound α-tocopherol is stored alongside cholesterol in NPCD,[239,240] while another suggests the same molecule as a therapy.[241]

Sphingolipids

Some lysosomal storage disorders result from an inability to metabolise gangliosides correctly (formed at stage ❻, Figure 4B); these lipids thus accumulate. The observations that NPCD patients have a secondary accumulation of gangliosides and present clinically similar symptoms to patients with a deficiency in ganglioside metabolism prompted the notion that gangliosides could be pathological in NPCD.[242] Given the absence of small molecule inhibitors of ganglioside synthases a logical treatment choice would therefore be to inhibit GlcCer synthesis (stage ❺, Figure 4A,B) and indeed GCS inhibitor N-butyldeoxynojirimycin (NB-DNJ) proved successful at alleviating symptoms in both cat and mouse models of the disease.[242] The first report of the effective treatment of a human patient emerged in 2004[243] and was followed by clinical trials which demonstrated stabilisation of disease progression and even some improvements.[244,245] These developments led to the approval of NB-DNJ (miglustat, Zavesca®, reviewed[246]) in Europe in 2009. Subsequent studies have questioned miglustat's mode of action. While the improvement in a murine model was confirmed, brain lipid analysis showed an increase in GlcCer (and no effects on gangliosides GM2 or GM3) - inconsistent with its postulated action as a GCS inhibitor.[247] Off-target effects at GlcCer hydrolase GBA2 were suggested (stage ⓯, figure 4B) and *in vitro* work later confirmed that miglustat was in fact a more potent inhibitor of this enzyme than of the synthase.[248] Use of a rationally designed GBA2 inhibitor[249] has recently been effective in treating NPCD mice[250] while genetic deletion of GM2 or -3 synthases in murine models failed to yield improvements.[251,252] This is consistent with miglustat being clinically effective but not altering GM2 or -3 levels and suggests that these gangliosides are

not the toxic lipids in NPCD. Thus the sub-population of GlcCer on the cytosolic face of membranes ('cytosolic GlcCer') emerges as an important factor in NPC disease. This topic will be examined in more detail in chapter 3.

There are some possible commonalities here with Gaucher disease which results from loss of function mutations of the lysosomal GlcCer hydrolase GBA1 (Figure 4B, stage ❾). Both Gaucher and NPCD feature lysosomal storage of GlcCer, both have upregulated GBA2[250,253] and both are clinically treated with GBA2 inhibitor miglustat. Thus it may be that, through upregulation of GBA2, GlcCer is the toxic lipid in both diseases. Whether this is genuinely the pathway, and if so whether it can be generalisable to other LSDs, remains to be seen.

Another important sphingolipid pool is that of sphingomyelin (SM) in the intra-lysosomal membranes mentioned above (Figure 1, ❻). These membranes are rich in specialised lipid lysobisphosphatidic acid (LBPA), also known as bis(monoacylglycero)phosphate (BMP).[254,255] SM is degraded at these membranes (analogous to stage ❾, Figure 4B) by acid sphingomyelinase (aSMase), a process which depends on the interaction of the enzyme with LBPA.[256,257] The activity of aSMase is reduced in NPCD[256,257] despite normal expression[256] and localisation.[257] This contributes to high levels of SM in NPCD endolysosomes which, as noted above, can permeabilise the limiting membrane[131–133] leading ultimately to apoptosis. Hsp70 stabilises the aSMase-LBPA interaction[258] and thus dosing recombinant Hsp70 corrects errors in a murine model of NPCD.[259] (These mice entirely lack NPC1 so it was not possible to assess whether Hsp70 also chaperoned transport of mutant NPC1 to endolysosomes[205] thus giving sufficient NPC1 activity.) The effect could be recapitulated by synthetic Hsp70 inducer arimoclomol.[259] A human clinical trial (NCT02612129) with this agent has recently concluded with positive results.[b] This research raises other questions. Both SM[260] and LBPA[254,255] are reported to associate strongly with cholesterol at the intra-luminal membranes; computational and model membrane studies also suggest SM has an inhibitory effect on cholesterol transfer[261,262] and increasing aSMase activity results in increased cholesterol export in normal cells.[263] More surprisingly, but consistently, increasing aSMase activity decreased lysosomal cholesterol in NPCD cells.[264] Comparable findings have recently been reported with LBPA.[265] Thus it would appear to be possible to reduce lysosomal cholesterol in NPCD by doing nothing more than altering the population

[b] See https://www.orphazyme.com/news-feed/2019/1/30/orphazyme-reports-positive-results-from-full-data-set-of-phase-iiiii-arimoclomol-trial-in-niemann-pick-disease-type-c-npc, accessed 21st August 2019

of another lipid inside the lysosome. Other work finds that the same result can be achieved by over-expression of rab7,[41] use of a viral rab7 equivalent,[266,267] by increasing expression of ABCA1[216,217] or by inhibiting O-glycosylation of lysosomal membrane proteins.[268] At the very least this suggests that NPC1 is not required for endolysosomal cholesterol export (though NPC2 may be[217,267]). By this account, and as previously argued on kinetic grounds,[54] cholesterol storage in NPCD is not primary but secondary and therefore the main or only function of NPC1 is not cholesterol export but some other form of endolysosomal regulation. We will return to these ideas in chapters 2 and 3.

Succesful treatment of NPCD by manipulating sphingolipids raises suspiscions that NPC1 may not be primarily a cholesterol exporter

This chapter has provided the tools necessary to understand the interplay of lipids and proteins, organelles and processes which characterises NPCD cells. Subsequent chapters will investigate how these interactions impact both the pathology and treatment of this disease in lysosomal function (chapters 2 and 3), endocytosis (chapter 3) and energy production (chapter 4).

Aims

- to investigate computationally the mode of action of NPC1 and -2 and particularly the idea that these proteins can process sphingosine in the same manner as cholesterol

- to use in silico tools to ask if the documented endolysosomal errors in NPCD cells can be understood in terms of lipid-protein interactions

- to measure the pH of the endolysosomal compartment in NPCD cells and to find if it is altered by GBA2 inhibition

- to ask if GBA2 inhibition can be a pharmacological treatment for other neurodegenerative diseases

- to measure the impact, if any, of GBA2 inhibition (and sphingolipid manipulations more generally) on the mitochondrial defect in NPCD cells

- to examine pharmacological manipulations of mitochondrial cholesterol overload in NPCD cells, postulated to be responsible for the respiratory defect

2

Modelling

In chapter 1 we briefly and sporadically encountered the idea that cholesterol is not the only lipid that accumulates in the lysosomes of Niemann-Pick type C disease (NPCD) cells. The idea to be explicated in this chapter is that these lipids interact with lysosomal proteins and that these interactions are ultimately responsible for the endocytic and autophagic defects present in NPCD. These interactions can be simulated by computer. Thus the methods used in this chapter see biological events as being essentially chemical, chemical change as driven by physics and physics expressed and quantitated by mathematics. The results derived from such a reductionist approach will be better understood with a brief sketch of the reverse process: how the basic idealisations of physics can be slowly elaborated to the real complexities of biology.

Introduction

Energy

It is important to realise that in physics today we have no knowledge of what energy is.

Richard Feynman
Six Easy Pieces

Our ignorance of energy's essential nature does not condemn us to a total absence of understanding of its role in the world. We do know that energy comes in different forms, such as those relating to electrical charge or to movement. We can also know, and indeed measure, if a given change in a given system either requires work to be done to that system, or conversely releases energy that is able to do work. Thus closing an electrical circuit releases electrical energy to perform work, for example causing a bulb to emit light, whilst pushing a stationary object into motion requires work to be done. Energy able to do work is termed 'free energy.' Changes that release free energy are favourable and are given a negative sign; changes that require free energy to be supplied are unfavourable and are given a positive sign. The size of the change is proportional to the degree of favourability or unfavourability. One change that can be quantitated in this way is that of the shape of a molecule.

Free energy as a measure of change

Molecular shape and interactions – basic considerations

Shapes of molecules and interactions between molecules are not fixed but determined energetically

Chemical compounds have a molecular structure defined by the constituent atoms and the bonds between them, but this does not necessarily define the shape the chemical will adopt, and indeed this shape will vary depending on the environment. That environment may include other molecules of the same or different types and this raises the question of how the molecules will interact with each other. (Interactions open the possibility of chemical reactions to give new molecules; the treatment here does not consider this possibility as such events are not relevant for work discussed in this chapter.) Both changes in the shape of one molecule and changes in interactions between molecules are determined by the free energy changes that accompany them – those which are more energetically favoured will be more likely. In turn the free energy changes can be usefully attributed to one of three sources: charge-charge interaction, hydrogen bonds and van der Waals bonding, all of which are weaker than covalent chemical bonds and vary in strength as now discussed.

Some biologically relevant entities such as the potassium ion (Figure 1A) carry electrical charges which generate repulsive force between them (Figure 1B) as defined by the equation:

$$F = \frac{kq_1q_2}{r^2}$$

where q_1 and q_2 are the electrical charges, r is the distance between them and k is Coulomb's constant. Thus forcing two such ions close together (making the inter-molecular distance small) results in a large, positive free energy change and so is unfavourable but at larger distances the energy penalty is much smaller, even negligible. Therefore the interaction energy is not fixed but may take a variety of values. Plots such as Figure 1B, and the equations that underlie them, show what the interaction energy may be and so are referred to as potential energy plots, or simply potentials. Of course in more complex systems containing multiple charges, both positive and negative, interaction could lead to a negative free energy change and so be favourable.

Even systems with simple biological molecules fit this description. This is partly because it is also possible for atoms to carry partial charges which result from differences in electronegativity between the two atoms at either end of a chemical bond. (This itself is actually a simplification, but the reasons for that need not detain us.) More electronegative atoms attract the electrons in the bond and thus

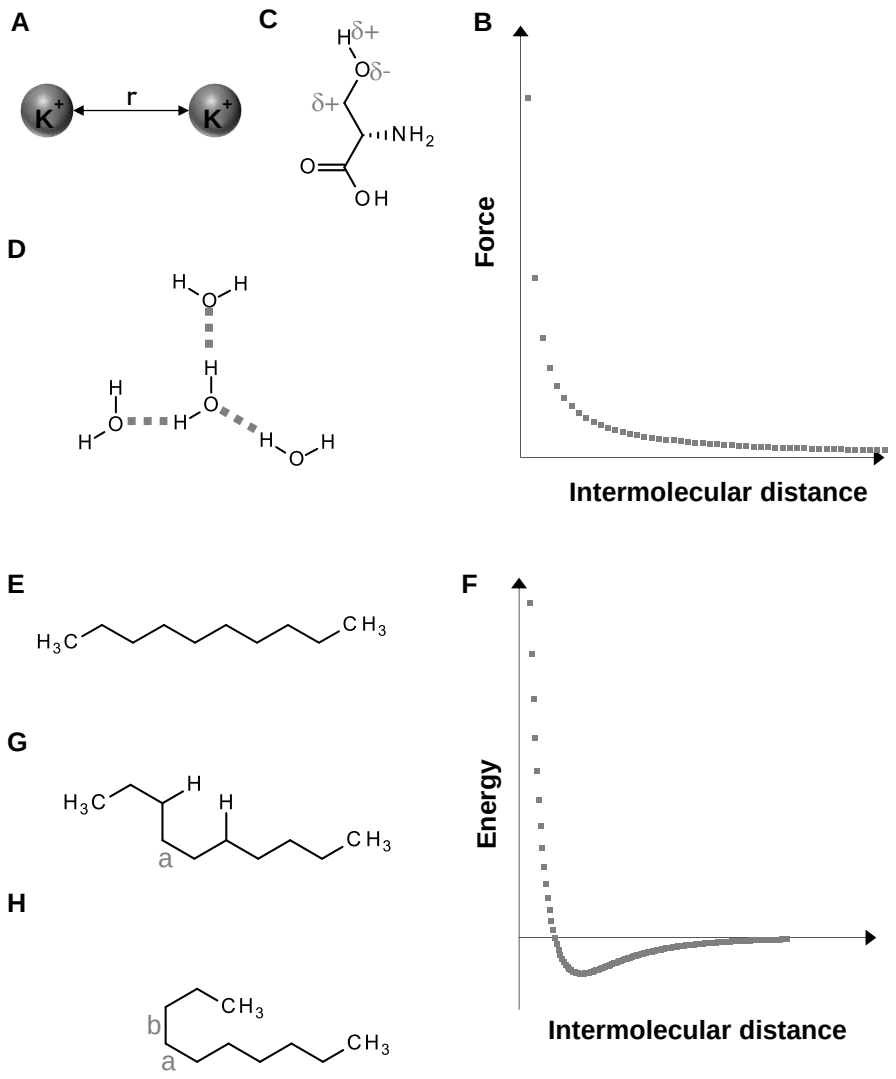

Figure 1 Interactions and shapes of molecules (**A**) Two potassium ions separated by inter-atomic distance r. (**B**) Electrostatic force between two entities of like charge. (**C**) Some of the partial charges on a serine molecule. (**D**) Hydrogen bonds illustrated for water. (**E**) Decane. (**F**) van der Waals interactions vary with intermolecular distance. (**G**) Rotation of decane about bond a produces a clash between the two hydrogens shown. (**H**) A second rotation about bond b produces a more serious clash.

have a partial negative charge (notated δ-) leaving the other atom with a partial positive charge (notated δ+). This is illustrated for the O-H and O-C_β bonds of serine in Figure 1C. These partial charges vary in size depending on the exact environment producing them. They induce inter-molecular attraction and repulsion just as the whole charge on a potassium ion does, but they also lead to the phenomenon of hydrogen bonding. This is where the size of the partial charges can be reduced by a hydrogen atom 'borrowing' some of the excess negative charge from another atom. (Describing this with a potential as for charged interactions in Figure 1B is not a simple task[269] and so is omitted here.) It is perfectly possible for molecules to form more than one hydrogen bond at a time, as illustrated for water in Figure 1D.

For reasons that are beyond the scope of this thesis atoms and molecules also experience van der Waals interactions – indeed in molecules which contain no charges (either full or partial) these are the dominating interactions. Van der Waals energies can either be attractive or repulsive and are approximated by the formula

$$V = \varepsilon\left[\left(\frac{a}{r}\right)^{12} - \left(\frac{a}{r}\right)^{6}\right]$$

where V is the potential energy, r is the distance between the relevant entities and a and ε are constants whose values are determined by the system. Thus if molecules of the simple hydrocarbon decane (Figure 1E) are brought very close together the energy change will be large and positive and so unfavourable (Figure 1F). At long distances the energy change will be close to zero but at intermediate distance the energy change is negative (Figure 1F) and so the interaction is favourable – uncharged, fatty molecules will tend to associate with each other. But such organic molecules often have flexible chains of atoms and this gives rise to a particular form of van der Waals interaction. Thus Figure 1G shows decane (Figure 1E) but with the bond labelled a rotated. Different shapes of a molecule that has undergone no chemical change are named conformations or conformers. This rotation brings the two hydrogen atoms shown so close together that they experience a van der Waals repulsion. This degree of rotation is thus unfavourable. A second rotation around bond b (Figure 1H) will lead to more severe clashes. The amount of rotation is measured by the torsion angle (also referred to as the dihedral angle) about the bond in question; the torsion potential follows a cosine function (not shown).

Molecular shapes and associations are determined by ionic interactions, hydrogen bonds and van der Waals interactions

These ideas enable us to say what will happen if a quantity of uncharged, fatty decane is added to an equal quantity of water and the vessel shaken. That process would disrupt the favourable van der Waals interactions (Figure 1F) between the decane molecules and the favourable hydrogen bonds (Figure 1D) between the water molecules. As no comparable compensatory process is available the change would be unfavourable. Oil and water don't mix.

Amphiphilic molecules

But what of molecules that contain both sorts of moieties? For example phosphatidylserine (PS, Figure 2A) has a headgroup with features permitting extensive hydrogen bonding and charged interactions both with other molecules of itself as well as any surrounding water molecules. As well as this polar or hydrophilic region it also has two fatty, and so hydrophobic, tails capable of extensive favourable van der Waals interactions both within and between PS

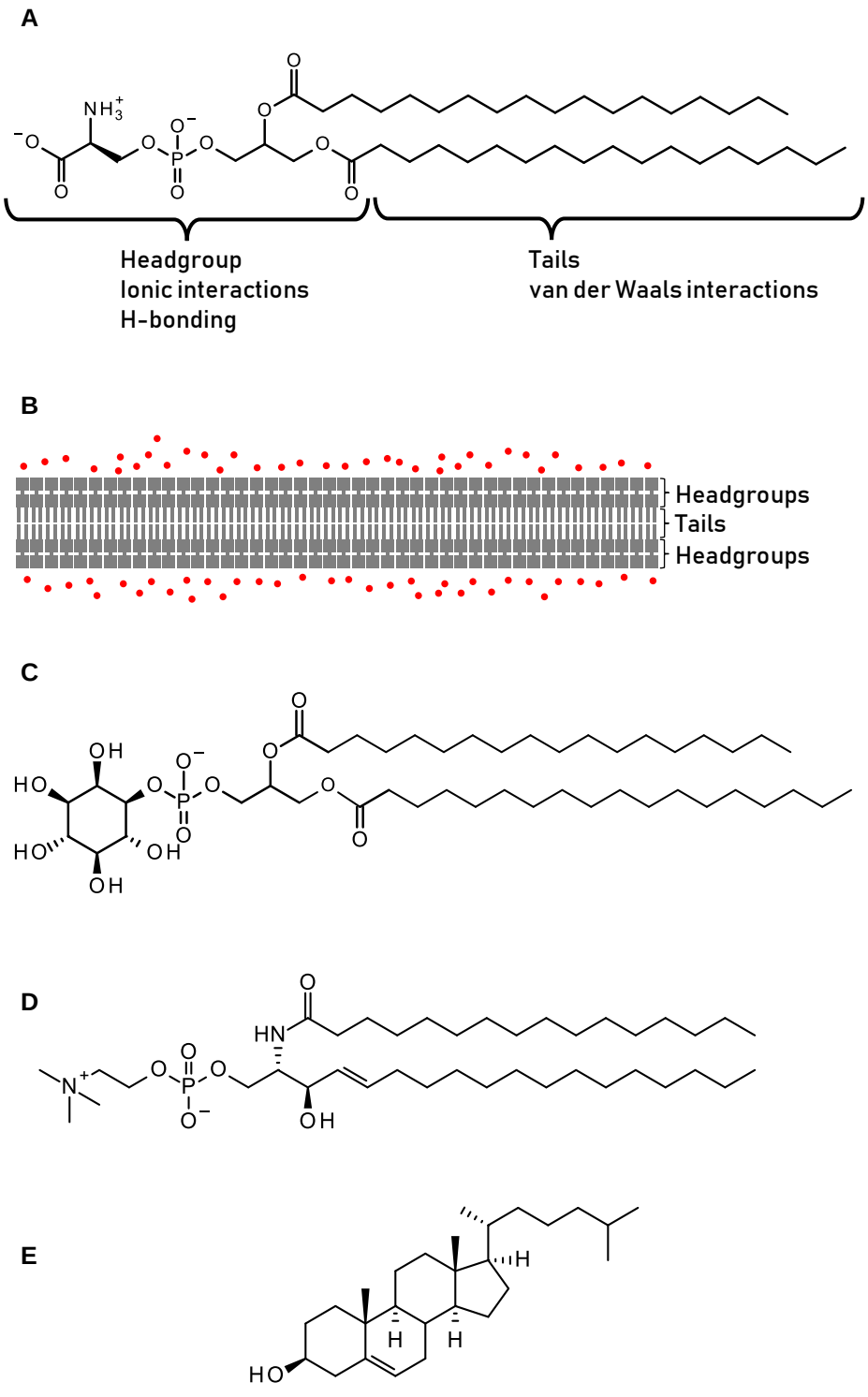

Figure 2 Structures and self-assembly properties of lipids (**A**) Phosphatidylserine (PS) has both a polar headgroup and non-polar (or lipophilic) tails (**B**) In water (represented by red dots) PS will arrange itself into bilayers where only the polar parts are in contact with the aqueous phase (**C**) Phosphatidylinositol (PI) has a structure which is both similar and different to PS (**D**) Sphingomyelin (SM), an exemplar sphingolipid has similar lipophilic tails but a headgroup with different H-bonding capacity (**E**) Cholesterol has a small headgroup and a rigid lipophilic region

molecules but whose interactions with water would not be favourable. The fatty tails have a slight preference to be straight to avoid the unfavourable interactions shown in Figure 1G,H. Placing such molecules in water, therefore, is likely to trigger a self-assembly process with the headgroups interacting with each other and the water and the tails interacting with each other but away from the water. Thus physics predicts the generation of a structure known to biology as a lipid bilayer (Figure 2B).

The lipid bilayer structure arises as a necessary consequence of physical laws

The real biological situation is more complicated because bilayers are not composed of one lipid type but of several. Thus phosphoinositide (PI, Figure 2C) differs from PS in being capped with not with serine but with a sugar which confers very different ionic and H-bonding properties. The sugar can also be phosphorylated in one or more places yielding the phosphoinositide phosphates which are important signalling lipids. The sphingolipids (eg sphingomyelin (SM), Figure 2D) have been introduced in chapter 1. The lipids shown in Figure 2 all have tails based on stearic acid. In reality tail lengths can vary and such differences can be important.[270,271] Not all lipids have such tails: cholesterol (Figure 2E) has a rigid tetracyclic core which imparts particular properties when cholesterol is mixed with other amphiphilic lipids.[272] Cholesterol also has a very small headgroup (just an OH) which gives rise to other phenomena in bilayers.[273] Thus real biological systems are considerably more complicated than the idealised cartoon of Figure 2B and such complication is only increased by the realisation that individual lipid molecules can move around in the bilayer. This raises the question of whether lipids show any preferences in their associations. For reasons that physics does not yet fully understand[274,275] cholesterol preferentially associates with certain other lipids, particularly sphingolipids such as GlcCer and SM[276] (Figure 2D). The resulting regions of membrane are termed lipid rafts (reviewed[277–280]) and have been implicated in diverse biological functions. These structures are shown in cartoon form in Figure 3. They are transient,[281] but show short-range order and are resistant to extraction with detergent, hence the alternative names of liquid-ordered phase (L_o) and detergent resistant membrane (DRM). Whilst phosphoinositides may or may not occupy lipid rafts[282,283] they are also clustered by cholesterol.[284,285] Fairly obviously such self-organisation will lead to areas of high local concentration of certain lipid species even if those species are a minor overall component of the cellular lipidome. Thus we would expect sphingolipids and PIs to accumulate in Niemann-Pick lysosomes and lipid rafts to be found there. All those expectations are fulfilled.[43,61]

Lipid-lipid associations, including rafts. Implications for Niemann-Pick disease

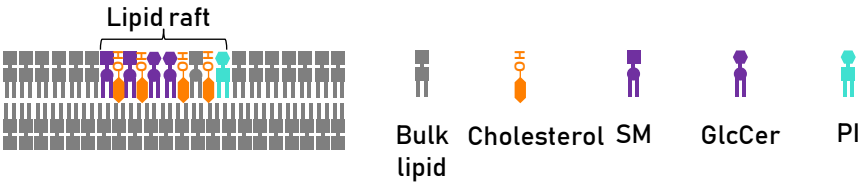

Figure 3 Lipid rafts Sphingolipids and cholesterol preferentially associate with each other to form semi-ordered domains called lipid rafts; phosphoinositides may be included

Proteins in membranes

Membranes contain not just a lipid bilayer but also proteins which interact with the lipids by one (or sometimes more) of four modes (Figure 4A-D). Peripheral membrane proteins (Figure 4A) such as AnxA2[286] typically bind by electrostatic interaction with the lipid head groups. Membrane-associated proteins have a small portion of their structure inserted into the membrane, either an α-helix (Figure 4B) or a lipid tail (Figure 4C). Examples of these are Syntaxin7[63] and rab7[287] respectively. Integral membrane proteins (figure 4D) span the bilayer completely often to allow hydrophilic substances to pass through.

How proteins associate with membranes

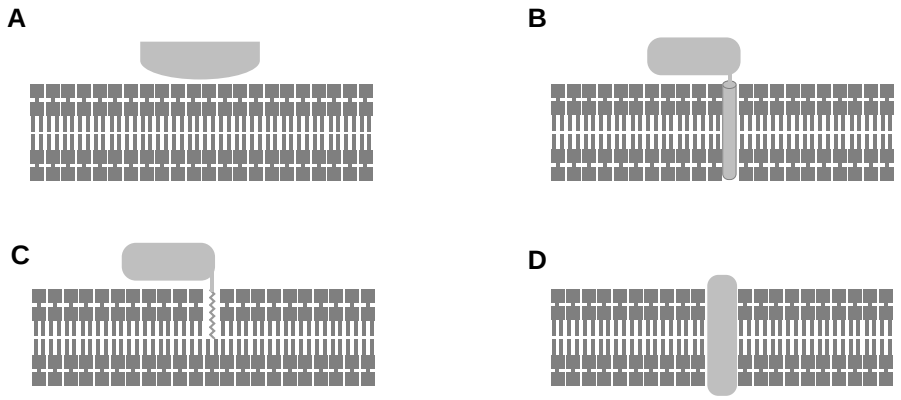

Figure 4 Four modes of protein-membrane association (**A**) Peripheral membrane proteins interact with lipids through polar residues on their surface (**B**) Membrane associated proteins possess an α-helix which is able to insert into the membrane (**C**) Other proteins become membrane associated by acquiring a lipid tail (**D**) Transmembrane proteins completely span the bilayer

As well as the trans-membrane segment they may contain very large domains on one or both sides of the membrane (eg NPC1, Figure 7). Each of these interaction modes places demands on the local lipid population, thus domains within membranes where local concentration of certain lipids is high, can influence the localisation and even function of proteins which interact with those membranes. Lipid-protein interactions form an important refinement of the classical fluid-mosaic model of membrane organisation[288] and have therefore become an important area of study[289–292] with much of the effort focussed on explaining how lipids can affect

Lipid-protein interactions are functionally important

the functions of proteins. (For further details of membrane organisation including protein inclusion see.[293])

Lipid-protein interactions

While implicating diverse cellular processes the review of NPCD in chapter 1 showed that lysosomal dysfunction is central to the pathology of this condition and identified the involvement of certain key proteins, most of them embedded in the lysosomal membrane. To that picture this chapter has added a disturbed distribution of lysosomal lipids. The question of the role of lipid-protein interactions in NPCD thus naturally arises. (The remainder of this chapter is an expanded version of[294].)

The idea of lipid-binding motifs in protein sequences. Deficiencies of algorithmic searching for them.

To examine lipid–protein interactions, it is necessary to identify the region of the protein where the lipid associates or binds. If a lipid-binding motif has been identified then a protein's sequence can be searched using computer algorithms (e.g., FuzzPro, bioinformatics.nl/cgi-bin/emboss/fuzzpro). The predictive power of this technique is variable. The most common cholesterol-binding motif, termed CRAC (Cholesterol Recognition Amino acid Consensus),[295] was first described on the protein TSPO[296] which we shall meet again in chapter 4. Using single letter amino acid code it is defined as L/V-X_{1-5}-Y-X_{1-5}-R/K (X can be any residue) and so is of variable length and strictly defined at only one position. Thus algorithmic searching for this motif typically generates numerous false positives for any given protein sequence. For example it is found over 5700 times in the proteome of a cholesterol-free bacterium.[297] The reverse motif CARC[298] also binds cholesterol but has a similarly lax definition and so identical concerns will apply. More recently, the protein p24 was found to bind to sphingomyelin via a defined region.[271] Analysing statistical over-representation enabled this finding to be generalised to a set of sphingolipid-binding motifs, e.g., $VX_2V_2X_2LF$, some of which were confirmed experimentally.[299] However, as far as can be ascertained, no interactions between sphingolipids and specific residues within these motifs were identified, nor is it clear whether the required terminal aromatic residue of the motif should be positioned closer to the edge of the membrane in which the protein is embedded or closer to the centre. Thus algorithmic searching of sequences for binding motifs offers only an approximate guide to where lipid–protein interactions may occur, and gives only limited information of three-dimensional features of such interactions. The work reported in this chapter set out instead to use molecular docking, which not only allows the exploration and rationalization of lipid binding in structural detail, but also allows ruling out some sites if binding proves impossible or implausible and so is much more reliable than merely identifying motifs.

Determining protein structure

Molecular docking can be performed only if the 3D structure of the protein is known. The determinants of molecular structure were set out above, though proteins are an exceptionally complex case – for example they are subject to particular constraints on dihedral angles[300] (Figure 2E, G-H). For this reason their structures cannot in general be predicted *ab initio* with any useful levels of accuracy and must therefore be experimentally determined. This has usually been achieved with x-ray crystallography[301] though recent advances in cryoEM have vastly increased the number of proteins whose structures are known. Protein structure can also be determined by NMR, though historically this has been limited to smaller molecules. Protein structures are deposited in the Protein Data Bank (PDB, rcsb.org) and can be freely downloaded.

The core of such pdb files is a list of all heavy atoms (atoms that are not hydrogen) together with their co-ordinates on an x,y,z grid. PDB entries are accompanied by numerous quality measures of which the most accessible is the resolution. This is quoted in ångstroms (Å) and is a measure of the average uncertainty in the position of the atoms – a useful comparison is the carbon-carbon single bond length of 1.4Å. Other ways to assess the quality of a PDB structure are discussed elsewhere.[302]

Homology modelling as a way of accessing the structure of a protein without an experimental determination

For proteins without a PDB entry a structure can sometimes be derived from the experimentally determined structure of a related protein by a technique known as homology modelling. The protein with known structure (called 'the template') is considered 'related' if about 30% or more of its amino acids are identical to those in the protein being modelled ('the target'). Modelling may still be possible if the two proteins share 25% sequence identity but below that threshold any models produced are generally unreliable.[303] The procedure next assigns the same x,y,z co-ordinates to all atoms of identical residues in the target protein as the corresponding residues in the template protein. Co-ordinates for the atoms in the remaining residues can then be inferred yielding what we might call a first-draft structure. This can then be adjusted to reduce or eliminate the kinds of unfavourable interactions discussed above and increase the favourable ones – this process is known as energy minimisation and various procedures are used. For individual proteins homology modelling has progressed to being an almost fully automated process run on webservers (eg[304,305]).

As the resulting models are not derived from experiments with measurable errors the question arises of how we measure their quality. The approach taken in this work is to use the QMEAN service.[306] Essentially this selects four mathematical

descriptors of protein structure and uses these to compare a model with a set of experimentally determined structures of proteins of a similar size. The closeness of similarity between the model and set of reference structures is taken as a measure of model quality. This approach yields not only a global score for the model as a whole but also a local score for each individual residue. Scores for the protein structures used in this work are shown in Table S2.

How to assess the quality and membrane positioning of protein structures

In this work we are mostly concerned with proteins that are integral to the lysosomal membrane or associated with it (Figure 4B-D) and so we need to know approximately where on the protein structure the boundaries of the membrane lie. The QMEAN service has been expanded (and named QMEANBrane[307]) to deal with membrane-bound proteins and the output provides an estimation of the protein's position in the membrane. For experimentally determined structures a similar service is provided by the OPM database (opm.phar.umich.edu).[308]

Docking lipids to proteins

With a structure of the protein in hand it is possible to progress to attempted docking of lipids. This was mostly done with AutoDock[309,310] software which holds the protein mostly rigid, but gives flexibility to some designated side chains. The lipid is allowed to vary its bond angles (Figure 2E, G-H) and both orientation and position within a defined search space. (Table S3 gives parameters for the docking runs used in this work.) The calculations were started with the bond angles of the ligand in an energy-minimised state; the docking software randomly selects a starting position and orientation. All these parameters are then systematically altered until an energetically favourable binding 'pose' – assessed by an energy scoring function – is discovered, if that is possible. This procedure is repeated multiple times and the results ranked to show more or less energetically favourable binding poses. These poses are grouped into clusters defined by root mean square difference (RMSD) of atomic positions with the cut-off for membership of a cluster set at > 2Å.

For some proteins the ROSIE-Rosetta ligand docking protocol[311–313] was also used (for an example of the critical comparison of somedocking programs see[314]) . Rather than specifying a search space as with AutoDock, ROSIE requires the user to provide co-ordinates for the starting position of the ligand. The small molecule is then randomly moved until its centre is in a position not occupied by the protein. (For this reason the academic group behind the software recommend ROSIE not be used for binding sites on the edge of proteins – the ligand tends to end up in empty space.) After positioning of the ligand ROSIE allows both amino acid side chains and the protein backbone to flex slightly in order to reduce unfavourable ligand-

protein interactions and increase favourable ones. The success of this process is measured by an energy scoring function which gives values both for the interface score (protein-ligand interaction) and the total score (measuring if the protein has adopted an unfavourable conformation). Thus ROSIE is much better than AutoDock at allowing for flexibility in the protein but its built-in conformer generator[315] does not generally produce molecular shapes significantly different from the starting conformer. Minor bond rotations (less drastic than those shown in Figure 2G-H) attract only a very small energy penalty meaning that some of the molecules considered in this chapter are very flexible.

Docking can investigate lipid-protein interactions computationally

However the calculations are run, they are limited by the accuracy of the scoring function and examine only a sample of all possible combinations of parameters. This second limitation can be circumvented by the use of a molecular dynamics (MD) simulation of the protein with bound lipid.

The x,y,z co-ordinates of all the atoms in such a system are known and, as discussed above, these atoms feel forces from interactions with other atoms. MD assumes the net force on any individual atom is the sum of all the different forces and then employs Newton's observation that force leads to acceleration. Thus each atom is constantly in motion. The basic premise of MD is that if we know the initial position of each atom in a lipid-protein complex and if we know the forces acting on each atom then we should be able to calculate the new position of each atom a short time later. This 'short time' is known as the time step and in this work is set to 2fs to accommodate bond vibrations which are the fastest events in protein molecules and occur approximately every 10fs. (Vibrations of bonds to hydrogen occur faster than this and are usually neglected in MD simulations.)

Molecular dynamics simulations can test the stability of binding poses from docking experiments

For the simulations to be realistic the protein should be embedded in an environment that at least approximates to its native one. The proteins simulated here are all soluble and so are placed in a 'box' which is filled with water molecules and salt molecules at a physiologically relevant concentration (Figure 5). This requires us to know something about how water behaves or, in MD terms, water should be parameterised. This is a solved problem. Various models are available – in this work the TIP3P model was used.[316] It is also a solved problem for protein structure[317] and for cholesterol;[318] for other small molecules of interest, eg sphingosine, acceptable parameterisation can be accomplished using CGenFF

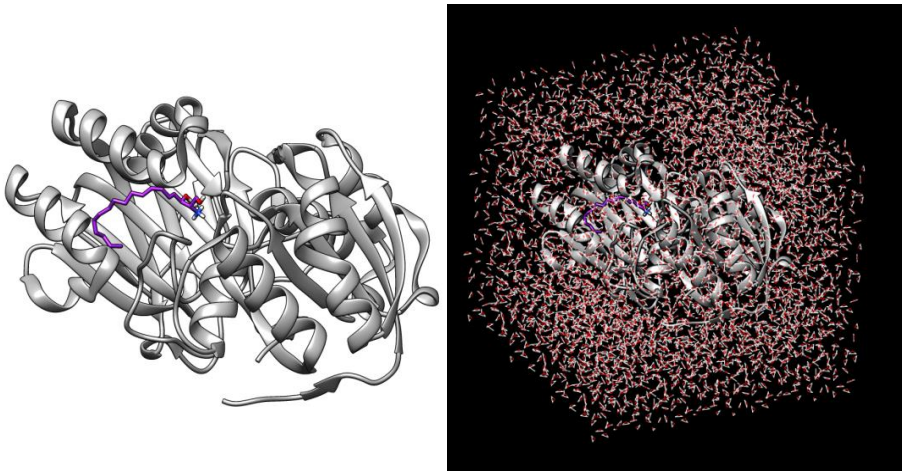

Figure 5 Illustration of a solvent box used in MD simulations (**A**) Sph (purple) bound to SphK (PDB: 3vzb[319]). (**B**) The same structure embedded in a 2Å water box.

(cgenff.paramchem.org/).[320] For proteins embedded in membranes it is not so easy. Single component lipid membranes have been well studied experimentally so their physical properties are known and they can be parameterised with relative ease. As we have seen lysosomal membranes are multi-component mixtures containing some non-standard lipids so parameterisation is non-trivial. For this reason, and the fact that we are only beginning to know the composition of the lysosomal membrane,[43,321] MD simulations of membrane-bound proteins are not conducted here.

The first phase of an MD simulation is equilibration, the aim of which is to find approximately the state of the lipid-protein complex under normal conditions. To accomplish this atoms are assigned initial velocities according to the Maxwell-Boltzmann distribution and the ensemble is slowly heated from 60 to 300K over the course of 1.2ns. The thermal energy thereby supplied to the system can be converted to other forms but the ensemble should reach a state of limited change. After this the production phase begins where the system is allowed to behave as it would in its native state. For this to be reliable correction terms are applied to the mathematics to ensure the ensemble experiences invariant temperature and pressure. This is done automatically by the software used.[322–324] The solvent box is also considered as a periodic boundary so that if a water molecule exits the box on one side then another enters from the opposite side In this work the production phase was set to 10ns; on completion the system can be analysed for changes, particularly H-bonds and RMSD of atomic positions. As the entire protein-lipid assembly is subject to random Brownian motion the RMSD analysis includes a step where this is factored out of the calculation leaving only the movements of interest. Should

the lipid remain in essentially the same orientation relative to the protein then this is good evidence that the binding pose is stable, at least on the timescale of the simulation. Stable binding poses imply control and control in turn implies design. Hence if a binding pose is stable under MD then this is good evidence that that pose really occurs.

No matter how closely computer simulations approach biological reality the results are hypotheses that need to be inspected and tested. Such testing will ultimately come from 'wet' lab experiments, but a useful first step is to ask if a binding pose is biologically plausible – a favourable energy score is no guarantee of that.

Biological plausibility of docking results

With membrane-bound and –associated proteins, such as most of those considered here, the orientation of the protein in the membrane offers a significant clue as to the biological plausibility of binding poses.

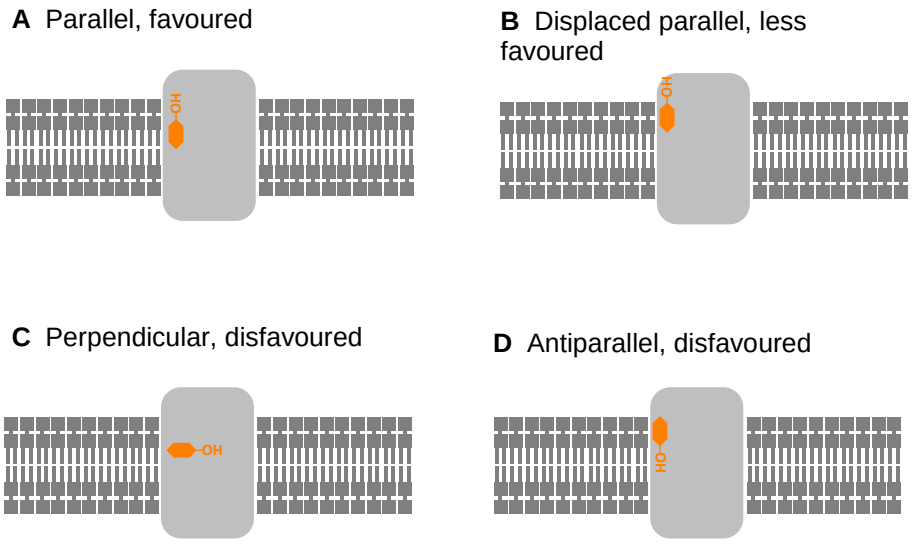

Figure 6 Four idealised possibilities for cholesterol binding to a trans-membrane protein Trans-membrane proteins (light grey) are embedded in the lipid bilayer (dark grey). (**A**) Cholesterol (orange) may bind parallel to the membrane (energetically favoured) (**B**) parallel to the membrane but vertically displaced from it (energetically less favoured) (**C**) perpendicular to the membrane (energetically disfavoured) or (**D**) antiparallel (energetically disfavoured).

Thus a lipid, illustrated by cholesterol (orange) in Figure 6, may bind to a trans-membrane protein (light grey) in various orientations which can be idealised as shown. Cholesterol can be parallel to the lipophilic section of the membrane and with the hydroxy group aligned with other lipid head groups (Figure 6A). This is the most energetically favourable situation. However the lipid may also be parallel to the membrane but vertically displaced from it (Figure 6B). Whilst possible, this

Considering the protein's position in the membrane can help decide if a docking result is plausible or not.

requires a deformation in the membrane and the consequential loss of some favourable van der Waals contacts between lipids (Figure 1F). Therefore this attracts an energy penalty and such a pose would be energetically less favoured. Burying the hydroxy group inside the lipophilic portion of the membrane by orienting it perpendicular (Figure 6C) or antiparallel (Figure 6D) is still possible,[325] but energetically disfavoured. In this work binding poses similar to those in Figure 6B-D were considered only when calculations did not generate poses corresponding to the more favourable situation shown in Figure 6A.

Calculations were made more computationally tractable by neglecting the membrane and thus we assess only lipid-protein interactions. Lipid-protein interactions considered in isolation may be energetically favourable with the lipid in perpendicular or antiparallel situations. As the lipid starting position and orientation are randomised, some of the iterations of the docking calculations will start with the lipid in a position perpendicular or antiparallel to the lipophilic section of the membrane. Thus some docking runs will start with the lipid in an orientation that is energetically favourable when considered in isolation but energetically disfavourable when considered in the context of the membrane as a whole. Such an orientation is biologically implausible. Energetic refinement of this orientation will not necessarily result in the lipid adopting a parallel orientation. Therefore some docking runs may result in binding poses that appear energetically favourable because they only consider lipid-protein interactions but would be energetically disfavourable overall and thus biologically implausible. This is a consequence of the randomisation of the initial position of the lipid, not a flaw in the docking experiments. If the docking algorithm is run a sufficient number of times then an energetically favourable, biological plausible binding mode should emerge, if one exists

Whilst this discussion applies mostly to cholesterol, similar considerations pertain to other lipids. Aliphatic lipid tails generally make non-specific interactions with trans-membrane proteins so docking calculations are routinely performed here with only the lipid head group to focus attention on the distinctive part of the molecule. These head groups include the first carbon atoms of the aliphatic chains and it is quite possible that the randomised initial positioning for the docking calculation will orient these atoms, and thus either or both alkyl chains, away from the membrane and into the cytosol. As discussed above this is highly energetically unfavourable. It is equally possible that the energy minimisation, because done in isolation from the membrane and solvent, will retain such an orientation if adopted by the initial random positioning. Thus once again docking calculations may output binding

poses that are energetically favourable in isolation but disfavourable overall and so biologically implausible. This does not indicate a flawed method.

For these reasons it is necessary that the output of such docking first be inspected for biological plausibility. The figures show representative binding poses that result from the docking runs – these are both energetically favourable and biologically plausible. (Table S4 presents extended data including number of clusters, cluster size, assessment of favourability and interacting residues.) Once filtered for energetic favourability and biological plausibility, the results of docking experiments should next be tested by 'wet' experiments. Whilst no new lab data is presented in this chapter, the results are fully consistent with existing findings from other labs.

Biological plausibility can also be assessed, for all proteins, using a surface conservation analysis, conducted here using the ConSurf server (http://consurf.tau.ac.il/).[326,327] The assumption here is an evolutionary one: that if a residue is conserved across numerous different organisms then it must be important to the function of the protein. ConSurf gives high scores to highly conserved residues, the presence of highly scored residues at putative lipid binding sites is taken as evidence that these sites are functionally important, which in turn suggests lipid binding may genuinely occur as calculated.

Results and discussion

What does the NPC system do?

All mammalian cells require cholesterol. LDL-derived cholesterol is delivered to the cell in the form of cholesteryl esters; transporting cholesterol imposes certain structural requirements on proteins (reviewed[328,329]). These esters are carried by the endocytic pathway to the lysosomes where they are hydrolysed by lysosomal acid lipase (LAL) at intraluminal membranes (Chapter 1, Figure 1, ❻). Unesterified cholesterol (sometimes termed ‘free cholesterol’) must then be exported to be used by the cell which is accomplished by the co-operative action of NPC2 and NPC1, as reviewed briefly in Chapter 1

NPC1 is a 13-TMH protein also containing 3 luminal loops (Figure 7A-C); loop 1 is usually referred to as the N-terminal domain (NTD), loop 2 as the middle luminal domain (MLD) and loop 3 as the C-terminal domain (CTD). The TM region was recognised as posessing a sterol sensing domain (SSD, Figure 7A,C) as well as other helices whose function is unknown. At the start of this work cholesterol binding had been experimentally verified only at the NTD (Figure 7B).[330] Binding at a second

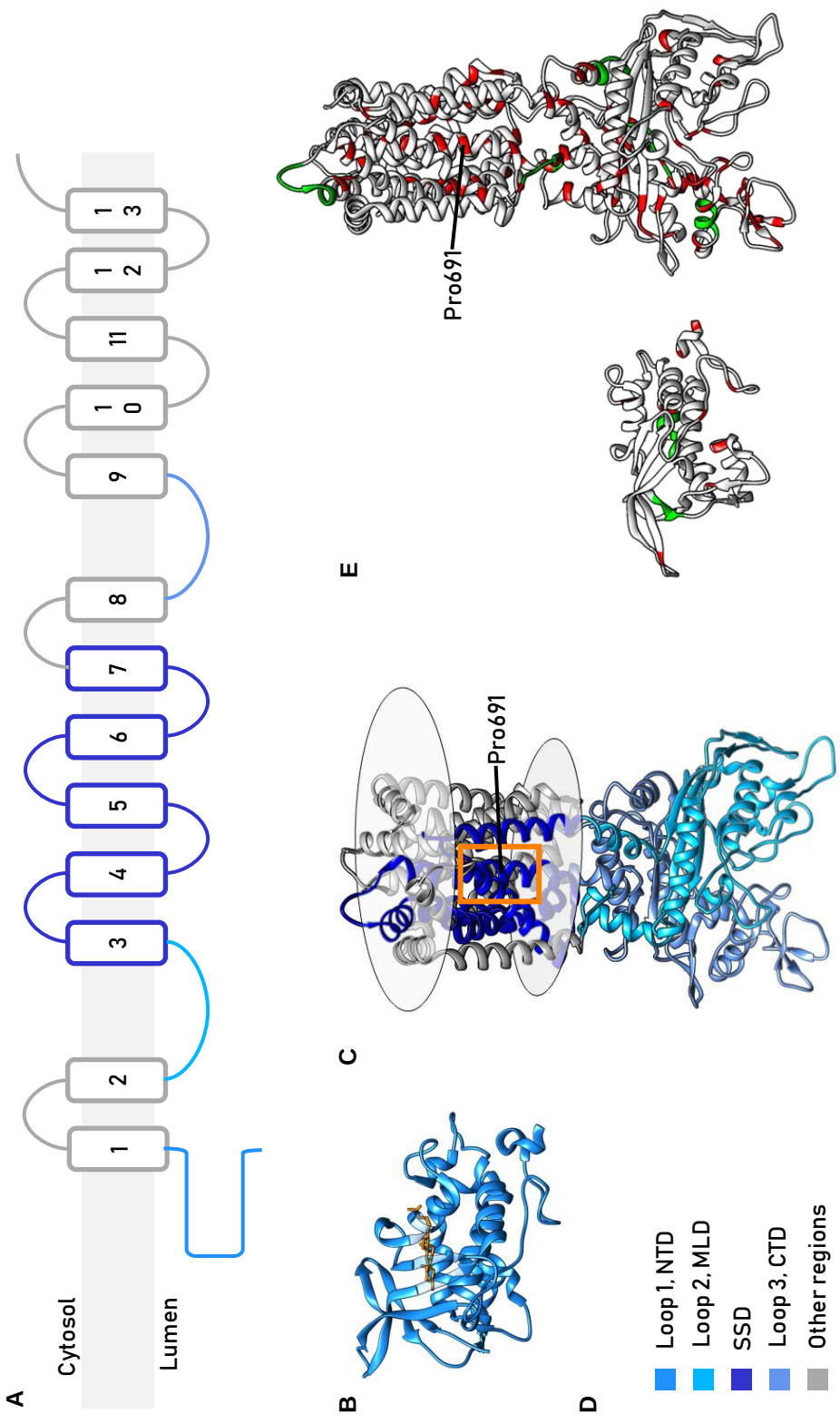

Figure 7 Structure and regions on NPC1 (**A**) Cartoon of NPC1. (**B**) Crystal structure of the NTD (PDB : 3gki). (**C**) Crystal structure of residues 334-1255 (PDB: 5u74) showing putative cholesterol binding site in the SSD (orange box). (**D**) Colours used in panels (**A**)-(**C**). (**E**) Structures of NTD (left) and 334-1255 (right) showing disease-associated mutations (red) and binding regions identified in (green).

site in the SSD (orange box in Figure 7C) had been suggested by ligand docking[331] and was also implied, not least because mutation of Pro691 reduced labelling by a fluorescent cholesterol analogue;[11] mutation of Pro691 is also disease-causing (Figure 7E).[10] The path from the NTD to the SSD was unknown but disease-associated mutations occur all through NPC1 (red residues in Figure 7E) suggesting that the whole protein may be involved. This idea is also supported by a proteomic study[332] with a tritiated cholesterol anaolgue which identified diverse binding sites in NPC1 (green in Figure 7E), though it should be noted that that study found no binding sites in the SSD and did not identify NPC2 as binding cholesterol at all. How cholesterol export is completed from the putative SSD binding site is not known.

The understanding of the export of unesterified cholesterol at the start of this work is shown in Figure 8. Cholesterol is first collected from the intraluminal membranes by NPC2 (Figure 8A, ❶). This carrier protein then binds to loop 2 of NPC1[333,334] in the correct position for the next step which is transfer of cholesterol to the NTD of NPC1[335] (Figure 8A, ❷). This transfer has not been observed in live cells but has been studied in model systems[336] and computationally.[337] At some point NPC2 presumably dissociates and the NTD, with the assistance of loop 3, then relays the cholesterol to the NPC1 sterol sensing domain (Figure 8A, ❸).[18,330,338,339] The geometry of these steps is likely to be important. It has been shown crystallographically that NPC2 binds cholesterol with the polar hydroxy group oriented toward the cytosol[15,334] (Figure 8C); transfer of cholesterol to NPC1's NTD therefore positions the hydroxy group inwards (Figure 8B) as confirmed by another x-ray study.[330] The orientation of the cholesterol molecule after its transfer to the SSD has not been unambiguously determined but an alignment parallel to the luminal side of the lysosomal limiting membrane would be expected (Figure 8A, ❸).

Despite the numerous studies that have contributed to our developed understanding of the NPC system, this account is not without its difficulties. NPC2 can transfercholesterol to model membranes lacking a glycocalyx with equal speed in the presence or absence of NPC1[18,340,341] so it would appear that the reason for this rather complicated relay mechanism of cholesterol export is to allow the lipid to pass through this thick, highly polar carbohydrate layer[342] which protects the luminal face of the lysosomal limiting membrane. Consistent with this idea is the finding that inhibiting O-glycosylation in NPC1-deficient cells leads to decreased lysosomal cholesterol.[268] Why, then, the need for the SSD? Given that cholesterol translocates (or 'flips') rapidly[343] from one face of the membrane to the other, isn't it sufficient

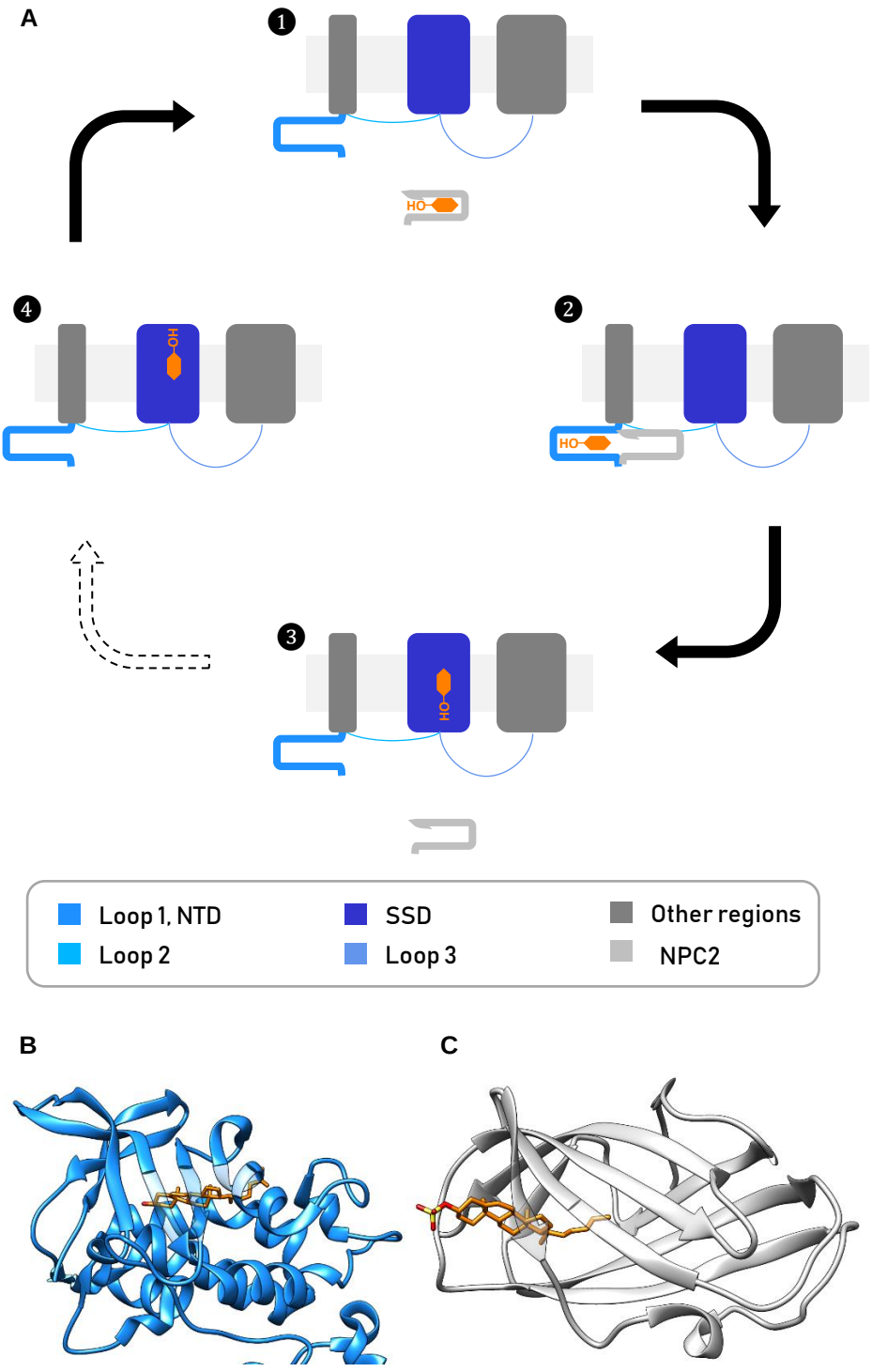

Figure 8 Cartoon of cholesterol export by the NPC system
(**A**) ❶ NPC2 collects cholesterol from intraluminal membranes and transports it to NPC1 in the limiting membrane. After binding at loop 2 cholesterol is transferred to the NTD of NPC1 ❷ and then to the SSD ❸. This work postulates that cholesterol can flip to a cytosolic facing binding site ❹. Export of cholesterol returns the system to its resting state ❶. (**B**) X-ray structure of cholesterol bound to NPC1 NTD (PDB: 3gki[330]). (**C**) X-ray structure of cholesterol-O-sulfate bound to NPC2 (PDB: 5kwy[334]).

just to get cholesterol to the membrane? If so, what is the purpose of NPC1's 13 transmembrane helices? Would not 1 or 2 TMHs suffice to anchor the N-terminal domain next to the membrane? And even if an SSD is necessary, what is the purpose of the remaining 8 helices (Figure 7)? The work described here attempts to begin an answer to these questions.

Ligand docking had previously identified a cholesterol binding site on the luminal side of the SSD of NPC1.[331] This experiment was repeated setting the search space as the entire SSD of NPC1 (Table S3) using a more recently published x-ray structure (PDB 5u74, see Table S1).[338] Lipid binding poses were found in not one but two energetically favourable clusters aligned to both the luminal and cytosolic faces of the membrane. Representative examples are shown in Figure 9A; extended results are given in Table S4. In both cases binding is anchored by an H-bond between the cholesterol hydroxy group and the side chain of an Asp residue whilst the remainder of the sterol is encased in a cavity formed from lipophilic side chains (Figure 9A, Table S4). These side chains make van der Waals contact with the cholesterol molecule. Crucially, Pro691 is among the residues predicted to interact with cholesterol (pink in Figure 9). Mutation of this residue has been shown to reduce cholesterol export[10] and to reduce labelling of NPC1 by a photoactivatable cholesterol analogue[11] implying that Pro691 plays an important role in cholesterol binding. The emergence of this residue from docking calculations forms an important agreement between *in vitro* and *in silico* approaches. The suggestion of two binding pockets means that NPC1 can potentially be added to the list of proteins featuring cholesterol binding in both leaflets of a lipid bilayer,[125,344] a phenomenon termed the 'mirror code.'[345] It also means that the cholesterol export narrative can possibly be extended to include stage ❹ (Figure 8) where the cholesterol is aligned with the cytosolic face of the lysosomal limiting membrane. This offers, for the first time, an idea of how cholesterol export can be completed. Both putative binding sites were supported by a surface conservation analysis (Figure 9B) showing that residues in these site are highly conserved, especially for the luminal site; similar considerations apply to the locations of disease-associated mutations which can be found in both binding sites (Figure 7E).

Discovery of a putative second cholesterol binding site in NPC1 may expand our understanding.

Shortly after this work was completed and published[294] a combined docking-MD study on cholesterol binding to NPC1 emerged.[346] While that study also found cholesterol binding aligned to both faces of the membrane the binding positions of the lipid in the protein are at variance with those suggested here. The root cause of the difference is likely to be the protein structure used in the other study (PDB: 3jd8[335]) which is more complete but significantly less accurate than the one used in

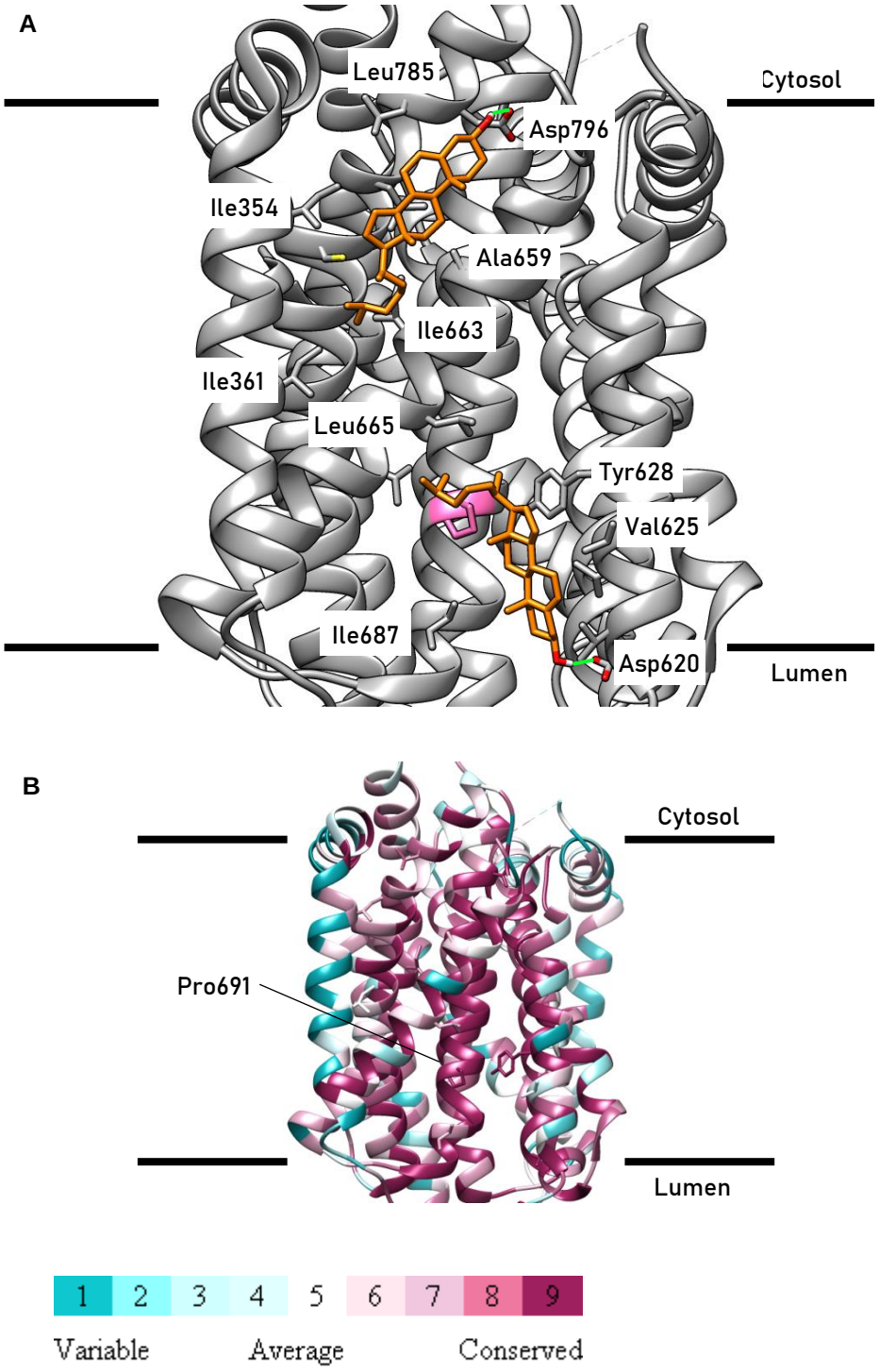

Figure 9 Docking identifies two potential binding pockets on NPC1 aligned to each side of the lysosomal membrane (A) Sample poses for both cholesterol (orange) show binding in these pockets consistent with evidence of NPC1's role as a cholesterol exporter. Selected interacting residues are labelled, H-bonds are shown in green. Pro691 is shown in pink; mutation of this residue results in reduced cholesterol binding.[10,11] (**B**) ConSurf analysis shows residues in the luminal pocket are highly conserved; residues in the putative cytosolic pocket slighly less so.

this work (resolution 4.4Å versus 3.3Å; for a full list of available NPC structures see Table S1). In particular the two structures locate key residue Pro691 differently (Figure S1). The other modelling study[346] did implicate this residue in binding cholesterol but, unlike the work reported here, the lipid contacted the proline only by forming an H-bond to the backbone carbonyl, an interaction that might be expected to persist on mutation and so explaining the loss of function induced by mutating that residue[10,11] is perhaps harder. Additionally the other study conducts docking experiments on the whole protein. Whilst this conveys the advantage of being completely unbiased, the necessary compromise is that the electrostatic grids are calculated at a lower resolution than those used here which unavoidably imparts computational errors of potentially greater magnigtude. This disadvantage is possibly mitigated by the MD simulations performed in the other study.

Cholesterol export may not be the only function of the NPC system. Indeed export of sphingosine (Sph) from NPC1-deficienct cells was found to be impaired using a photo-activatable analogue that localises to lysosomes and whose export can then be followed by pulse-chase experiments.[347] This implies either that storage of Sph is induced by storage of cholesterol or that sphingosine uses the NPC export machinery. The second explanation is favoured by experiments using pharmocological inhibition of NPC1 which induced lysosomal accumulation of sphingosine at an earlier time point than accumulation of cholesterol.[54] NPC1 has also been identified as a sphingosine-binding protein in a proteomic screen.[c]

Docking suggests that sphingosine can bind to NPC1 in the same manner as cholesterol

To investigate this further the docking experiments described above were repeated with Sph in place of cholesterol. Consistent with the studies just cited plausible binding poses were found for sphingosine aligned to both sides of the LEL membrane (Figure 10). Reminiscent of cholesterol the polar head group of Sph forms H-bonds or ionic interactions with the side chains of Asp residues while the lipophilic tail makes van der Waals contact with the same set of lipophilic side chains as cholesterol (Figure 10, Table S4). Thus it seems plausible that sphingosine can use the cholesterol export machinery as suggested by previous experiments.[347] Indeed the presence of anionic Asp residues on both sides of the membrane may suggest that this protein is better suited to exporting cationic Sph than neutral cholesterol. (The pKa of sphingosine has been reported as 6.6 in solution[348] and 9.1 in a model membrane.[349] Thus Sph will likely be protonated both in the acidic endolysosomal lumen and when incorporated in the cytosolic face of the membrane

[c] Dr Per Haberkant (EMBL), personal communication

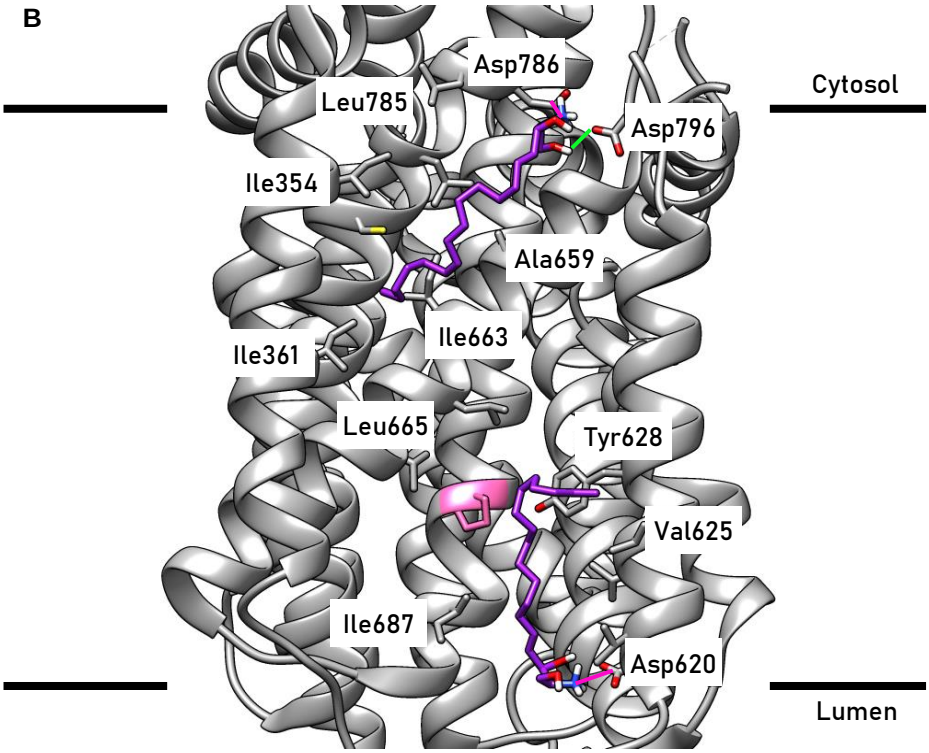

Figure 10 Putative binding of sphingosine to the SSD of NPC1. Docking experiments suggest that sphingosine can bind to the SSD of NPC1 in the same two sites as cholesterol.

so these and subsequent docking experiments were performed with protonated sphingosine.)

This raises the expectation, given also that Sph is generated in the lysosome at the same intraluminal membranes as cholesterol (Chapter 1, Figure 4, ❿), that both NPC2 and the NTD of NPC1 would be able to bind sphingosine. Investigations of this began with the published x-ray structure[330] of cholesterol bound to the NTD (PDB: 3gki, Figure 11A). Cholesterol was removed from the structure and redocking of the lipid to the *apo* protein attempted using AutoDock. This successfully replicated the binding pose in the crystal (Figure 11B) with the hydroxy group of cholesterol pointed inwards (the 'in' orientation, Table S4) and forming H-bonds with Asn41 and Gln79. H-bonds like these between a bound ligand and 'buried' residues confer particular strength to the ligand-protein bond.[346] Repeating the docking procedure with sphingosine yielded analogous results (Figure 11C, Table S4). Sph was found predominantly in the 'in' orientation with the positively charged lipid headgroup making additional making ionic interactions with Glu30; lipophilic side-chains making van der Waals contact with Sph were the same as those doing so with cholesterol (Table S4).

Similar results with the NTD of NPC1 and with NPC2

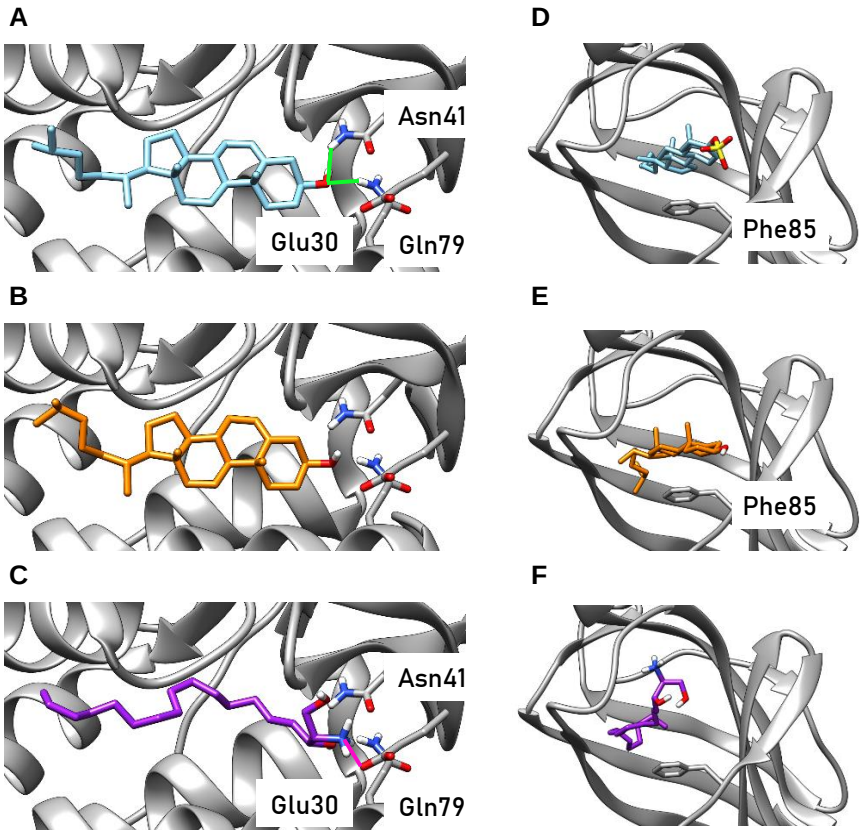

Figure 11 Comparison of cholesterol and sphingosine docking with crystallographic conformations (**A**) Cholesterol in the NTD of NPC1 (PDB: 3gki[330]) forms H-bonds (green) to Asn41 and Gln79 (**B**) Docking of cholesterol reproduces the binding found in the crystal (**C**) Docking of sphingosine preferentially orients the molecule the same way as cholesterol; as well as H-bonds to Glu30 and Gln79, an ionic interaction (magenta) with Glu30 is present (**D**) Cholesterol-O-sulfate in NPC2 (PDB: 5kwy[334]) forms a CH-π interaction with Phe85 (**E**) Docking of cholesterol reproduces the binding found in the crystal (**F**) Docking of sphingosine preferentially orients the molecule the same way as cholesterol.

An exactly similar procedure with was followed with NPC2. PDB entry 5kwy was selected as, although it also includes the MLD of NPC1, it is the only structure of human NPC2 with a bound sterol, cholesterol-*O*-sulfate (Table S1, Figure 11D).[15] This has the polar end of the lipid facing outwards (the 'out' orientation), has no hydrogen bonds between lipid and protein but doesfeature a CH-π interaction between the sterol's smooth α face and the aromatic ring of Phe85,This particular form of van der Waals interaction as well as the lipid's orientation were replicated in docking experiments between the free protein and cholesterol (Figure 11E). Docking of sphingosine yielded binding poses much less energetically favourable than cholesterol, but the vast majority had the ligand adopting the biologically correct 'out' orientation (Figure 11F, Table S4) and interacting with the same lipophilic residues lining the pocket as had been found for cholesterol.

Given that binding of Sph to NPC proteins has not yet been experimentally demonstrated it was decided to employ MD simulations to investigate putative binding further – similar previous work on NPC2[350] has examined only cholesterol and structural analogues thereof. These simulations were set up as described briefly above using the QwikMD plug-in[323] to the VMD interface[351] of NAMD software.[322] By default QwikMD sets the solvent box as the width of the protein in each dimension plus an extra 15Å. Whilst rather large this size is a useful feature as it provides enough space for a lipid to escape into if that is more energetically favourable than remaining bound to the protein. Simulations were performed for the binding poses of cholesterol and Sph shown in Figure 11B, C, E and F. As an additional control a simulation of the same length was performed on Sph bound to sphingosine kinase (SphK, PDB: 3vzb[319]) – see video SphK_3vzb_SphH.

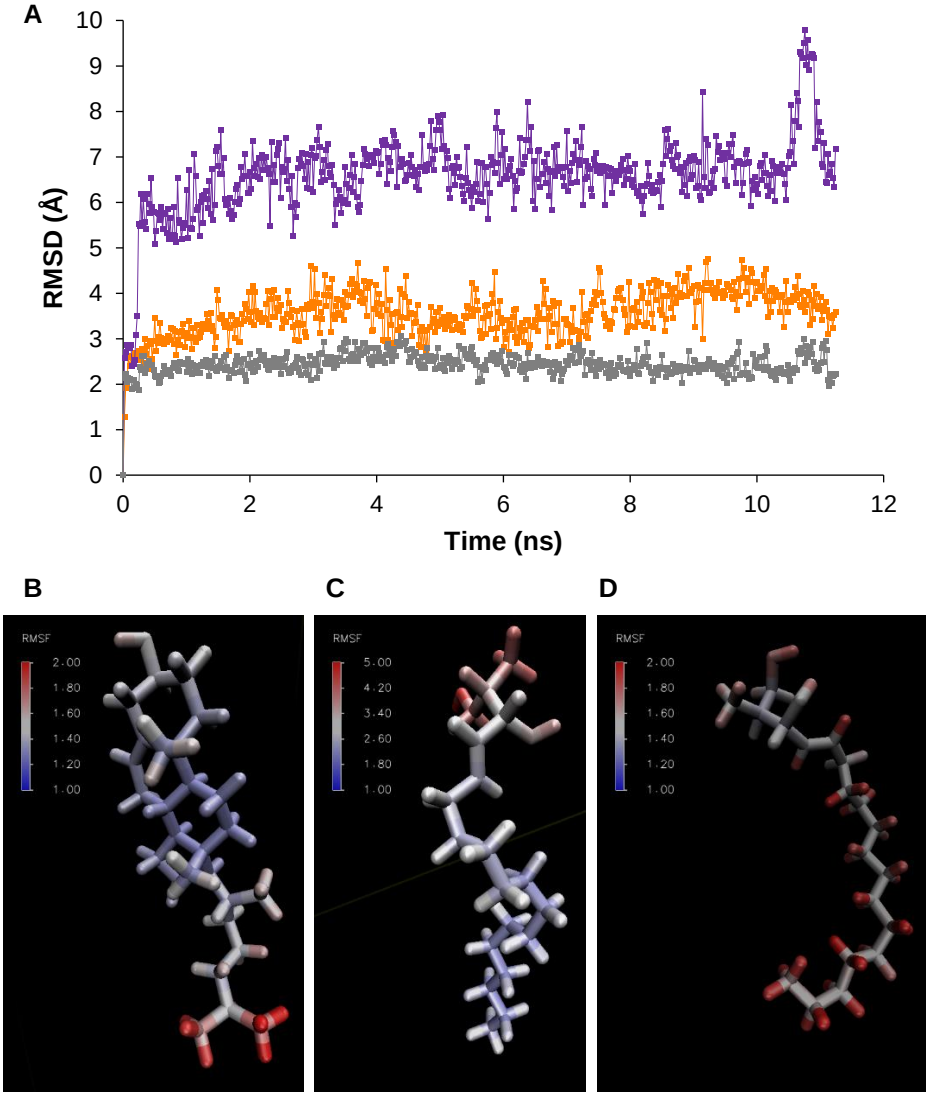

Figure 12 Output of MD simulations (**A**) Ligand RMSDs for Sph in NPC2 (purple), cholesterol in NPC2 (orange) and Sph in SphK (grey). (**B**) RMSF of cholesterol in NPC2. (**C**) RMSF of Sph in NPC2. (**D**) RMSF of Sph in SphK.

In NPC2 cholesterol moves slightly from its starting position (Video NPC2_5kwy_chol) and thereafter is relataively stable as shown by its low ligand RMSD values (Figure 12A). Movement can also be quantitated by a root mean square fluctuation (RMSF) analysis which asks how much each atom moves on average over each time-step. Thus Figure 12B shows cholesterol's movement is limited, larger fluctuations being found only in the atoms at the end of the flexible tail. Sphingosine in NPC2 behaves rather differently. The head group moves away from the protein almost immediately (Video NPC2_5kwy_SphH) to form H-bonds with solvent (data not shown) – the starting binding pose does not H-bond with the protein. Thereafter the highly polar headgroup acts almost as a free molecule within the solvent and moves around considerably while the carbon atoms at the other end of the chain move no more than the corresponding atoms in cholesterol (see RMSF analysis in Figure 12C, note the scale difference to Figure 12B). The high RMSD values for Sph in NPC2 (Figure 12A) mostly reflect the extreme mobility of the headgroup. RMSD of NPC2 α-carbon atoms were comparable regardless of bound ligand and approximately the same as those for SphK with sphingosine bound (Figure S2). Under MD simulation, therefore, the cholesterol-NPC2 complex behaves similarly to the sphingosine-SphK complex while sphingosine in NPC2 is rather less tightly bound. Crucially sphingosine remained stably within the NPC2 cavity.

When considering the lipids in the N-terminal domain (NTD) of NPC1 a slightly different picture emerges. Figure 11A,B showed that docking replicated the experimentally found binding pose of cholesterol in the NTD with the lipid forming H-bonds with Asn41 and Gln79 at the back of the cavity. This arrangement remained stable under MD simulation. Asn41 formed an H-bond with cholesterol for 71% of the production phase while Gln79 did so for 79% of this time period. (Figure 13A). This is reflected in the small RMSD for cholesterol in this protein (Figure 13B). See video NPC1_3gki_chol. The simulation of Sph in the NTD of NPC1 began with the binding pose shown in Figure 11C. The lipid headgroup is located at the back of the pocket where it makes an ionic interaction with Glu30 and an H-bond with Asn41; these interactions persist for the duration of the simulation (residues coloured grey in Video NPC1_3gki_SphH). After about 0.3ns of equilibration the Sph forms an additional hydrogen bond with Asn86 (dull bronze in video) located midway along the pocket. This persists until 1.4ns of the production phase, at which point the lipid undergoes a sudden movement and establishes an H-bond with Gln79 (video). This arrangement remains stable till the end of the simulation and thus replicates the binding arrangement of cholesterol but

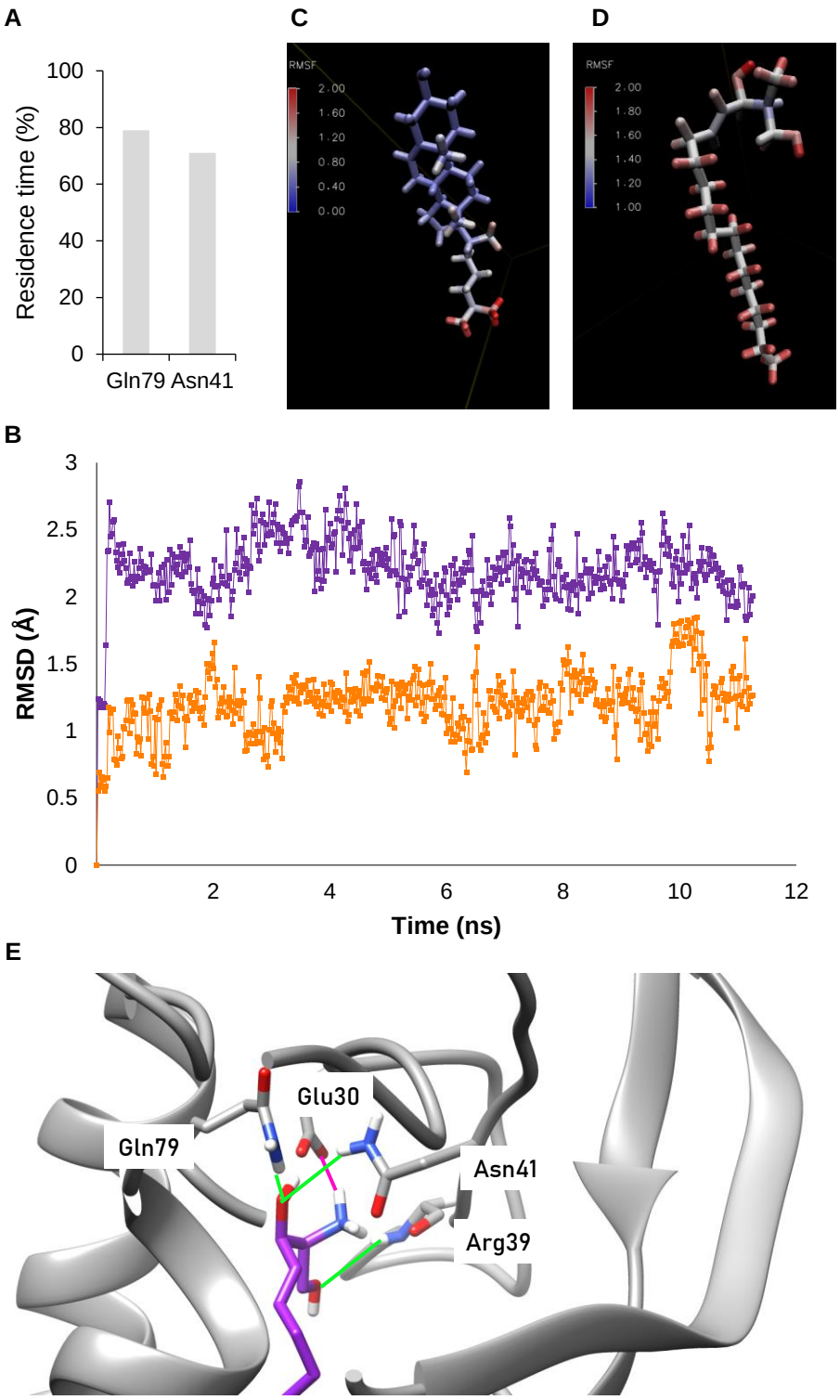

Figure 13 MD simulations of lipids bound in NPC1 NTD (**A**) Residence times of cholesterol at key binding residues. (**B**) RMSDs of sphingosine (purple) and cholesterol (orange) bound in NPC1 NTD. (**C**,**D**) RMSF of sphingosine and cholesterol during MD simulation. (**E**) Final binding pose of sphingosine; H-bonds shown in green, ionic interaction in magenta.

with the addition of the ionic interaction with Glu30. An H-bond with the backbone of Arg39 also forms. Video NPC1_3gki_SphH shows all these changes; Figure 13E shows the final binding arrangement. Thus MD refines the binding pose suggested by docking - the final arrangement of the lipid having a greater number of bonded interactions with the protein. The RMSD for Sph in this protein is slightly larger than that for cholesterol but comparable with that for Sph in SphK (Figure 13B, compare Figure 12A). RMSF analyses for both lipids are comparable (Figure 13C,D) as was RMSD of protein α-carbon atoms (Figure S3).

MD simulations of sphingosine in NPC proteins support the docking experiments

Docking calculations suggest that Sph can bind to both NPC2 and the N-terminal domain of NPC1 in same orientation as cholesterol in the vast majority of cases (Table S4); this geometry is biologically significant (Figure 8). MD simulations suggest that Sph is not tightly held in NPC2 but that the binding pose is stable; however this technique yields a very stable binding of Sph to the NPC1 NTD. We may question whether or not NPC2 was designed to bind sphingosine (although it is able to do so) but the calculated binding of Sph to the NPC1 NTD features bonded interactions with three residues, including a charged interaction, and so is unlikely to be an experimental artefact.

Hence the idea, suggested but not proved by various experiments,[54,114,347] that the NPC system can act to export sphingosine as well as cholesterol is endorsed by this computational work. This idea would explain the accumulation of sphingosine in NPCD,[61] although favourable interactions with cholesterol may also be a factor.[352,353] Sphingosine's protonated, highly polar headgroup would make energetically unfavourable contacts with membrane lipids meaning that it likely requires a flippase for export from the lysosome. This work tentatively identifies that flippase as NPC1. The flipping pathway will nonetheless require the Sph headgroup to be shielded from the lipophilic section of the membrane, a requirement that is probably not met by the binding sites identified here (Figure 10) as these are open to surrounding membrane. NPC1 helix 1 (Figure 7) could probably not serve this purpose as a low-resolution cryoEM structure (PDB: 3jd8)[335] places it on the opposite side of the protein. Shielding could, however, plausibly be accomplished by one of the proteins with transmembrane domains noted to interact with NPC1.[354,355] The question was raised above of why NPC1 has 13 trans-membrane helices when far fewer than that would probably suffice to facilitate cholesterol export. This question receives a tentative and partial answer from this work: some of the helices are needed to export Sph which, unlike cholesterol probably does not flip rapidly and so requires binding sites on both faces of a membrane. Thus dysfunctional NPC1 would precipitate a

failure of sphingosine export; the functional consequences of this failure will be considered again in chapter 3.

NPC1 protein-protein interactions

Earlier in this chapter various questions were raised about NPC1 function and in particular why cholesterol, which flips rapidly,[343] requires an export protein at all, let alone one with a cytosol-facing binding site. The presupposition underlying this interrogation of NPC1 is that cholesterol needs merely to reach the cytosolic face of the LEL membrane to become available to the rest of the cell, initially the ER at LEL-ER membrane contact sites. This in turn requires either that cholesterol diffuse freely away from the LEL membrane, or be collected by another protein which will convey it to another organelle. Whilst free diffusion happens surprisingly rapidly ($t_{½}$ ~ 30 minutes)[356] this mechanism would lack control and so the idea of a relay protein is more attractive. The picture of cholesterol trafficking within the cell is still emerging[102–105] and it appears that multiple pathways operate. In an attempt to integrate the cytosol-facing binding site of NPC1 with this developing account, its interactions with a StAR protein were investigated to ask if cholesterol might be transferred from NPC1 to a member of this family.

Where might cholesterol go after it leaves NPC1?

The StAR protein family contain a cytosolic START domain which binds lipids and transfers them between membranes at contact sites.[357,358] Connected to the common START domain by a flexible linker are varying domains which localise the proteins to the correct organelles; for example StARD3 (also known as MLN64) contains a MENTAL domain which targets it to endolysosomes. The common START domain is comprised of an α/β-helix grip structure (Figure 14A). We will meet these proteins more fully in chapter 4 but for now we note that it is believed that the Ω1 loop (Ala335-Arg345, Figure 14A) flexes to allow cholesterol to enter or leave the binding domain, and that cholesterol's polar OH group is oriented toward the back of the pocket (the part of the domain coloured orange in Figure 14A).[359,360]

To investigate the putative transfer of cholesterol directly from NPC1 to a StAR protein the best available structure of a member of this family (StARD3, PDB 5i9j[360]) was used. To simulate Ω1 opening this loop was removed from the structure and the resulting truncated protein assigned a 'best guess' position close to the cytosolic part of NPC1 (PDB 5u74).[338] The resulting complex was then submitted to ROSIE which is able to simulate protein-protein interactions[361] by essentially the same procedure as outlined above for lipid-protein interactions. A relatively large perturbation from the initial guessed position resulted in an orientation of the two

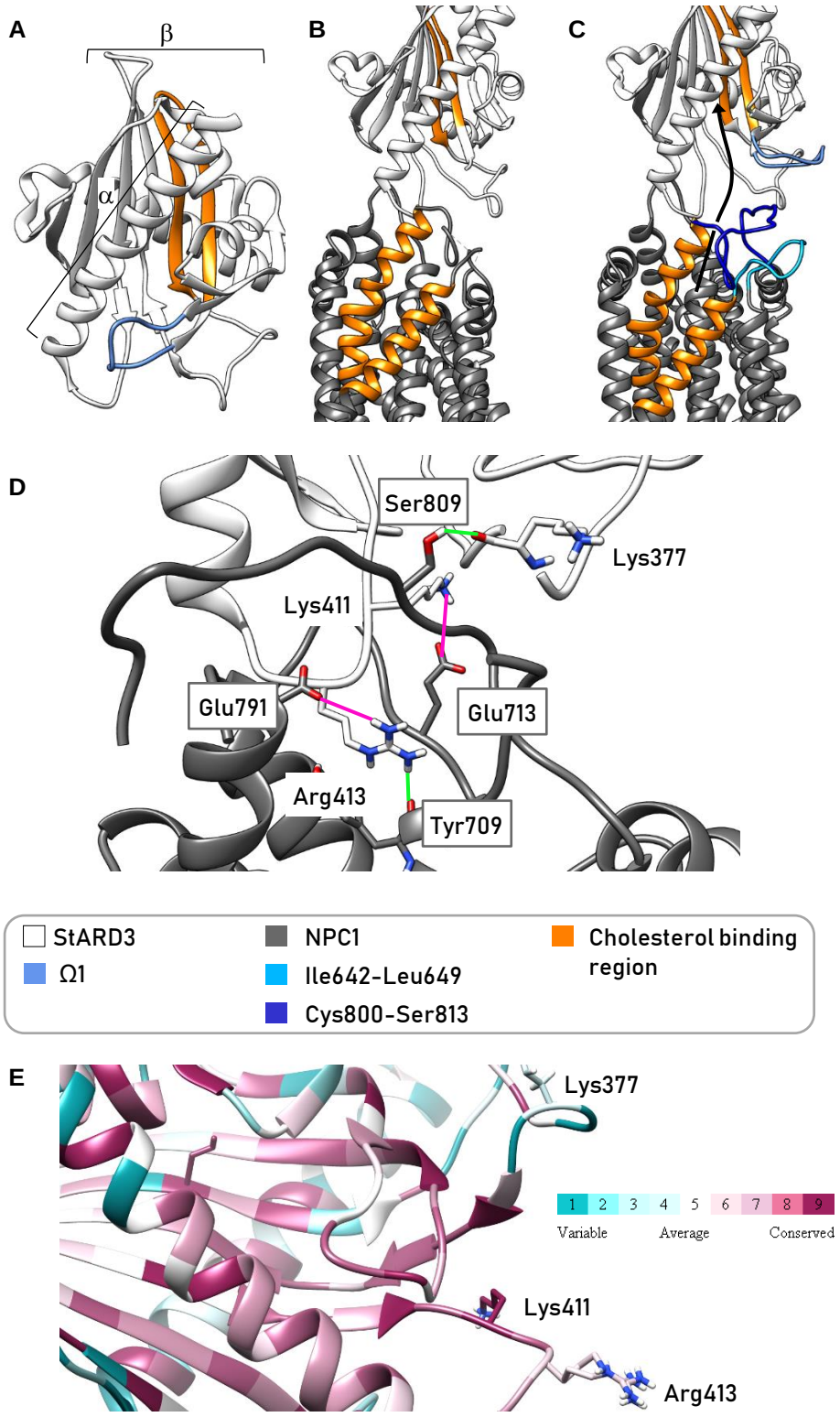

Figure 14 Putative cholesterol transfer between NPC1 and StARD3
(**A**) StARD3 showing the Ω1 loop; the cholesterol binding pocket composed of a-helix and b-sheet elements (**B**) Initial protein-protein interaction result showing alignment of the cholesterol binding regioins (**C**) Protein complex with (re)built loops; a plausible cholesterol transfer pathway is indicated with an arrow (**D**) Plausible bonding interactions between the two proteins in refined orientation; NPC1 residue labels are edged in grey; H-bonds are shown in green, ionic interactions in magenta; some protein structure is omitted for clarity (**E**) Analysis of the StARD3 structure predicts key interacting residues are conserved (some of Lys377 missing in the crystal).

proteins that aligned the known cholesterol binding pocket of StARD3 with the putative cytosolic cholesterol binding pocket of NPC1 (Figure 14B). This binding pose was also energetically favourable (Figure S4).

Cholesterol egress from NPC1 may be blocked by the Cys800-Ser813 and/or Ile642-Leu649 loops of this protein both of which are missing from the PDB structure,[338] usually a sign of a region being highly flexible.[302] Thus the possible structures of these loops, together with Ω1, were predicted using the program Modeller[362] implemented in UCSF Chimera.[363] As expected a diverse set of results was obtained (consistent with high flexibility) all with favourable energy scores (data not shown). Among these were loop models with Ω1 open and neither Cys800-Ser813 nor Ile642-Leu649 obstructing the putative cytosolic binding pocket. Thus cholesterol's path from NPC1 to StARD3 is potentially open (Figure 14C).

NPC1 may interact directly with StARD3 to facilitate transport of cholesterol out of the lysosome

To check the (re)built loops did not interfere with protein-protein interaction the ensemble was resubmitted to ROSIE. This resulted in a smaller RMSD of atomic positions and improved energy scores for the most favourable poses (Figure S4) suggesting that the initial binding arrangement had been refined rather than contradicted. Manual inspection of a sample of results also showed a relatively small positional deviation. Closer examination of one arrangement showed the likelihood of a set of ionic and H-bond interactions holding the two proteins together (Figure 14D). As analysed by ConSurf Lys377 is quite variable, but this residue forms a backbone H-bond so the variability is not significant, while the residue forming ionic interactions (Lys 411 and Arg413) are both conserved (Figure 14E). Thus it is plausible that StARD3 binds to NPC1 to collect cholesterol and that this interaction explains the presence of a lipid binding site on the cytosolic face of the endolysosomal membrane. StARD3 can then dissociate from NPC1 and insert cholesterol to the ER membrane.

Another family of sterol transporting proteins with a soluble domain is the oxysterol binding protein related proteins (ORPs). ORP5 localises to the ER by a single trans-membrane helix and has been implicated in the transfer of cholesterol from endolysosomes to the ER[102,109] using its large cytosolic domain. Thus an exactly similar approach was taken to simulate NPC1-ORP5 interaction using a model of ORP5 derived from a structure of a yeast homologue from the osh family (36% sequence identical, PDB 4ph7,[364] see Table S2 for details). Repeated attempts failed to yield an arrangement of the two proteins that was energetically favourable and allowed unimpeded transfer from the NPC1 cytosolic pocket to the lipid carrying domain of ORP5. Whilst this may be due to shortcomings in the model or the

docking procedure it is consistent with *in vitro* studies of osh4 which suggest a sterol-phosphoinositide exchange mechanism[365] (ORP5 can also transport PIs[366]) and MD work suggesting that osh4 interacts with membranes[367] rather than another protein.

Hence we may hypothesise models for post-NPC1 cholesterol transfer (Figure 15). In one route cholesterol is collected from the cytosolic pocket of NPC1 by the START domain of StARD3 before rearrangement of the flexible linker positions this domain at the ER membrane allowing the completion of cholesterol transfer. The second route depends on cholesterol leaving NPC1 – the open binding sites suggested here (Figure 9) and elsewhere[331] would permit this. Once on the cytosolic face of the membrane cholesterol could be collected by ORP5, possibly in exchange for a phosphoinositide; ORP5 would then rearrange itself just like StARD3 before inserting cholesterol into the ER membrane. Both these mechanisms depend on a stable tethering of LELs to the ER – varying accounts attribute this to the interaction of VAP-A with ORP1L[24] (as shown in Figure 15) or with StARD3 itself.[368]

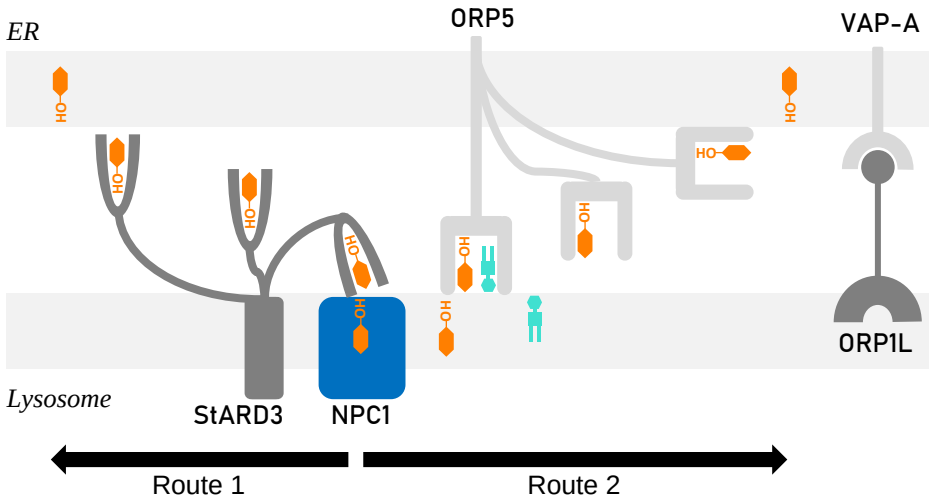

Figure 15 Models of post-NPC1 cholesterol transport Cholesterol (orange) may be collected from the cytosolic pocket of NPC1 by the StARD3 START domain which then transfers it to the ER membrane (route 1) or may diffuse from NPC1 and be collected by ORP5, possibly in exchange for a phosphoinositide (turquoise), and thereby conveyed to the ER.

Revising the BK-cholesterol interaction site

BK is a cholesterol-sensitive lysosomal potassium channel

Whatever the function of NPC1, cholesterol accumulation resulting from its failure will likely affect the big potassium channel (BK, also known as MaxiK and KCa1.1) which has recently been found on lysosomes.[369,370] It has long been recognised as being sensitive to its lipid environment with cholesterol suggested as the key

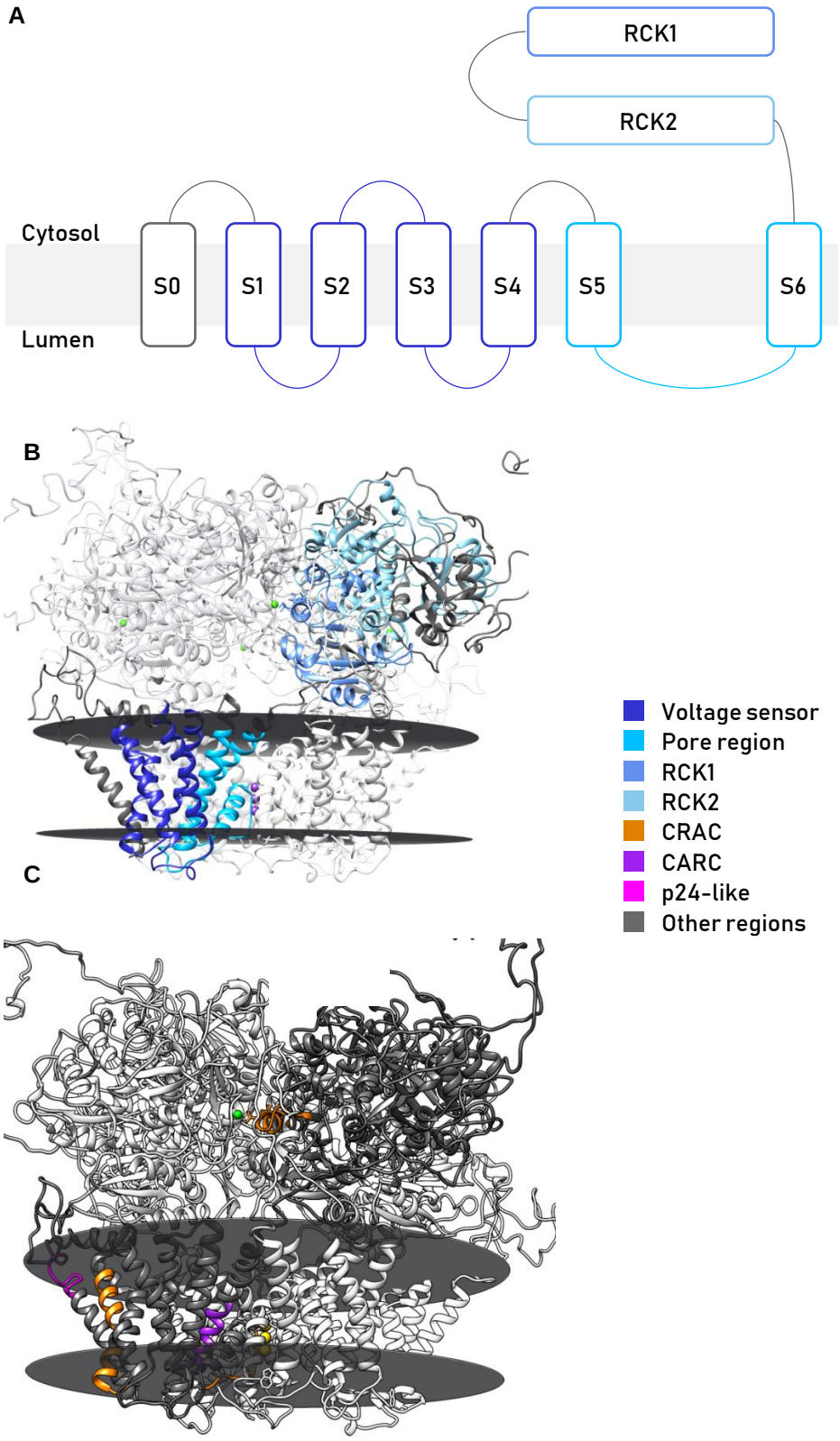

Figure 16 The BK channel (**A**) functional domains in a cartoon representation of one of the 4 proteins that comprise the homotetramer. (**B**) functional domains shown in one of the proteins from the model based on 5tj6.[371] (**C**) Putative lipid binding domains of interest. In (**B**) and (**C**) three of the proteins are shown in white for clarity; approximate position of the membrane shown by translucent discs.

species[372–375] and there is evidence, not least structure-activity studies, to suggest a specific interaction rather than an influence on bilayer thickness.[376,377] Thus we would expect cholesterol to bind to the BK protein. BK is composed of 4 identical subunits each of which contain a voltage sensor and two regulatory of conductance for potassium (RCK) domains. Each subunit also contributes two helices to the channel pore (Figure 16). A 2012 paper[378] traced cholesterol sensitivity to a motif (Val509-Lys518) positioned in RCK1; this sensitivity was lost when the protein was cleaved before Val509. This cleavage was quite drastic removing all of RCK1 and -2, thus significantly weakening the link between Ca^{2+} binding and channel opening and questioning the physiological relevance of these findings. Additionally MD simulation of lipid binding did not identify a stable binding pose. More importantly still, recent structural work on the protein,[371,379] locates the region identified as binding cholesterol in the cytosol where levels of cholesterol will be lower than in the membrane. Given that the membrane region has 4 cholesterol binding motifs (Figure 16C) this seems unlikely. Thus the question of where cholesterol binds to BK was deemed worthy of re-examination.

To do this a model of the membrane section of the human BK channel was built based on a recent cryoEM structure (PDB 5tji)[371,379] of an orthologue from a sea hare. Docking of cholesterol was attempted at each of the intra-membrane cholesterol binding motifs. For the CARC or for CRAC1 or CRAC3 (all defined as in[378]) no poses could be found that were both energetically favourable and biologically plausible, as discussed above, even when flexibility was allowed in residue side chains. Docking cholesterol was then attempted in the space near CRAC2 (Val258-Arg266, located on the voltage sensor) allowing various combinations of side chains to be flexible. Using this procedure a number of plausible binding poses were found (Figure 17). These poses feature the classical elements of binding at a CRAC motif - H-bond to polar residue, CH-π interaction with an aromatic residue and favourable van der Waals bonding with a lipophilic residue - but not derived from a contiguous section of protein sequence. This has previously been found for the β_2 adrenoceptor[380] and illustrates the perils of trying to identify lipid-binding by searching sequences. Neither illustrative pose shown in Figure 17 is likely to represent a static binding situation, rather cholesterol will flit between these and other poses with residue sidechains adopting a set of conformations. Surface conservation analysis of these residues (Figure 17C) was less than fully convincing, although it is not clear that cholesterol modulation of BK activity is a natural mode of regulation (this role is usually accorded to the β subunit that has no role in pore forming[381–383]) so we would not necessarily expect to find these residues conserved. Whilst these docking results cannot disprove cholesterol

Docking suggests cholesterol binds to a previously unappreciated site on the BK voltage sensor.

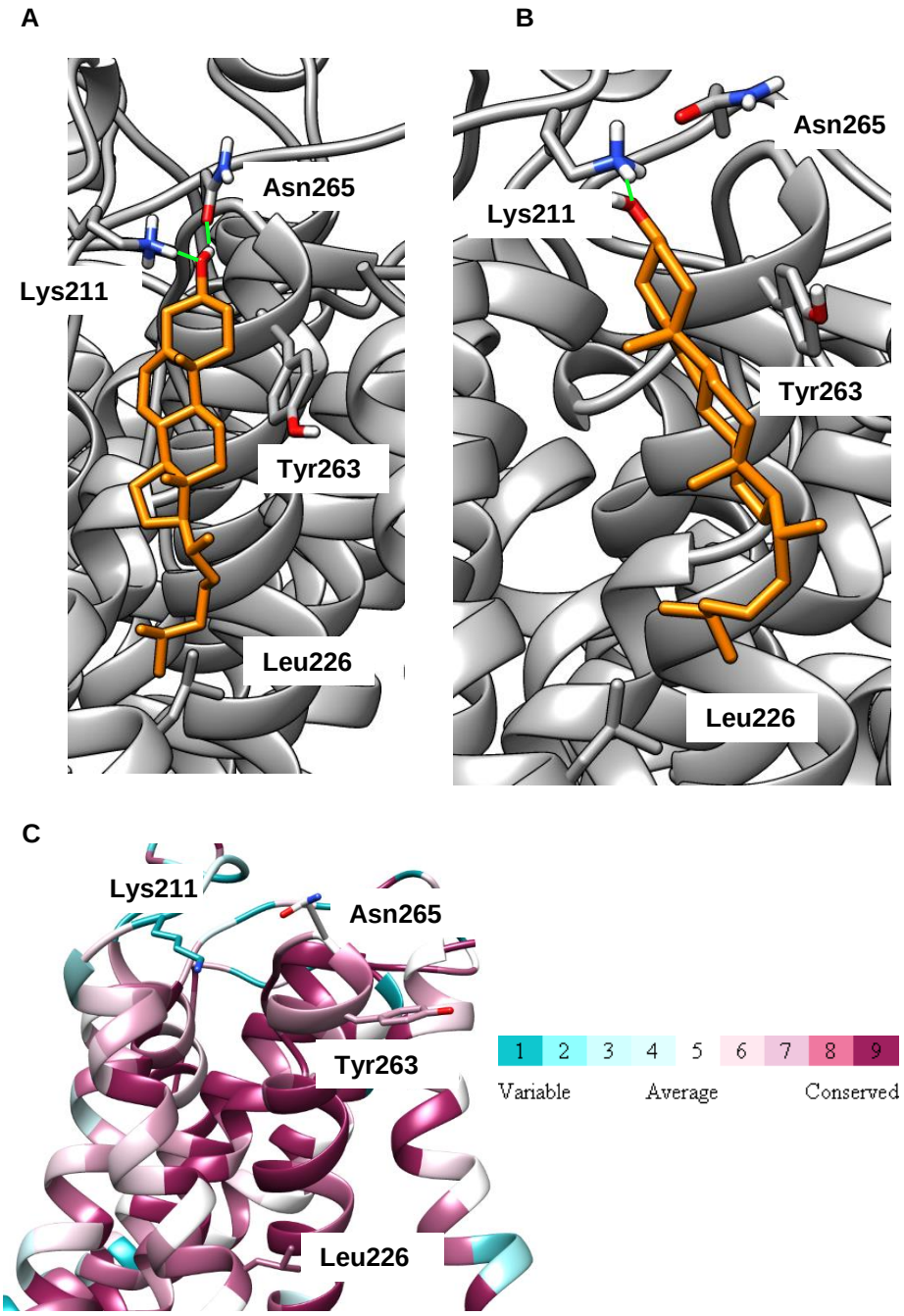

Figure 17 Putative cholesterol binding at the voltage sensor of BK
Cholesterol (orange) is able to form H-bonds (green) with Lys211 (**A**, **B**) and Asn265 (**A**), CH-π interaction with Tyr263 (**B**) and hydrophobic interaction with Leu226 (**A**, **B**). (**C**) Surface Conservation analysis of putative binding residues

binding in the cytosolic domains, they are fully consistent with all relevant data on BK being a cholesterol sensitive channel and offers a plausible explanation for this observation.

So when the NPCD lysosome accumulates cholesterol its BK channel activity will be reduced; conversely channel agonism[384] or over-expression[370] repairs the

endocytic defect in this disease. As BK has been reported as a regulator of LEL-ER membrane contact sites (MCSs)[385] these are likely to be impaired in formation and/or function. A key function of MCSs is refilling endolysosomal Ca^{2+} stores which become depleted as the organelles acidify along the endocytic pathway.[52] Thus we would expect that BK impairment in NPCD would lead, indirectly, to reduced endolysosomal calcium which has indeed been found by multiple groups[53–55] (though not without some dissent[115]).

.

LEL calcium and TRPML1

Reduced LEL Ca^{2+} will result in impaired calcium release via the TRPML1 channel which has been observed in NPCD.[115] (Dysfunction of TRPML1 causes the storage disorder mucolipidosis type IV, which we will meet again in chapter 3.) But as with so much else, TRPML1 impairment in NPCD actually results from multiple factors. This channel exists as a homotetramer whose assembly is driven by interactions between the loop 1 regions on adjacent subunits (Figure 18A).[386] An aspartate-rich region on each loop forms a pore which confers pH-sensitivity on the channel. At low pH the aspartate residues are all protonated so Ca^{2+} ions can pass freely through. As pH rises the aspartates become deprotonated and the resulting anionic carboxylate moieties bind Ca^{2+} which thereby inhibits its own conductance as demonstrated by the structural study.[386] We saw in chapter 1 that the pH of the LEL compartment in NPCD is increased - something to which chapter 3 will return - and this is another reason for expecting reduced TRPML1 function in NPCD. The increased levels of cholesterol in the LELs of NPCD cells is associated with the accumulation of sphingomyelin (SM) which has also been reported to inhibit Ca^{2+} efflux through TRPML1.[115,387] The question thus arises of where SM binds to TRPML1.

There are at least 3 possibilities for the site of this interaction: (1) SM binds at the same site as synthetic ligand ML-SA1, (2) SM uses its anionic portion to compete with the natural ligand $PI(3,5)P_2$, (3) SM inhibits assembly of the four proteins into the channel (Figure 18A). The first of these is precluded as the ML-SA1 binding site lies in the intra-membrane region (Figure 18A)[388,389] and will thus be inaccessible to the SM headgroup. (The headgroup is the distinctive part of lipid molecules with two tails (Figure 2A,C,D) and so likely to be the part of the molecule that determines lipid-protein interactions.) The second possibility was investigated by docking the relevant lipid head groups to a region of the human protein (PDB: 5wj9)[388] equivalent to that recently identified in a marmoset TRPML3 channel[390] as being the ligand binding site (sequence alignment in Figure 16B). Both $PI(3,5)P_2$ and natural

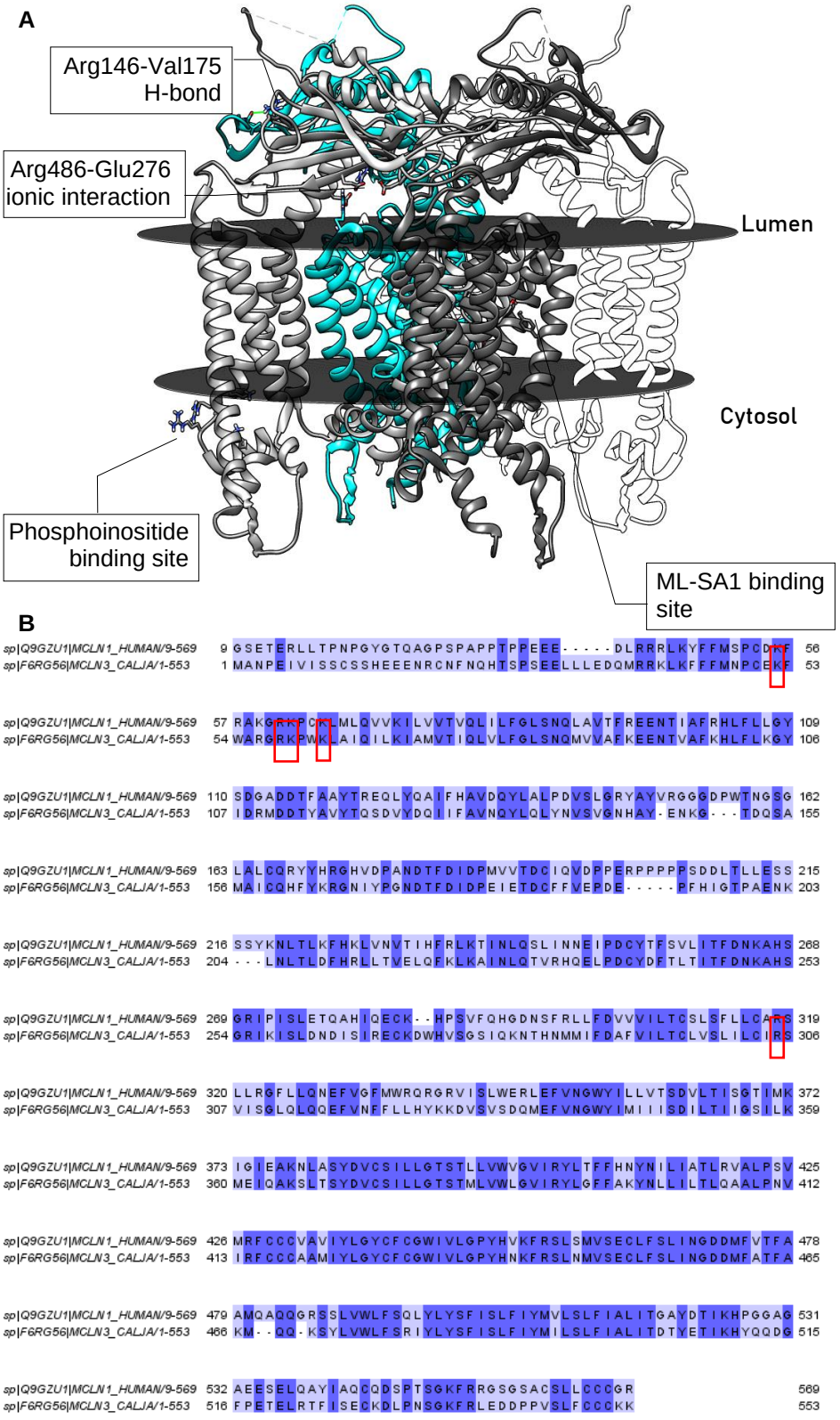

Figure 18 Possible SM binding sites on the TRPML1 channel (**A**) SM may bind at one of 4 locations – two ligand binding sites and two sites of interaction between neighbouring protein chains. Chains are shown in different colours and the approximate location of the membrane is indicated with discs. (**B**) Alignment of human TRPML1 (PDB: 5WJ9[388]) and marmoset TRPML3 (PDB: 5W3S[390]) locates conserved residues (red boxes) of the phosphoinositide binding site.

inhibitor $PI(4,5)P_2$ were found to bind to this polybasic region (Table S4) thus supporting mutagenesis experiments[390] locating binding here (After this work was completed crystallography confirmed this as the ligand binding site.[389]) SM was also successfully docked to this region (Table S4) but the energy of interaction was much weaker than with the phosphoinositides suggesting that SM will not effectively compete with endogenous ligands for this binding site.

The third possibility for SM inhibiting TRPML1 function is inhibition of channel assembly which has previously been shown to lead to reduced TRPML1 function.[386] Two sites of inter-chain binding have been identified in structural studies: Arg146-Val175 (H-bonded) in the linker region[386] and Arg486-Glu276 (zwitterionic) in the juxta-membrane region[388] (Figure 18A). The Arg146-Val175 site is too far from the membrane to be relevant. Docking of the SM headgroup to the Arg486-Glu276 region suggested that, whilst the residue side chains are very flexible, they preserve interactions between them rather than become separated by SM. Channel assembly is thus maintained in the presence of this polar lipid (Figure 19). Considering this, direct effects of SM on the TRPML1 channel appear unlikely and thus the inhibitory properties of this lipid may well derive from indirect effects, perhaps mediated through membrane organisation.

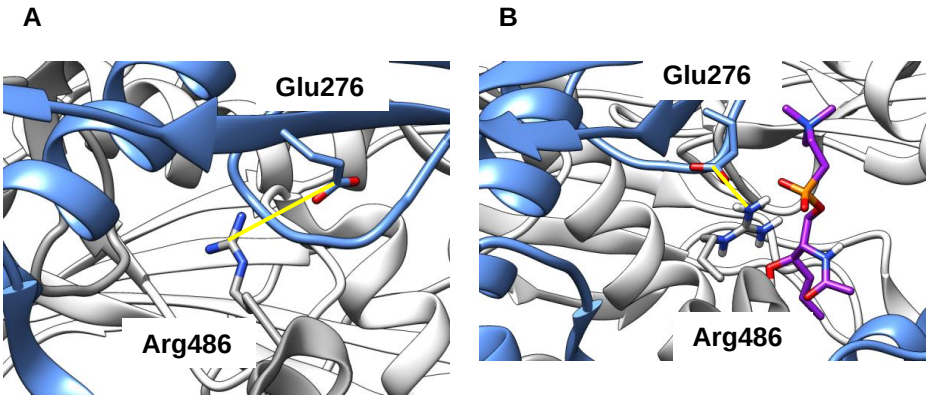

Figure 19 Putative binding sites of lipids at TRPML1 (**A**) Glu276 from one chain (blue) forms a charged interaction with Arg486 from another (grey); interatomic distance 3.77Å. (**B**) Modelling suggests plausible binding poses for SM (example shown) but these do not disturb the inter-residue interactions present in the *apo* state; interatomic distance 2.97Å. Protein oriented as in Figure 18.

TRPML1 plays roles in endocytosis[391,392] and autophagy[393] so the failure of these process in NPCD[41,42,394,395] is unsurprising, though there may be some redundancy with the TPCs,[396,397] $P2X_4$ [398] and P/Q-type VGCC.[113,399]

Annexins and phosphoinositides

Endocytosis[27] and autophagy[400] also involve the peripheral membrane protein annexin A2 (AnxA2, previously annexin II). This is reported to mislocalise in NPCD, associating with late rather than early endosomes[27,61] thereby raising the expectation that its membrane binding will involve cholesterol, something later confirmed by experiment.[27,57] Closer examination reveals phosphoinositides, and especially PI(4,5)P_2, to have a key role.[286,401,402] These observations can be harmonised by the result that cholesterol acts to aggregate PIs[284,285] in a similar manner to its function in raft organisation so that NPCD triggers an accumulation not just of cholesterol but also other lipids including PIs.[43] Significantly, the only study to report that AnxA2 membrane association is cholesterol-independent was conducted in model membranes that did not contain phosphoinositides.[403] Thus it seemed reasonable to ask if phosphoinositides could bind to AnxA2. If binding is favourable then the protein will go where the lipid is and AnxA2 mislocalisation would be thereby explained. Other work reverses this direction of causality and suggests that AnxA2 induces lipid raft formation[401,404] – it is quite possible that both process occur simultaneously.

A published x-ray structure of AnxA2 (PDB: 2hyw[405]) was used in preference to a previous structure (PDB: 1xjl[406]) as the earlier work had slightly worse resolution (2.59 vs 2.1Å) and quite a high number of water molecules per protein (212 for 319 residues) which can be an indication of lower quality.[302] The search was concentrated in a region including Lys279, Lys281 (as site-directed mutagenesis had identified these residues as important for PI(4,5)P_2 binding[401]); a nearby residue Arg284 was also included in the search space. All these residues are basic and are thus likely to protonated and positively charged *in vivo*. The presence of a nearby bound Ca^{2+} ion was a difficulty as by default AutoDock sets charges on metals to zero. This is not only unrealistic in itself but also leads to errors in the partial charges computed for atoms co-ordinated to the metal and others in the vicinity. Thus Atomic Charge Calculator[407] (webchem.ncbr.muni.cz/Platform/ChargeCalculator) was used to calculate the charges on all the atoms in the system and the AutoDock files manually edited to change the charge on the calcium and on all atoms nearby. Docking experiments could then be performed as normal.

Accumulating cholesterol induces increases in phosphoinositides which bind to AnxA2. This explains why AnxA2 mislocalises in NPCD.

Consistent with the previously reported results[286,401,402] the cationic residues interact with the two anionic phosphates while the two lipid side chains point away from the protein and remain in the membrane (example binding pose shown in Figure 20A). Docking of SM was also performed and the results were much less energetically favourable than for PI(4,5)P_2 (Table S4) suggesting that the

phosphoinositide is genuinely responsible for AnxA2 binding. Thus in NPCD AnxA2 will be expected to mislocalise away from early endosomes and to cholesterol-rich late endosomes as observed[27,61] and contribute to the documented endocytic defect.[41,42] (Surface conservation analysis suggested this region of the protein is rather variable (data not shown); however given the in vitro demonstration that phosphoinositide binding depends on Lys279 and Lys281[401] the value of this output is unclear.)

Previous studies have reported conflicting results on the Ca^{2+}-dependence of membrane binding by AnxA2.[57,286,408] Consistent with *in vitro* work[401] the results here support a direct interaction of the protein with PI lipids and thus do not require a specific role for calcium. This is consistent with an MD study[409] which found Lys281 interacting with membranes without requiring Ca^{2+} even as the interaction overall remained dependent on calcium and phosphatidylserine.

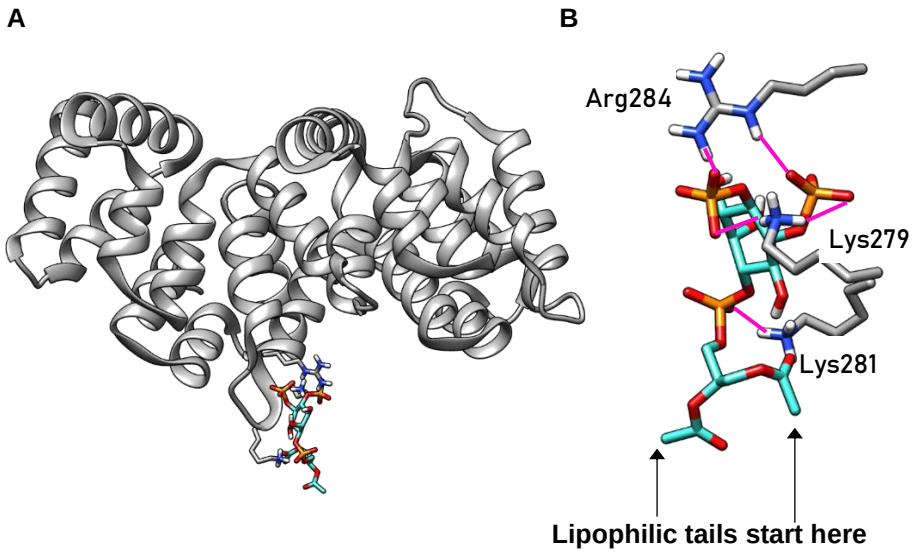

Figure 20 Site of PI(4,5)P_2 binding to AnxA2 (**A**) PI(4,5)P_2 (turquoise) binds to the convex face of AnxA2 (grey) driven (**B**) by zwitterionic interactions (magenta) with Lys279, Lys281, Arg284.

Another member of the annexin family, AnxA8,[d] has also been reported to have roles in regulating endocytosis where it localises to late endosomal membranes.[410] However, this association increases on pharmacological inhibition of NPC1[411] and AnxA8 is found to bind phosphoinositides including PI(4,5)P_2.[412] Given also the accumulation of PIs in NPCD the question arises of whether AnxA8 binds these lipids in a similar manner to AnxA2. Sequence alignment of AnxA8 with –A2

[d] I am grateful to Prof Volker Gerke (Universität Münster) for drawing this area to my attention.

revealed a similar polybasic region, though with one lysine mutated to an alanine (Figure 21A, red box). The AnxA8 crystal structure (PDB: 1w3w[413]) shows that these residues are on the convex face of the protein where annexins tend to interact with membranes[409,414] and so docking was attempted in this region. When the equivalent basic residues (Lys267 and Arg272) were allowed to be flexible no binding pose could be found where PI(4,5)P_2 interacted with both sidechains (data not shown).

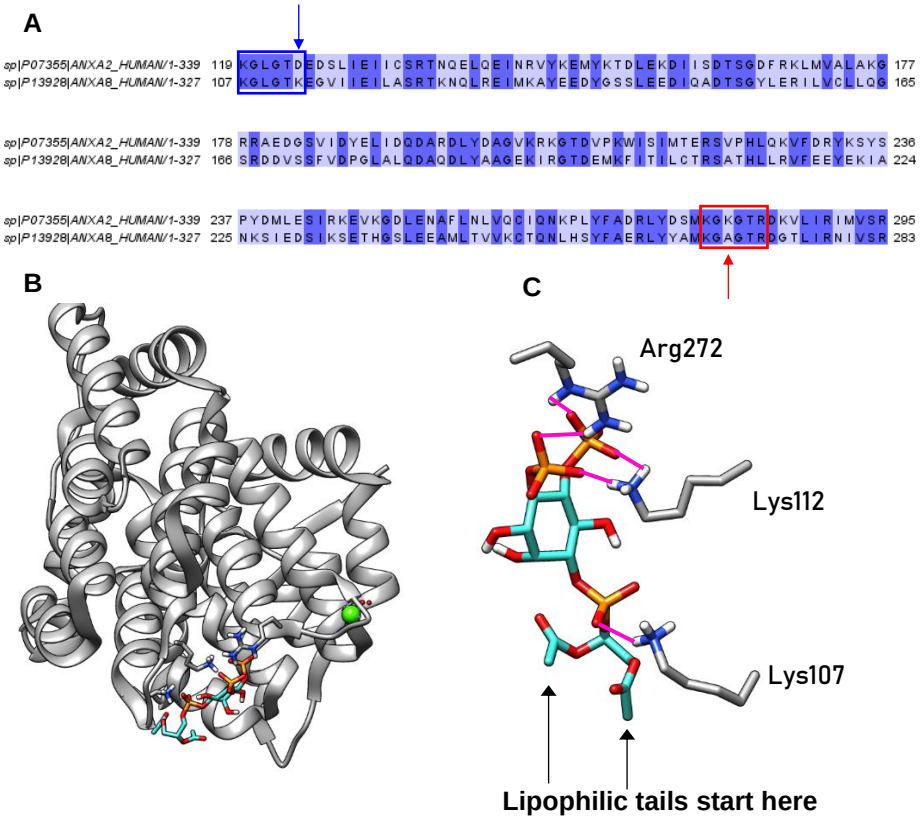

Figure 21 Phosphoinositide binding to AnxA8 (**A**) Sequence alignment of AnxA8 with –A2 reveals two dissimilar basic regions. (**B**) PI(4,5)P_2 binds on the convex face of AnxA8. (**C**) Detailed view of the binding site showing zwitterionic interactions.

Inspection of the structure revealed that Arg272 was proximately located to Lys107 and Lys112, a region where AnxA2 contained an aspartate residue (Figure 21A, blue box). When docking was attempted in this region, allowing the basic sidechains to be flexible, numerous plausible binding poses featuring interactions with all 3 positively charged centres were found (representative example shown in Figure 21B,C, extended data in Table S4). This binding, which requires validation from in vitro experiments may have functional consequences for NPCD which will be discussed later.

SNARE proteins and phosphoinositides

Whilst it is clear that AnxA2 is important in endocytosis, its precise role has not yet been discovered (though recent work suggests it may assemble into dimers or heterotetramers to bridge membranes[29]). The same could not be said of SNARE proteins such as syntaxins and VAMPs (also known as synaptobrevins). These are membrane-associated proteins, generally with one trans-membrane helix (Figure 4B), which form complexes with SNAP-29 thereby mediating membrane fusion events (Chapter 1, Figure 1, ❾). These complexes are subsequently disassembled so that the individual components can be re-used. This disassembly is retarded in cholesterol rich membranes[65] such as those present in the endolysosomal compartment of NPCD cells. The molecular reasons for cholesterol-mediated slowing of this process are not known.

Significant work has been done on the juxta-membrane region of syntaxin 1 (Stx1) which is polybasic and thus polycationic *in vivo*.[415–418] Many other syntaxins have a similar region, as do their VAMP partners (see multi-sequence alignments, Figure 22C) where less extensive work has been reported.[419] This raises the questions of how two protein regions with like charges can get close enough together to form a complex, and how the complex stays assembled despite the electrical repulsion present. These questions could be plausibly answered by invoking a bridging role for a negatively charged phosphoinositide lipid similar to that repeatedly found for Stx1.[415–418]

To investigate this a model of a SNARE complex featuring Stx7 and VAMP8 – a combination reported necessary for endocytosis[32–34] – was built based on an x-ray structure (PDB: 3hd7[420]) of a related bundle. Docking was then attempted with $PI(3,5)P_2$ allowing various combinations (Table S4) of juxta-membrane basic residues (VAMP8: Arg67, Lys68, Lys72; Syntaxin 7: Arg232, Lys233, Arg235) to be flexible. Numerous plausible poses were found where the anionic ligand bound to cationic residues of both SNARE partners (Figure 20A,B). This would be expected to promote SNARE interaction and thus inhibit complex disassembly. The previously reported cholesterol-mediated clustering of $PI(3,5)P_2$[284,285] means not only that this lipid will accumulate in NPCD but that it will accumulate in defined areas which thus have a high local concentration of phosphoinositide. Thus should an assembled SNARE cluster escape one phosphoinositide molecule and begin diffusing through the bilayer it will likely encounter another phosphoinositide and so remain trapped. Thus the recycling defect observed in cholesterol rich membranes[65] can be explained by appealing to the effect of cholesterol on another lipid rather than on the protein directly. (The apparent paradox of Stx7, a cholesterol binding protein that lacks a

Phosphoinositides bind to two partners in a SNARE bundle and thus inhibit its recycling

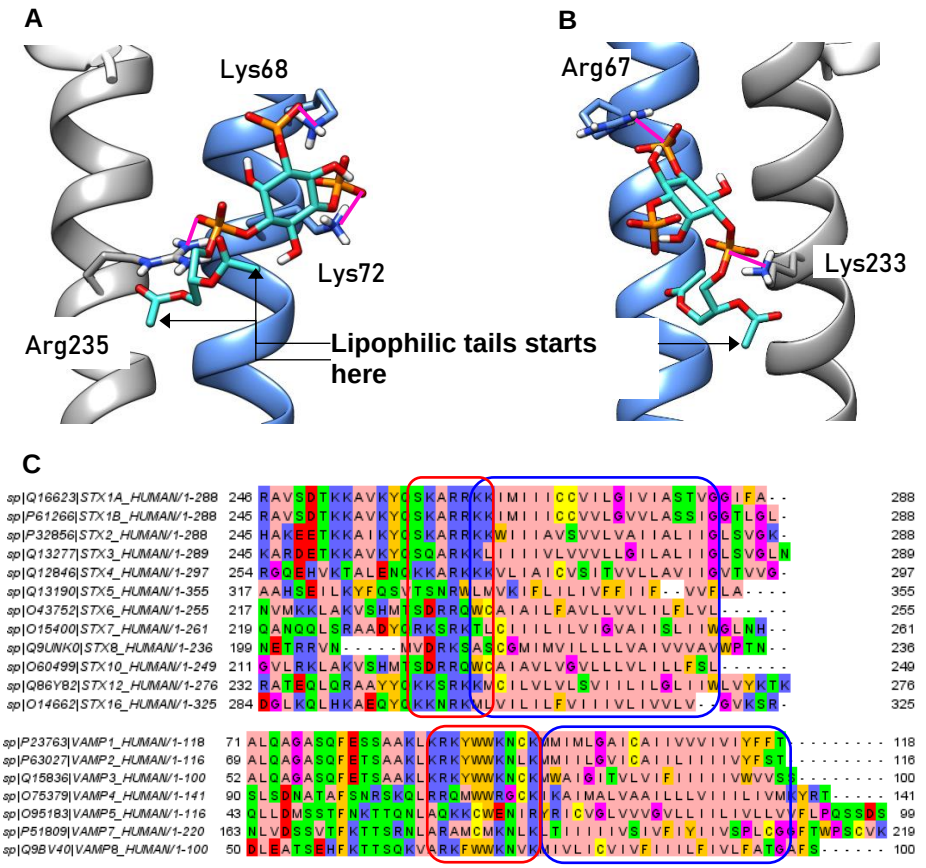

Figure 22 PI(3,5)P2 can bind to two members of a SNARE bundle simultaneously. Sample poses from juxta-membrane region 1 (**A**) and 2 (**B**) of PI(3,5)P_2 (turquoise) bridging VAMP8 (blue) and syntaxin 7 (grey) in the assembled SNARE bundle with zwitterionic interactions (magenta). (**C**) Multi-sequence alignment of human Stx (top) and VAMP (bottom) proteins showing the common polybasic region (red boxes) next the the TMH (blue boxes).

recognised cholesterol binding motif,[63] can plausibly be resolved along similar lines.) Repeated attempts to dock PI(4,5)P_2 to the model consistently failed to give plausible binding poses (data not shown) suggesting that clustering is dependent on only the 3,5-isomer.

The situation with autophagy is more complicated as this has been reported to rely on Stx17 in both mammals and Drosophila;[94,421] Stx7 does not appear to be involved.[95] Stx17 is unusual in its possession of two trans-membrane helices, neither of which has a polybasic juxta-membrane region (Figure 22).

Proteins where modelling is not currently helpful

Annexin A6

Chapter 1 advanced various ways in which Annexin A6 (AnxA6) might be implicated in NPCD pathology. A typical annexin protein consists of a bundle of 4 ankyrin repeats;[422] AnxA6 is atypical in that it has two such bundles connected by a flexible

linker[423] (Figure 23) which means it can undergo internal re-organisation on membrane binding.[424] Consistently, two groups report it binding membranes in more than one conformation but remaining peripheral[425,426] (Figure 4A) Other workers disagree finding it binds membranes in an integral mode[427] (Figure 4D) possibly even trimerising and forming an ion channel.[428] The Trp343 residue has been reported as key to binding[58,428] though other reports do not examine this possibility. In similarity with AnxA2 this protein has been reported to associate with phosphoinositides.[429]

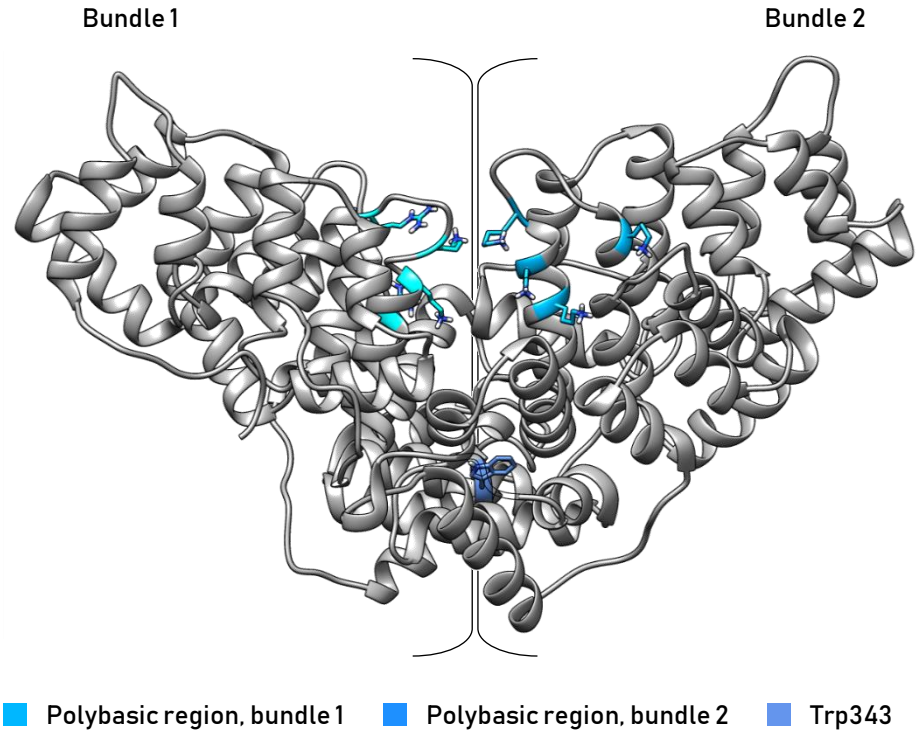

Figure 23 Key areas of AnxA6 The polybasic regions aligning with those in AnxA2 and Trp343 all localise away from the periphery of the protein (structure taken from 1m91).

To investigate if membrane association could occur by the same mechanism the AnxA6 sequence was split into its two halves and each multi-aligned with AnxA2 (data not shown). The polybasic region of AnxA2 implicated in membrane binding has approximate counterparts in each half of human AnxA6 and these can be located in a published crystal structure of the protein[423] (PDB 1m9i, Figure 23). However both these regions are at least partly buried in the interior of the protein (Figure 23) so for them to bind phosphoinositides in a membrane would require either forcing other parts of the protein to contact the membrane (so making modelling computationally very expensive[409]) or exposing the basic residues by large-scale conformational change (which is in the category of speculation). Trp343 is also located in the interior of the protein in the crystal structure (Figure 23) but it is also part of the flexible linker and may be more or less exposed dependent on

conditions[423] so using computation to examine its role in binding lacks the necessary well-defined starting point.

rab7 and -9

As we saw in chapter 1 rab7 apparently associates with cholesterol-rich membranes on NPCD endolysosomes from which it is recycled slowly thus contributing to the endocytic defect.[26,50] Rab proteins become membrane-associated through the acquisition of geranylgeranyl tails[287] which insert into lipid bilayers (Figure 4C); however such a tail is generally considered excluded from lipid rafts.[430] Raft-inclusion and hence impaired recycling of rab7 thus appear paradoxical and require further investigation as part of ongoing work to understand the complexities of membrane dynamics. It may be postulated that lipid head groups interact with the residues close to the lipidation sites at the protein's C-terminus in a manner similar to that advanced above for the SNAREs. Indeed this region contains residues likely to carry charges at cytosolic pH (data not shown) so ionic interactions with accumulating charged lipids such as PIs and SM are possible; modelling could be a good way to investigate this. Unfortunately in all of the published structures of human[431,432] or rat[433] rab7 the relevant C-terminal region is missing rendering such an approach impossible. Exactly similar considerations apply to rab9.[434–436]

ClC channels

There are excellent reasons for studying the ClC chloride transporters, not least that in mice knockout[81,83] or mutation[82] of members of this family led to neurodegeneration. ClC3, -6 and -7 are localised to the endolysosomal compartment[437–439] where they associate with lipid rafts[437,440] which are reported to disrupt their activity.[440] They are likely to be implicated in maintaining the acidity of the lysosomal lumen[75,439,441] (though there is some dissent about this[442]) and therefore storage of unmetabolised material in the lysosome.[83] A proteomic study reports two members of this family upregulated in NPCD[113] while a sub-population of NPCD lysosomes appears deficient in both H^+ and chloride.[441] The best available structures[443,444] of eukaryotic ClC proteins have only low sequence identity with endolysosomal transporters (ca 25%, data not shown) and low resolution (ca 4Å) meaning models derived from them are likely to be of very low quality and therefore unsuitable for modelling lipid-protein interactions. Provocatively, one of the published structures (PDB: 5tr1)[443] has a cholesterol associated with it.

Two-pore channels

Confusion characterises our current understanding of two-pore channels (TPCs)[445] extending as far as the ions they conduct where calcium,[396] sodium[446] and even hydrogen[447] have all been reported. While localised to the endolysosomal compartment[448] and implicated widely in its functions,[396,397,449] no disease is yet associated with knockout or mutation of these proteins, unlike the better known calcium release channel TRPML1.[80] (The possible involvement of the TPCs in Parkinson's disease[450] is an interesting hypothesis that has yet to be established.) The only definite link with NPCD is the report that sphingosine targeted to the lysosome results in Ca^{2+} release via TPC1.[114] Whilst the pathogenic relevance of this finding has yet to be established the accumulation of Sph in NPCD endolysosomes[61] is suggestive. Sphingosine has a chemical structure markedly dissimilar to the reported endogenous[396,451] and synthetic[452] ligands of the TPCs meaning its binding site requirements will be very different. In turn this suggests that the Ca^{2+} release is unlikely to arise from direct binding to the ligand binding-sites determined by structural work (PDB: 5dqq and 6c9a)[451,452] and so modelling work is unlikely to yield new insights.

TMEM192

TMEM192 is a lysosomal transmembrane protein[453] implicated in autophagy;[454] it also binds sphingolipids[e] and so may well have a role in NPCD, though no study has yet investigated that and knockout of the protein in mice did not lead to lysosomal dysfunction.[455] Algorithmic searching of its primary sequence reveals a p24-like sphingolipid binding motif (discussed above) on one of its predicted[456] transmembrane helices (data not shown). As previously noted this motif contains a compulsory aromatic residue at one end, however whether that residue should be near the membrane edge or near the membrane centre is not defined. In fact this residue in TMEM192 (Trp55) is positioned near the membrane centre whereas the corresponding residue in p24 (Tyr189) is positioned near the membrane edge.[271] This questions whether or not sphingolipid binding occurs at this site and until the roles of the individual residues in the p24-like motif are understood more clearly modelling of lipid-TMEM192 interactions will likely provide nothing more than curiosities.

TMEM175

TMEM175 is a lysosomal potassium channel[76] implicated in numerous aspects of degradative function including acidification.[76,85] Intriguingly knockout of this

[e] Dr Per Haberkant (EMBL), personal communication

protein also results in reduced mitochondrial oxygen consumption.[85] Given such widespread effects on metabolic function it is perhaps unsurprising that mutation of this protein has been associated with decreased age of onset of Parkinson's disease[84,457] and raises the question of whether it has roles in other neurodegenerative diseases. The recent disclosure of the structure of a similar bacterial channel[458] with ca. 30% sequence identity opens the possibility of constructing a homology model of this protein. However no studies have yet examined lipid modulation of TMEM175 function so even if lipid binding could be successfully modelled its functional consequences would be unclear.

Open questions and future work

Extensive modelling work has generated evidence for NPC1 and -2 as binding cholesterol (which is widely accepted) and sphingosine (which is more controversial). These ideas could be tested by mutating residues predicted to be key for binding; in particular Glu30 of the NPC1 NTD is an attractive target as this plays no role in cholesterol binding but is predicted to be important for sphingosine. If mutating this residue provoked an NPCD-like phenotype then that would be good evidence of the involvement of Sph in the pathogenesis of this condition. Equally the reality of sphingosine binding to NPC2 and the NPC1 NTD could be tested by co-crystallising the lipid and the protein in the same way as has been done for cholesterol.[15,330] Recent MD studies of the transfer of cholesterol from NPC2 to the NTD of NPC1[337,459] could be repeated with Sph. The question of whether or not NPC1 acts to transfer cholesterol from one binding pocket in the SSD to the other (Figure 9) could be addressed using the methods of a separate MD study of NPC1 in a model membrane.[346] Whilst caveats should be attached to this work – the possibility that NPC1 occurs in complex with other proteins,[354,355] the question of whether the composition of the model membrane adequately approximates reality – it would be significant if a similar result could be obtained with sphingosine.

The question of NPC1 transferring lipids directly to soluble domains of carrier proteins, as predicted in Figure 14, could be addressed by mutating those residues identified as key to the association, especially those involved in charged interactions. If the proposed NPC1-StARD3 complex is real then such mutation would be expected to reduce the interaction and thus the transfer of lipid to other organelles. The opposite experiment, relief of disease burden by activating post-NPC1 cholesterol transport by over-expression of StARD3 or ORP5, is unlikely to be successful. Cholesterol transfer to the ER depends on formation of LEL-ER contact

sites (Figure 15) and multiple lines of evidence suggests the disruption of these in lysosomal storage disorders like NPCD.[24,48,56]

Whilst this protein-protein interaction might explain the need for the 5 TMHs of NPC1's SSD (Figure 7) it does not, as noted above, explain why NPC1 has an additional 8 helices spanning the bilayer. It has recently been proposed that NPC1 exports cholesterol via a pathway featuring wholesale conformational change in the protein[460] so that the lipid passes not round the edge of the protein, as suggested here and elsewhere,[331] but through the middle. This would potentially be consistent with the finding that NPC1 regulates the activity of cathepsin D via binding to luminal loop 3[461] – if cholesterol passing through the protein causes it to rearrange then cathD binding may be altered. In the absence of any structural information supporting this pathway the modelling approaches used here are inappropriate. However, should such information emerge the modelling the putative NPC1-cathD interaction becomes feasible and interesting.

The evidence that the BK channel is cholesterol sensitive is extensive[372–375] but the binding site predicted here is novel. This hypothesis could be tested by mutagenesis experiments involving key hydrogen-bonding residues Lys211 and Asn265 which would be likely to reduce binding and therefore cholesterol sensitivity. If either of these mutations produced a fully functional but cholesterol-insensitive channel then it would be interesting to produce the same mutant protein in NPCD cells as this might correct the endocytic defect as has been demonstrated by channel agonism[384] or over-expression.[370] If such a mutation also corrected with lysosomal Ca^{2+} refilling defect (proposed to be dependent on BK[369]) then this would give great insight into the molecular pathology of NPCD.

The failure of docking approaches to identify a binding site for SM on TRPML1 is disappointing in view of the reported channel inhibition by this lipid and hence reduced calcium efflux through it.[115] That report did not demonstrate direct SM-channel binding and found lysosomal calcium normal in NPCD, a result at odds with multiple other studies which report a reduction.[53–55] Given that calcium efflux through TPC1 is also reduced in NPCD cells[114] perhaps the simplest explanation is that lysosomal calcium is genuinely reduced in this pathology. Such a reduction could account for the reduced TRPML1 calcium current without the need to invoke lipid-induced malfunction.

The work on Annexin A2 reported here is in excellent agreement with existing *in vitro* studies (especially[401]). Next it would be interesting to extend a recent high-

level MD study of the interaction of AnxA2 with membranes[409] to consider the interaction of the basic residues identified in Figure 20 with anionic membrane lipids. To investigate further the reported accumulation of phosphoinositides in NPCD disease[43] cells could be transfected with a YFP-tagged plekstrin homology (PH) domain[177] (which recognises phosphoinositides). Co-localisation of this protein with fluorescently-tagged antibodies to an LEL maker protein, eg LAMP2, would be expected. If AnxA2 also held a fluorescent tag which co-localised with YFP-PH then the pathological relevance of the PIP-AnxA2 interaction would be confirmed. A similar approach with AnxA8 is also likely to be profitable as the mislocalisation of this protein in disease cells has not yet been demonstrated, only in cells treated with a pharmacological inhibitor of NPC1.[411] The functional consequences of AnxA6 and –A8 (if confirmed) mislocalisation and likely to form a profitable area for investigation. Both proteins have been reported to interact with actin[412,462] and so may contribute to the defect in lysosomal localisation,[24,26,51] although the current absence of small molecule modulators of the function of these proteins may restrict their usefulness in NPCD treatment.

The association of the juxta-membrane region of syntaxin 1 with phosphoinositides has been demonstrated using a fluorescently tagged protein[415,416] – the same approach could be taken with Stx7 and VAMP8. It might also be possible to tag these two proteins with different fluorescent labels and use FRET to measure their association. The modelling work in this chapter would predict that the degree of association would be greater in membranes with reasonable phosphoinositide content than in membranes devoid of those lipids. Such an experiment would not demonstrate that the recycling defect from cholesterol-rich membranes[65] is actually a direct result of PI-protein interaction, as this work proposes, but would point in that direction. It would also be possible to extend the docking work described here to an MD simulation of the assembled SNARE bundle (as has been done with Stx1[417]) which would increase confidence in the reality of PI-protein binding. A further extension to simulation of complex disassembly is more challenging as the mechanism of this process is only just emerging[463] and simulation has not yet been attempted using an explicit lipid component.[464]

Summary

Docking and MD simulations have supported the idea of NPC1 as a cholesterol export protein and postulated a direct interaction with StARD3 as part of the onward pathway. Dysfunctional NPC1 will lead to the accumulation of cholesterol in the lysosome which will inhibit BK channel function. This accumulation will also trigger the secondary storage of sphingomyelin (which may inhibit TRPML1) and phosphoinositides (which will mislocalise AnxA2 and impair SNARE recycling). As consequences of all this endocytosis and autophagy will be impaired. This chapter has also supported the idea of NPC proteins as a sphingosine export system; the next chapter will examine what might be the functional consequences of the impairment of this function.

Materials and methods

Multi-sequence alignments were performed in Clustal Omega (ebi.ac.uk/Tools/msa/clustalo/)[465] and visualised in JalView.[466] Lipid binding motifs were located using Fuzzpro (bioinformatics.nl/cgi-bin/emboss/fuzzpro).

Protein structures were either downloaded from the PDB or models built using SwissModel[304] (swissmodel.expasy.org/). Quality was assessed using QMEANBrane;[306,307] see Table S2. Approximate positions in the membrane were found using the OPM database (http://opm.phar.umich.edu/).[308] The AnxA2 structure features calcium ions which by default are set to zero charge by AutoDock. Thus atomic charges for these and spatially proximate atoms were calculated using the Atomic Charge Calculator (webchem.ncbr.muni.cz/Platform/ChargeCalculator)[407] and the relevant AutoDock files manually edited. Ligand structures were prepared in Avogadro (avogadro.cc/) and minimized using the MMF94 force field with at least 5000 steps; other settings were defaults.

Docking of lipids to proteins was performed using AutoDock 4.2.6[309,310] using default settings. AutoDock requires a search space (in which the docked ligand must fit) to be defined; this is accomplished by specifying the region's centre, its offset from this centre in each of the x,y,z directions measured in points (1 point = 0.375Å) and its dimensions also measured in points. For each protein this information is given in Table S3 along with the residue sidechains allowed to be flexible. The various descriptors of the ligand's relation to the protein (position, orientation, bond angles) are then altered and a certain amount of mixing between different states allowed; hence the procedure is termed a genetic algorithm (GA). This is run a set number of times. AutoDock clusters binding poses by RMS distance (cut-off > 2Å); extended data are given in Table S4. Docking scores were used as a preliminary assessment followed by manual inspection for biological plausibility as discussed.

For MD simulations sphingosine was parameterised using CGenFF (cgenff.paramchem.org/);[320] the lipid structure file was the same as used in docking calculations but converted to sdf format (https://cactus.nci.nih.gov/translate/). CGenFF calculates approximate values for partial charges, bond angles and dihedral angles; the degree of approximation is given by a penalty score which should be less than 10 and must be less than 50. The partial charge penalty scores of concern are given in Figure 24. All these charges were considered reasonable given the electronegativity of the atoms in question. Penalty scores above 20 were returned for some bond angles and dihedrals in the grey oval but the angles were also considered acceptable given that sphingosine was used in its energy minimized conformation. In any case the sphingosine sdf file from the ZINC database,[467]

recommended by the authors of CGenFF, gave identical results. Cholesterol has already been parameterised.[318]

Pdb files containing both bound ligand and protein were made in UCSF Chimera[363] and then manually edited so that the atom numbers matched those in the lipid parameter files.

MD simulations were run using the VMD interface[351] of NAMD software;[322] for ease the QwikMD plug-in[323] was used to set up calculations. Simulations were run in a 15Å water box with 0.1M NaCl as an approximation for the complex ionic environment of the lysosome lumen.[101] The equilibration phase was set at 1.24ns and the production phase at 10ns; CHARMM36 force field was used.[317] Post-simulation analysis was conducted in QwikMD;[323] images for videos were recorded using the MovieMaker plug-in of VMD,[351] made into videos using Adobe Photoshop. Protein structures, including docking results, were visualised in UCSF Chimera.[363]

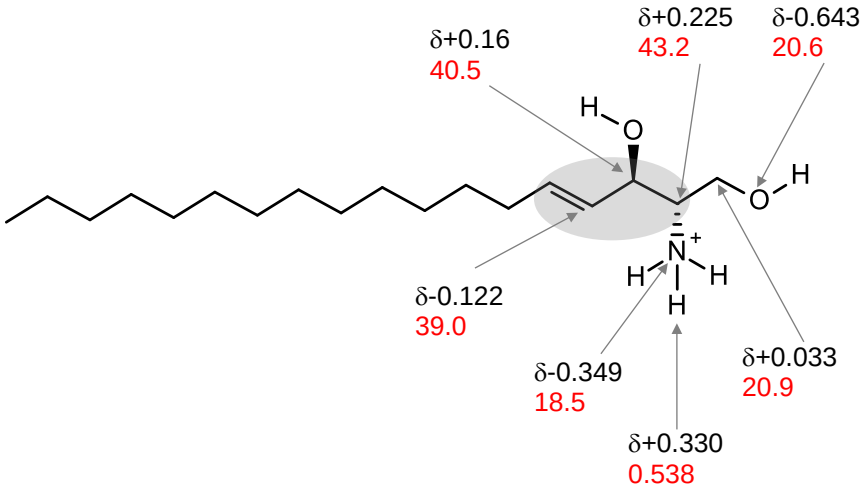

Figure 24 CGenFF penalty scores for protonated sphingosine For details see text

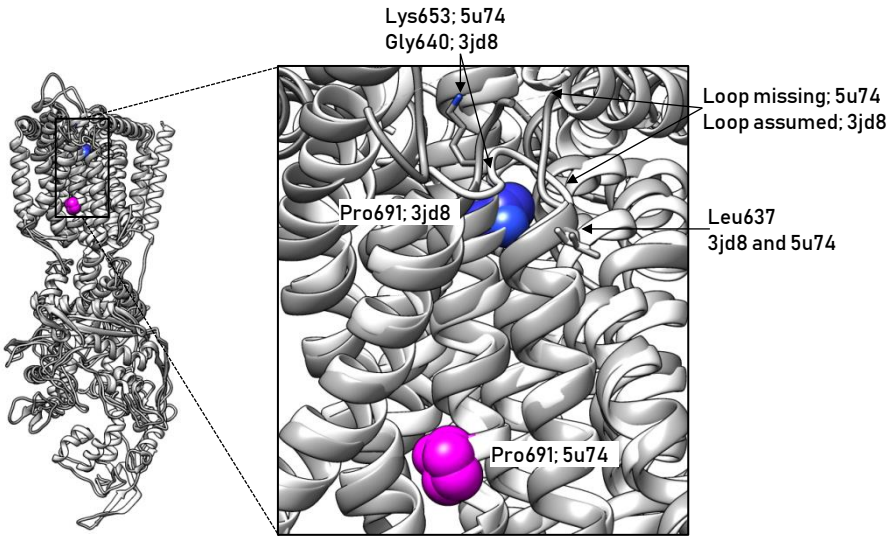

Figure S1 Differences between published structures of NPC1 Structure of NPC1 (PDBs 3jd8 shown in white and 5u74 shown in grey) adopt approximately the same overall shape (left panel). In the SSD (right panel) they locate Leu637 essentially identically near the cytosolic end of helix 3 (right panel). Because 5u74 resolves all side chains the authors realised that the loop between helices 3 and 4 was missing (dashed line) from their x-ray data whereas the authors of 3jd8, where the side chains are not resolved, assumed the structure was continuous at that point. Thus the two structures position different residues at the cytosolic end of helix 4 (Lys653 for 5u74 (and as predicted by InterPro) but Gly640 for 3jd8). The significance of this for the current study is that key residue Pro691 is in a dramatically different location in the two structures (pink for 5u74, blue for 3jd8).

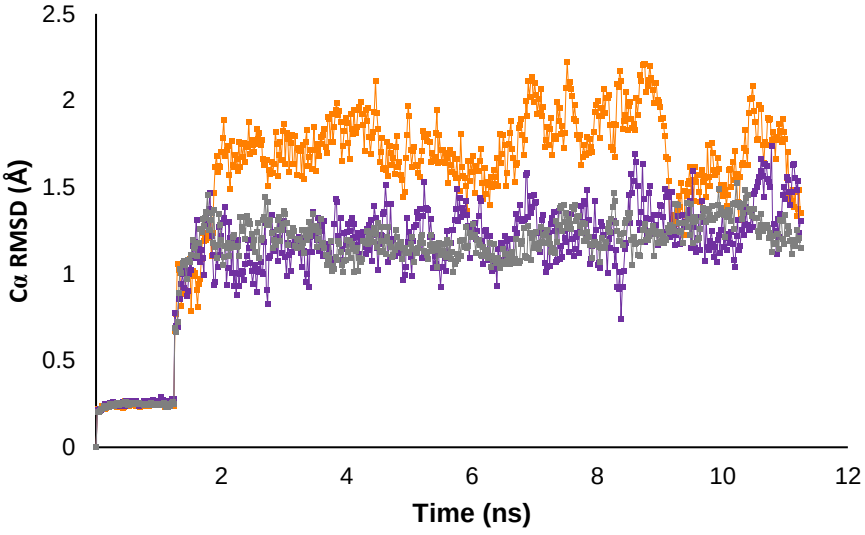

Figure S2 Output of NPC2 MD simulations RMSD of protein C_α atoms of NPC2 with bound cholesterol (orange), NPC2 with bound sphingosine (purple) and SphK with bound sphingosine (grey).

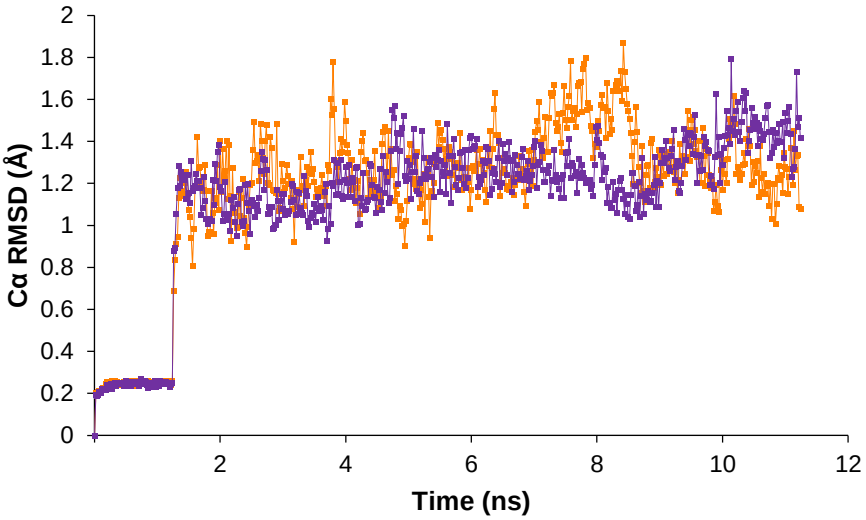

Figure S3 Output of NPC1 NTD MD simulations RMSD of protein C_α atoms of NPC1 NTD with bound cholesterol (orange) and bound sphingosine (purple).

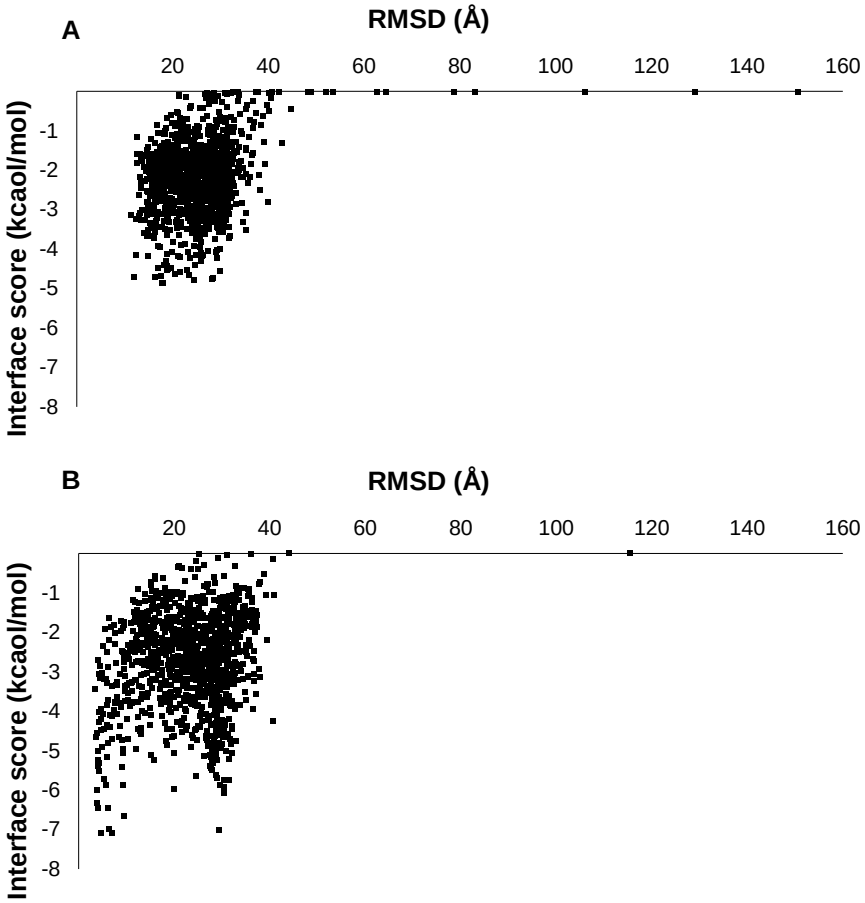

Figure S4 Extended data for modelled interaction between NPC1 and StARD3 (**A**) Initial simulation of NPC1 and StARD3 interaction results in energetically favourable binding poses; some of these align the cholesterol binding regions (see main text). (**B**) Refinement of a selected initial result with (re)built loops generates smaller changes in position and a more favourable energy score.

Table S1 Available stuctures of NPC proteins

Protein, Residues	PDB	Method	Resolution (Å)	Comments	Ref
NPC2 1-130	1nep	X-ray	1.7	Bovine	[14]
NPC2 1-130	2hka	X-ray	1.8	Bovine In complex with cholesterol-O-sulfate	[15]
NPC1 23-247 (NTD)	3gkh	X-ray	1.8	-	[330]
NPC1 23-247 (NTD)	3gki	X-ray	1.8	In complex with cholesterol	[330]
NPC1 23-247 (NTD)	3gkj	X-ray	1.6	In complex with 25-hydroxycholesterol	[330]
NPC1 23-1251	3jd8	cryoEM	4.4	-	[335]
NPC1 390-604 (MLD)	5f1b	X-ray	2.3	In complex with Ebola virus glycoprotein	[468]
NPC1 390-604 (MLD)	5f18	X-ray	2.0	-	[468]
NPC1 392-606 (MLD)	5hns	X-ray	2.5	-	[469]
NPC1 23-1251	5jnx	cryoEM	6.6	In complex with Ebola virus glycoprotein	[335]
NPC1 400-607 (MLD) NPC2 20-152	5kwy	X-ray	2.4	In complex with cholesterol-O-sulfate (in NPC2)	[334]
NPC1 334-1255	5u73		3.4	New designation for 5i31	[331]
NPC1 334-1255	5u74		3.3	New version of 5u73 with sidechains resolved	[338]

Table S2 Protein models used in this work Experimentally determined and model structures are shown; QMEANBrane scores give a measure of quality from good (higher score) to bad (lower score). QMEANBrane output also offers an idea of the position of the protein in the membrane which shows local quality scores from good (blue) to bad (orange).

Protein	Struc -ture	Model based on	Resolu-tion (Å)	QMEAN Brane score	Position in membrane	Ref
NPC1 membrane region	5u74		3.34	-4.23	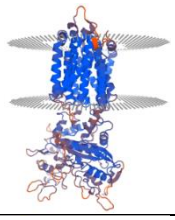	338
NPC1 NTD	3gki		1.8	0.64[a]	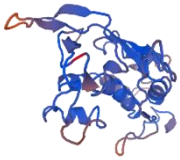	330
NPC2	5kwy		2.41	-0.2 [a]	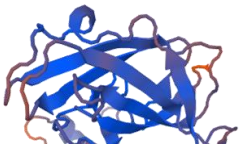	334
StARD3	5i9j		1.74	0.93 [a]	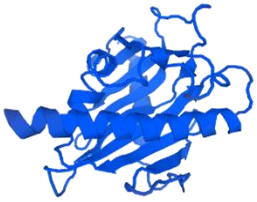	360
ORP5		4ph7 36% identical	2.55	-1.66 [a]	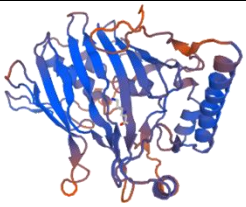	364
BK		5tji 55.7% identical	3.8	-5.85	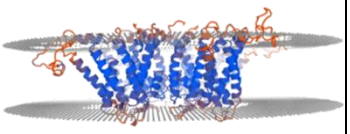	371
TRPML1	5wj9		3.49	-5.08	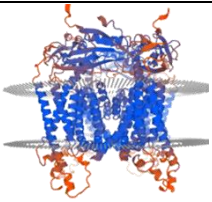	388

Protein	Struc-ture	Model based on	Resolu-tion (Å)	QMEAN Brane score	Position in membrane	Ref
AnxA2	2hyw		2.1	0.48 [a]	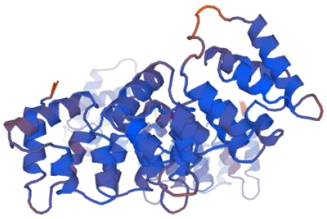	405
AnxA8	1w3w		2.1	0.69 [a]	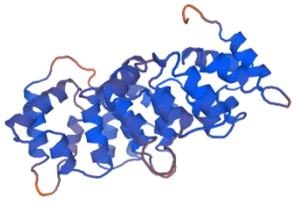	413
Stx7 VAMP8 bundle		3hd7 (Stx7 36.2% identical, VAMP8 35.6% identical)	3.4	-2.87	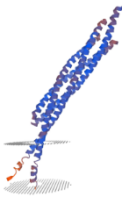	420

Notes: [a] soluble protein, score generated by QMEAN.

Table S3 Particulars of docking procedures In AutoDock the search space is centred on an atom and has a length in points (1 point = 0.375Å) in each of the three spatial dimensions. This space can be moved by the specified offset amounts. While AutoDock holds the protein backbone rigid, it does allow the sidechains of certain residues to be made flexible. The various descriptors of the ligand's relation to the protein (position, orientation, bond angles) and then altered and a certain amount of mixing between different states allowed; hence the procedure is termed a genetic algorithm (GA). For more details on the procedures used to perform docking and calculate the grids used, see.[309,310]

Protein, region	**Grid centre**	**Grid dimensions (points)**	**Grid offsets (points)**	**Residues with flexible sidechains**	**Lipid (number of GA runs)**
NPC1, SSD	Phe779, C_β	x=80 y=76 z=126	x=-7.583 y=5.5 z=7	none	Cholesterol (100) Sphingosine (300)
NPC1, NTD	Asn86, C_α	x=40 y=40 z=60	x=3 y=0 z=0	none	Cholesterol (20) Sphingosine (200)
NPC2	Protein centre	x=80 y=80 z=80	x=0 y=0 z=0	none	Cholesterol (50) Sphingosine (200)
BK, CRAC2	Tyr263, C_α	x=46 y=40 z=60	x=0 y=-2.5 z=3.75	Lys211 Asn265 Tyr263	Cholesterol (300)
TRPML1, Juxta-membrane	Asp114 (chain A), C_Z	x=40 y=50 z=60	x=10 y=-3.75 z=0	Glu276 (chain A) Arg486 (chain D)	Sphingomyelin (300)
TRPML1, agonist	Pro52, C_γ	x=40 y=40 z=40	x=8.5 y=-6.5 z=0	Lys55 Arg61 Lys65 Arg318	$PI(3,5)P_2$, $PI(4,5)P_2$, Sphingomyelin (all 500)
AnxA2	Gly279, C_α	x=60 y=40 z=60	x=0 y=-2.75 z=-2	Lys279 Lys281 Arg284	$PI(4,5)P_2$ (400)
AnxA8	Gly274 C_α	x=50 y=40 z=70	x=0 y=0 z=6	Lys107 Lys112 Arg272	$PI(4,5)P_2$ (400)
Stx7/VAMP8, juxta-membrane 1	Lys62 (VAMP8), C_α	x=60 y=60 z=60	x=4 y=0 z=0	Lys66 (VAMP8) Lys72 (VAMP8) Arg235 (Stx7)	$PI(3,5)P_2$ (600)
Stx7/VAMP8, juxta-membrane 2	Lys161 (Stx7), N_Z	x=54 y=58 z=50	x=-1.5 y=0 z=-1.75	Arg67 (VAMP8) Lys233 (Stx7)	$PI(3,5)P_2$ (400)

Table S4 Details of AutoDock output AutoDock clusters binding poses by RMSD (cut-off > 2.0Å) and orders clusters by binding energy of most favourable member. For each binding experiment the clusters are given with the number of members of each in parentheses. The mean binding energy is given; AutoDock's margin for error is ± 1.5 kcal/mol so clusters with mean energies within this margin are energetically indistinguishable. The status of each cluster (assessed as described in main text) is given. The interacting residues for each cluster are listed along with the position in the LEL membrane. H-bonds were detected by AutoDock, ionic interactions were assumed when oppositely charged groups were within 4Å of each other, the cut-off previously identified. The binding pose from each cluster chosen as representative and shown in the main text is indicated; the difference from the mean binding energy of the cluster (kcal/mol) is given in parenthesis – a negative value indicates more favourable and a positive value less favourable.

Protein, region	**Lipid**	**Cluster (members)[a]**	**Mean binding energy (kcal/mol)**	**Status**	**Position Interactions (side-chain van der Waals unless stated)**	**Member shown in text**
NPC1, SSD	Cholesterol	1 (74)	-9.50	Parallel, favoured	Luminal Asp620 (side-chain, H-bond), Val 621, Val624, Val625, Tyr628, Leu665, Val668, Ile687, Glu688, Pro691	1 (-0.38)
		2 (4)	-9.42	Parallel, favoured	Luminal Ser627 (side-chain, H-bond), Val 621, Val624, Val625, Ala629, Tyr628 Phe632, Ile687, Glu688, Pro691	
		4 (3)	-8.93	Anti-parallel, disfavoured	-	
		5 (7)	-8.51	Parallel, favoured	Cytosolic Ile654, Ile361Ala695, Leu663, Ser655, Cys778, Leu782, Leu785, Asp786 (side-chain, H-bond), Arg789	1 (-0.25)
		6 (10)	-8.25	Anti-parallel, disfavoured	-	
	Sphingosine	1 (115)	-5.67	Parallel, favoured	Luminal Ser627 (backbone, H-bond), Asp620 (side-chain, ionic), Val 621, Val625, Tyr628, Ile687, Glu688, Pro691, Phe1221	1 (-1.36)
		2 (47)	-5.53	Parallel, favoured	Luminal Ser617 (backbone, H-bond), Asp620 (side-chain, ionic), Val 624, Val668, Leu672, Val686, Ile687, Leu682, Glu688, Ile690, Pro691, Phe1221	
		3 (24)	-5.59	Parallel, favoured	Luminal Ser617, Asp620 (side-chain, ionic), Val621, Val 624, Tyr628, Leu665, Val668, Ala669, Glu688 (side-chain, H-bond), Pro691, Phe1221	
		4 (22)	-5.30	Parallel, favoured	Luminal Asp620 (side-chain, ionic), Val621, Val 624, Val625, Tyr628, Phe632, Leu665, Glu688, Pro691, Phe1221	
		5 (5)	-5.26	Parallel, favoured	Luminal Asp620 (side-chain, ionic), Val621, Val 624, Val625, Tyr628, Phe632, Ile687, Glu688, Pro691, Phe1221	
		6 (8)	-4.43	Parallel, favoured	Luminal Asp620, Val 624, Tyr628, Leu665, Ile687, Glu688 (side-chain, H-bond), Pro691, Leu695, Phe1221	

Protein, region	Lipid	Cluster (members)[a]	Mean binding energy (kcal/mol)	Status	Position Interactions (side-chain van der Waals unless stated)	Member shown in text
		7 (5)	-3.99	Anti-parallel, disfavoured	-	
		8 (13)	-4.54	Parallel, favoured	Cytosolic Ile354, Ile361, Ser655, Ile662, Ile663, Leu665, Cys778, Leu785, Asp786, Arg789, Asp796 (side-chain and backbone, H-bonds)	3 (-0.76)
		9 (5)	-4.76	Perpendicular, Disfavoured	-	
		10 (10)	-4.34	Parallel, favoured	Luminal Ser617 (side-chain and backbone, H-bonds), Asp620 (side-chain, H-bond), Val621, Val 624, Val625, Tyr628, Ile687	
		11 (8)	-4.11	Anti-parallel, disfavoured	-	
		12 (9)	-4.39	Parallel, favoured	Luminal Ser617 (side-chain and backbone, H-bonds), Asp618, Val621, Val 624, Tyr628, Phe632, Leu684, Pro691	
		13 (8)	-4.38	Perpendicular, Disfavoured	-	
NPC1, NTD	Cholesterol	1 (18)	-13.11		Asn41 (side-chain H-bond), Gln79 (side-chain, H-bond), Thr82, Leu83, Pro90. Phe108, Thr112, Leu176, Tyr192, Met193, Ala201, Phe203	1 (-0.19)
		2 (2)	-12.18		Out	
	Sphingosine	1 (107)	-7.12		In Glu30 (ionic), Asn41 (side-chain H-bond), Gln79 (side-chain, H-bond), Thr82, Leu111, Thr112, Tyr192, Met193, Ala201, Pro202, Phe203, Ile205	1 (-1.25)
		2 (31)	-6.33		In Asn41 (side-chain H-bond), Thr82, Leu83, Asn86 (side-chain, H-bond), Leu111, Leu176, Met193,Ile205, Phe108, Phe203, Ile205	
		3 (16)	-5.51		Out	
		4 (15)	-5.79		In Leu83, Asn86 (side-chain, H-bond), Leu87, Pro90, Phe106, Thr112, Met193, Tyr192	
		5 (14)	-5.59		Out	
		6 (7)	-5.53		In Leu83, Pro90, Phe108, Thr112 (side-chain, H-bond), Leu176, Met193, Ala201, Pro202, Phe203, Ile205	
		7 (8)	-5.12		Out	
NPC2	Cholesterol	1 (19)	-11.51		Out Leu49, Tyr55, Ser56, Val57, Gly76, Val83, Phe85, Leu113, Pro114, Tyr119, Leu124	1 (-0.11)
		2 (1)	-11.16		In	
	Sphingosine	1 (3)	-4.71		Out Val39, Tyr55, Val57, Val74, Phe85, Leu113, Pro114 (backbone, H-bond), Tyr119 (side-chain, H-bond), Val126, Trp128	
		2 (30)	-3.92		Out	1

Protein, region	Lipid	Cluster (members)[a]	Mean binding energy (kcal/mol)	Status	Position Interactions (side-chain van der Waals unless stated)	Member shown in text
					Val39, Tyr55, Leu113, Pro114, Val115, Tyr119, Pro120 (side-chain, H-bond), Ile122, Val126, Trp128, Trp141	(-1.36)
		3 (40)	-4.46		Out Tyr55, Gly76, Val83, Pro84, Phe85, Leu113, Pro114, Val115, Tyr119, Ile124, Val126, Trp128, Trp141	
		4 (23)	-4.00		In	
		5 (31)	-4.40		Out Tyr55, Val57, Gly76, Val83 (backbone, H-bond), Leu113, Pro114, Val115, Leu124, Val126	
		7 (23)	-4.04		Out Val39, Leu47, Tyr55, Val57, Val74, His75 (backbone, H-bond), Gly76, Phe85, Leu124, Trp128, Val145	
		8 (14)	-3.97		Out Val39, Tyr55, Ser56, Val57, Val74, Gly76, Val83, Pro84 (backbone, H-bond), Phe85, Leu124, Trp141	
BK, CRAC2	Cholesterol	1 (109)	-6.26	Displaced parallel, disfavoured	-	
		2 (72)	-6.05	Parallel, favoured	Lys211 (side-chain, H-bond), Leu215, Val223, Leu226, Val255, Val262, Tyr263, Asn265 (side-chain, H-bond)	22 (-0.27)
		3 (56)	-6.05	Parallel, favoured	Leu215, Val223, Leu226, Val255, Val262 (side-chain, H-bond and van der Waals), Tyr263, Asn265 (side-chain, H-bond)	
		4 (6)	-5.49	Parallel, favoured	Lys211 (side-chain, H-bond), Leu215, Val223, Leu226, Val255, Val262, Tyr263 (side-chain, CH-π)	4 (+0.34)
		5 (3)	-5.57	Perpendicular, disfavoured	-	
		8 (7)	-5.63	Displaced parallel, disfavoured	-	
		9 (5)	-4.68	Anti-parallel, disfavoured	-	
		10 (3)	-4.93	Displaced parallel, disfavoured	-	
		11 (17)	-5.14	Anti-parallel, disfavoured	-	
TRPML1, Juxta-membrane	SM head group	1 (2)	-3.40	Splayed Disfavoured	-	
		2 (2)	-3.04	Anti-parallel, disfavoured	-	
		3 (3)	-2.60	Splayed Disfavoured	-	
		4 (3)	-2.35	Anti-parallel, disfavoured	-	
		6 (2)	-2.53	Anti-parallel, disfavoured	-	
		7 (2)	-3.12	Splayed Disfavoured	-	

Protein, region	Lipid	Cluster (members)[a]	Mean binding energy (kcal/mol)	Status	Position Interactions (side-chain van der Waals unless stated)	Member shown in text
		8 (2)	-3.05	Perpendicular, disfavoured	-	
		9 (8)	-1.41	Anti-parallel, disfavoured	-	
		11 (5)	-2.76	Anti-parallel, disfavoured	-	
		12 (6)	-1.71	Parallel, favoured	Asp114 (side-chain, H-bond), Glu276 (side-chain, ionic), Arg486 (side chain, ionic)	1 (-1.63)
		14 (4)	-2.21	Anti-parallel, disfavoured	-	
		15 (3)	-3.02	Splayed Disfavoured	-	
		16 (2)	-2.71	Perpendicular, disfavoured	-	
		17 (3)	-1.45	Perpendicular, disfavoured	-	
		20 (3)	-1.41	Splayed Disfavoured	-	
		21 (7)	-1.73	Anti-parallel, disfavoured	-	
		22 (2)	-2.50	Splayed Disfavoured	-	
		23 (2)	-1.92	Anti-parallel, disfavoured	-	
		25 (2)	-2.37	Perpendicular, disfavoured	-	
		28 (4)	-1.84	Anti-parallel, disfavoured	-	
		29 (3)	-1.44	Perpendicular, disfavoured	-	
		31 (2)	-2.37	Perpendicular, disfavoured	-	
TRPML1, agonist	$PI(3,5)P_2$ headgroup[c]	1 (27)	-17.40	Parallel, favoured	Lys55 (side-chain, ionic), Arg67 (side-chain, ionic), Lys65 (side-chain, ionic), Arg318 (side-chain, ionic)	
	$PI(4,5)P_2$ headgroup[c]	2 (22)	-19.11	Parallel, favoured	Lys55 (side-chain, ionic), Arg67 (side-chain, ionic), Lys65 (side-chain, ionic), Arg318 (side-chain, ionic)	
	SM headgroup[c]	8 (9)	-6.05	Parallel, favoured	Lys55 (side-chain, ionic), Arg67 (side-chain, H-bond), Lys65 (side-chain, ionic), Arg318 (side-chain, H-bond), Arg322 (side-chain, H-bond)	
AnxA2	$PI(4,5)P_2$ headgroup[d]	1 (1)	-7.82	Parallel, favoured	Lys279 (side-chain, ionic), Lys281 (side chain, ionic and H-bond), Arg284 (side-chain, ionic)	
		2 (4)	-7.07	Parallel, favoured	Lys279 (side-chain, ionic and H-bond), Lys281 (side chain, ionic and H-bond), Arg284 (side-chain, ionic)	
		3 (4)	-4.07	Parallel, favoured	Lys279 (side-chain, ionic and H-bond), Lys281 (side chain, ionic and H-bond; backbone, H-bond), Arg284 (side-chain, ionic)	
		7 (3)	-2.76	Parallel, favoured	Lys279 (side-chain, ionic), Lys281 (side chain, H-bond), Arg284 (side-chain, ionic)	2 (+0.18)
		9 (3)	-3.32	Parallel, favoured	Lys281 (side chain, H-bond;), Arg284 (side-chain, ionic)	

Protein, region	Lipid	Cluster (members)[a]	Mean binding energy (kcal/mol)	Status	Position Interactions (side-chain van der Waals unless stated)	Member shown in text
		10 (2)	-4.36	Splayed, disfavoured	-	
		13 (2)	-4.73	Perpendicular, disfavoured	-	
		15 (4)	-3.48	Splayed, disfavoured	-	
		20 (3)	-3.62	Parallel, favoured	Lys279 (side chain, H-bond) Lys281 (side chain, H-bond), Arg284 (side-chain, ionic)	
		21 (4)	-4.00	Parallel, favoured	Lys279 (side-chain, H-bond), Lys281 (side chain, ionic and H-bond), Arg284 (side-chain, ionic)	
		25 (2)	-3.40	Splayed, disfavoured	-	
		27 (4)	-3.58	Anti-parallel, disfavoured	-	
		38 (2)	-3.37	Perpendicular, disfavoured	-	
		40 (2)	-3.88	Perpendicular, disfavoured	-	
		43 (3)	-3.73	Perpendicular, disfavoured	-	
		44 (3)	-3.31	Perpendicular, disfavoured	-	
		46 (2)	-4.02	Anti-parallel, disfavoured	-	
		50 (3)	-3.55	Perpendicular, disfavoured	-	
AnxA2	SM headgroup	1 (7)	-3.09	Anti-parallel, disfavoured	-	
		2 (3)	-3.34	Anti-parallel, disfavoured	-	
		3 (3)	-3.63	Anti-parallel, disfavoured	-	
		5 (3)	-2.36	Anti-parallel, Disfavoured	-	
		6 (4)	-3.17	Anti-parallel, disfavoured	-	
		8 (2)	-3.39	Perpendicular, disfavoured	-	
		9 (3)	-2.55	Splayed, disfavoured	-	
		1 (7)	-3.09	Anti-parallel, disfavoured	-	
		2 (3)	-3.34	Anti-parallel, disfavoured	-	
		3 (3)	-3.63	Anti-parallel, disfavoured	-	
		5 (3)	-2.36	Splayed, disfavoured	-	
		6 (4)	-3.17	Anti-parallel, disfavoured	-	
		8 (2)	-3.39	Splayed, disfavoured	-	
		9 (3)	-2.55	Anti-parallel, disfavoured	-	
		10 (3)	-2.83	Anti-parallel, disfavoured	-	

Protein, region	Lipid	Cluster (members)[a]	Mean binding energy (kcal/mol)	Status	Position Interactions (side-chain van der Waals unless stated)	Member shown in text
AnxA8	$PI(4,5)P_2$ headgroup	1 (4)	-10.96	Parallel, favoured	Lys107, Lys112, Arg272 (all electrostatic), Thr275 (sidechain H-bond)	
		2 (5)	-9.38	Parallel, favoured	Lys107, Lys112, Arg272 (all electrostatic), Leu109 (backbone H-bond)	
		3 (9)	-8.51	Parallel, favoured	Arg85, Lys112, Arg272 (all electrostatic), Lys107 (side chain H-bond)	
		4 (6)	-9.29	Parallel, favoured	Arg85, Lys107, Lys112, Arg272 (all electrostatic)	
		5 (3)	-7.60	Anti-parallel, disfavoured	-	
		6 (15)	-8.83	Parallel, favoured	Arg85, Lys107, Lys112, Arg272 (all electrostatic)	2 (-1.58)
		8 (4)	-9.65	Parallel, favoured	Arg85, Lys107, Lys112 (all electrostatic), Arg272 (electrostatic and sidechain H-bond)	
		10 (7)	-8.89	Anti-parallel, disfavoured	-	
		11 (6)	-9.22		Lys107, Lys112, Arg272 (all electrostatic), Leu109 (backbone H-bond)	
Stx7/VAMP8, juxta-membrane 1	$PI(3,5)P_2$ headgroup	1 (10)	-10.56	Parallel, favoured	Lys68 (VAMP8, side-chain, electrostatic and H-bond), Lys72 (VAMP8, side-chain, electrostatic), Arg235 (Stx7, side-chain, electrostatic and H-bond)	2 (-2.15)
		2 (3)	-11.58	Parallel, favoured	Lys68 (VAMP8, side-chain, electrostatic), Lys72 (VAMP8, side-chain, electrostatic and H-bond), Arg235 (Stx7, side-chain, electrostatic and H-bond)	
		3 (5)	-9.99	Parallel, favoured	-	
		4 (5)	-10.70	Parallel, favoured	Lys68 (VAMP8, side-chain, electrostatic), Lys72 (VAMP8, side-chain, electrostatic and H-bond), Arg235 (Stx7, side-chain, electrostatic)	
		5 (2)	-12.97	Anti-parallel, disfavoured	-	
		6 (2)	-13.46	Anti-parallel, disfavoured	-	
		7 (6)	-9.83	Anti-parallel, disfavoured	-	
		8 (6)	-10.60	Anti-parallel, disfavoured	-	
		9 (10)	-9.94	Anti-parallel, disfavoured	-	
		10 (7)	-10.50	Anti-parallel, disfavoured	-	
		11 (8)	-9.91	Anti-parallel, disfavoured	-	
		12 (4)	-10.10	Parallel, favoured	Lys68 (VAMP8, side-chain, electrostatic), Lys72 (VAMP8, side-chain, electrostatic and H-bond), Arg235 (Stx7, side-chain, electrostatic and H-bond)	
		14 (8)	-10.00	Perpendicular, disfavoured	-	

Protein, region	Lipid	Cluster (members)[a]	Mean binding energy (kcal/mol)	Status	Position Interactions (side-chain van der Waals unless stated)	Member shown in text
		15 (2)	-11.20	Parallel, favoured	Lys68 (VAMP8, side-chain, electrostatic), Lys72 (VAMP8, side-chain, electrostatic), Arg235 (Stx7, side-chain, electrostatic and H-bond)	
		17 (6)	-9.97	Perpendicular, Disfavoured	-	
		18 (6)	-8.82	Anti-parallel, disfavoured	-	
		19 (6)	-11.93	Parallel, favoured	Lys68 (VAMP8, side-chain, electrostatic), Lys72 (VAMP8, side-chain, electrostatic), Arg235 (Stx7, side-chain, electrostatic)	
		20 (3)	-10.36	Parallel, favoured	Lys68 (VAMP8, side-chain, electrostatic), Lys72 (VAMP8, side-chain, electrostatic), Arg235 (Stx7, side-chain, electrostatic)	
		22 (4)	-9.91	Parallel, favoured	Lys68 (VAMP8, side-chain, electrostatic and H-bond), Lys72 (VAMP8, side-chain, electrostatic), Arg235 (Stx7, side-chain, electrostatic and H-bond)	
		23 (3)	-10.91	Perpendicular, disfavoured	-	
		24 (6)	-9.48	Parallel, favoured	Lys68 (VAMP8, side-chain, electrostatic), Lys72 (VAMP8, side-chain, electrostatic), Arg235 (Stx7, side-chain, electrostatic and H-bond)	
		25 (7)	-8.68	Parallel, favoured	Lys68 (VAMP8, side-chain, electrostatic), Lys72 (VAMP8, side-chain, electrostatic and H-bond), Arg235 (Stx7, side-chain, electrostatic and H-bond)	
		26 (5)	-9.97	Parallel, favoured	Lys72 (VAMP8, side-chain, electrostatic), Arg235 (Stx7, side-chain, electrostatic)	
		28 (2)	-11.04	Perpendicular, disfavoured	-	
		30 (9)	-9.21	Perpendicular, disfavoured	-	
		31 (4)	-9.16	Perpendicular, disfavoured	-	
		32 (5)	-9.20	Parallel, favoured	Lys68 (VAMP8, side-chain, electrostatic), Lys72 (VAMP8, side-chain, electrostatic), Arg235 (Stx7, side-chain, electrostatic)	
Stx7/VAMP8, juxta-membrane 2[f]	$PI(3,5)P_2$ headgroup	1 (8)	-3.37	Perpendicular, disfavoured	-	
		2 (2)	-4.75	Parallel, favoured	Arg67 (VAMP8, side-chain, electrostatic), Lys233 (Stx7, side-chain, H-bond)	
		3 (4)	-2.75	Parallel, favoured	Arg67 (VAMP8, side-chain, electrostatic), Tyr230 (Stx7, side-chain, H-bond), Lys233 (Stx7, side-chain, electrostatic and H-bond)	1 (-2.50)
		4 (18)	-2.20	Antiparallel, disfavoured	-	
		5 (12)	-1.92	Parallel, favoured	Lys233 (Stx7, side-chain, electrostatic)	
		6 (4)	-2.76	Antiparallel, disfavoured	-	

Protein, region	Lipid	Cluster (members)[a]	Mean binding energy (kcal/mol)	Status	Position Interactions (side-chain van der Waals unless stated)	Member shown in text
		7 (8)	-2.23	Antiparallel, disfavoured	-	
		8 (6)	-2.45	Perpendicular, disfavoured	-	
		9 (8)	-2.69	Perpendicular, disfavoured	-	
		10 (5)	-3.41	Perpendicular, disfavoured	-	
		11 (4)	-3.30	Perpendicular, disfavoured	-	
		12 (3)	-2.99	Parallel, favoured	Lys233 (Stx7, side-chain, electrostatic and H-bond)	
		13 (12)	-2.65	Perpendicular, disfavoured	-	
		14 (6)	-2.87	Parallel, favoured	Lys233 (Stx7, side-chain, electrostatic)	
		17 (3)	-3.68	Parallel, favoured	Lys233 (Stx7, side-chain, electrostatic)	
		19 (4)	-3.41	Antiparallel, disfavoured	-	
		20 (10)	-1.62	Antiparallel, disfavoured	-	
		21 (6)	-1.97	Perpendicular, disfavoured	-	
		22 (6)	-2.49	Parallel, favoured	Arg73 (VAMP8, side-chain, electrostatic), Lys233 (Stx7, side-chain, electrostatic)	
		23 (2)	-2.46	Perpendicular, disfavoured	-	
		24 (4)	-2.28	Parallel, favoured	Asn73 (VAMP8, side-chain, H-bond), Lys233 (Stx7, side-chain, electrostatic and H-bond)	
		25 (3)	-1.95	Antiparallel, disfavoured	-	
		26 (16)	-2.00	Parallel, favoured	Asn73 (VAMP8, side-chain, H-bond), Lys233 (Stx7, side-chain, electrostatic)	
		27 (10)	-2.16	Perpendicular, disfavoured	-	
		28 (2)	-3.45	Perpendicular, Disfavoured	-	
		29 (12)	-2.54	Perpendicular, Disfavoured	-	
		30 (4)	-2.03	Perpendicular, disfavoured	-	

Notes: [a]Docking experiments generally produce a long 'tail' of small clusters with less favourable binding energies. These are omitted as are clusters with only 1 member. [b]The smaller size of the clusters aligned to the cytosolic face relative to those aligned to the luminal face is likely a consequence of the larger size of the luminal binding pocket. When cholesterol is positioned randomly at the start of the calculation run it is more likely to be close to the luminal pocket. The energetic favourability of binding poses aligned to the cytosolic face was confirmed by independent docking experiments using ROSIE-Rosetta software (rosie.rosettacommons.org/ligand_docking, data not shown). [c]Data given for the most energetically favourable and biologically plausible cluster only. [d]Increasing the RSMD cut-off to 4.0Å dramatically reduced the number of clusters but clustered some antiparallel binding poses together with parallel ones (data not shown). [e]An abbreviated list of results is shown due to the diffuse nature of the clustering and that many of the clusters have indistinguishable interactions. [f]RSMD cut-off of 2.5Å was used.

3

Lysosomes

Chapter 1 introduced Niemann-Pick type C disease (NPCD) as most frequently originating with dysfunction of NPC1, a protein of late endosomes and lysosomes, and consequently featuring widespread errors of the endocytic system. Chapter 1 also questioned whether the traditional role of NPC1 and its partner NPC2 as mediating cholesterol export from the lysosome is their main or only function. Chapter 2 provided evidence that these proteins may also export sphingosine. This chapter attempts to connect those two strands of thought by examining endocytic dysfunction in NPCD cells and asking if this can be corrected in a way that mimics the correction of faulty sphingosine export.

Introduction

Measuring the functions of the endocytic system

Perhaps the most widely known feature of the endocytic system is the acidic pH of the lumen of the lysosome, the key degradative organelle. Quantifying this acidity, however, proves less easy, especially in the context of NPCD. One approach is to use acridine orange[73,470,471] which undergoes a pH-dependent colour change but the behaviour of this probe can also be affected by cholesterol levels[472] making its use in NPCD problematic. LysoTracker red (Figure S1) is a useful probe for labelling acidic organelles by virtue of its weakly basic nature (pKa = 7.5[473]). The same property ensures, however, that it is almost fully protonated at all pH values below *ca.* 6.5 meaning it is likely insensitive to any lysosomal pH changes thus rendering results, including from NPCD cells,[474] difficult to interpret. Both acridine orange and LysoTracker red diffuse freely through membranes; their basicity means they become protonated in acidic organelles and so are trapped inside as the resulting positive charge stops their free diffusion. An alternative approach is to use pH probes conjugated to dextrans,[54,73,475] polysaccharides which are internalised through the endocytic pathway. Such probes access cells in a given time period (the 'pulse' time) and are then 'chased' into cells for the time required to localise them correctly. The trouble is that lysosomal storage disorders (LSDs) like NPCD feature delayed endocytosis – colloquially referred to as a traffic jam[45,476] – meaning that defining the chase time is not easy. This difficulty means that it is perfectly possible for dextran probes to measure a subtly different compartment in control compared with disease cells. This complication becomes yet more apparent in the light of recent

work which suggests that, rather than being homogeneous, the cell's population of lysosomes contains differing sub-groups.[441,477,478] Ideally then, we require a lysosomal pH probe which is lipid-insensitive, sub-population specific, and that works across the relevant pH range. Such probes have only recently been reported[441,479] and are not commercially available making compromise inevitable. The present work used LysoSensor yellow/blue (Figure S1),[480] a freely diffusing probe which protonates in acidic compartments (and consequently remains trapped there) and fluoresces at two wavelengths – the ratio of the intensities correlates with pH in the range 3-7.5. In comparison with these virtues its disadvantages are minor: various experimental parameters must be carefully controlled,[481] and simultaneous measurement of all acidic organelles is unavoidable. This second fact means that this chapter refers to endolysosomes (ELs) to signify the totality of the endocytic acidic compartment.

LysoSensor yellow/blue as the best compromise pH probe

Other assays of the functions of the endocytic system are subject to less ambiguity. Thus LysoTracker red (Figure S1) can be used to label all acidic organelles and thereby assess the size of the endolysosomal compartment. BODIPY-LacCer (Figure S1) is a lipid labelled with a fluorescent tag which inserts into the outer leaflet of the cell's plasma membrane. Pulse-chase experiments transport the marker, and therefore the fluorescence, to the preferred destination of its carrier lipid, in this case the Golgi via a pathway dependent on NPC1, rab7 and -9 and TRPML1.[41,391] Examining cells for the location of the fluorescence thus gives a measure of any delay in the endocytic process.

Whilst the obvious platform for studying NPCD at the cellular level is to use cells obtained from patients a pharmacological approach is also popular. This involves the use of U18666a (Figure S2), a blocker of NPC1[112,482] which is likely to be trapped in lysosomes by virtue of its weakly basic nature.

Results and Discussion

Defining the endocytic defects in NPCD

U18666a has traditionally been used at concentrations in the low micromolar range. In mouse RAW macrophages this treatment gave an endolysosomal pH of 6.3±0.4, significantly higher than the control value of 5.3±0.2 (Figure 1A) and consistent with a previous report in baby hamster kidney cells.[475] However a lysosome with a luminal pH of 5 will have an H^+ concentration of ca. 10μM so the alkalinising effect of 5μM U18666a could be attributed to simple acid-base chemistry. Indeed 9 basic

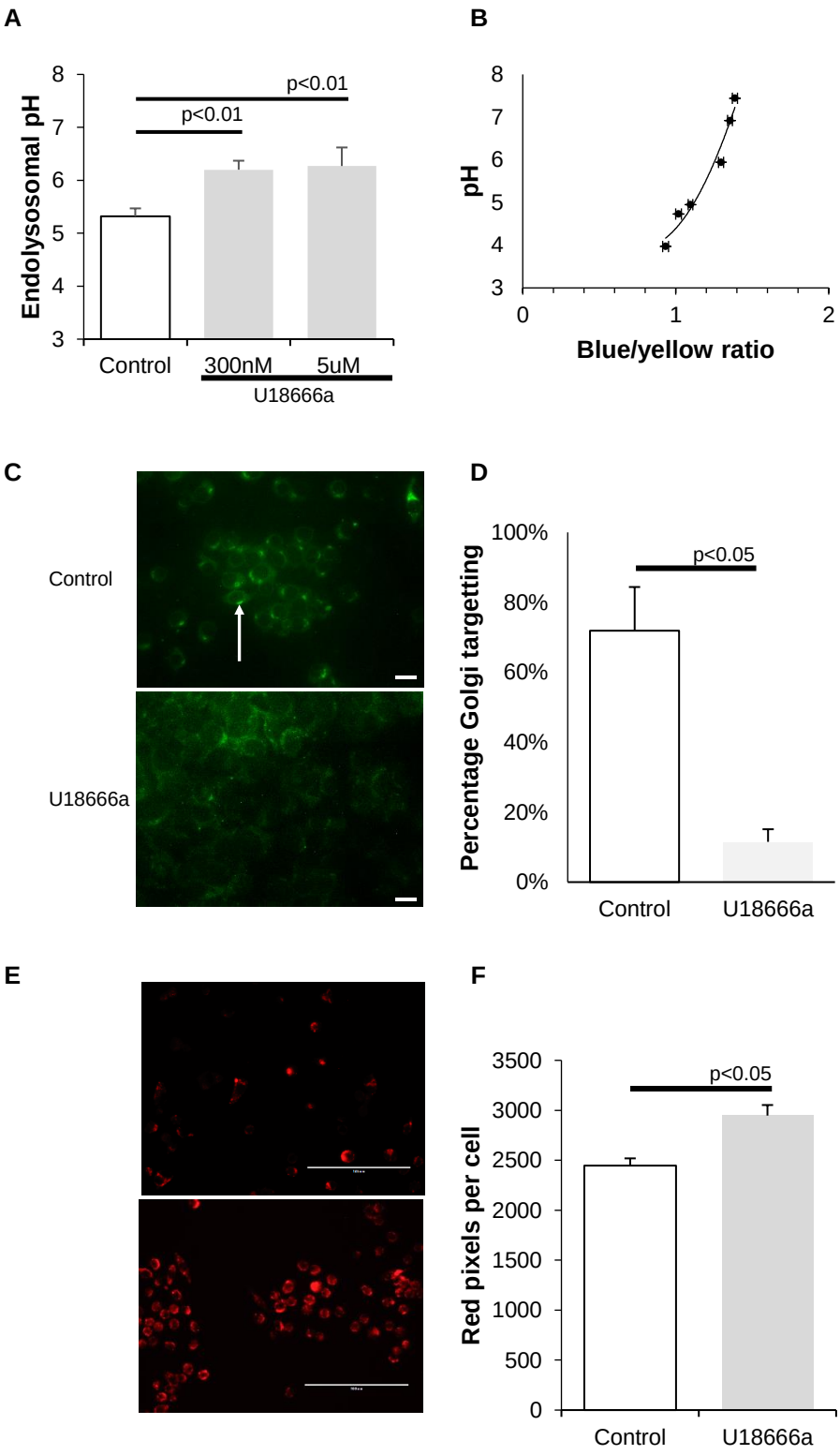

Figure 1 Effect of U18666a treatment on RAW cells (**A**) U18666a at a dose of either 5µM or 300nM induces increases in endolysosomal pH; results are the mean ± SEM of at least 4 independent experiments. (**B**) Correlation curve for LysoSensor yellow/blue in RAW cells; points are mean ± SEM from independent experiments (n=24, r^2=0.965). (**C**) Representative images of BODIP-LacCer endocytosis in RAW cells; scale bar 10µm. (**D**) Quantitation of Golgi targeting; results are mean ± SD from at least 2 independent experiments examining at least 150 cells per experiment. (**E**) Representative images for LysoTracker experiments in RAW cells (**F**) Quantitation of acidic compartment volume; results are mean ± SEM of at least 3 independent experiments examining at least 100 cells per experiment.

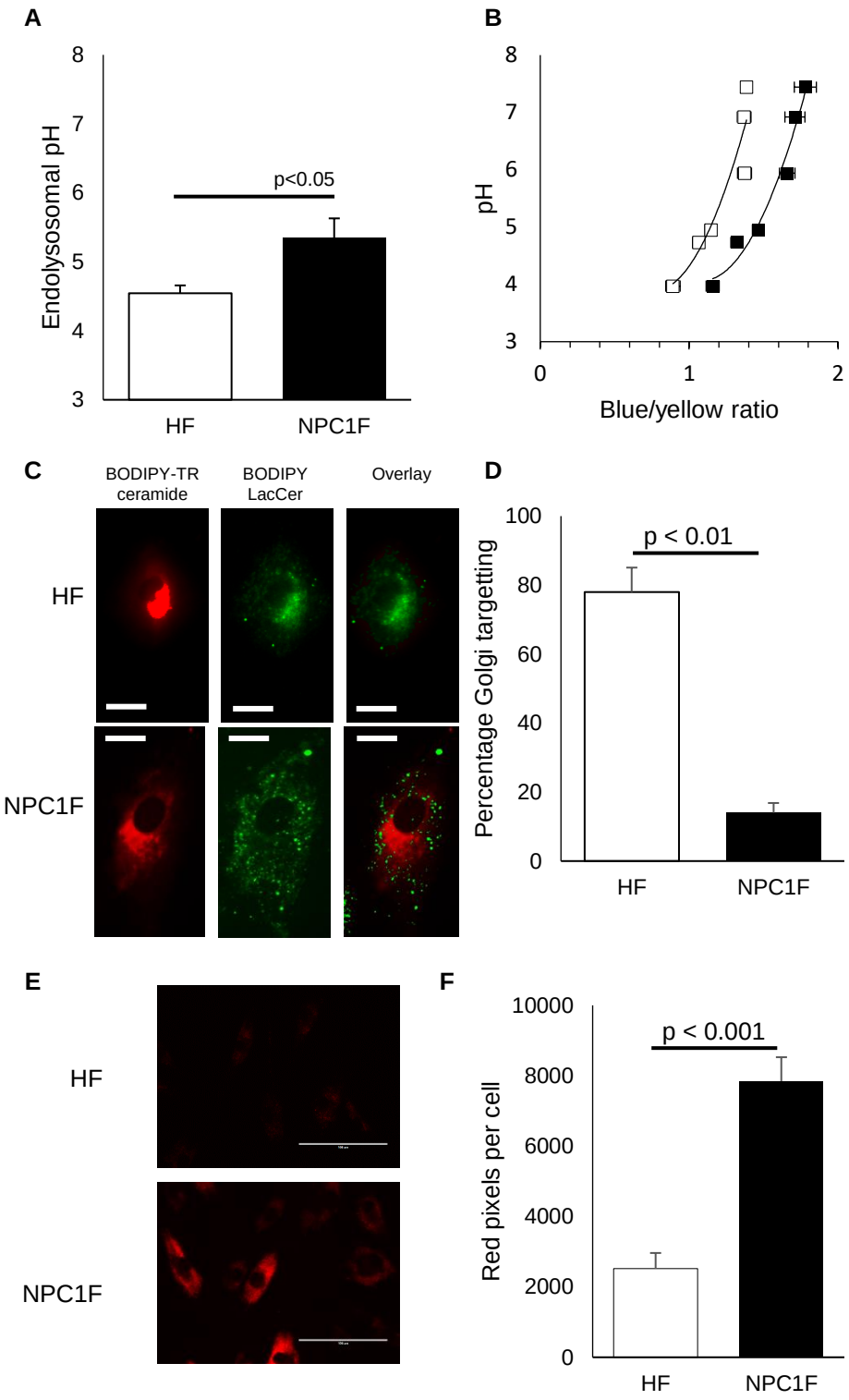

Figure 2 Endolysosomal defects in NPCD (**A**) Endolysosomal pH is increased in NPCD; results are the mean ± SEM of at least 4 independent experiments. (**B**) Correlation curve for LysoSensor yellow/blue in fibroblasts under various conditions with non-significant differences between datasets; points are mean ± SEM from independent experiments (for HF (white squares) n=6, r^2=0.89, for NPC1F (black squares) n=8, r^2=0.97). (**C**) Representative images of BODIPY-LacCer endocytosis in fibroblasts; scale bar 10µm. (**D**) Quantitation of Golgi targeting; results are mean ± SD from at least 2 independent experiments examining at least 90 cells per experiment. (**E**) Representative images for LysoTracker experiments in fibroblasts (**F**) Quantitation of acidic compartment volume; results are mean ± SEM of at least 3 independent experiments examining at least 30 cells per experiment.

drugs used at a dose of 10μM all induced a lysosomal storage disorder (LSD)-like phenotype[483] (possibly involving calcium and mTOR[484]). This was despite the drugs having a diversity of chemical structures and none of them resembling U18666a making it highly unlikely that they would all bind to NPC1. Thus potentially highly significant is the finding that U18666a inhibits lysosomal cholesterol export with a potency in the sub-micromolar range (while LDL degradation remains normal).[482] At such a dose the numerous off-target effects[485–487] of U18666a are eliminated or reduced as confounding factors; perhaps more significantly a dose of around 300nM would be insufficient to neutralise an H+ concentration of 10μM

Treatment of RAW cells with 300nM U18666a gave a pH increase indistinguishable from that seen with the higher concentration (Figure 1A). Some previous work suggests that correct acidification is necessary for the successful completion of endocytosis.[37,38] Thus pulse-chase experiments with BODIPY-LacCer, a Golgi-targeted marker[41] showing green fluorescence, were performed RAW cells and the proportion of cells where a fluorescently labelled Golgi could be seen was quantitated. This proved considerably reduced on treatment with 300nM U18666a (Figure 1C for typical images (Golgi indicated by white arrow) and D for quantitation). LSDs are often marked by a proliferation of the endocytic compartment which can be visualised by LysoTracker red[488] and quantitated by counting red pixels – for full details see Materials and Methods. Treatment of RAW cells with 300nM U18666a effectively simulated this disease phenotype (Figure 1E for typical images and F for quantitation).[f]

Cells deficient in NPC1 show increased endolysosomal pH, an endocytic delay and an expansion of the endolysosomal volume

When fibroblasts from patients deficient in NPC1 (denoted NPC1F, see Table S1) were examined all the features found in the drug induced phenotype were again observed. Thus endolysosomal pH in control fibroblasts (denoted HF) was found to be 4.5±0.1 in line with previously reported values obtained with LysoSensor yellow/blue[489,490] while in NPC patient fibroblasts this increased to 5.4±0.3 (Figure 2A). This is in contrast to previous reports that NPCD does not change endolysosomal pH[54,73,470,474] though these accounts may suffer from the methodological flaws discussed earlier. (After this work was completed other reports emerged of increased endolysosomal pH in NPCD disease models.[43,72,441]) The delay in appearance of BODIPY-LacCer fluorescence at the Golgi was also observed: the percentage of cells showing a clear Golgi after 90 minutes chase was reduced from 78% in healthy cells to 13% in cells deficient in NPC1 (Figure 2C and D). Consistent

[f] These experiments were performed by my colleague Meenakshi Bhardwaj; I am grateful for the use of her data.

with previous reports of NPCD[491,492] and indeed other lysosomal storage disorders (LSDs)[488] the LysoTracker red assay showed an increase in the size of the acidic compartment in NPC1-deficient fibroblasts (Figure 2E for typical images, 2F for quantitation).

Does cholesterol accumulation increase endolysosomal pH?

Given that NPCD lysosomes accumulate cholesterol an obvious hypothesis to explain the pH increases is that the lipid inhibits the vATPase proton pump responsible for acidifying the lysosomes. This multi-subunit protein associates with lipid rafts,[475,493,494] areas of high cholesterol concentration (see Chapter 2, Figure 3 and accompanying discussion), while the lysosome has both the lowest amount of cholesterol and the most acidic pH of all the endocytic vesicles.[495] Furthermore a photo-activatable tritiated cholesterol analogue labelled the c subunit of vATPase.[332] Each assembly has 10 of these subunits arranged in a rotating ring[496] (grey in Figure 3) and the Glu139 residue co-operates with Arg735 on the a subunit (blue in Figure 3) to move the proton into the lysosomal lumen.[36] The c subunit has been identified as the location of the binding site for almost all known inhibitors of vATPase whose interaction has been studied at the molecular level. This includes three natural product families the conconamycins,[497] bafilomycins[498] and archazolides,[499] a synthetic conconamycin analogue[500] and an inhibitory protein.[501] The inhibitors salicylihalamide[502] and apicularen[503] are exceptions to this pattern, though the apicularen binding site is partially on subunit c and partially on subunit a. Thus a model was built (for details see Materials and Methods) of the decameric c ring of human vATPase based on the recently disclosed cryoEM structure of a yeast homologue (PDB:5tj5, 70% identical).[496] This proved of acceptable quality (see Table S3) with a higher score than an alternate model based on the x-ray structure of a bacterial protein[504] (data not shown). Docking of the inhibitor archazolide gave results consistent with those previously reported[505] increasing confidence in the model (data not shown).

Attempted docking of cholesterol at a CARC motif (Arg126-Leu133) with the arginine sidechain allowed to be flexible indeed uncovered energetically favourable binding modes (Figure 3B) consistent with the localisation of this protein assembly to lipid rafts. A similar tactic with Lys155 delivered similar results (Figure 3B). However neither set of binding poses covers Glu139 – as the inhibitor archazolide does[499] – and so this residue remains free to collect the proton to be pumped into the lysosome. Thus it is questionable whether such binding would be inhibitory. Some binding poses were found with the cholesterol covering Glu139 and lying

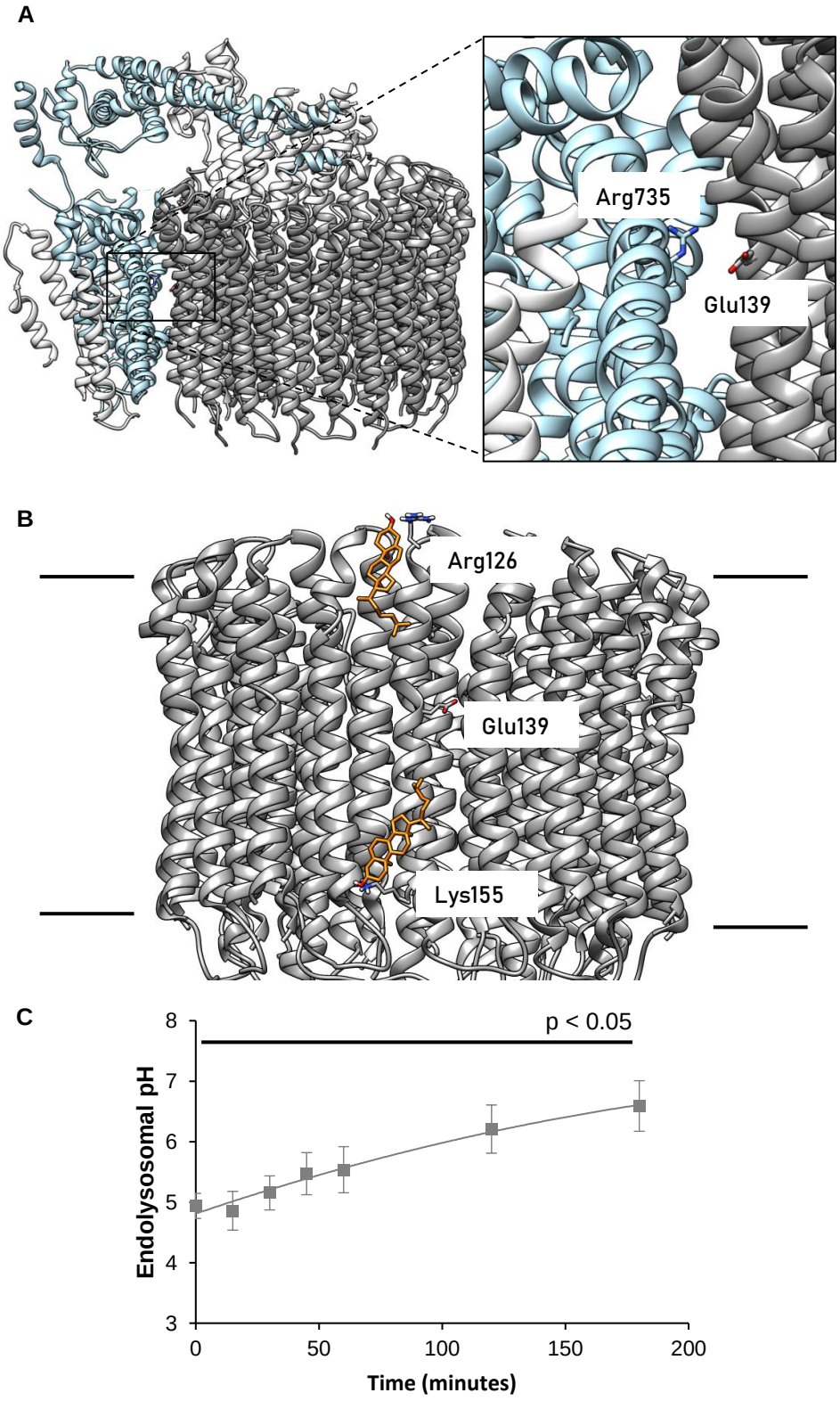

Figure 3 Cholesterol is unlikely to account for the acidification defect in NPC1 cells (**A**) Structure of the *S. cerevisiae* vATPase (PDB: 5tj5[496]); decameric c subunit ring in grey, a subunit in blue, other subunits in white; key residues for proton transport shown. (**B**) Cholesterol docking poses are unlikely to impede proton pumping. (**C**) Incubation of RAW cells with 300nM U18666a gives a pH increase in 2.25 hours, quicker than cholesterol accumulates under identical conditions ($r^2 = 0.979$).

perpendicular to the bilayer (data not shown). While such an orientation is possible its probability is low in thick membrane regions such as the rafts where vATPase resides.[325] Thus direct inhibition of vATPase by cholesterol seems unlikely to be responsible for the pH defect in NPC1-deficient cells.

Accumulating cholesterol is unlikely to be responsible for the pH defect in NPC1-deficient cells

In vitro studies led to the same conclusion. Thus when RAW cells were treated with 300nM U18666a an increase in endolysosomal pH was apparent almost immediately (Figure 3C); after 2.25hours the value had reached 6.6±0.4 ($p<0.05$ versus untreated), a value indistinguishable from the 16 hour incubation (Figure 1A). Previous studies in the same cell line had shown that U18666a begins to stimulate cholesterol accumulation only after 4 hours[54] suggesting that this lipid is not responsible for the endolysosomal pH increase. As it appeared difficult to follow the pathological steps of NPCD from protein dysfunction to increased endolysosomal pH a different approach was tried.

Can endolysosomal defects be repaired?

In chapter 1 we encountered NB-DNJ (miglustat, Zavesca®, Figure S2), approved in Europe for the treatment of NPCD and an inhibitor of GBA2 the enzyme that breaks down glucosylceramide on the cytosolic leaflet of membranes ('cytosolic GlcCer,' Chapter 1, Figure 4B, stage ⓯).[248] Miglustat features a 4-carbon chain attached to the ring nitrogen atom (Figure S2). Reasoning that GBA2 acts on a membrane bound lipid led to the idea that increasing the length of this chain would incorporate the inhibitor into membranes and so increase its effective concentration at the site of action. This tactic led to AMP-DNJ (Figure S2),[249] a compound with greater GBA2 potency than miglustat (1nM compared with 5-300nM[248]), though some loss of selectivity over GlcCer synthase (GCS, IC50 150nM versus 20-50μM[248]) and lysosomal hydrolase GBA1[248] (Chapter1, Figure 4, stages ❺ and ❾, IC50 50-200nM versus 400-500μM[248]). (This is consistent with the success of the same tail-lengthening tactic in preparing GBA1 inhibitors.[506] Unfortunately neither study performs a lipophilic ligand efficiency analysis,[507,508] which can sometimes unmask phantom inhibitory potency, eg.[509] In any case assessing inhibitory potency against these enzymes is difficult.[248,510,511]) AMP-DNJ rather than miglustat was selected for use in this study[g] as its greater potency is likely to reduce off-target effects and its efficacy in a mouse model of NPCD has been demonstrated.[250] It also has lower potency than miglustat at ERGluII (ca. 200μM[249] compared with 5-13μM[512,513]);

[g] I am indebted to the laboratory of Prof Johannes Aerts (Universiteit Leiden) for a gift of a generous sample of this material prepared as previously described.[249,682]

Inhibitory activities at instestinal glucosidases have not been reported for either compound, though annecdotally GI side-effects are a common reason for discontinuing miglustat treatment.

Wider considerations supported the investigation of sphingolipids, which accumulate in this disease,[43,61] as having a role in pathology and indeed normal physiology. (Sphingolipid (SL) metabolism was introduced in chapter 1 (Figure 4) including the elaboration to glycosphingolipids (GSLs). Drugs which act on this pathway are shown in Figure S2 and detailed in Table S3.) Endolysosomal acidification has been found to be controlled by glycolipids in neurons,[514] melanocytes,[515] plant vacuoles,[516] and *C. elegans*.[517] It is increasingly apparent that aberrant lysosomal GlcCer in Gaucher disease, another LSD, is associated with elevated endolysosomal pH.[518–521]

Following precedent[522,523] 20nM was selected as the dose of AMP-DNJ. This treatment indeed reduced the aberrant endolysosomal pH of NPC1 cells from 5.4±0.3 to 4.5±0.2 (Figure 4A). When normal fibroblasts were subjected to the same treatment the endolysosomal pH also reduced to 4.1±0.1 (Figure 4A). This dose also restored disrupted BODIPY-LacCer targeting in NPC1Fs (Figure 4B); Golgi targeting of this fluorescent lipid in healthy cells was not affected (data not shown). These findings are consistent with previous work linking endolysosomal pH with endocytic trafficking[37,38] and with previous experiments in Gaucher disease where inhibiting GlcCer synthase gave aberrant trafficking which was repaired by specifically replenishing cytosolic GlcCer by adding GlcSph.[524] In contrast, treatment of NPC1Fs with various concentrations of AMP-DNJ did not repair the defect in endolysosomal volume as measured by LysoTracker Red (Figure 4C).[h] This is at odds with findings using B-lymphocytes from patients treated with miglustat[243,492] where the volume of the acidic compartment, measured with LysoTracker red, was increased in untreated patients and normalised on therapy. This disparity may reflect a cell type difference or may be indicative that the effect is chronic (the miglustat studies used time points of days to weeks while this work used 24 hours). The possibility that miglustat and AMP-DNJ have subtly different pharmacologies is less probable but cannot be excluded. That AMP-DNJ corrects the acidification of the endolysosomal compartment when taken as a whole, while leaving endosomal proliferation unaffected, suggests that this drug increases acidification of endocytic organelles.

GBA2 inhibition repairs some, though not all, endocytic defects in NPC1-deficient cells

[h] These experiments were conducted by BSc student Lukasz Stolarczyk under my supervision; I thank him for his efforts.

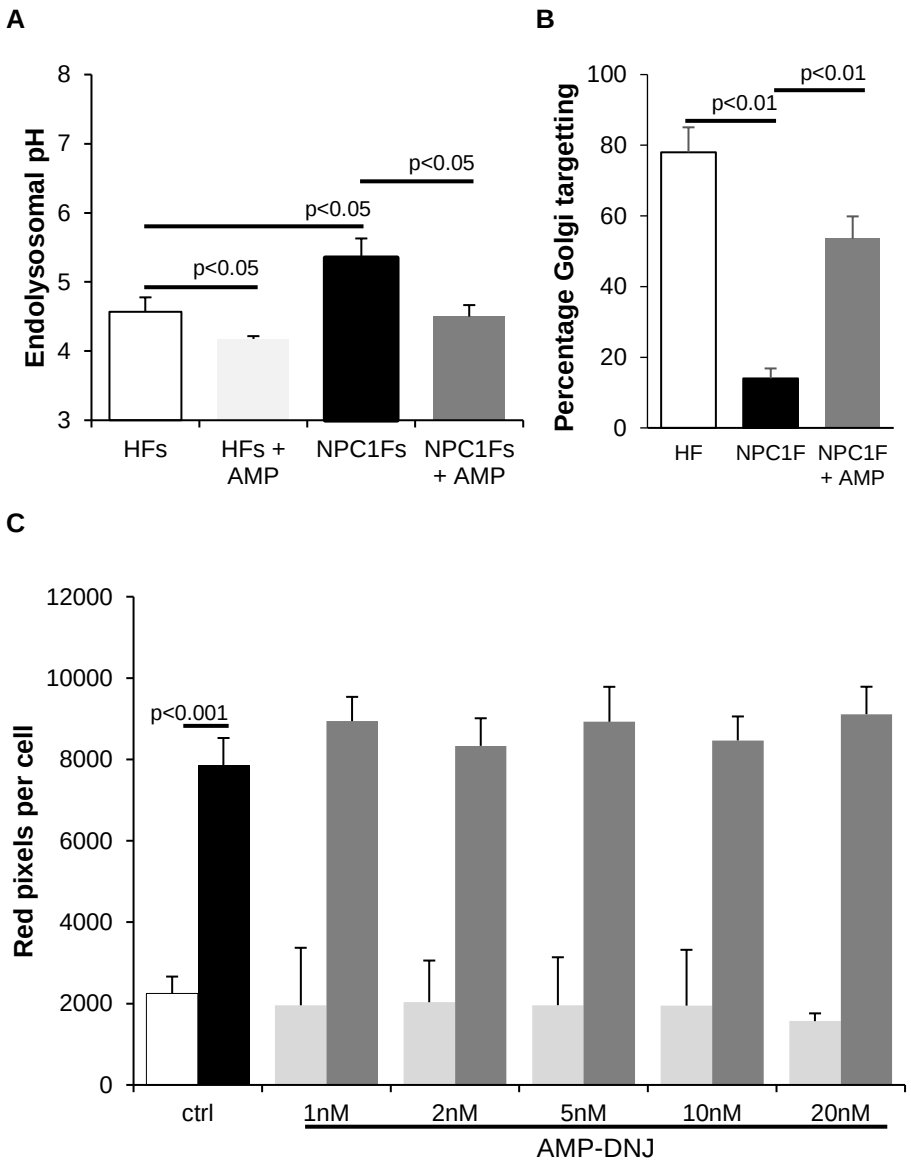

Figure 4 Effect of AMP-DNJ on some endolysosomal parameters (**A**) 20nM AMP-DNJ reduces endolysosomal pH in both healthy and NPC1 deficient cells; results are the mean ± SEM of at least 4 independent experiments. (**B**) 20nM AMP-DNJ repairs mistargeting of BODIPY-LacCer in NPC1 deficient cells. (**C**) 1-20nM AMP-DNJ does not correct increased endolysosomal volume in NPC1 deficient cells; results are the mean ± SEM of 4 independent experiments. White bars represent untreated healthy cells, black represent disease; light grey bars represent treated healthy cells, dark grey treated disease.

Increasing GlcCer on the cytosolic face of membranes reduces endolysosomal pH in both healthy and NPCD cells

Confirmation that the pH effect was dependent on the cytosolic pool of GlcCer was sought by using brefeldin A (Figure S2) which merges the ER and Golgi thus co-localising ceramide and GlcCer synthase (Chapter 1, Figure 4) thereby increasing cytosolic GlcCer.[525] In fibroblasts this tactic delivered similar reductions in endolysosomal pH in both control and disease cells (4.5±0.1 to 4.2±0.1 for control, 5.4±0.3 to 4.6±0.1 for disease cells) as had been observed with AMP-DNJ (Figure 5A). To exclude the possibility of off-target pharmacology endolysosomal pH was also measured in a near-haploid chronic myelogenous leukaemia cell line (HAP1

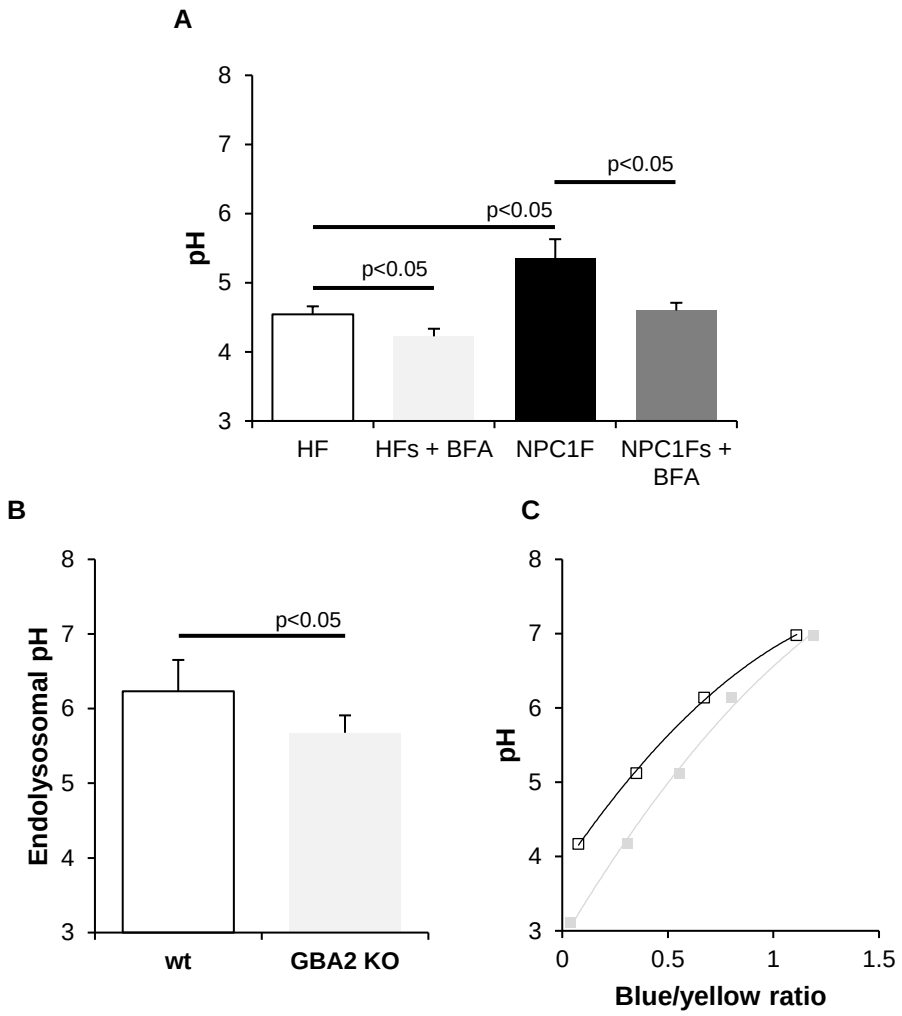

Figure 5 Confirming the effect of cytosolic GlcCer on endolysosomal pH (**A**) Brefeldin A reduces endolysosomal pH in healthy and disease fibroblasts; results are the mean ± SEM of at least 3 independent experiments. (Correlation curves as Figure 2B.) (**B**) GBA2 KO in HAP cells reduces endolysosomal pH ; results are mean ± SEM of 4 independent experiments. (**C**) Sample correlation curve for LysoSensor yellow/blue in wt HAP cells (white squares, r^2=0.999) and GBA2 KO cells (grey squares, r^2=0.997). White bars represent untreated healthy cells, black represent disease; light grey bars represent treated healthy cells, dark grey treated disease.

cells).[i] Consistent with previous results, CRISPR genetic knockout of GBA2 led to a decrease in endolysosomal pH (Figure 5B).

How does cytosolic GlcCer acidify endolysosomes?

Given that increasing cytosolic GlcCer uniformly led to increased endolysosomal acidification it was postulated that this lipid could activate vATPase the lysosomal proton pump. Previously activation of this potein complex has been found to depend

[i] These cells (wt and KO) were a generous gift from Prof Dagmar Wachten (CAESAR, Bonn); the pH measurements were undertaken by my colleague Meenakshi Bhardwaj. I am grateful to them both.

on raft-inclusion[475] and on raft components, including GlcCer.[515,526] Molecular docking was identified as a useful tool to investigate this.

Cytosolic GlcCer may help assemble the vATPase complex

Attention was focussed on the interface between the membrane-bound a and c subunits (blue and grey respectively in Figure 3A) as any lipid binding could potentially bridge these two proteins and hence hold the protein assembly together. (Building of a model including one a and 3 c subunits was conducted as described in Materials and Methods.) The ROSIE-Rosetta ligand docking protocol was used in preference to AutoDock to allow maximum flexibility of the proteins; the calculation was simplified by using just the GlcCer headgroup (Figure S3). This calculation was performed at the interface between the a subunit and each of the 3 c subunits in the model. For each of the starting positions the 30 binding poses with most favourable interface score were surveyed (data in Figure S4) and in all cases about half oriented GlcCer correctly relative to the bilayer. There was sufficient space for a GlcCer headgroup in each search space with the sugar forming H-bond bridges between a and c subunits on two; representative examples are shown in Figure 6. Thus cytosolic GlcCer may help assemble the vATPase complex. (After this work was completed and published[471] a study emerged showing a yeast vATPase has lipid molecules associated with it and that these lipids increase pump activity.[527])

From Figure 6A emerges the potentially key role of Asn437 on the a subunit which is conserved across the 3 human protein isoforms and in other mammals. In *C. elegans*, which also contains GlcCer, it is conservatively mutated to Asp while in *S. cerevisiae*, which lacks this glycolipid the residue is a glycine (Figure 7A). This point can be expanded by considering this protein across the yeasts,[j] some of which contain GlcCer and some of which do not.[528,529] The presence or absence of GlcCer broadly correlates with whether or not the residue equivalent to Asn437 can participate in H-bonding (Figure 7B) – yeasts with GlcCer mostly have an Asp at this position, those without mostly have a Gly. (Tyr386 and Gln720 (Figure 6B) are conserved across all mammal and yeast species examined - data not shown.) Whilst this is only circumstantial evidence for the action of GlcCer in activating vATPase by this mechanism, it is highly suggestive when taken with the *in vitro* data presented here and previous findings in the area.[475,515] The question thus arises of how mutant NPC1 leads to a deficiency in cytosolic GlcCer.

[j] I am grateful to Dr Stephen Muench (Leeds University) for suggesting this experiment.

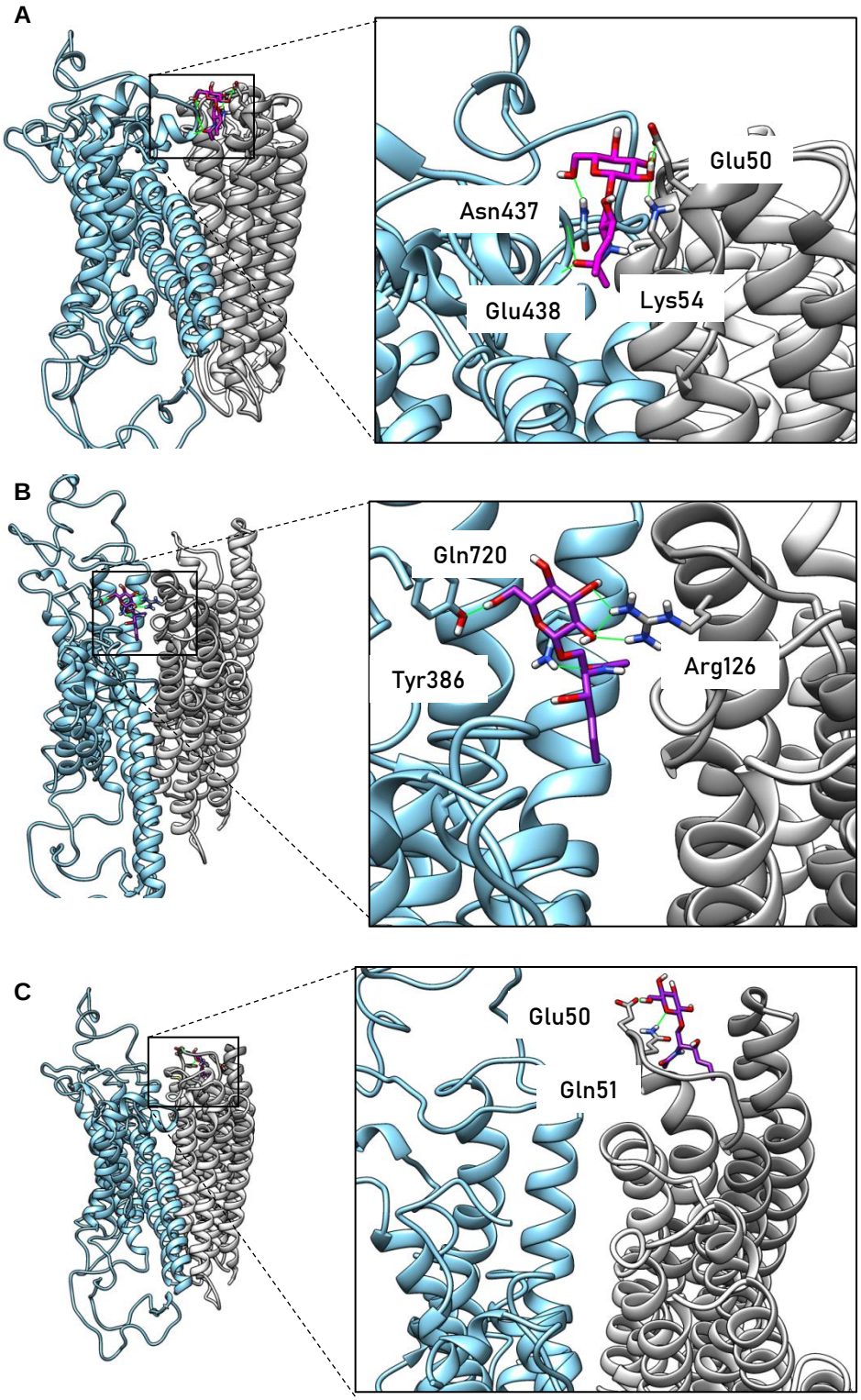

Figure 6 Docking suggests cytosolic GlcCer can activate the vATPase (**A**) GlcCer (purple) uses H-bonds (green) to bridge the a subunit (blue) and adjacent c subunit (chain N, grey). (**B**) GlcCer (purple) uses H-bonds (green) to bridge the a subunit (blue) and an adjacent c subunit (chain B, grey) (**C**) GlcCer (purple) uses H-bonds (green) to bind to the third adjacent c subunit without bridging (chain D, grey) without bridging to the a subunit (blue). Subunits shown not contacted by GlcCer shown in white; chain designations taken from 5tj5.[496]

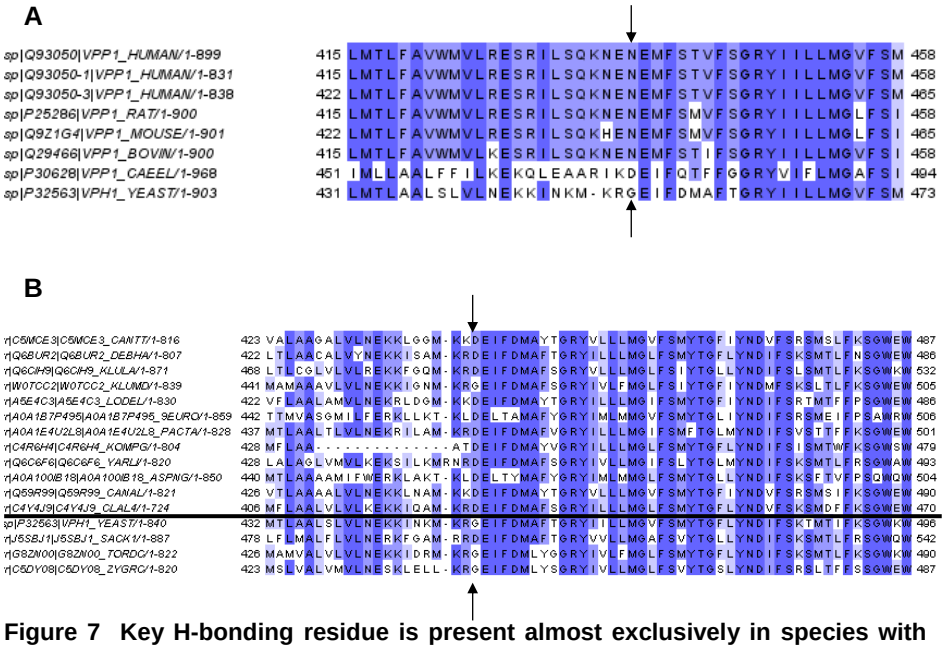

Figure 7 Key H-bonding residue is present almost exclusively in species with GlcCer (**A**) Multi-sequence alignment of human a subunit isoforms and homologues from other mammalian species, *C. elegans* and *S. cerevisiae.* The residue corresponding to Asn427 (Figure 6A) is mutated to non-H-bonding Gly in *S. cerevisiae* (which lacks GlcCer) but conserved as an H-bonding residue across all other species (which do express GlcCer). (**B**) Yeast expressing GlcCer[528,529] (above the line) largely have an H-bonding residue at the position equivalent to Asn427 while yeast lacking GlcCer (below the line) largely have the non-H-bonding Gly.

How do NPC cells become deficient in cytosolic GlcCer?

The obvious explanation, given that NPC1 has been suggested as a transporter of a diversity of types of molecule,[6,7,9,54] is that NPC1 itself can act as a GlcCer export protein. This attractively simple solution would have the added virtue of solving another problem of sphingolipid biology. GlcCer is made on the cytosolic face of the Golgi but emerges onto the topologically non-equivalent cell surface (Chapter 1, Figure 4, stages ❺ and ❽); therefore GlcCer requires a flippase.[194] Results presented so far in this chapter imply that NPC1 could be that protein while Chapter 2 uncovered lipid binding sites on NPC1 aligned with both faces of the lysosomal membrane. If NPC1 indeed acts as a GlcCer flippase then reduced GlcCer on the cell surface might be expected. This is indeed found in CHO cells treated with 5μM of NPC1 blocker U18666a (Figure 8A), reflecting similar findings in NPC1-deficient cells.[471] Intriguingly galactosyl-ceramide (GalCer) does not suffer from a similar defect (Figure 8B).[k]

[k] These experiments were performed by Dr Per Haberkant (EMBL); I am grateful for his expertise.

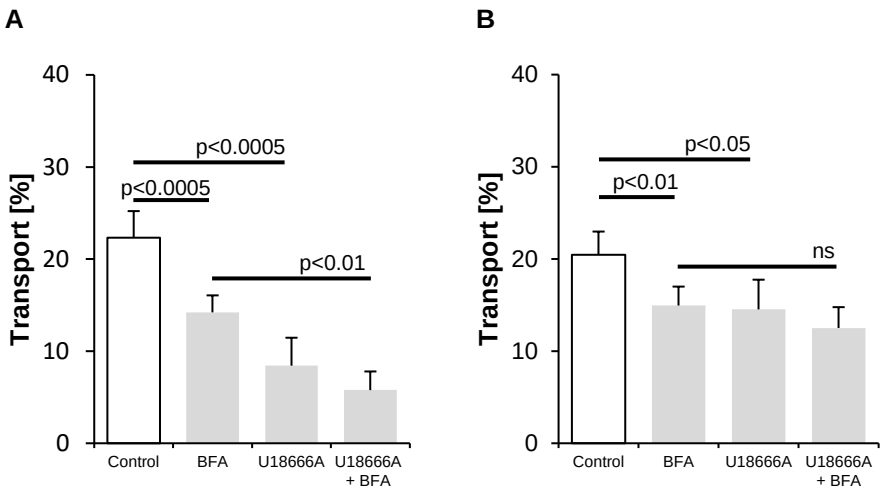

Figure 8 The effect of blocking NPC1 on transport of sphingolipids to the cell surface. Transport of newly synthesised GlcCer to the cell surface is reduced in NPCD cell culture models. The effect of 1 μg/ml of brefeldin A (BFA) and 5 μM U18666A on transport of GlcCer (**A**) and GalCer (**B**) in CHO cells expressed as % transport to the cell surface; results are mean ± SEM from at least 3 independent experiments conducted in triplicate.

Docking of GlcCer to NPC2 and the NTD of NPC1 showed that the lipid is too large to fit into the cavities of these proteins (data not shown) consistent with *in vitro* findings with GalCer.[261] Therefore saposin C (Chapter 1, Figure 4, stage ❾) is probably required to transport GlcCer from intra-luminal membranes to the transmembrane section of NPC1 though this role has not been explicitly demonstrated.[530] Attempted docking of GlcCer to the SSD of NPC1 is not as straightforward as might be wished. AutoDock can only handle 32 rotatable bonds so one of the long alkyl chains (Figure S3) used in the docking was artificially shorted to only nine carbon atoms in addition to the carbonyl carbon to satisfy this criterion (15,9-GlcCer, Figure S3). These chains are rather easily flexible (Chapter 2, Figure 1) adopting a huge range of conformations when unconstrained. The presence of a membrane usually acts as such a constraint, but this was absent from the docking procedure, resulting in a diffuse set of clusters each with a small number of binding poses (extended data not shown for this reason). These caveats must be borne in mind when considering the energetically favourable binding poses aligned to the luminal edge of the protein that did emerge (eg Figure 9A). Additionally, docking results with GalCer gave approximately equivalent results (data not shown) which renders difficult an explanation of the difference in cell surface transport data (Figure 8 and[471]).

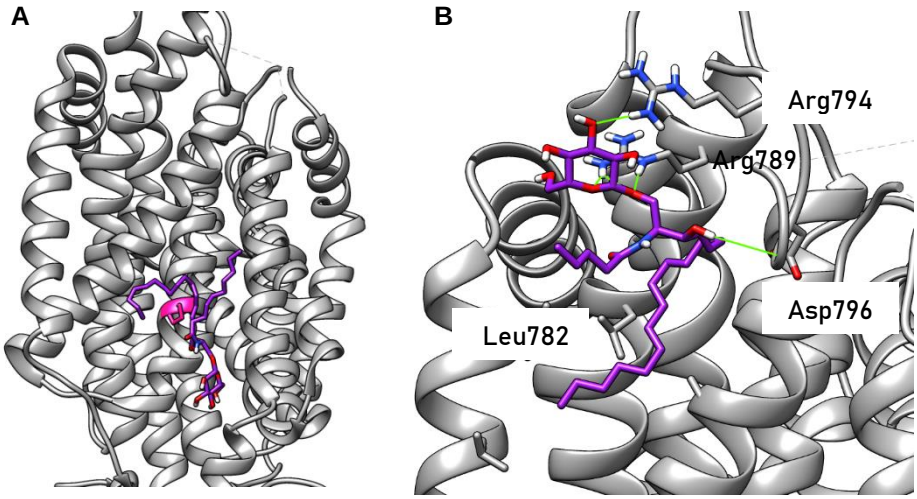

Figure 9 Docking of GlcCer to NPC1 (**A**) GlcCer (purple) binds to the SSD in the same manner as cholesterol contacting the key Pro691 (pink, see Chapter 2, Figure 8) (**B**) GlcCer (purple) binds to the luminal pocket but only one alkyl chain can be accommodated; H-bonds shown in green.

The putative cytosolic binding site is rather smaller than its luminal equivalent so the ROSIE ligand docking protocol was adopted due to its ability to allow protein flexibility. Limitations in the software reduced the possible number of rotatable bonds still further (15,4-GlcCer (Figure S3) was used). Whilst energetically favourable binding in this pocket was uncovered (eg Figure 9B), many poses were energetically unfavourable (Figure S5). The large sugar headgroup forces the lipid away from the residues implicated in cholesterol and Sph binding (eg Asp796) and the second alkyl chain cannot be accommodated meaning that the protein likely cannot retain the lipid in its binding pocket unassisted. Therefore the presence of a partner protein capable of interacting with NPC1 eg TMEM97[354] or LAMP2,[355] is probably required for NPC1 to process GlcCer in this way. Overall this work cannot rule out a role for NPC1 in exporting unmetabolised GlcCer from the endolysosome but it offers support for the idea that is tentative at best.

NPC1 probably doesn't export GlcCer

An alternative explanation relies on the potential role of NPC1 as a sphingosine export protein (Chapter 2 and[54,347]). This lipid has been reported as an inhibitor of GBA2.[531] Thus in healthy cells lysosomal metabolism releases Sph which is exported by NPC1 to the cytosolic face of the limiting membrane. There it acts as an endogenous negative regulator of GBA2 thus increasing the amount of GlcCer available to activate vATPase (Figure 6). It is even possible to imagine this system acting as a nutrient sensor whereby metabolic processes nearing completion result in reduced Sph export, reduced GBA2 inhibition, reduced cytosolic GlcCer and therefore reduced vATPase pumping of the protons for which there is now a reduced need. In cells deficient in NPC1 this situation pertains constitutively leading to

Hypothesis: NPC1 exports sphingosine which inhibits GBA2 increasing cytosolic GlcCer and activating vATPase. Failue of this process explains NPCD endocytic defects

increased pH as observed (Figure 2A). Consistent with this model, supplying AMP-DNJ, an exogenous GBA2 inhibitor, compensates for the deficiency in sphingosine and repairs the pH defect (Figure 4A). There is currently no known cytosolic hydrolase for GalCer so this model would leave cell surface transport of this lipid unaffected, as was found (Figure 8 and[471]).

Testing the sphingosine-GBA2-GlcCer hypothesis

NPCD can arise not only from defects in NPC1, but also the soluble cholesterol carrier NPC2 (Chapter 2, Figure 7, stages ❶ and ❷). As might be expected for a minor cause of a rare disease NPC2 deficiency has been little studied and there is only one exception[532] to the pattern of a phenotype identical to that in cells with mutant NPC1. It could be argued on the basis of Chapter 2 Figures 9 and 10 that NPC2 deficiency could be used as a test of the hypothesis that reduced sphingosine is responsible for the pH increase seen in cells lacking functional NPC1. This is not entirely clear, however, as Sph would be expected to have much greater solubility in the aqueous and acidic lysosomal lumen than cholesterol and so it cannot be ruled out that Sph would arrive at the NTD of NPC1 by diffusion unassisted by NPC2. In any case endolysosomal pH and the effects of GSL manipulation have not yet been studied in NPC2-deficient cells and so such fibroblasts were treated with AMP-DNJ at a variety of concentrations, and also with 50μM miglustat, a concentration likely to inhibit GlcCer synthase (GCS)[248] and thus potentially lead to a pH increase. More usual GCS inhibitors such as (D)-PDMP and PPMP were deprioritised due to potential cell toxicity.[533]

Increased endolysosomal pH in NPC2-deficient cells does not respond to AMP-DNJ questioning the sphingosine export hypothesis

Endolysosomal pH had a value of 5.34±0.04 in cells with defective NPC2 (Figure 10A) equivalent to NPC1 deficiency but significantly higher than healthy cells. In contrast to mutant NPC1 cells this increase was not corrected by AMP-DNJ at any tested concentration (Figure 10A). This result is less surprising than it might first appear. As NPC2 acts at intralysosomal membranes deficiency in this protein is arguably less similar to deficiency in NPC1 than to deficiency in acid sphingomyelinase (aSMase) which has the same site of action and also leads to lipid accumulation. We shall see later (Figure 12) that cells with defective aSMase have increased endolysosomal pH which does not respond to AMP-DNJ. Cells deficient in NPC2 did not show altered endolysosomal pH on miglustat (Figure 10A) but were free of gross signs of toxicity (Figure 10C,D).

The pH defect in NPC2 deficient cells cannot therefore result from disinhibited GBA2 and it is simpler, though not necessarily correct, to think that the same defect

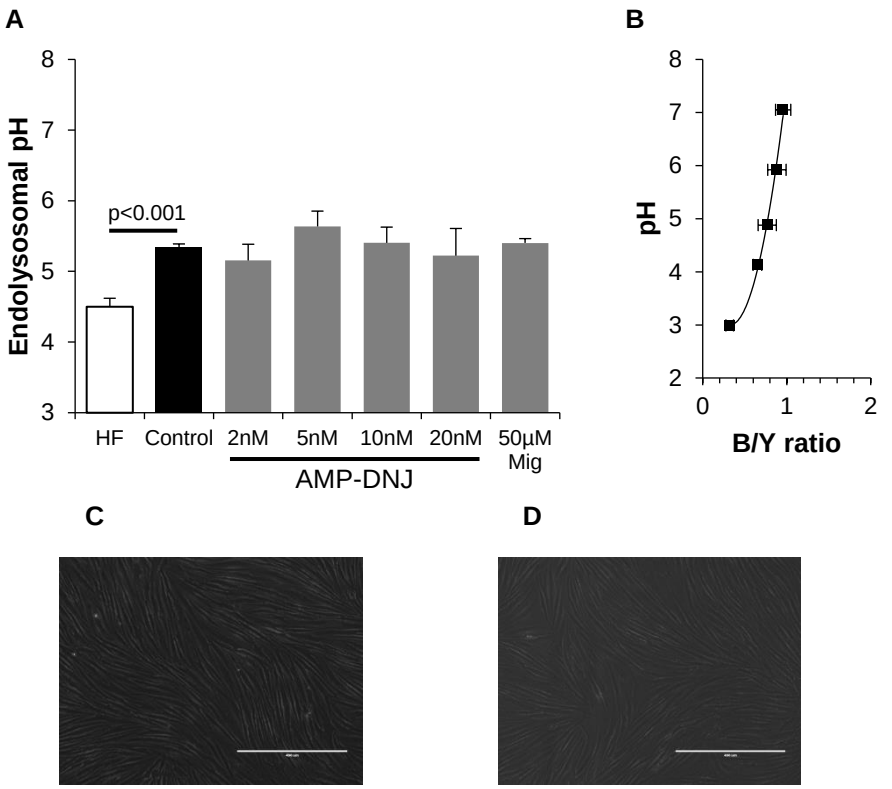

Figure 10 The effect of glycolipid alterations on NPC2 deficient fibroblasts (**A**) Increased endolysosomal pH is not changed by AMP-DNJ or miglustat; results are mean ± SEM from at least 3 independent experiments. (**B**) Correlation curve for LysoSensor yellow/blue in NPC2Fs; points are mean ± SEM from independent experiments (n=3, r^2=0.996). Cells treated with 50µM miglustat (**D**) appear the same as those treated only with vehicle (**C**). White bars represent untreated healthy cells, black represent disease and dark grey treated disease.

in NPC1 deficient cells does not result from disinhibited GBA2 either. Thus it becomes more likely the aberrant endolysosomal pH in these cells results from pathologically upregulated GBA2, as found in NPC1 KO mice.[250] This will be discussed in more detail later.

The gene for GBA2 has a nearby promoter region known to bind 124 transcription factors (data from the GeneCards[534] database).[l] 61 of these transcription factors are also known to upregulate >50 of the 120 proteins found with increased expression in NPCD[113] meaning that tracing the pathway from mutant NPC1 to over-expressed GBA2 is not easy.

Another way of testing the ideas about lipids and lysosomal acidification is to measure lipid levels in cells. A complication is that only changes in the cytosolic pool are proposed to be relevant and the technology to measure individual pools of lipid does not yet exist. Thus only whole-cell quantitation is possible and if cytosolic

[l] genecards.org/cgi-bin/carddisp.pl?gene=GBA2, accessed 10th September 2019.

lipids are a minor population then changes may not be detectable, or may be swamped if changes also occur in more numerous populations. It is also not certain which lipids are relevant for pH changes. GlcSph, generated by the action of neutral ceramidase (nCerase) on cytosolic GlcCer, can be safely neglected. An NPCD mouse model featured increased GBA2 activity and accumulation of GlcSph[250] while a mouse model of aging also showed increased GlcSph despite decreased GBA2 activity.[535] Therefore GlcSph levels do not correlate with GBA2 action. A complication does arise from the ability of GBA2 to use GlcCer as glucosyl donor for cholesterol thereby generating GlcChol.[523] The role of this lipid, if any, in modulating endolysosomal pH is not known. Appropriate caveats duly noted, treatment of cells with a GBA2 inhibitor would be expected to increase GlcCer, decrease Cer and also possibly decrease Sph generated through the action of nCerase.

Analysis of changes in lipid levels shows AMP-DNJ has more than one target

This was tested in both healthy and disease cells[m] and as expected all lipids were present in greater quantity in cells deficient in NPC1 (Figure 11, $p \leq 0.04$). Closer examination reveals that AMP-DNJ is likely to have off-target effects for a dose of 20nM reduces total GlcCer in healthy cells (Figure 11A) whilst leaving the amount of ceramide, which is both its immediate precursor and catabolite, unchanged (Figure 11C). Sphingosine, from which some ceramide is made and to which some ceramide is hydrolysed, (Chapter 1, Figure 4) is reduced at the same dose (Figure 11E) reinforcing the conclusion of mixed pharmacology. The same conclusion can be drawn from other doses in healthy cells where GlcCer is unchanged while both other lipids are increased (Figure 11A,C,E). The non-specific effects of AMP-DNJ, combined with the confounding factors noted above, mean it is impossible to draw simple conclusions from this data.

With NPC1Fs the larger sample variability makes interpretation less sure, but a similar picture emerges. 5-10nM AMP-DNJ generates peak amounts of both GlcCer and Sph (Figure 11B,F), something that would be unexpected from inhibition of a single enzyme. Healthy cells also showed the largest changes in lipid levels in the 5-10nM dose range suggesting that the literature[522,523] dose of 20nM used in the pH experiments may be too high. This issue will be repeatedly alluded to in the remainder of this chapter.

[m] Lipid quantitation was performed accoring to a previously published procedure[590] by Dr Maria Ferraz in the laboratory of Prof Hans Aerts (Universiteit Leiden) on cell pellets I provided. I thank them for the generous gift of time and skills.

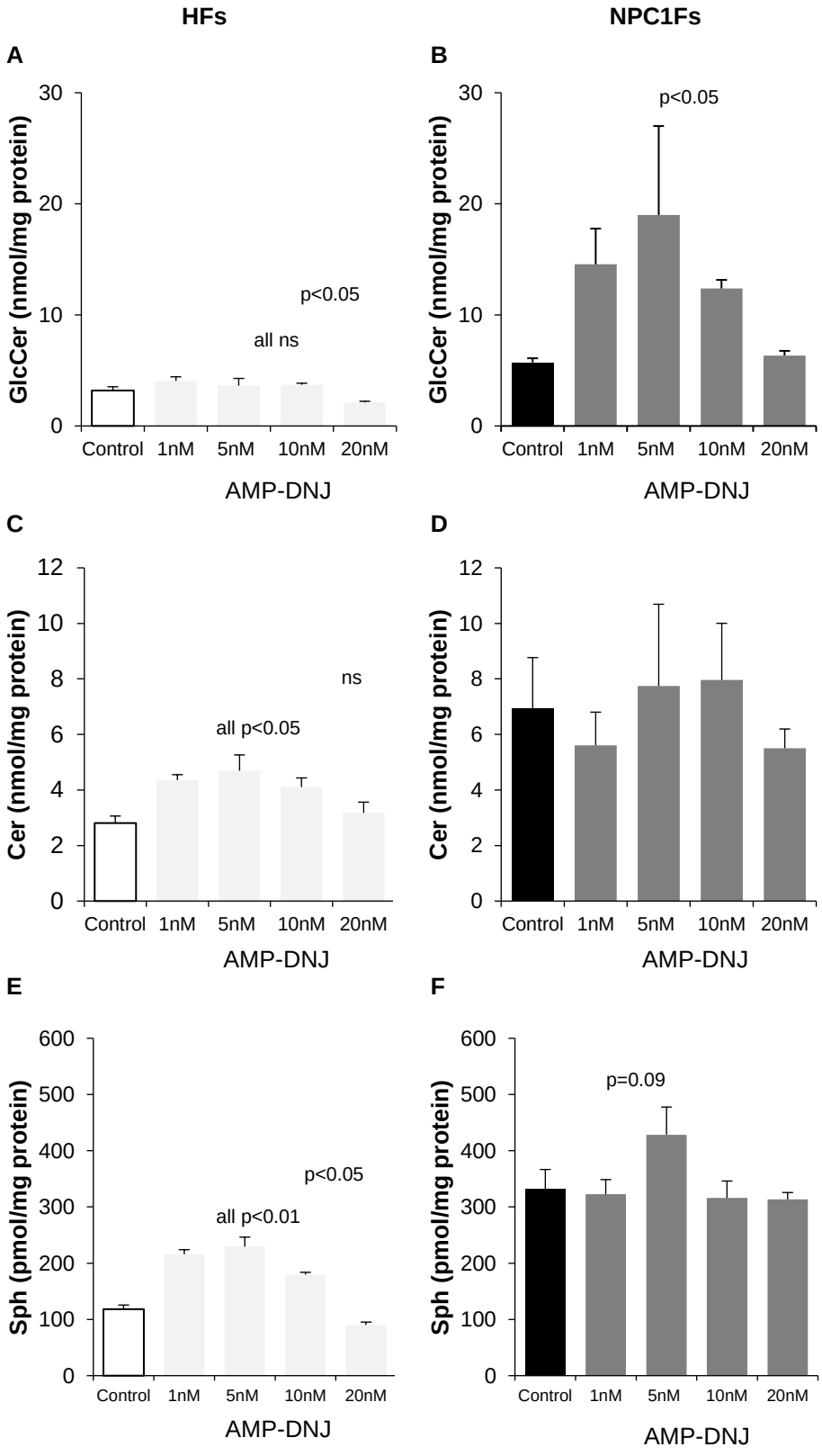

Figure 11 The effect of AMP-DNJ on cellular lipid levels. GlcCer, Cer and Sph were quantitated in healthy (**A**,**C**,**E** respectively) and NPC1 deficient fibroblasts (**B**,**D**,**F** respectively); results are mean ± SEM from 3 independent experiments. White bars represent untreated healthy cells, black represent disease; light grey bars represent treated healthy cells, dark grey treated disease.

The utility of AMP-DNJ in correcting errors in cell culture models of NPC1-deficiency is clear even though neither its mechanism of action nor the origins of the endolysosomal pH error are unambiguously established. It is also unclear whether or not the clinical success of GBA2 inhibition can be attributed to this correction of endoctic defects. It would potentially be both informative and useful to examine the actions of this drug in related diseases.

Application to other diseases

Niemann-Pick type A disease (reviewed[536]) results from a deficiency in acid sphingomyelinase[537] (aSMase) the lysosomal enzyme responsible for hydrolysing sphingomyelin which thus accumulates[538] in the lysosome but also at the cell membrane.[539] Total cell cholesterol does not appear to increase,[538–540] which is surprising given the close physical[276] and physiological[264] relationship between this lipid and SM, though errors in cholesterol handling have been reported.[541,542] Total cell GlcCer is also unchanged[538] although an increase in sphingosine has been reported.[540,543] Despite these differences faulty endocytosis[544] and wider lysosomal dysfunction,[132] including increased endolysosomal pH,[441] are found, just as they are in NPCD. The impact of drug-induced GSL alterations on endolysosomal pH has

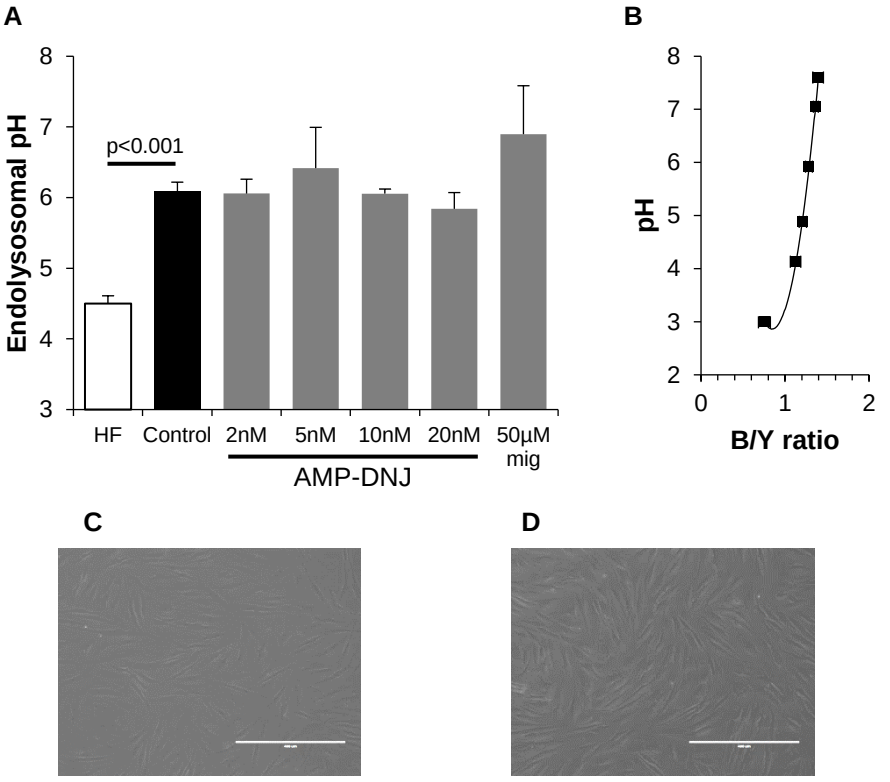

Figure 12 The effect of glycolipid alterations on NPA fibroblasts (**A**) Increased endolysosomal pH is not changed by AMP-DNJ or miglustat; results are mean ± SEM from 3 independent experiments. (**B**) Correlation curve for LysoSensor yellow/blue in NPAFs; points are mean ± SEM from independent experiments (n=3, r^2=0.999). Cells treated with 50µM miglustat (**D**) appear the same as those treated only with vehicle (**C**). White bars represent untreated healthy cells, black represent disease and dark grey treated disease.

not yet been studied and is both interesting for an understanding of cellular physiology and potentially useful for therapy.

The endolysosomal pH defect in Niemann-Pick type A disease does not respond to AMP-DNJ

Fibroblasts from NPAD showed an elevated endolysosomal pH of 6.1±0.1 compared to healthy controls (Figure 12A) consistent with a recent literature report.[441] Whilst GCS inhibition through 50μM miglustat gave a non-significant increase to 6.9±0.7 GBA2 inhibition with AMP-DNJ did not reduce endolysosomal pH in cells from this disease. Gratifyingly miglustat did not show any gross signs of toxicity in this cell line (Figure 12C,D).

As briefly mentioned in chapter 1, NPCD is a member of the class of lysosomal storage disorders which result from diverse failures of the physiology of this organelle but whose clinical manifestations all feature neurodegeneration. Mucopolysaccharidosis type IIIa (MPSIIIa, also known as Sanfilippo syndrome[545]) arises from mutant heparan-N-sulfatase, a member of a class of enzymes responsible for hydrolysing glycosoaminoglycans, linear carbohydrates formerly known as mucopolysaccharides, and the consequent accumulation of unmetabolised enzyme substrate. Mucolipidosis type IV (ML-IV) is caused by mutation and therefore dysfunction of the Ca^{2+} release channel TRPML1[80,546] (Chapter 1, Figure 1, stage ❽) and results in defects in endocytosis[547] and autophagy.[393] TRPML1 function is decreased at higher pH.[386] Fibroblasts from MPSIIIaand ML-IV were thus treated with a range of concentrations of AMP-DNJ. GlcCer synthase (GCS) inhibitor PPMP (Figure S2) was also used with the expectation that this would reduce cytosolic GlcCer and thus increase endolysosomal pH. This parameter has not previously been measured in cells from these diseases. Preliminary data from these experiments, performed twice, were mixed (Figure 13).

AMP-DNJ is sometimes, but not always effective in LSDs with increased endolysosomal pH.

The endolysosomal pH of MPSIIIa cells was found to be 5.3, higher than healthy controls (Figure 13A), but was not corrected by AMP-DNJ consistent with the failure of a clinical trial of marketed GBA2 inhibitor miglustat in this disease.[548] Endolysosomal pH was also insensitive to PPMP (Figure 13A). ML-IV cells had a higher endolysosomal pH (5.8) than healthy controls which was corrected by AMP-DNJ treatment (Figure 13E) – perhaps consistent with the lipid quantitation data above (Figure 11) the largest effect was seen at 10nM where an endolysosomal pH of 4.6 was observed. This effect is also consistent with the efficacy of miglustat in a mouse model of ML-IV.[549] (Intriguingly PPMP, even at half the usual concentration, led to a greater reduction in endolysosomal pH (Figure 13E) though this may be the result of the toxicity of this agent.[533]) Thus AMP-DNJ appears to correct elevated endolysosomal pH in cells from a disease where GBA2 inhibition

has been successful *in vivo*, but conversely apparently fails to correct the same error in cells from a disease where GBA2 inhibition is ineffective clincially. The idea that the success of GBA2 inhibition to treat disease results from correction of endocytic defects is thus strengthened. This connection was not known when this work was begun.

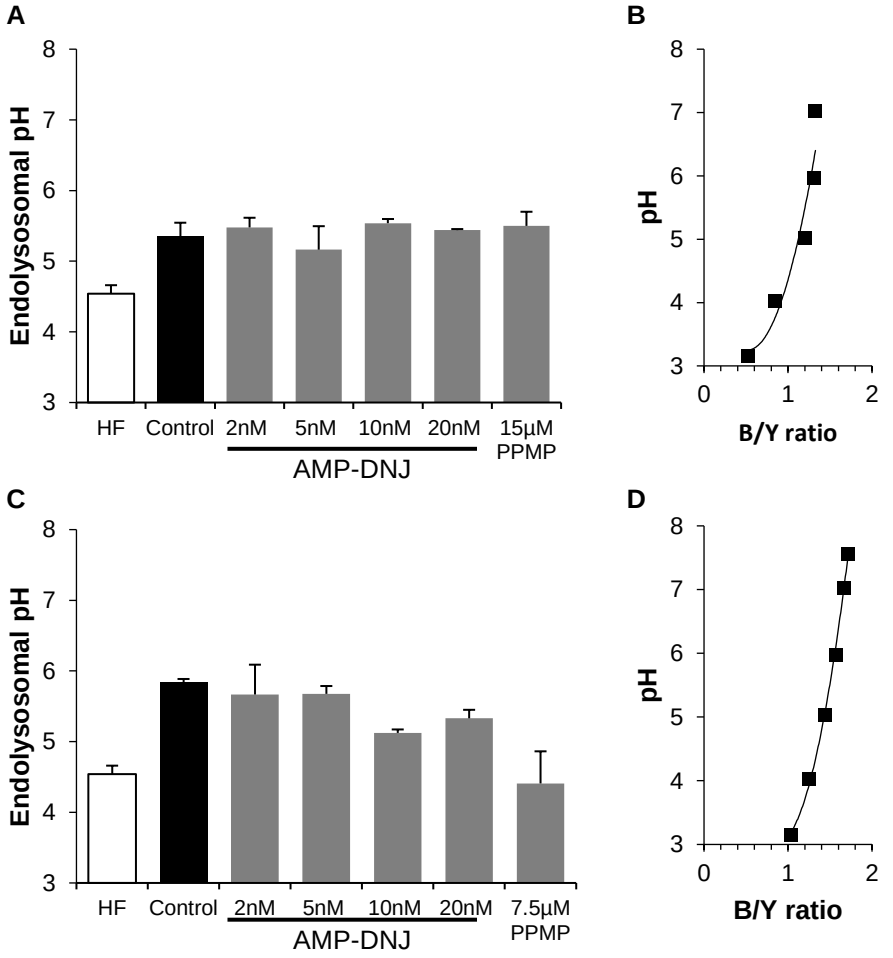

Figure 13 The effect of altering glycolipids on endolysosomal pH in LSDs (**A**) In MPSIIIa increased endolysosomal pH is unchanged on glycolipid alteration. (**B**) Correlation curve for LysoSensor yellow/blue in MPSIIIa fibroblasts; (r^2=0.913). . (**C**) In ML-IV fibroblasts increased endolysosomal pH is reduced on inhibition of GBA2 or GCS. (**D**) Correlation curve for LysoSensor yellow/blue in ML-IV fibroblasts; (r^2=0.998). All data are from one representative example (mean±SD) of two independent experiments conducted in duplicate. White bars represent healthy cells, black disease and dark grey treated disease.

Experiments in another LSD, Krabbe disease (previously known as globoid cell leukodystrophy), complicate the picture still further. This disorder stems from deficiency in galactosylceramidase, the lysosomal enzyme responsible for the digestion of GalCer[550] (analogous to Chapter 1, Figure 4, stage ❾). It is widely believed, though not yet proved, that accumulating GalCer is hydrolysed by acid

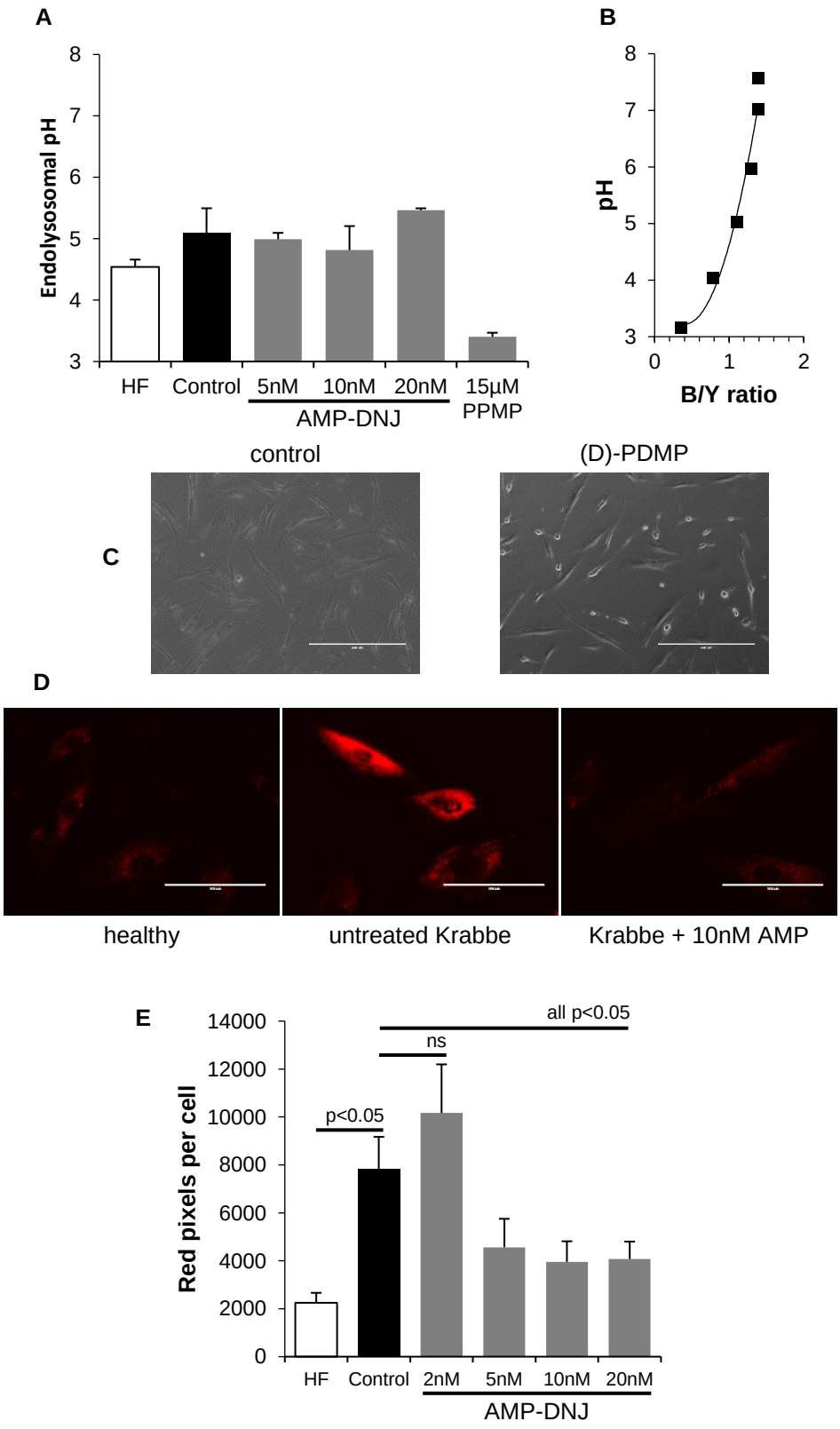

Figure 14 The effect of AMP-DNJ on Krabbe fibroblasts (**A**) AMP-DNJ does not correct increased endolysosomal pH (mean±SD) from one representative experiment conducted in duplicate. (**B**) Correlation curve for LysoSensor yellow/blue in Krabbe fibroblasts; (r^2=0.967). (**A**,**B** are a representative example of two independent experiments.) (**C**) GCS inhibition produces apoptotic appearance in Krabbe fibroblasts. (**D**) Representative images from LysoTracker experiment (**E**) Quantitation of acidic compartment volume (mean ± SEM examining at least 40 cells per condition). White bars represent healthy cells black represent disease and dark grey treated disease.

ceramidase to give GalSph (also called psychosine) which escapes the lysosome by an unknown mechanism and leads to damage to organelles, particularly mitochondria, and cell death.[551] While endolysosomal pH was elevated in fibroblasts[n] from this disorder, consistent with measurements in rat oligodendrocytes treated with psychosine,[236] treatment with AMP-DNJ did not correct it while PPMP again led to a reduction (Figure 14A; data is a representative example of two independent experiments). This reduction may be an experimental artefact as a closely structurally related GCS inhibitor, (D)-PDMP (Figure S2), led to cell toxicity (Figure 14C). However AMP-DNJ did correct the error in lysosomal volume (Figure 14D,E). Thus in Krabbe disease AMP-DNJ corrects the proliferation in endocytic vesicles, but not the pH defect while in NPCD the exact opposite applies (Figure 4A,C) and it is thus an open question whether or not endocytic proliferation is dependent on correct acidification. Just as the lipid quantitation data did, these results also point to multiple modes of action for AMP-DNJ.

Application to amyloid-related diseases

Amyloid precursor protein (APP) is a plasma-membrane resident molecule of unknown function. It is cleaved by the actions of two proteases: β-secretase at sites outside membranes and γ-secretase, unusually, at sites within them. The resulting protein fragments, termed amyloid beta (Aβ) and released into the cytosol, are of varying lengths and are named after the number of residues each contains, eg Aβ40. When secreted from the cell Aβ forms the basis of amyloid plaques, the aberrant accumulation of which is widely held to be responsible for Alzheimer's disease (AD). A logical goal of therapy is therefore to reduce Aβ.

The reasons for the increased amounts of Aβ in AD have yet to be unravelled although this is a feature shared with NPCD, both cells[552] and the CSF of patients.[157] In NPCD the CSF levels can be corrected by miglustat therapy.[157] Endolysosomal dysfunction also occurs in AD and it has been suggested that this is linked to reduced clearance of Aβ (see[553] and references therein). At the same time clozapine (Figure S4), an anti-psychotic drug with mixed pharmacology which has been proposed to include GlcCer,[554] has been reported to reduce Aβ in a mouse model of AD.[555] The pathway included p35 and cdk5 providing echoes of NPCD as dealt with in Chapter 1, Figure 3 and surrounding discussion. Very recently a TRPML1 agonist has been reported to acidify endolysosomes in AD model cells and to block the accumulation of Aβ induced by LDL.[556] All these lines of evidence suggested that AMP-DNJ could

[n] These cells were a gift from Prof Frances Platt (University of Oxford) to whom I am grateful.

be used to reduce the pH of endolysosomes in AD model cells and thereby to reduce levels of Aβ.

Due to the well-documented difficulties of growing neuronal cells in culture, experiments were performed in two neuroblastoma cell lines, one of which (SH-SY5Y) had been transfected[557] to overexpress APP stably.º Preliminary experiments (Figure 15) showed that AMP-DNJ did indeed increase endolysosomal acidity in the untransfected NB7 cells (6.2 to 5.4 with 10nM, though only n=2); little if any reduction was observed in the SH-SY5Y cells (data not shown). Thus the rationale of using AMP-DNJ to acidify lysosomes as a means of reducing Aβ was provisionally and partially supported. A pH increase was not observed with GlcCer synthase inhibitor PPMP, as might be expected, testament to the complexity of the operating pathways.

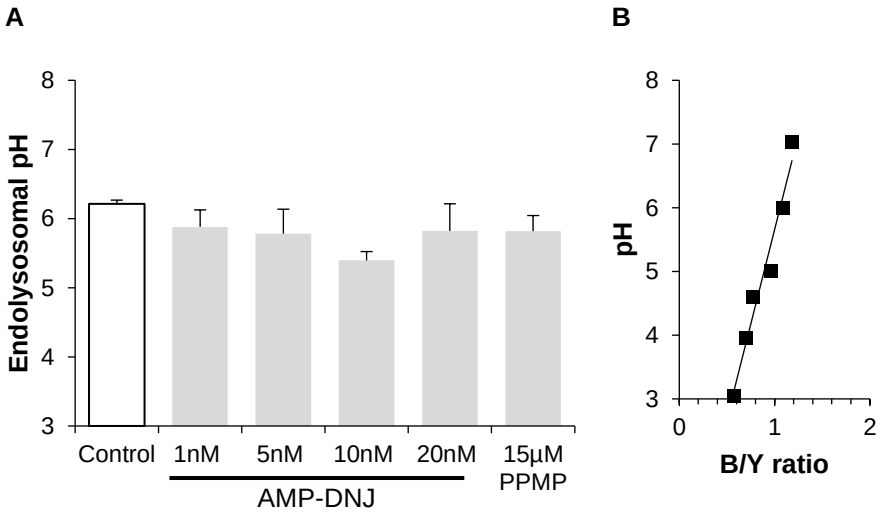

Figure 15 The effect of AMP-DNJ on endolysosomal pH in neuroblastoma cells (**A**) In NB7s endolysosomal pH is reduced on treatment with AMP-DNJ. (**B**) Correlation curve for LysoSensor yellow/blue in NB7 cells; (r^2=0.961). Data are (mean±SD) of two independent experiments conducted in duplicate.

In order to obtain as full a picture as possible of the effect of sphingolipids on Aβ production studies in these cells employed a diversity of drugs in addition to AMP-DNJ and PPMP. Myriocin, an inhibitor of serine palmitoyl transferase (Chapter 1, Figure 4, stage ❶) reduces synthesis of sphingosine and thereby, in principle, all

other sphingolipid populations. NPC1 blocker U18666a was also used to see if Aβ would increase consistent with the higher levels observed in cell culture models and

º These cells were a gift from Prof Nigel Hooper (University of Manchester); I thank him for his generosity.

patients with this disease[157,552] and clozapine to check consistency with the previous report of reduced Aβ in an AD mouse.[555] Aβ levels were measured both in the media and in cell lysates; NB7 cells, which are not transfected with APP, had lower levels of Aβ generally and undetectable levels of the shortest fragment Aβ38. After

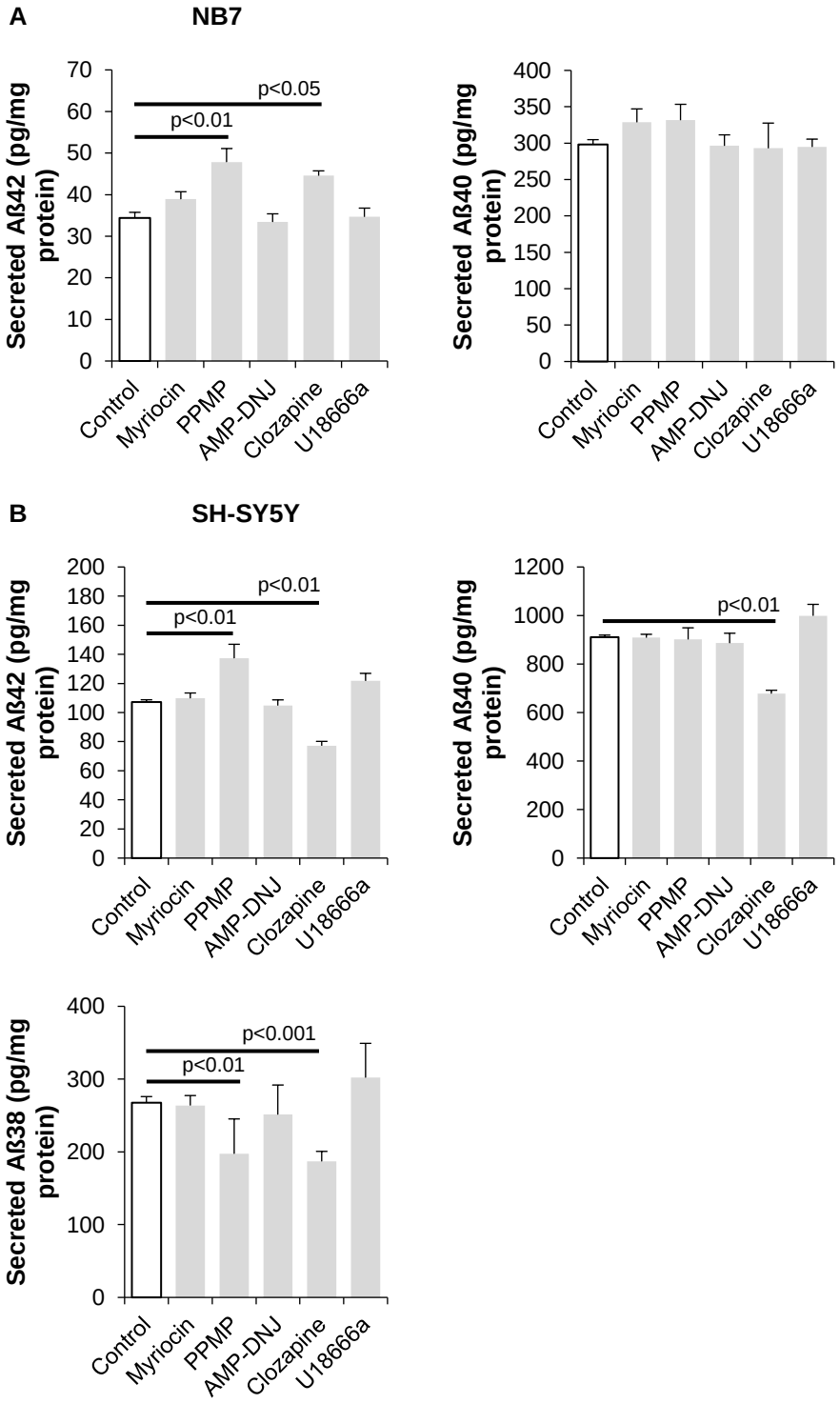

Figure 16 Effect of lipid alteration on secreted Aβ NB7 (**A**) and SH-SY5Y (**B**) cells were treated with the indicated drugs overnight before quantitation of Aβ in the media; results are mean ± SEM from 3 samples.

a 24 hour incubation none of the drugs tested gave effects on levels of secreted Aβ that were consistent across both cell type and protein length (Figure 16).[p]

Whilst clozapine reduces all forms of this protein in SH-SY5Y cells it has no effect on Aβ40 secreted by NB7s and even increases Aβ42 exported by this cell line. PPMP does not affect Aβ40 in either cell line but increases Aβ42 in both. Neither U18666a nor AMP-DNJ affected levels of any form of secreted Aβ suggesting that in these models endolysosomal pH is not the key determinant of how much protein is formed.

AMP-DNJ reduces endolysosmal pH but leaves Aβ levels unchanged in two neuronal model cell lines

To examine levels of Aβ in cell lysates the drug panel used above was supplemented with (D)-PDMP, an inhibitor of GlcCer synthase, and its (L)- isomer (Figure S3). These two compounds are both reported to reduce Aβ in a transfected neuroglioma cell line[558] despite having opposite effects on GSL levels in the same cells;[559] they are also effective in transfected CHO cells.[533] Disappointingly, none of the agents significantly reduced Aβ in lysates of SH-SY5Y cells, though some led to small and significant increases. (Figure 17A). (These experiments were not conducted in NB7 cells as Aβ is not present in measurable amounts in the lysates of untransfected cell lines.) PPMP gave a large increase, though that may result from increased expression of APP with this compound (Figure 17B).

Thus the picture that emerges of the relationship between lipids and levels of Aβ is exceptionally complex. Lipids affect endolysosomal pH (Figure 15A,C) and potentially other lysosomal ion fluxes (Chapter 2), APP expression (Figure 17B) and, in multiple ways, γ-secretase activity.[560–562] All these factors can, at least in principle, affect Aβ levels. Thus the therapeutic goal of reducing Aβ by altering lipid levels, even if it is possible, is likely to be met only by identifying and precisely targeting one or more crucial sub-populations of lipids. Even if such a pool could be identified, selective manipulation is difficult to achieve. AMP-DNJ is probably the available drug with the greatest ability to target a defined lipid population but data from fibroblasts (Figure 11) suggests that even this agent is not perfectly selective.

Less well known than AD is the involvement of amyloid in Down syndrome (DS), the triplication of chromosome 21 on which the gene for APP is located. Individuals with this condition are at vastly increased risk of developing amyloid plaques;[563]

[p] Aβ quantitation assays were performed by Kate Kellett and Kate Fisher of the Hooper lab at Manchester university on samples I provided. I thank them both for their diligence and for informative discussions of the results.

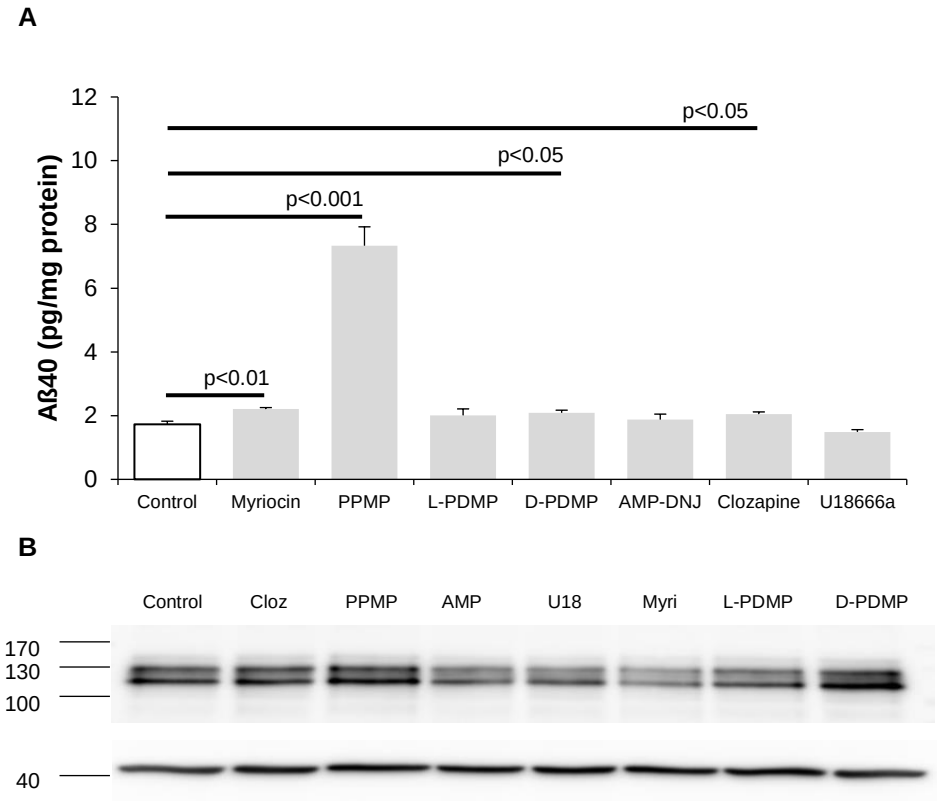

Figure 17 Effect of lipid alteration on Aβ levels in cell lysates of SH-SY5Y cells (**A**) quantitation of Aβ levels in cell lysates of SH-SY5Y cells treated with the indicated drugs; results are mean ± SEM from 3 samples. (**B**) Western blot of APP (upper panel) in cell lysates of SH-SY5Y cells treated with the indicated drugs; actin (lower panel) was used as a loading control.

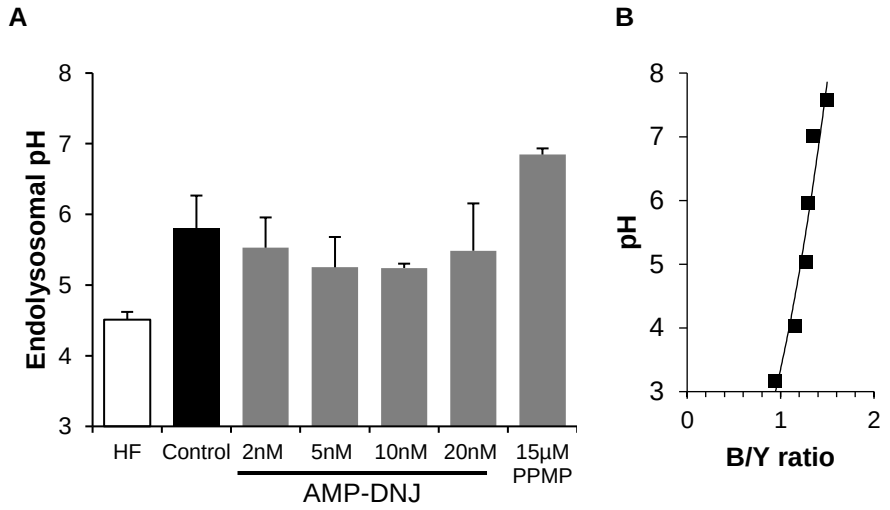

Figure 18 The effect of AMP-DNJ on endolysosomal pH in DS fibroblasts (**A**) In DS fibroblasts endolysosomal pH is increased but reduced on treatment with AMP-DNJ. (**B**) Correlation curve for LysoSensor yellow/blue in DS fibroblasts (r^2=0.915). Data are representative examples of two independent experiments. White bars represent untreated healthy cells, black represent disease and dark grey treated disease.

Endolysosomal pH is elevated in a Down syndrome cell line; AMP-DNJ corrects this

endolysosomal dysfunction has also been documented[564] and very recently an amyloid-dependent endolysosomal pH increase has been reported.[565] Preliminary experiments (data shown are a representative example of two independent experiments) replicated this latter finding: endolysosomal pH in untreated cells was 5.8 (Figure 18A). Furthermore the acidity was found to by GSL-sensitive as AMP-DNJ reduces endolysosomal pH (an optimum dose of 10nM gives a pH of 5.2) while PPMP increases it further (Figure 18A). The very idea that DS might be susceptible to drug treatment is novel.

Open questions and future work

I don't know, Sophie thought. Surely nobody really knows. And yet - Sophie thought it was a fair question.

Jostein Gaarder
Sophie's World

The following discussion will make two assumptions. The first is that the preliminary results reported above on the effects of GBA2 inhibition on endolysosomal pH in pathologies other than Niemann-Pick are accurate. Whilst these findings are consistent with *in vivo* data where those are available,[548,549] and each disease was tested twice, the experiments should be repeated until statistical significance is obtained. More controversially we will also assume that neither AMP-DNJ inhibiting GBA2 nor brefeldin A merging the ER and Golgi has any significant effect other than increasing cytosolic glucosylceramide.[525,566] This assumption is incomplete (see Figure 11 and surrounding discussion) but both useful and necessary as the other targets of AMP-DNJ are unknown. From these two assumptions and the results reported above several deductions follow.

The finding that both AMP-DNJ and brefeldin A reduce endolysosomal pH in healthy cells (Figure 5A) implies that the regulation of this parameter by cytosolic GlcCer is a general, though possibly minor, pathway. Next it is possible to divide LSDs into those where endolysosomal pH is normal (currently only CLN2 deficiency, Figure 13C) and those where it is increased. In some of these defective acidification is rescued by increasing cytosolic GlcCer (NPC1 deficiency and ML-IV, as well as Down syndrome) which in turn implies that this sub-population of lipid is reduced in these pathologies. Therefore other explanations for increased endolysosomal pH are correspondingly less likely.

Such explanations may include an association between NPC1 and components of the vATPase as suggested by two studies[125,461] which may be impaired in the presence of mutant NPC1. More difficult is the potential involvement of growth regulating complex mTORC1. Cholesterol accumulation, such as occurs in NPCD, has variously been reported to result in mTORC1 inhibition,[126] mTORC1 activation[125] and no difference in mTORC1 status.[98] GlcCer is also reported to bind mTORC1[517] meaning that it may become necessary to include this complex in the account of action of AMP-DNJ, though the explanation offered above is simpler and therefore preferable. Other secondary effects of cholesterol may be implicated. (Consistent

with the argument advanced in this section about the importance of cytosolic GlcCer *in silico* modelling (Figure 3) has suggested that a direct effect of cholesterol on the vATPase is unlikely.) Secondary effects could be investigated by using cells from patients with Wolman disease, a genetic LAL deficiency which features endolysosomal cholesterol accumulation. Lysosomal pH has previously been reported as normal in such cells[53] but with a dextran probe, the deficiencies of which were noted above; only the most basic quantitation of secondary lipid accumulation has been performed to date.[567] Combining lipidomics with measurements of endolysosomal pH in this disease and the repair of any defect with AMP-DNJ might help confirm the putative key role of cytosolic GlcCer.

Why is the crucial cytosolic sub-population of GlcCer reduced? This work postulated a Niemann-Pick specific mechanism in which mutant NPC proteins fail to fulfil their roles as sphingosine exporters[54,347] (Chapter 2, Figures 8-11) reducing the reported inhibition of GBA2 by this molecule[531] and hence depleting the cytosolic pool of GlcCer. The failure of AMP-DNJ to correct the pH error in NPC2-deficient cells suggests that this pathway is incorrect and so leaves unanswered the question of the pathological role, if any, of sphingosine accumulation in NPCD. However this very failure also opens the door to a more generally applicable understanding of the role of GBA2 in disease.

If GBA2 is not disinhibited in NPCD but its substrate pool is depleted then either the enzyme has become activated or its expression is upregulated. No activation mechanisms are known for GBA2 and so the idea that NPC pathology leads to upregulation is preferred; confidence in this deduction is increased by the observation of such upregulation in a murine model of NPCD.[250]

This conclusion, however, does not tell us why the cytosolic pool of GlcCer should be so important. The case was made above, and suggested by previous work, that this sub-population,[515] or at least raft components or inclusion,[475,526] activates vATPase but this is far from being proved. If vATPase can be isolated then GlcCer binding can be assessed using an ELISA assay with immobilised lipid. Whilst this would evidence the fact of lipid-protein binding, it would not identify how the two partners interact. Mutagenesis experiments changing the key reside Asn437 to an alanine could be more useful. Assuming the mutant protein was expressed, localised and functioned correctly then it should prove insensitive to GSL alterations, eg those produced by AMP-DNJ. The ultimate experiment would be to characterise structurally the protein complex with adventitious lipids intact. This should be

possible using lipo-paticles followed by examination of the complex by MS and cryoEM.[568,569]

Other pathways of AMP-DNJ action are possible. Clearly lysosomal acidification depends on vATPase expression which was found to be increased by AMP-DNJ at both the mRNA and protein levels.[471] Provocatively, Myb-binding protein 1a, a protein involved in transcription, has been found to bind sphingolipids in three independent proteomic screens[q] implying a possible link between GlcCer and numerous proteins, not just vATPase. Mapping these pathways will be an essential component of future attempts to understand the impact of sphingolipid perturbations on the cell (compare Chapter 1, Figure 2). A more direct link to protein expression is supplied with the disclosure that GBA2 localises to the ER and Golgi.[570] Earlier work found that miglustat can prevent interaction between calnexin and the ΔF508 mutant CFTR channel[571] thereby normalising protein expression and restoring a chloride current which has been implicated in control of lysosomal acidity.[236] This miglustat study[571] used a dose of 100μM which will also inhibit GCS[248] requiring caution in the interpretation of this result. Nonetheless it opens the possibility that AMP-DNJ may acidify endolysosomes by increasing expression of CFTR whose activity has been reported as cholesterol-dependent.[572] Were this the case then we would expect to be able to measure an increase of CFTR expression and to find that a CFTR blocker[573] negates the effects of AMP-DNJ.

A role for GBA2 inhibitors at the ER may also invoke calcium in the explanation. Two independent studies have suggested that GlcCer indirectly activates the ryanodine receptor (RyaR) leading to increased cytosolic calcium[210,574] which could potentially refill the depleted lysosomal Ca^{2+} stores in NPCD cells[53–55] thereby normalising calcium efflux through channels such as TRPML1. (The open probability of this channel increases with higher cytosolic calcium.[546]) Corrected lysosomal calcium could restore defective endocytosis and autophagy and possibly be a counter-current necessary to balance endolysosomal acidification. Consistent with these observations thapsigargin, an inhibitor of the sarco-/endoplasmic reticulum calcium pump, was found to normalise lysosomal calcium rapidly in NPCD cells and to relieve lipid storage.[54] Expression of proteins related to calcium handling was found to be altered in NPCD cells.[113] The question thus arises of whether AMP-DNJ prevents GlcCer hydrolysis not at the lysosome but at the ER and the resulting increased GlcCer leads to calcium release which normalises lysosomal function.

[q] Per Haberkant (EMBL) and Cliff Lingwood (Sick Kids, Toronto), personal communications; MPharm student Zain Mohammed analysed the overlap of these large data sets with my guidance. I am grateful to all of them.

Experiments to test this idea have thus far been unsuccessful. If the effect of AMP-DNJ were Ca^{2+}-mediated we would expect it to be blocked by the cell-penetrant calcium-selective chelator BAPTA-AM. When used alone this reagent unexpectedly led to a reduction in endolysosomal pH (data not shown) rendering it unsuitable for competition experiments with other drugs. The effect of non-toxic SERCA inhibitor curcumin could not be assessed using LysoSensor yellow/blue due to this compound's strong yellow colour, an observation that will only enhance its reputation as interfering with assays.[575] The restoration, or otherwise, of endolysosomal calcium by AMP-DNJ could be assessed using confocal microscopy loading cells with calcium probe Fura2 and lysing lysosomes with Gly-Phe-ß-naphthylamide (GPN).[54]

Whatever the function of the cytosolic sub-population of GlcCer it is possible manipulations of it might have effects in NPCD more widespread than those demonstrated above (Figure 5). As noted in chapter 1 (Figure 1, stage ❸) some very early endocytic vesicles are formed from the plasma membrane in a manner dependent on both GSLs and galectin-3.[21] Given that cell surface GlcCer is reduced in NPCD (Figure 8) we might expect disease cells to show deficiencies in this process, and for these to be repaired by AMP-DNJ. Further along the endocytic pathway, traffic from early to late endosomes can be assessed using horse radish peroxidase as a fluid phase marker.[61] This endocytic segment is impaired in NPCD, probably driven by the mislocalisation of the key protein AnxA2.[27] Assessing whether or not AMP-DNJ corrects this defect is a worthwhile enterprise. It is possible that GBA2 inhibition will have no effect on either galectin-3 or AnxA2 dependent process which would suggest, in combination with the results in Figure 4, that AMP-DNJ targets late, but not early, endocytosis.

What the work presented here does not demonstrate is the extent of repair of the late endolysosomal (LEL) compartment – are these organelles normalised or merely adjusted? In particular is lipid accumulation reversed? AMP-DNJ corrects endolysosomal pH (Figure 4) but not necessarily cholesterol export as the NPC1 protein is still dysfunctional. Thus the misdistribution of lipids such as SM and PIs in the lysosomal limiting membrane, which accumulate through energetically favourable interactions with cholesterol,[276,284] may not be altered and so many of the protein-mediated errors investigated in chapter 2 may remain uncorrected. Whilst sophisticated subcellular lipidomics techniques can assess changes in specific lipids,[43] the use of filipin as a fluorescent cholesterol marker is a simpler assay common in the NPCD field (eg[203]). The question of whether AMP-DNJ reduces lysosomal cholesterol storage is thus relatively easy to address. In addition lipid

accumulation can permeabilise lysosomes releasing their degradative contents into the cytosol[131–133] (Chapter 1, Figure 3, stage ❷). Various techniques are available to assess lysosomal permeabilisation[576] and the impact of AMP-DNJ on this parameter should be investigated.

Lipids in the internal membranes such as triglycerides also accumulate in NPCD[43] but probably because they are processed by hydrolases such as LAL which have low pH optima and high substrate flux[515,577] and so their activity declines with reduced acidity. Normalising pH with AMP-DNJ will therefore be expected to reduce the accumulation of these fats, provided their lysosomal export pathway is operable. A similar case might be constructed regarding the cathepsin proteases. Optimal pH for activity is 3-4 for cathD[578] and 4-5 for cathB[579] and cathB activity is correspondingly reduced in NPC1 deficient cells.[74] The relatively simple experiment of using Magic Red to assess cathB activity[74] in NPCD cells treated with AMP-DNJ should be revealing.

Closely related to endocytosis is the process of autophagy where correct lysosomal acidification is also necessary[89–91] and so it would be expected that AMP-DNJ treatment would correct the errors evident in NPCD (see Chapter 1). This could be assessed by looking for a reduction in the number of vesicles positive for autophagy marker protein LC3-II. A new, simpler technique using acridine orange[580] may suffer from the pitfalls noted above with this reagent; nor is it clear how autolysosomes would be distinguished from acidic endocytic vesicles.

What of the LSDs where pH is increased but not repaired by AMP-DNJ (MPSIIIa, Krabbe, NPA and NPC2 deficiency)? From the argument presented thus far it may be suggested that GBA2 is not upregulated in those diseases. This might be surprising as the only other LSD where GBA2 regulation has been investigated is Gaucher which stems from mutation of lysosomal glucosylceramidase (GBA1, Chapter 1, Figure 4, step ❾). Here GBA2 was also upregulated[253] explaining the therapeutic effectiveness of pharmacological inhibition (miglustat is approved for use in Gaucher) or genetic knockout[581] of this enzyme. No data on the effect of GBA2 inhibition on the elevated[518] endolysosomal pH found Gaucher cells has yet been reported.

The GBA2 status of diseases whose increased endolysosomal pH is unresponsive to AMP-DNJ could be investigated by blotting for the protein and measuring enzyme activity.[253,510] Speculatively, this may reveal that GBA2 upregulation is a general feature of LSDs. In those circumstances we would be forced to re-examine the

assumptions with which we began this section, and in particular the idea that increasing cytosolic GlcCer is the only relevant effect of AMP-DNJ. In fact Figure 11 and the accompanying discussion made it clear that this agent has widespread effects on the cellular lipid profile. The possibility thus arises that it is these effects, as well as or instead of changes to cytosolic GlcCer that mediate endolysosomal pH changes. This could perhaps be clarified by performing subcellular lipidomics[43,180,582] on cells from a variety of disease types with and without AMP-DNJ treatment. Given the apparently crucial role of the cytosolic pool of GlcCer even organellar lipidomes may not offer sufficient resolution and it may be necessary to subfractionate, something that has been achieved for lysosomes,[583] before measuring the lipid profile. In the meantime the opposite responses to AMP-DNJ of the pH and endocytic volume defects in NPC and Krabbe cells (Figure 4 and 14) fuel the impression that lysosomal storage disorders are superficially similar but fundamentally different.

Other diseases: endolysosomal pH and the effects of AMP-DNJ

The outlook for the use of GBA2 inhibitors in Alzheimer's disease is yet more complicated. As noted above manipulation of lipid sub-populations can have a variety of effects on the cell, some of them undesirable, like increasing APP expression. The lipid quantitation data from fibroblasts (Figure 11) where AMP-DNJ affects at least two processes suggests that precisely targeting such manipulations is extremely difficult. To this should be added the differences between cell models (transfected glioma[558] and CHO[533] cells responded differently to PDMP than the blastoma cells used here) and the unresolved controversy over the relevance of transfected cells to disease in patients. It then becomes difficult to see how to proceed empirically with a lipid-altering approach to AD. Nonetheless the general tendency of clozapine to reduce Aß levels (Figure 16) and the suggestion that GSLs may mediate this compound's effects[554] may offer a way forward. Interesting next experiments would be to measure clozapine's effects on endolysosomal pH and lipid levels and to quantify any changes to APP expression on clozapine treatment (Figure 17B shows little apparent alteration). These experiments may allow us to tease out which factors are important in Aβ reduction.

Parkinson's disease (PD) is another relatively common neurodegenerative disorder but here the prospects are perhaps better. Deficiency in one copy of the GBA1 gene (Chapter 1, Figure 4, stage ❾) is the most common risk factor yet identified for PD;[584] deficiency in both copies is the cause of the LSD Gaucher disease which features raised endolysosomal pH.[518] Consistent with both this observation and the report of increased GBA2 activity in Gaucher,[253] this disease is treated clinically with

miglustat. Thus there may be pathological and treatment pathways common to both disease, and ultimately GBA2 inhibition may treat PD. There are several intermediate questions of interest: Does one defective GBA1 gene lead to increased GBA2 activity? What about other PD risk factors such as mutant LRRK2[585] or PARK9?[586] If so, is endolysosomal pH increased as it is in a PD model[521]? Does this increase contribute to the accumulation of the toxic α-synuclein protein? Can increased endolysosomal pH be corrected by GBA2 inhibition? If so does this prevent, or even reduce, the build-up of α-synuclein? These questions could be addressed using activity-based probes[510] and the LysoSensor technology from this chapter in patient fibroblasts, neuroblastoma cells or iPSC-derived neurones.

Materials and methods

General

Unless otherwise stated incubation of cells was conducted at 37°C in a humidified atmosphere containing 5% CO_2 and media were supplemented with 10% FBS (Gibco 10500-064) and 50U penicillin – 50µg streptomycin per mL penicillin-streptomycin (Gibco 15070-063). Fibroblasts and SH-SY5Ys were grown in cell culture flasks using high glucose DMEM supplemented with 10mM glutamine (Gibco 41965-039), NB7s were grown in cell culture flasks in RPMI (Gibco 61870-010) and RAW macrophages which were grown in untreated petri dishes in RPMI. Cells were passaged or media refreshed every 2-5 days. Cells used are shown in Table S1.

Table S1 Cells used in this chapter

Cell type	Tissue source	Supplier Code	Aberrant protein Mutation	Gender and age of donor
Monocyte macrophage	Blood	ECACC 91062702	-	mouse
Fibroblast	Skin	Coriell Institute GM00380	-	♀, 35 years
Fibroblast	Skin	Coriell Institute GM03123	NPC1 Pro237Ser/Ile1061Thr	♀, 9 years
HAP wt	Bone marrow	Horizon -	-	No information
HAP GBA2 KO	Bone marrow	Horizon HZGHC004109c001	CRISPR KO of GBA2	No information
Fibroblast	Skin	Coriell Institute GM18424	NPC2 Val30Met; other allele uncharacterised	♀, no data
Fibroblast	Skin	Coriell Institute GM13205	aSMase Premature stop at Leu382; other allele uncharacterised	♀, 2 years
Fibroblast	Skin	Coriell Institute GM01739	Heparan-N-sulfatase 1307del9; other allele normal	♀, 6 years
Fibroblast	Skin	Coriell Institute GM02048	TRPML1 Heterozygous; exons missing	♀, 2 years
Fibroblast	Skin	Coriell Institute GM02571	- Trisomy 21	♀, 3 months
Neuroblastoma NB7	Bone marrow	See footnote o	- Various chromosomal defects[587]	No information
Neuroblastoma SH-SY5Y	Bone marrow	ATCC, CRL-2266	Stably over-expressing APP[557]	♀, 4 years

Trypsin (Gibco 25200-072) was used to remove cells from flasks except for RAW macrophages which required only scraping. PBS was sterile (Gibco 10010-015) unless otherwise stated; non-sterile PBS, MES+ and RIPA buffers were prepared according to the formulae given below. Protease inhibitor

cocktail (PIC) tablets (Pierce A32955) were suspended in 400µL ddH_2O to give 25x stock solution. Other chemicals were obtained and used as set out in Table S3.

Non-sterile PBS: 5 PBS tablets (Sigma P4417) were dissolved in 1L ddH_2O with stirring. The resulting solution was stored at 4°C.

MES+: MES (3.2g, Sigma 69892) $MgSO_4.7H_2O$ (177mg), KCl (5.144g) and NaCl (125mg) were dissolved in 600mL ddH_2O with stirring to give fc values of MES (25mM) $MgSO_4$ (1.2mM) KCl (115mM) and NaCl (5mM). The solution was divided into 6 equal portions and cooled to 4°C. Each portion was adjusted to a pH value in the range 3-7.5. Buffers were stored at 4°C.

RIPA: NaCl (876mg), Nonidet-P40 (1mL, Sigma N6507), Na-deoxycholate (500mg, Acros 218590150) and Tris (655mg) were dissolved in 100mL ddH_2O with stirring to give fc values of NaCl (150mM), Nonidet-P40 (1% v/v), Na-deoxycholate (0.5% w/v) and Tris (50mM). Buffer was stored at 4°C and used within 1 month.

Endolysosomal pH

Procedure is for fibroblasts and is based on previous work.[65,480,481] Cells were grown in one T225 (flask a) and six T75 (flasks b-g) cell culture flasks until confluent. Medium was removed and replaced with fresh; drugs were added as appropriate (see Table S2) and cells incubated overnight. Media was decanted and the cells trypsinised; media was re-added and the cells centrifuged (5mins, 1500rpm). Media was removed and the pellets resuspended in 1mL (flask a) and 200µL (flasks b-g) of original medium. LysoSensor yellow/blue DND-160 (Invitrogen, L7545, 1mM in DMSO) was added - 5µL to pellet a, 1µL to pellets b-g (fc 5µM) - and the samples incubated in a water bath at 37˚C for 5 minutes. The centrifuge tubes were filled with ice-cold non-sterile PBS and centrifuged (4˚C 5mins, 1500rpm). All supernatants were discarded. Pellet a was resuspended in 3mL ice-cold non-sterile PBS and 500µL placed in each of six 1.5mL Eppendorf tubes (pellets a1-a6); pellets b-f were resuspended in 500µL ice-cold non-sterile PBS and placed in each of six 1.5mL Eppendorf tubes; all tubes were centrifuged (4˚C 5mins, 2000rpm). Supernatants were discarded. To pellets a1-a6 were added 430µL ice-cold MES+ of different pH values in the range 3-7.5; monensin and nigercin (each 4.3µL of a 0.1mM solution) were added; to pellets b-f were added 430µL ice-cold non-sterile PBS. All tubes were vortexed. 2x200µL of each sample were placed in separate wells in a black non-treated 96-well plate pre-cooled to ice temperature. 6x200µL ice-cold non-sterile PBS were also added to separate wells. The plate was incubated at ice temperature on the bench for 10 minutes after monensin and nigericin were added. The plate was examined by fluorescence exciting at 320 and 360nm and measuring emission at 451 and 520nm (cut-off values set at 455 and 515nm) using a SpectraMax Gemini instrument. If needed repeat readings were taken at 10 minute intervals until an acceptable correlation curve ($r^2 \geq 0.9$) was obtained. Yellow/blue ratios for pellets a1-a6 gave the correlation curve; yellow/blue ratios for pellets b-g were calculated and pH values obtained by comparison with this curve.

Variations: for RAW macrophages one large (15 cm diameter) and six small (9 cm diameter) petri dishes were used; for NB7 and SH-SY5Y cells a centrifuge speed of 3500rpm was used. Incubation time with brefeldin A was 2hours.

Table S2 Drugs used in this chapter
All solutions and dilutions were made with DMSO unless otherwise stated.

Drug	Mode of action	Supplier, Catalogue number	Initial concen-tration	Dilution	Volume added to (media volume)	Final concen-tration	Ref
U18666a	NPC1 blocker	Tocris 1638	1mg/mL	-	10.6µL (5mL)	5µM	
U18666a	NPC1 blocker	Tocris 1638	1mg/mL		0.64µL (5mL)	300nM	[482]
AMP-DNJ	GBA2 inhibitor	See footnote g	1mg/mL	1:250	10µL (5mL)	20nM [a]	[523,588]
Brefeldin A	COP-1 blocker, merges ER and Golgi	Sigma B7651	1mg/mL	-	10µL (10mL)	1µg/mL	
Miglustat	GBA2 inhibitor	Tocris 3117	6.4mg/mL	-	10µL (5mL)	50µM	[248]
(D)-PDMP	GCS inhibitor	Matreya 1756	2.1mg/mL	-	10µL (5mL)	10µM	[518]
(L)-PDMP		Matreya 1749	2.1mg/mL	-	10µL (5mL)	10µM	
PPMP	GCS inhibitor	Cayman 17236	10mg/mL	-	3.8µL (5mL)	15µM [a]	
Myriocin	SPT inhibitor	Sigma M1177	2mg/mL	-	10µL (5mL)	10µM	
Fumonisin B_1	Cer synthase inhibitor	Cayman 62580	5.4mg/mL	-	10µL (5mL)	15µM	[589]
Clozapine	GlcCer modulator?	Tocris C444	2mg/mL		16.3µL (5mL)	20µM	[554]
Monensin	Na^+/H^+ ionophore	Sigma M5273	6.9mg/mL 10mM	1:10 [b]	4.3µL (430µL)	10µM	
Nigericin	K^+/H^+ ionophore	Sigma N7143	7.5mg/mL 10mM	1:10 [b]	4.3µL (430µL)	10µM	

Notes: [a] Lower concentrations were achieved by using a reduced amount of drug solution and normalising the volume with DMSO. [b] Dissolved and diluted in methanol

Endolysosomal pH time course

Seven petri dishes containing RAW macrophages were grown to confluence. Medium was removed and replaced with fresh; U18666a (fc 300nM, see Table S3) was added 0, 15, 30, 45, 60, 120 and 180 minutes before cells were harvested and yellow/blue ratios measured as above. Comparison with the correlation curve obtained by averaging results for other independent experiments gave the pH values.

Measurement of endocytic vesicles

Cells were placed in a Nunc 6-well plate (Thermo Scientific 140675) at ca. 50% confluence and incubated overnight. Media was removed; cells were washed with 1mL PBS and fresh media (2mL) added. AMP-DNJ was added at requisite concentrations and the cells incubated overnight. Cells were washed with 3x2mL warm (37˚C) medium containing 0% serum ('0% medium') before adding 1.5mL warm 1% medium containing 400nM LysoTracker red (prepared by adding 4µL LysoTracker red DND-99 (1mM in DMSO; Invitrogen L7528) to 10mL 1% medium). Cells were incubated for 15 minutes. Medium was removed and each well washed with 3x2mL warm 10% medium for 1 minute each time. After the final wash 2mL ice-cold 10% medium was added to each well. Cells were examined by fluorescence microscopy using an EVOS instrument and the RFP filter; 40x magnification and 40% light intensity were used. Typically 10 images per well were recorded. For each image red pixels were counted in ImageJ using the Color Pixel Counter plugin with default settings (imagejdocu.tudor.lu/plugin/color/color_pixel_counter/start); the number of cells in each image was counted manually.

Golgi trafficking

Procedure is for fibroblasts and is based on previous work.[41] 5x100µL of cells suspended in medium (control or containing drug (Table S3)) were placed on a coverslip in a petri dish and incubated overnight. Medium was removed and each coverslip washed with 3x100µL 0% medium. 95µL 1% medium containing 1.5µM BODIPY-LacCer (prepared by adding 7µL of BODIPY-LacCer (1mg/mL in ethanol; Invitrogen, discontinued) to 0.5mL 1% medium) was added to each coverslip and petri dishes incubated for 45 minutes (pulse time). Medium was them removed for each coverslip and the dish washed with 3x10mL 10% medium for 1 minute each time. 10mL of fresh 10% medium was placed in the dishes which were then incubated for 90 minutes (chase time). The medium was then removed and 10mL ice-cold 10% medium added. Coverslips were retrieved individually and examined by fluorescence microscopy using an EVOS instrument and the GFP filter. Typically 40-50 images were recorded. Images were analysed manually for the presence of Golgi staining.

Variations: for RAW macrophages BODIPY-LacCer complexed to BSA (Invitrogen B34402, 1mg dissolved in 1mL ddH_2O) and a chase time of 60 minutes were used.

Lipid quantitation

Cells were grown until confluent, treated with drug (DMSO for controls) and incubated overnight. Cells were harvested, the pellets rinsed x3 with PBS and stored at -20°C. Pellets were transported to Universiteit Leiden in a container packed with solid CO_2 where they were analysed for lipid content as described.[590]

Aß assay

Cells were grown in Nunc 6-well plates (Thermo Scientific 140675) until confluent. Media were then removed, the cells washed with PBS (2x1mL) and 1mL OptiMEM (Gibco 31985-062) added. Drugs were added (see Figure S2 and Table S3) and cell incubated overnight. 800µL medium was removed from each well, centrifuged (3mins, 3000rpm) and then 750µL placed in a 1.5mL Eppendorf containing 30µL 25x PIC (see above). Samples were stored at -20°C until they were transported to Manchester University in a container packed with solid CO_2 where they were analysed for Aß content as previously described.[557] The remaining OptiMEM was removed from each well and cells washed with 2x1mL warm PBS. 200µL RIPA buffer containing PIC (see above) was added and the cells scraped; the suspension transferred to a 1.5mL Eppendorf and incubated at ice temperature for 30 minutes. The mixtures were then centrifuged (4°C, 10mins, 13000rpm), 75µL of lysate removed and stored at -20°C until transport and analysis as above.

Multi-sequence alignment

The human, mammalian and *C. elegans* sequences were downloaded from UniProt (uniprot.org) and aligned in Clustal Omega (ebi.ac.uk/Tools/msa/clustalo/).[465] For yeast the *S. cerevisiae* sequence was subjected to a BLAST search in UniProt and the resulting 250 sequences imported to JalView where they were sorted according to GlcCer status[528,529] (sequences from species with no GlcCer information were removed).

Protein modelling

Protein modelling was performed as described in chapter 2 except for the vATPase model with one a and three c subunits which required sequence alignment in DeepView and the project mode of SwissModel (swissmodel.expasy.org/).[304,306,591] Details are given in Table S3.

Table S3 Properties of protein structures used in this chapter

Protein	Struc-ture	Model based on	Resolu-tion (Å)	QMEAN-Brane score	Position in membrane	Ref
vATPase (c subunit decamer)		5tj5	3.9	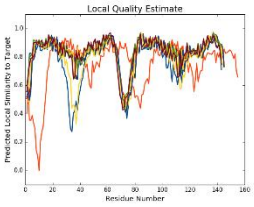	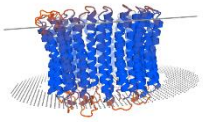	496
vATPase (a subunit and three c subunits)		5tj5	3.9	-5.75	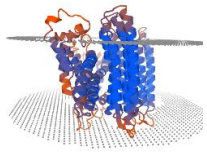	496
NPC1 (membrane region)	5u74		3.34	-4.23	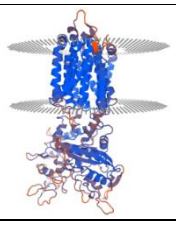	338

Molecular docking

Molecular docking was performed as described in chapter 2. Details for the AutoDock docking of cholesterol to the c subunit decamer are given in Table S4. For ROSIE-Rosetta ligand docking of the GlcCer headgroup to the ac_3 model, the starting position was the terminal N of Lys54 of each of the three c subunits; for GlcCer to NPC1 the starting position was $C_ß$ of Ser666; in both cases all other settings were defaults.

Table S4 Docking parameters for AutoDock For more details on the procedures used to perform docking and calculate the grids used, see Chapter 2 Table S3 and.[309,310]

Protein, region	Grid centre	Grid dimensions (points)	Grid offsets (points)	Residues with flexible sidechains	Lipid and (number of GA runs)
vATPase c subunit decamer, luminal face	Phe137, Cβ	x=60 y=80 z=90	x=-3.25 y=-11 z=17	Lys155	Cholesterol (100)
vATPase c subunit decamer, cytosolic face	Phe137, Cβ	x=76 y=90 z=90	x=-2 y=-12 z=-9	Arg126	Cholesterol (100)
NPC1, luminal face	Leu693, Cα	x=80 y=110 z=126	x=0 y=-2.25 z=-9.5	-	15,9-GlcCer 15,9-GalCer (both 500)

A

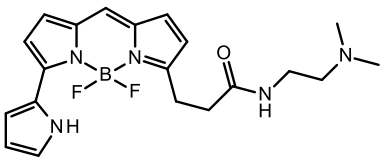

Lystotracker Red

B

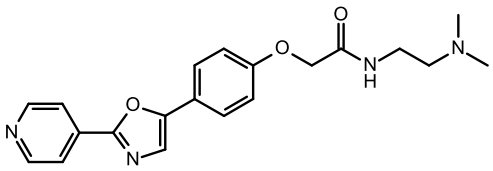

Lysosensor yellow/blue

C

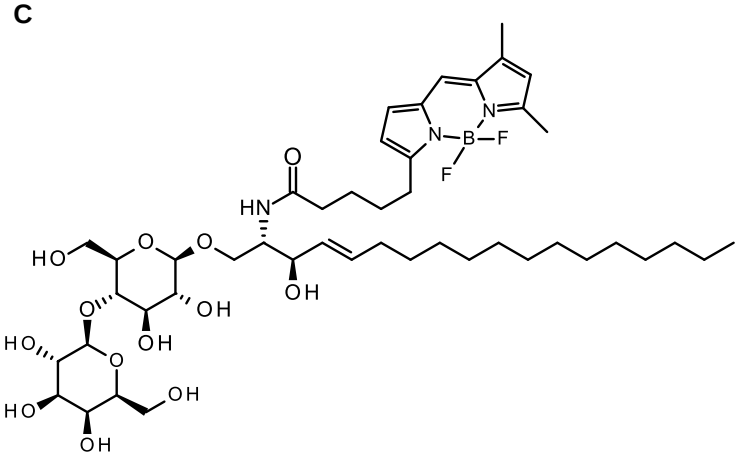

BODIPY-LacCer

Figure S1 Chemical probes used in this work

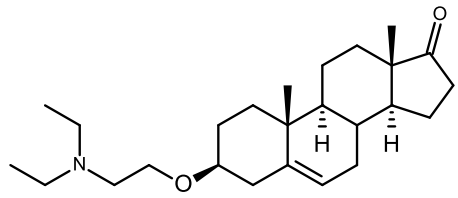

U18666a

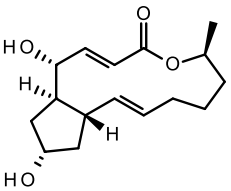

Brefeldin A

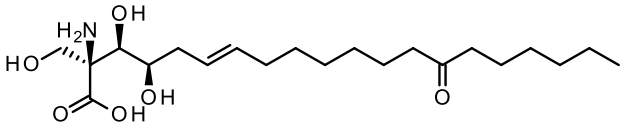

Myriocin

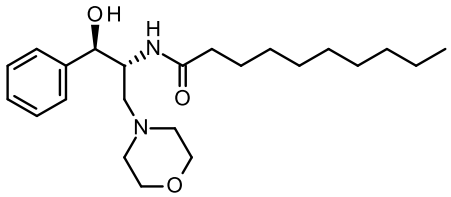

(D)-PDMP

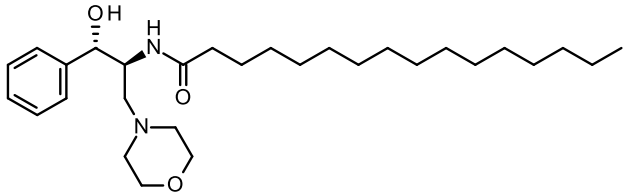

PPMP

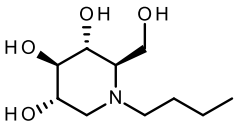

NB-DNJ
miglustat
Zavesca ®

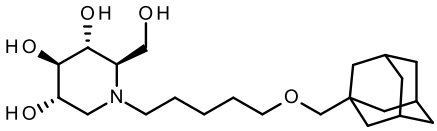

AMP-DNJ

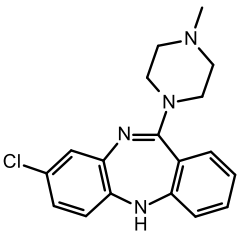

Clozapine

Figure S2 Sphingolipid manipulating drugs used in this work

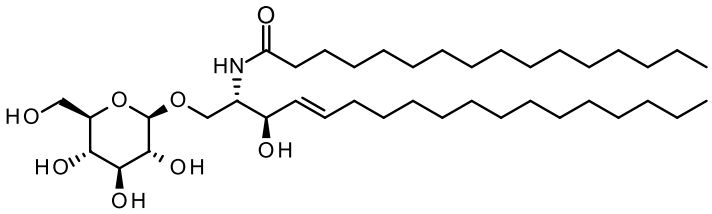

Natural GlcCer

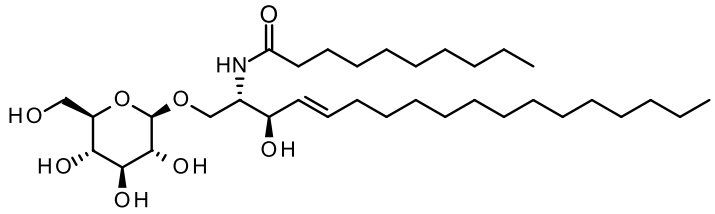

15,9-GlcCer

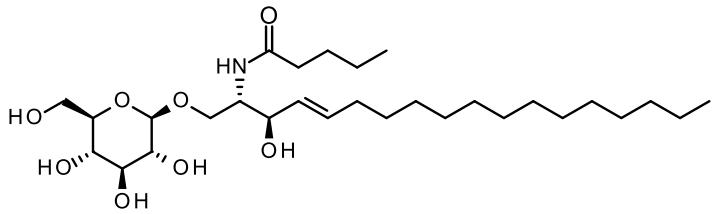

15,4-GlcCer

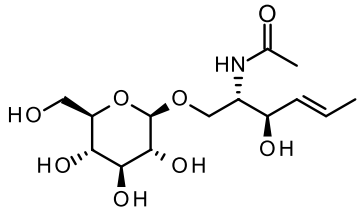

GlcCer headgroup

Figure S3 Natural GlcCer and short chain surrogates used for molecular docking

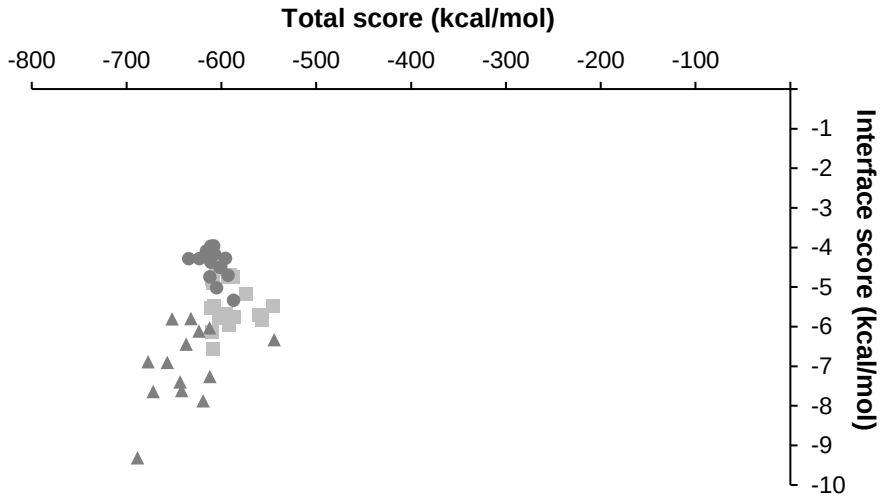

Figure S4 ROSIE-Rosetta ligand docking output for GlcCer at vATPase Squares represent binding poses between the a subunit and c subunit chain N (Figure 6A), triangles represent binding poses between the a subunit and c subunit chain D (Figure 6B) and circles represent binding poses between the a subunit and the c subunit chain B (Figure 6C). Only correctly oriented conformations from the 30 poses with most favourable interface scores are shown.

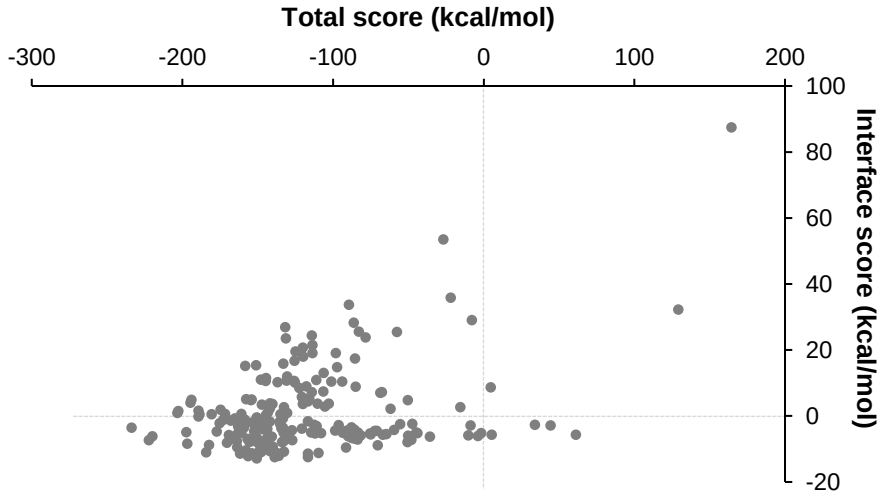

Figure S5 ROSIE-Rosetta ligand docking output for GlcCer at the luminal pocket of NPC1 Dotted lines mark the boundaries of the energetic favourability for both total score and interface score. Only poses in the lower left quadrant are favourable.

4

Mitochondria

Chapter 1 introduced the phenomenon of mitochondrial dysfunction in NPCD and the idea that it results from damage caused by cathepsins escaping damaged lysosomes. That chapter also surveyed the evidence for the more popular notion that mitochondrial insufficiency is caused by cholesterol overload and found the data highly suggestive but ultimately inconclusive. This chapter will consider the idea that reduced mitochondrial function results not from cholesterol but from sphingolipids and considers the possibility that this aspect of NPCD might be treated by manipulating levels of this class of molecule, as chapter 3 showed was successful for endocytosis. Finally it returns to the cholesterol hypothesis and proteins of the mitochondrial membranes.

Introduction

Basics of mitochondrial function

The generation of adenosine triphosphate (ATP), a molecule stable to biological conditions and yet readily hydrolysed to release energy, occurs in the mitochondria by a multi-stage process involving multi-protein complexes embedded in the inner mitochondrial membrane (Figure 1A). Pyruvate, derived from glycolysis in the cytosol, enters the mitochondria where it participates in the Krebs cycle. At various points in this cycle NADH and $FADH_2$ are produced (Figure 1, ❶ and ❷). These are organic sources of hydride ion (H^-) and are processed by Complex I and Complex II respectively. The hydride is split into an H^+ ion (proton) and two electrons (❸). The electrons are passed, via ubiquinone (Q), to complex III (❹) and the energy liberated thereby used to transport a proton across the inner membrane against its concentration gradient and into the inter-membrane space (❺). An electrical potential is also generated by this separation of ions and is termed $\Delta\Psi$. Further transport of electrons from Complex III to Complex IV by cyt *c* (❻) allows another proton to be exported. Protons can then flow back into the mitochondrial matrix down their concentration gradient via the ATP synthase (fATPase, ❼) and the energy release allows the synthesis of ATP (❽). The protons are recombined with the electrons in the presence of oxygen to give water (❾).

If electrons escape this transport chain into the inter-membrane space they can react with oxygen to give, after further chemistry, hydrogen peroxide, and the superoxide and hydroxide radicals. These molecules are collectively known as reactive oxygen species (ROS), are toxic to cells but generally rendered harmless by peroxisomes.

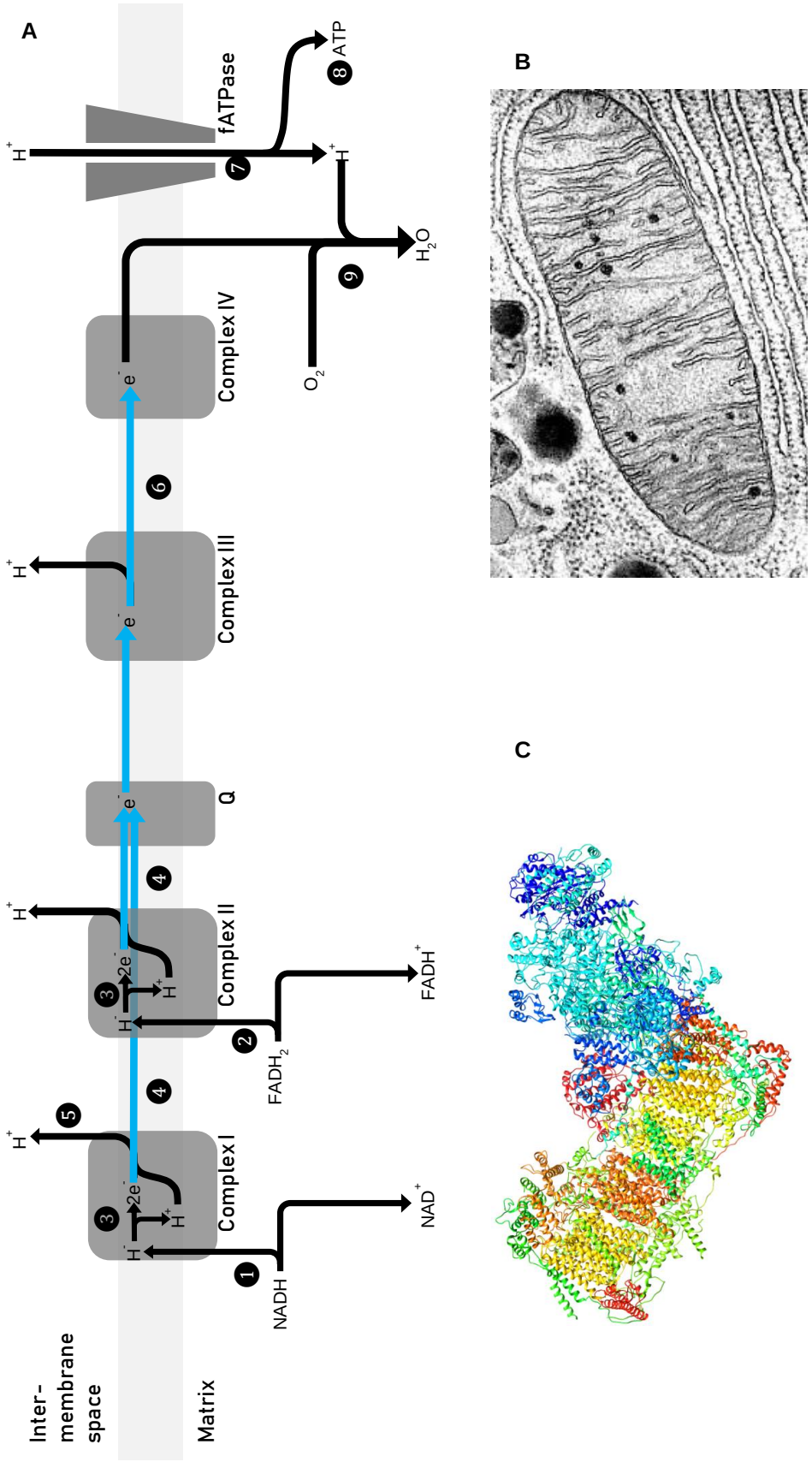

Figure 1 Mitochondrial physiology (**A**) Schematic of the respiratory chain, for details see text. (**B**) Electron micrograph of a mitochondrion taken from biology-pages.info/C/CellularRespiration.html (accessed 18/07/2019). (**C**) Structure of complex I (PDB: 5txd[592]) proteins coloured differently.

Measuring mitochondrial function

This work uses two complementary measures of mitochondrial function: oxygen consumption and ATP production, both experiments being performed in healthy and disease fibroblasts. Oxygen consumption was measured using an OxyGraph machine[593] (details given in Materials and Methods). This experiment places two samples of *ca.* 10^6 cells in a buffer in sealed glass chambers where oxygen concentration can be measured using electrodes. The cells are first permeabilised with digitonin causing the loss of small molecules including Krebs substrates and consequent decline in oxygen consumption to almost zero. Cells are then supplied with a large excess of malic and glutamic acids which produce NADH, substrate for complex I. Additional supply of ADP renders possible the production of ATP and thus oxygen consumption increases sharply, though reliant only on complex I. Feeding the cells with succinic acid, which produces $FADH_2$, substrate for complex II, increases oxygen consumption still further. The cells can then optionally be treated with rotenone, an inhibitor of complex I, to evaluate oxygen consumption reliant only on complex II. Further optional treatments include mitochondrial uncoupler CCCP (to assess total respiratory capacity) and fATPase inhibitor oligomycin (which should abolish oxygen consumption almost entirely). Whilst this assay has the advantage of being able to resolve any deficiencies specific to individual complexes, its drawbacks are the need for a large number of cells and relatively low throughput.

ATP production was measured using a repurposed cell viability assay that assess the number of cells in a sample by consuming their ATP to produce a fluorescent signal - the amount of ATP is correlated with the number of cells present. Thus if the number of cells is fixed a measure of ATP levels is produced instead (details given in Materials and Methods). This assay lacks the detail of oxygen consumption (it cannot even distinguish mitochondrial from glycolytic function) but the use of only 6000 cells per sample means that it can be run in a 96-well plate so the throughput is high. The underlying assumption is that there are only negligible differences in growth rates between cell types and within the same cell type treated with different drugs.

Fibroblasts are an appropriate cell type to study mitochondrial function

As noted in chapter 1 all cells need to import cholesterol to mitochondria so that Cyp27A1 and related proteins can synthesis LXR ligands as part of the cell's cholesterol homeostatic processes. Mitochondria of steroidogenic cells also contain Cyp11A1 (also known as $P450_{scc}$) which mediates the first committed step in steroid hormone synthesis raising the possibility that such cells may have a higher demand

for cholesterol than those from non-steroidogenic tissues. It is therefore important to note that while mitochondrial dysfunction has been observed to result from NPC1 deficiency in CHO cells[138,185] it has also been found in brain,[137,171] muscle,[171] liver[171] and skin.[55] Fibroblasts thus constitute a valid and convenient platform for the study of respiratory insufficiency in NPC disease.

Results and Discussion

Defining the mitochondrial defect in NPC1-deficient cells

In accordance with previous work[138] oxygen consumption was found to be reduced in untreated NPC1-deficient cells compared to healthy controls (Figure 2A).

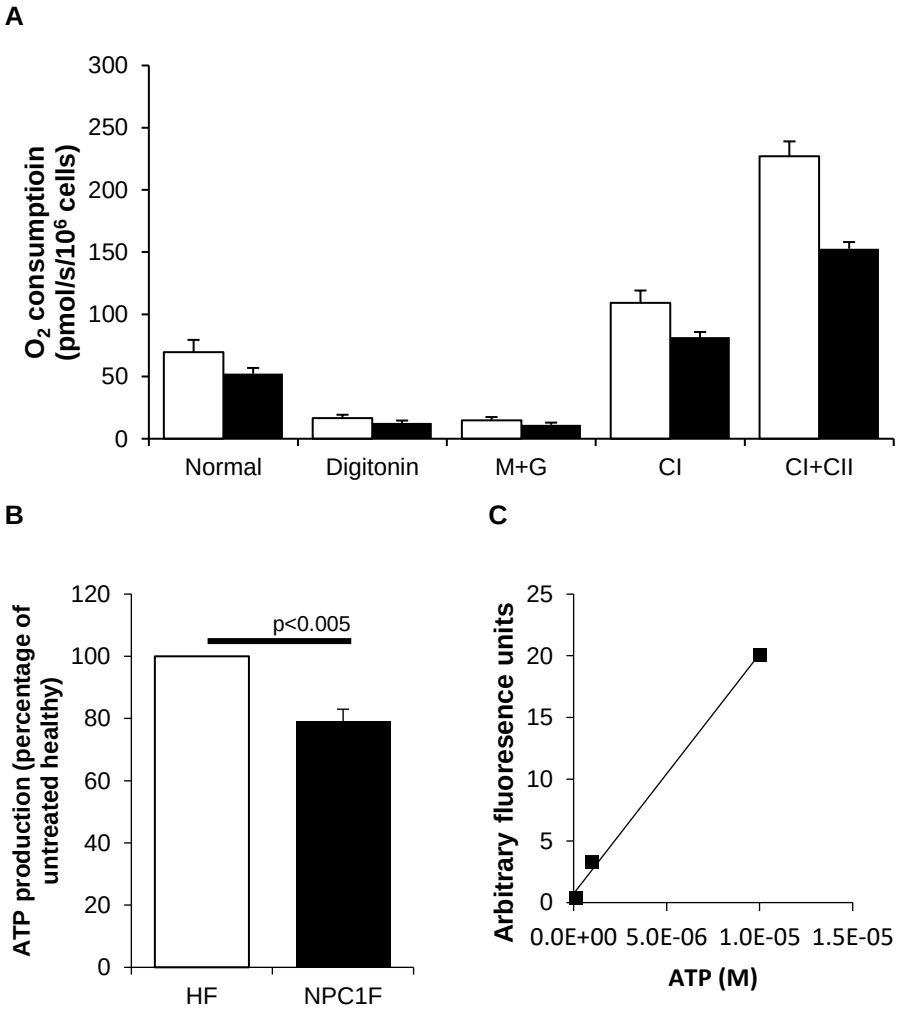

Figure 2 Respiratory dysfunction in NPC1-deficient cells (**A**) Oxygen consumption if reduced under all conditions tested (mean±SEM, n=4). (**B**) ATP production is ca. 80% of healthy cells (mean±SEM of 6 independent experiments conducted in triplicate). (**C**) Sample correlation curve for the Glo ATP assay (r^2=0.997) carried out with each experiment as per the manufacturer's instructions.

This respiratory error was again apparent when feeding complex I alone and even more pronounced when feeding complex I together with complex II (Figure 2A) suggesting a pernicious error of mitochondrial function rather than something that can be localised to a particular protein complex. This contrasts with previous work where, using an incomplete mitochondrial fraction, the error was localised to the fATPase.[171] ATP production was also reduced in disease fibroblasts (Figure 2B) as has been found previously.[138,171]

Which lipid is responsible?

In chapter 1 we encountered the idea that mitochondrial dysfunction in NPCD stems from cholesterol overload of that organelle and observed that the direct evidence for this is not quite conclusive as cholesterol quantitation was performed on mitochondrial fractions that were pure but incomplete.[138,171,181,186] (Other studies[594,595] do not attempt to demonstrate the purity or completeness of their mitochondrial fractions.) While cholesterol overload has been reported to result in mitochondrial dysfunction in both liver and pancreatic cells[173,174] mechanisms by which this might lead to respiratory insufficiency have only recently been put forward, and on evidence which is quite slim.[172,175] At the same time the build-up of lipids other than cholesterol raises the possibility that one or more of these might actually be the culprit. Consistent with this notion are reports of deleterious effects on mitochondrial function of Sph[596,597] (though not at pathophysiologically relevant concentrations) GlcSph[598] and GlcCer.[598] The LSD Gaucher disease, caused by an impaired ability to metabolise GlcCer, also features mitochondrial dysfunction[599] and in a yeast model of NPCD respiratory defects were attributed to excess ceramide.[600,601] These observations open the possibility that multiple lipid defects lead to mitochondrial dysfunction in NPCD and hence even the experimentally challenging[180] subcellular lipidomics approach might not clarify matters.

To investigate the possibility that sphingosine might poison mitochondria respirometry was undertaken in HEK cells where sphingosine-1-phosphate (S1P) lyase (Chapter 1, Figure 4, stage ⓮) had been knocked out.[r] This is the terminal enzyme in sphingolipid catabolism which catalyses an irreversible carbon-carbon bond cleavage, hence its loss causes cells to accumulate both S1P and sphingosine[602] even while continuing to grow normally in culture. This phenotype is similar to NPC1-deficient cells. These Sph-enriched cells displayed lower oxygen consumption than the parent cells from which they were derived (Figure 3) thus possibly giving credence to the idea that in NPCD excess sphingosine leads to mitochondrial

[r] These cells were a gift from Dr Per Haberkant (EMBL) to whom I am grateful.

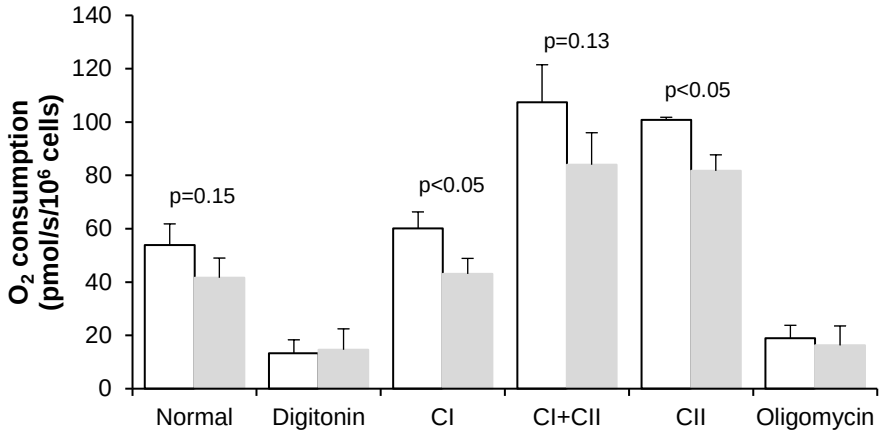

Figure 3 S1P lyase knockout in HEK cells impairs oxygen consumption Oxygen consumption is reduced, though not always significantly, under all conditions tested (mean±SEM, n=4).

dysfunction. (Attributing mitochondrial toxicity to the excess of S1P is perhaps less likely as a mimic of this lipid has been shown to reduce ROS in a neuronal cell culture[603] whereas ROS increases in NPCD.[138])

It is plausible that excess sphingosine, rather than cholesterol, poisons mitochondria in NPCD

Next the question was asked whether this was an effect specific to sphingosine, as is sometimes observed in other areas (eg[114]), or generalisable to similar molecules. Thus healthy fibroblasts in the OxyGraph were fed with 5μM dihydrosphingosine (dhSph, see chapter 1, Figure 4, stages ❶-❷) and incubated for 40 minutes. After this time respiratory activity reduced to 60-70% of that present in untreated cells (Figure 4) thus reducing the likelihood that a specific Sph-protein interaction is responsible for respiratory dysfunction. (These experiments were conducted in PBS as no change could be detected when adding dhSph to cells in the usual respiration buffer (data not shown) - this can probably be attributed to dhSph binding to the BSA that is present in the buffer.) This is consistent with work in mice where knocking out ceramide synthase (Chapter 1, Figure 4, stage ❷) led to an expected increase in dihydrosphingosine as well as mitochondrial insufficiency.[604]

These experiments may hint at a mechanism of action for these sorts of molecules. Previously sphingosine had been implicated in mitochondrial dysfunction through induction of Ca^{2+} errors[605,606] though the possible equivalence of dhSph was not examined. A simpler explanation may suffice: it may be that any amine can poison mitochondria - the basic portion of the molecule reacting with H^+ ions in the intermembrane space (Figure 1A) and so reducing their concentration thus reducing $\Delta\Psi$ and hence fATPase activity. The localisation of both sphingosine kinase[607] and monoamine oxidase[608] (for which Sph is not a substrate) to mitochondria argues in

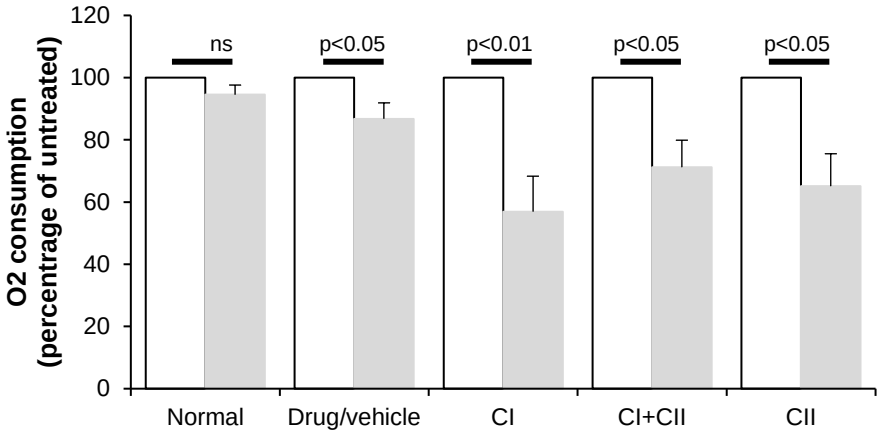

Figure 4 Dihydrosphingosine reduces oxygen consumption Dosing healthy fibroblasts in PBS with 5μM dhSph reduces oxygen consumption under all conditions tested (mean±SEM, n=3).

favour of this idea. Thus it is plausible that other amines, eg GalSph that is believed to be responsible to toxic effects in Krabbe disease,[609] also poison mitochondria. This raises a transport question: how does a lipid stored in the lysosome end up in the mitochondrion? This is a relevant question whether the lipid is sphingosine, cholesterol or a different species entirely.

Transport of lipids from lysosomes to mitochondria

Mitochondria are unable to synthesise their own lipids and so must acquire them from elsewhere, most obviously the ER via membrane contact sites;[610,611] the question for this study is whether lipids can also be provided from the lysosome. In some pathologies this seems possible. Thus traumatic brain injury leads to activation of lysosomal enzyme aSMase which acts on sphingomyelin in a metabolic process equivalent to Chapter 1, Figure 4, stage ❾ for GlcCer. This hydrolase generates ceramide and thence sphingosine; ultimately sphingosine is increased in mitochondria where it disrupts normal function.[612] (Previously expressed caveats regarding purity and completeness of the mitochondrial fraction apply here also.) The simplest explanation is that sphingosine generated in the lysosome is transported to the mitochondrion. Studies with cholesterol have suggested that such a pathway does not require functional NPC1 but is mediated by NPC2[185] and lysosomal cholesterol transport protein StARD3[181,186,613] (also known as MLN64) which we met in chapter 2. Thus NPC2 conveys cholesterol to the lysosomal limiting membrane where it presumably flips before being collected by the START domain of StARD3 and inserted into the outer mitochondrial membrane. (This study[185] of the role of NPC2 is contextualised by the work cited in chapter 1 showing that various devices[41,216,217,264,266–268] promote cholesterol export from the lysosome even in the

absence of functional NPC1 and makes yet more opaque the role of NPC1, as discussed in chapter 2.)

But why can NPC1-deficient cells transport lipid to the mitochondrion not, as reviewed in chapter 1, to its normal destination in the ER? Vacuole-mitochondrion contact sites have been described in yeast;[614] and more recently the equivalent in human cells[71] has been found to be mediated by rab7, a protein whose dysfunction is implicated in NPCD (see chapter 2). This chapter will therefore assume that a key feature of NPCD pathology is the formation of lysosome-mitochondria MCSs. It will further assume that, even in the absence of functional NPC1, significant amounts of cholesterol and sphingosine accumulate on the cytosolic face of the lysosomal membrane from where they can potentially be transported to the mitochondria. This second assumption is to an extent at odds with the model of NPC1-mediated lipid export discussed in chapter 2 but is an appropriate paradigm given the paucity of our knowledge of NPC1 and the data on mitochondrial dysfunction in NPCD.

Unlike NPC2[15] and the NTD of NPC1[330] no StAR protein has been crystallised with a bound sterol so the best method for elucidating binding is through molecular docking using the recently published crystal structure of StARD3 (PDB: 5i9j[360]) combined with the analysis of sterol binding in StAR-like proteins. The ROSIE ligand docking protocol[312,615,616] allows great protein flexibility and works best with enclosed pockets like the one in StARD3 so this was selected. Binding poses can be named according to the orientation of the cholesterol hydroxy group and consistent with previous work[359] binding poses were found in both the 'IN' and 'OUT' orientations (Figure 5A). The previous study could not distinguish between these two clusters of results using docking or MD, though the total simulation time of 1.5ns may be too short. On inspecting the 30 most favourable ROSIE binding poses (those with the most negative interface score) a statistically significant ($p<10^{-5}$) preference for the IN orientation was evident (Figure 5B) as has previously been reported for StARD5.[617] This is consistent with studies on StARD1[618] (also known as STAR) and StARD4[619] which both suggest that the Ω1 loop (blue in Figure 5A) flexes to allow lipids to enter the cavity. Thus the StARD3 opening created by a flexed Ω1 loop could interact with the polar surface of a membrane; cholesterol could then leave the membrane polar-end first and enter the binding cavity and hence the IN orientation would arise naturally. (An exactly similar situation pertains if StARD3 were to collect cholesterol from the putative luminal binding site of NPC1, see Chapter 2, Figure 13.) Most cholesterol IN poses featured an H-bond

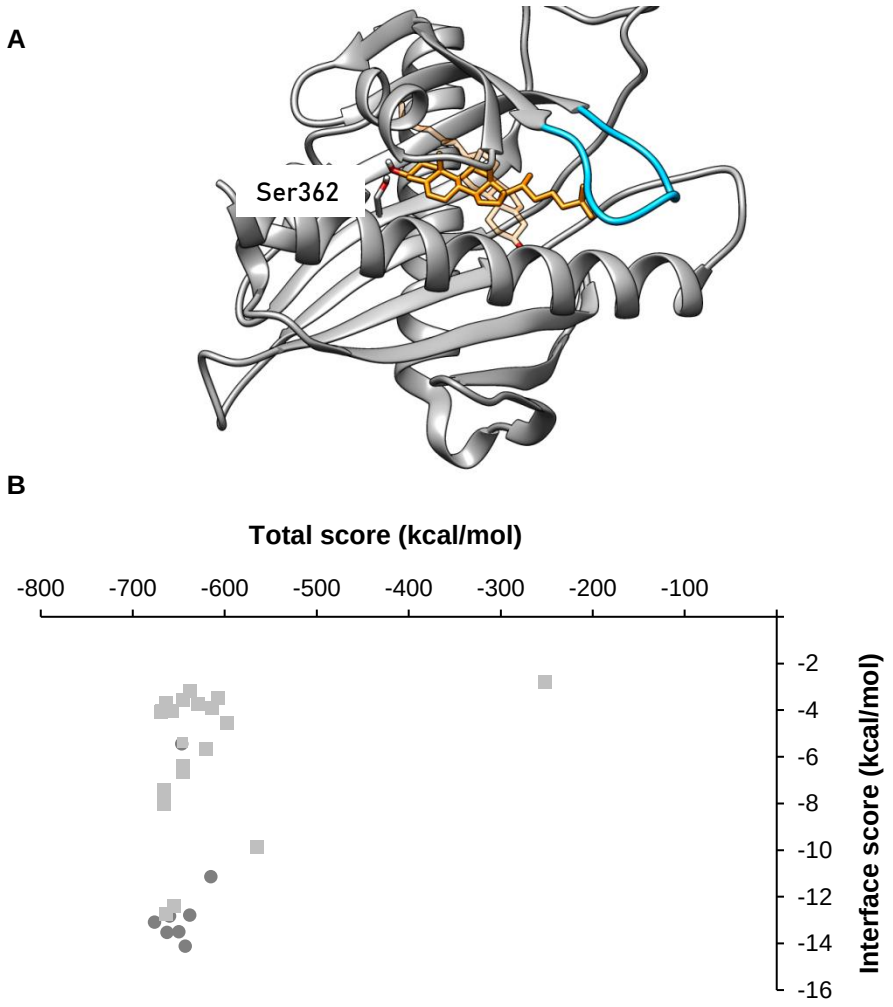

Figure 5 Docking of cholesterol in StARD3 (**A**) Docking of cholesterol in StARD3 (PDB: 5i9j) yields both IN (orange) and OUT (pale orange) poses; the Ω1 loop is shown in blue. (**B**) The interface score of the cluster of IN poses (circles) is significantly more favourable than that of the OUT poses (squares).

to Ser362 which is shown in Figure 5A and was also identified as key in the previous study.[359]

After this docking work had been completed the crystal structures of three yeast StAR orthologues[s] with bound sterols were published;.[620–622] the orientations of these bound ligands show similarities as well as differences (Figure 6A,B) to the results emerging from the docking experiments (Figure 5). Most obviously all sterols are bound with the IN geometry (Figure 6A) supporting the idea that this is biologically important.[359] All are bound with the methyl groups of the sterol β-face oriented similarly (Figure 6A, though only StARD3 features a CH-π interaction involving the sterol α-face (with Trp404, Figure 6B). All sterols make hydrophobic

[s] These structures were found using the DALI search tool[683,684] for similar protein structures. I am grateful to Dr Pietro Roversi (University of Leicester) for bringing this technique to my attention.

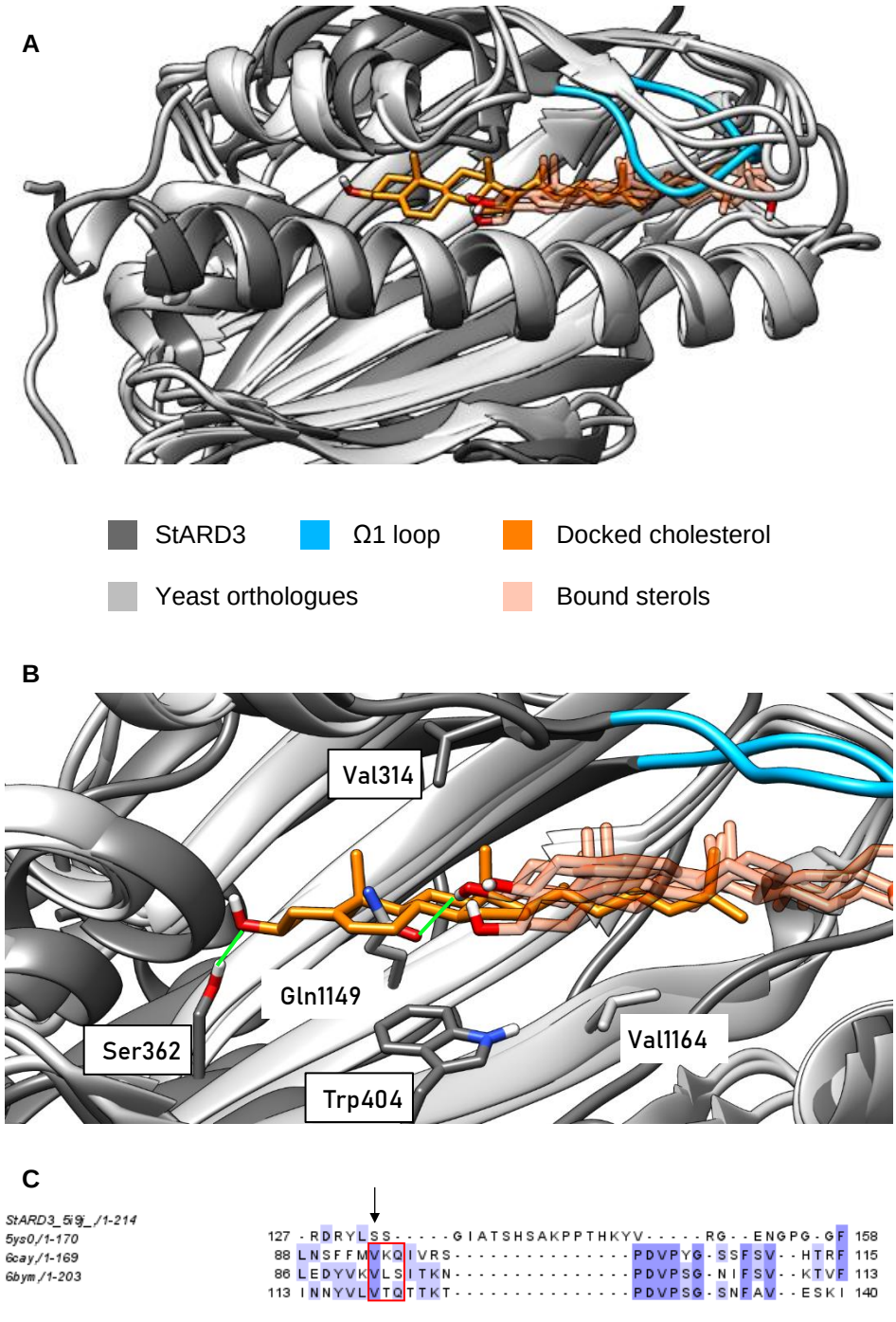

Figure 6 Conservation of structure amongst StARD3 and related proteins (**A**) Human StARD3 with docked cholesterol is shown overlaid with *S. cerevisiae* Lam4 (PDB 6bym) and two sterol binding domains of *S. cerevisiae* Lam2 (PDB 5ys0 and 6cay) with bound sterols. (**B**) Detailed view of lipid-protein interactions with selected binding residues; StARD3 residue labels are edged in black; some protein structure omitted for clarity. For details see text. (**C**) Section of overlay-based multisequence alignment of the sterol binding domains from (**A**) and (**B**). For details see text.

contacts with aliphatic sidechains inside the pocket (eg Val1151 of Lam2 and Val314 of StARD3, Figure 6B). Simple multi-sequence alignment of these four proteins shows the fungal structures have <20% sequence identity to StARD3 and positions

residues equivalent to putative key H-bonidng residue Ser362 outside the lipid binding pocket (data not shown). Thus the sequences were re-aligned based on the structure overlay (performed in UCSF Chimera[363]). This gives an even lower sequence identity to human StARD3 (ca. 12% in every case) but sheds more light on lipid binding. Thus Ser362 aligns with a valine in every case (Figure 6C, arrow) but an H-bonding residue occurs two positions further on (Figure 6C, red box; eg Gln1149 of Lam4) and these are found crystalographically to bind the sterol –OH,[621,622] (Figure 6B) with an intermediate water in one case.[620] (Some of the residues aligning with position 363 of StARD3 are capable of H-bonding but their sidechains are positioned outside the binding pocket.) This perhaps explains why the bound sterols in the crystal structures only partially overlay with cholesterol

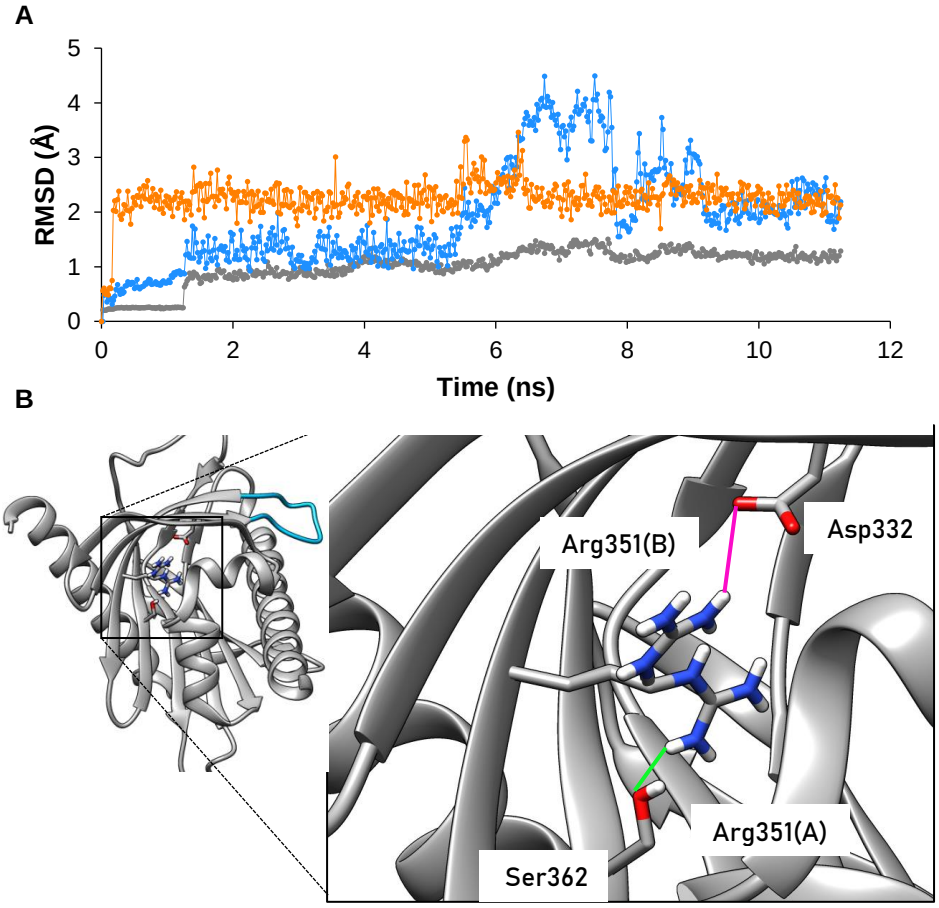

Figure 7 Flexibilities in StARD3 with potential functional consequences (**A**) MD simulation of a sample IN binding pose shows the C_a atoms of the protein backbone (grey) experience minimal fluctations while the the C_a atoms of the Ω1 loop (blue) have considerable flexibility. The cholesterol (orange) remains stably bound suggesting loop opening alone is insufficient to provoke cholesterol off-load. (**B**) Cholesterol unloading may be prompted by Arg351 switching between the two conformations found in the crystal where it can form an H-bond (green) with key cholesterol binding residue Ser362 (conformation A) and ionic interactions (magenta) with Asp332 (conformation B).

docked to StARD3 (Figure 5A) and why the RMSD for the carbon atoms in these lipids compared to docked cholesterol is usually larger than the RMSD for the protein overall (9.40Å vs 5.81Å for 5ys0, 8.70Å vs 6.37Å for 6cay and 8.77Å vs 8.35Å for 6bym). Perhaps as a consequence of this the regions of yeast proteins corresponding to the Ω1 loop appear more open (Figure 6A), though these loops are still found important for yeast protein function.[620–622] Overall, then, docking predicts a binding mode of cholesterol to StARD3 very similar to that found experimentally for fungal orthologues.

In a 10ns MD simulation a sample pose of cholesterol bound to StARD3 rapidly underwent a small rearrangement preserving the Ser362 H-bond and then remained stable with minimal movement in the protein backbone (Figure 7A, video StARD3_5i9j_chol; protein in grey, Ω1 in blue, cholesterol in orange). Also evident from Video StARD3_5i9j_chol and Figure 7A is Ω1 opening and then closing during the lifetime of the simulation while cholesterol remains bound; this may suggest that an additional trigger is needed for lipid release. Intriguingly the crystal structure of StARD3[360] found the Arg351 sidechain in two conformations: one forming an ionic interaction with Asp332 and the other (a slight majority) forming an H-bond with Ser362 (Figure 7). We may thus conjecture that something about membrane binding triggers the re-establishment of this H-bond thereby ejecting the cholesterol molecule.

This chapter has supplied evidence that sphingosine (Figure 3) and possibly other amines (Figure 4) can lead to reduced mitochondrial function while chapter 2 repeatedly found sphingosine capable of binding to proteins in the same manner as cholesterol. The question thus arises of whether the NPCD respiratory defect can be attributed to sphingosine transported from lysosomes to mitochondria by StARD3. Here we are faced with a complication. The pKa of sphingosine has been reported as 6.6 in solution[348] and 9.1 in a model membrane[349] meaning that it will likely be electrically neutral in the cytosol but protonated (and positively charged) in the membrane. It is not obvious whether or not it will lose its charge on moving from a membrane into the lipid binding pocket of StARD3 although the geometrical considerations of lipids entering and leaving membranes discussed above suggest that Sph should adopt the same IN binding mode as cholesterol.

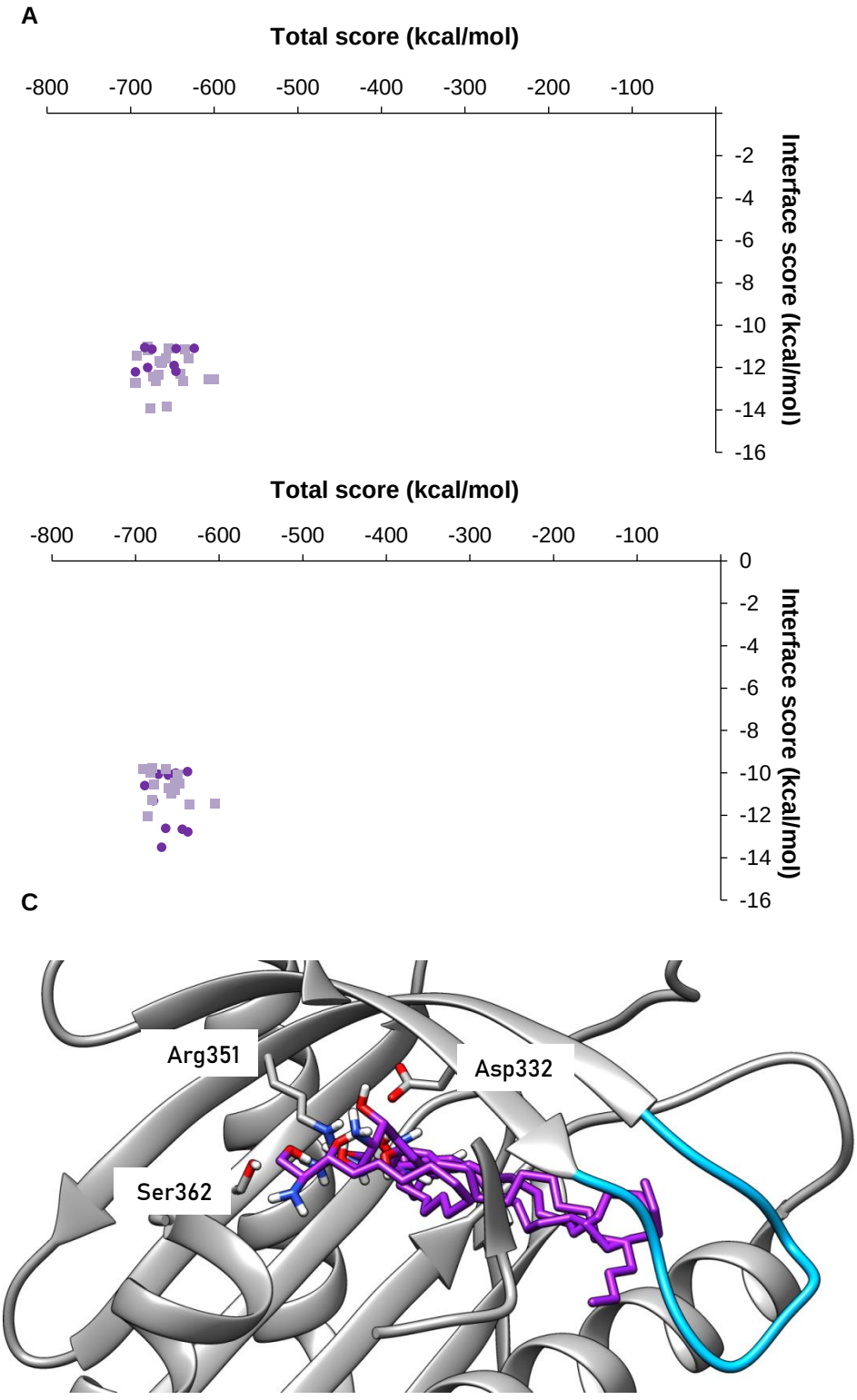

Figure 8 Sphingosine binds to StARD3 in a variety of conformations (**A**,**B**) Unprotonated (**A**) and protonated (**B**) sphingosine bind StARD3 (PDB: 5i9j) in poses where the IN clusters (circles) are energetically indistinguishable from the OUT clusters (squares). (**C**) Selected IN binding poses of unprotonated sphingosine in StARD3; some protein omitted for clarity, Ω1 loop shown in blue.

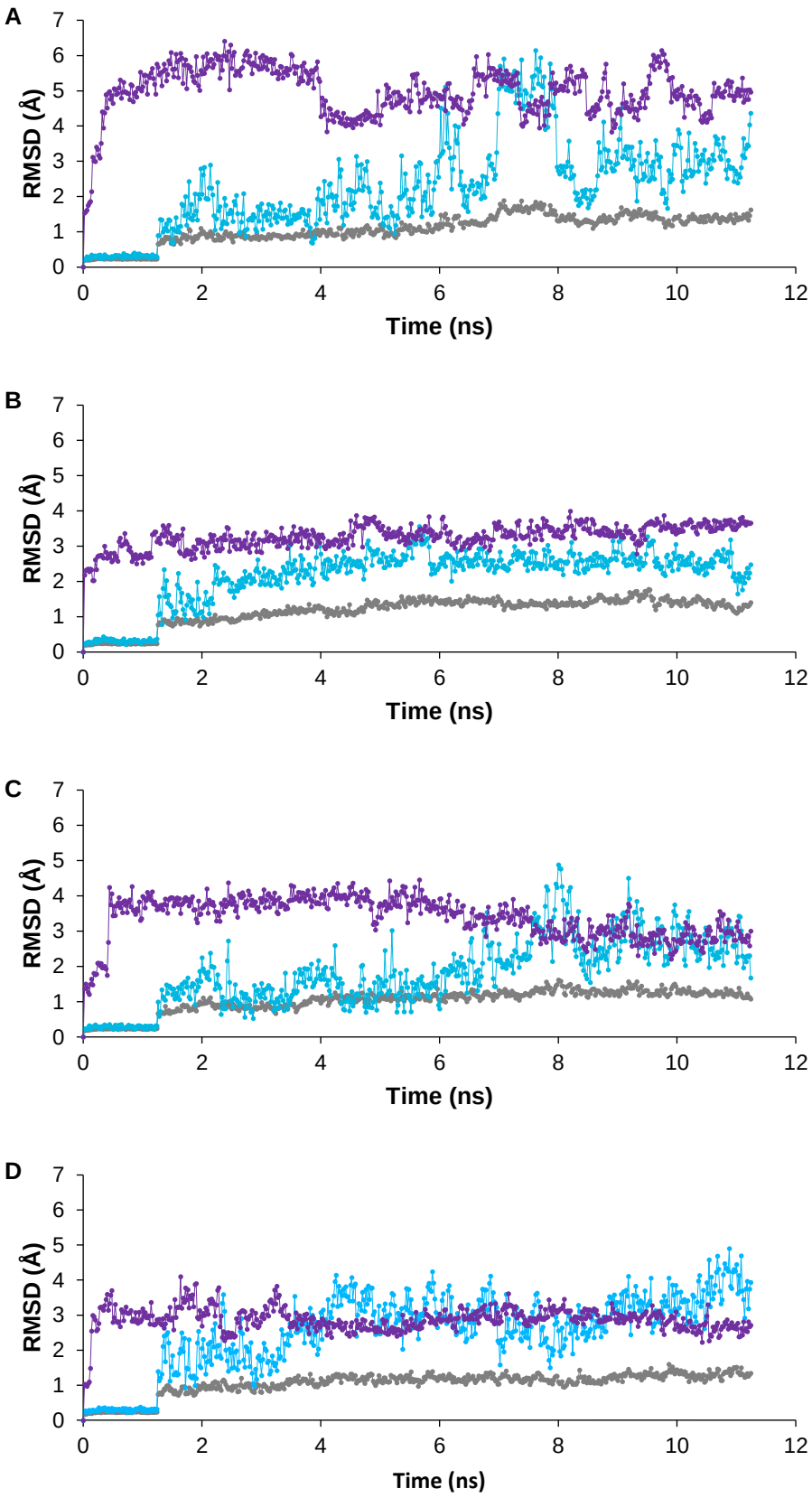

Figure 9 Stability of Sph binding poses in StARD3 under MD simulation Simulation data from starting poses 1, 2, 3 and 4 (Figure 7) are shown in (**A**), (**B**), (**C**) and (**D**) respectively; C_α (whole protein) is in grey C_α (Ω1) blue and Sph purple.

ROSIE ligand docking was performed with sphingosine both neutral and protonated and the 30 binding poses with most favourable interface scores were surveyed. (The built-in conformer generator[315] used in ROSIE tends to give only very small variations from the initial molecular shape thus Frog2[623] was used in preference.) Neutral sphingosine (Figure 8A) gave slightly more energetically favourable binding overall than protonated sphingosine (Figure 8B); for neither species was there a discernible differences between those poses categorised as IN and those denoted 'OUT' and nor was binding dominated by Ser362 - a diverse range of residues formed H-bonds with the lipid. Four representative binding poses (Figure 8C) of neutral sphingosine were subjected to 10ns MD simulations. RMSD analysis of the results for each suggested that the protein experienced limited fluctuations (Figure 9A-D, grey) while Ω1 moved around much more as expected (Figure 9A-D, blue). Sph in poses 1 and 3 did not appear to be stable (Figure 9A,C, purple) while Sph in poses 2 and 4 underwent much smaller displacements from its initial position (Figure 9B,D, purple). An analysis of residence time (the percentage of the production phase the lipid forms H-bonds to a given residue, Table) led to the same conclusions - the H-bonds formed by poses 2 and 4 remain largely stable for the duration of the simulation while those in poses 1 and 3 do not persist. Similar findings pertain to protonated sphingosine (data not shown).

Modelling supports the accepted transport pathway of cholesterol to mitochondria; sphingosine probably cannot use the same mechanism.

	Ile301	Asp332	Arg351	Ser362	Gly384	Asn407
Pose 1	0	24	2	0	0	0
Pose 2	8	0	48	59	0	0
Pose 3	0	0	15	0	34	0
Pose 4	0	0	0	0	68	5

Thus for Sph there is no energetic difference between the biologically relevant IN mode and its likely irrelevant OUT counterpart, some IN poses are unstable and some of the stable IN poses bind the protein in a manner likely to be different to cholesterol, a genuine[613] biological substrate. The failure of Sph docking/MD experiments to converge on a single stable solution suggests the conclusion that StARD3 is not involved in any sphingosine-induced mitochondrial pathology even though such dysfunction can be artificially induced as shown above (Figure 3).

Does GBA2 inhibition correct mitochondrial defects?

The effectiveness of AMP-DNJ in NPCD mice[250] suggests that the effect of GBA2 inhibition on mitochondrial dysfunction in this disease, which has not previously been studied, is worthy of investigation. (There is some evidence of benefit from a very small human study.[140]) A necessary caution is that while $A_{2A}R$ agonists have

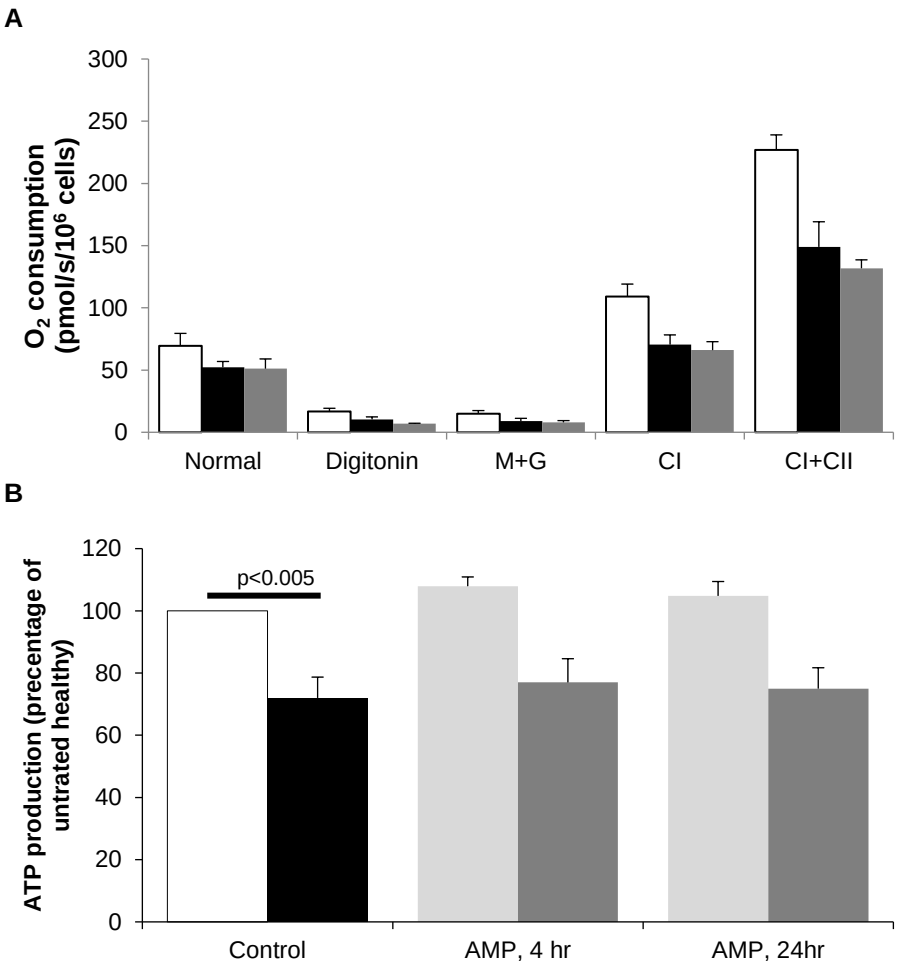

Figure 10 AMP-DNJ does not correct respiratory insufficiency in NPC1-deficient cells Neither reduced oxygen consumption (**A**, mean±SEM, n=4) nor reduced ATP production (**B**, mean±SEM of 4 independent experiments conducted in triplicate) in NPC1-deficient fibroblasts is corrected by AMP-DNJ. White bars represent untreated healthy cells, black bars untreated disease cells; light grey bars represent treated healthy cells, dark grey treated disease.

corrected both lysosomal and mitochondrial errors in cells[55,234] they produced only limited improvements in a mouse disease model[238] and so translation between cellular and *in vivo* models is not necessarily straightforward.

GBA2 inhibition by AMP-DNJ does not repair mitochondrial dysfunction.

Experiments showed that incubating NPC1-deficient fibroblasts for 24 hours with the dose of 20nM AMP-DNJ,[t] which had successful rectified errors in the endolysosomal system (Chapter 3), did not improve the reduced oxygen consumption (Figure 10A). Oxygen consumption was also unchanged in healthy cells under these conditions (data not shown). Likewise ATP production remained deficient despite treatment (Figure 10B) and was similarly unaffected in healthy

[t] I am indebted to the laboratory of Prof Johannes Aerts (Universiteit Leiden) for a gift of a generous sample of this material prepared as previously described.[249,682]

cells. Reducing the incubation time to 4 hours in search of a more transient effect was unsuccessful (Figure 10B). This strengthens the idea, advanced in Chapter 3, that the clinical usefulness of GBA2 inhibitors in NPCD arises from their ability to correct endocytic defects and adds the contribution that such drugs' failure to halt disease progresion completely may stem from their ineffectiveness at correcting mitochondrial defects.

Searching for other sphingolipid effects

Whilst the failure of GBA2 inhibition to correct mitochondrial dysfunction was disappointing there are compelling reasons for connecting energy production with sphingolipids more widely. The lysosomal storage disorders Gaucher disease and Krabbe disease are both caused by a failure of sphingolipid metabolism and feature mitochondrial dysfunction among their cellular characteristics.[551,599] The mitochondrial lipid transporter ABCB10 has recently been identified as a GlcCer binding protein[u] while ceramide,[624] as well as sphingosine, is toxic to this organelle. Thus despite the potential problems[625] it was considered worthwhile to examine the effects of pharmacological manipulation of sphingolipids on mitochondrial function in both healthy and NPC1-deficient cells. Details of the drugs and concentrations used are given in Table S1 and Figures S1-3.

None of the drugs employed led to changes in ATP production in either cell type (Figure 11A). Whilst perhaps surprising it is worth noting the difficulties described in chapter 3 of precisely manipulating defined lipid populations and that many sphingolipids are toxic to mitochondria so increasing the amount of one lipid at the expense of another may lead to no overall change. The CBE result is perhaps particularly unexpected for this compound is an inhibitor of GBA1 whose dysfunction leads to Gaucher disease. These results are nonetheless consistent with previous work that found CBE-induced mitochondrial defects only after a 10 day incubation.[626]

Attempting to alter sphingolipid populations by feeding lipids to cells was similarly unsuccessful. Neither GlcSph nor GalSph nor a cell-penetrant GlcCer analogue (AdaGlcCer) at either of its recommended concentrations[627] corrected inadequate ATP production in NPC1-deficient cells or changed ATP production in healthy cells (Figure 11B). This was a surprise as GalSph incubation is often used to simulate the LSD Krabbe disease and has been shown to induce mitochondrial dysfunction.[609] Thus, hypothesising that GalSph and other sphingolipids bound to protein in the

[u] Prof Cliff Lingwood (Sick Kids, Toronto), personal communication

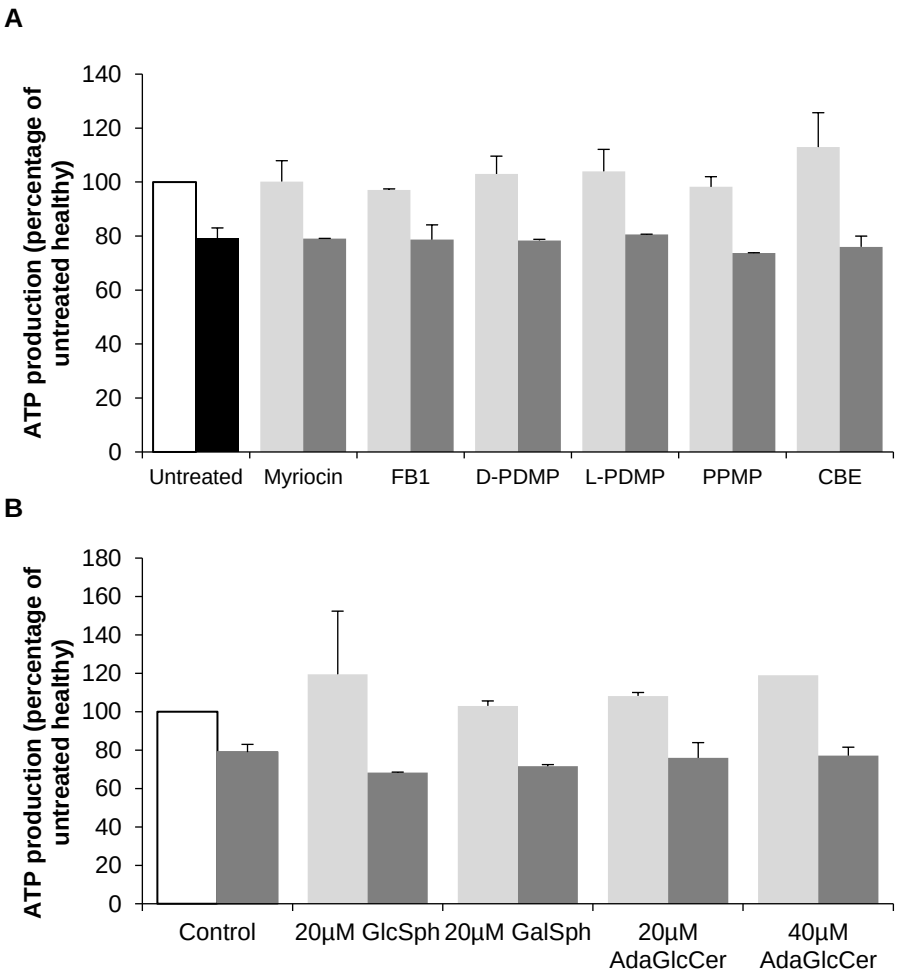

Figure 11 Sphingolipid manipulations do not correct impaired ATP production in NPC1-deficient cells Neither pharmacological inhibition of sphingolipid metabolism (**A**, mean±SD of 2 independent experiments conducted in triplicate) nor incubation with sphingolipids (**B**, mean±SD of 2 independent experiments conducted in triplicate) alter ATP production in healthy or NPC1-deficient fibroblasts. White bars represent untreated healthy cells, black bars untreated disease cells; light grey bars represent treated healthy cells, dark grey treated disease.

media (consistent with experiments in[628]) these experiments were repeated in serum-free media. Microscopic inspection of the cells revealed blebbing and fragmentation, features of apoptosis, in a manner that appeared to be dose-dependent (Figure 12) suggesting that measured ATP levels would be more likely to be a consequence of cell death than a less controlled disease process.

The results presented thus far show that sphingolipids may be part of the problem of mitochondrial dysfunction in NPCD; they do not appear to be part of the solution.

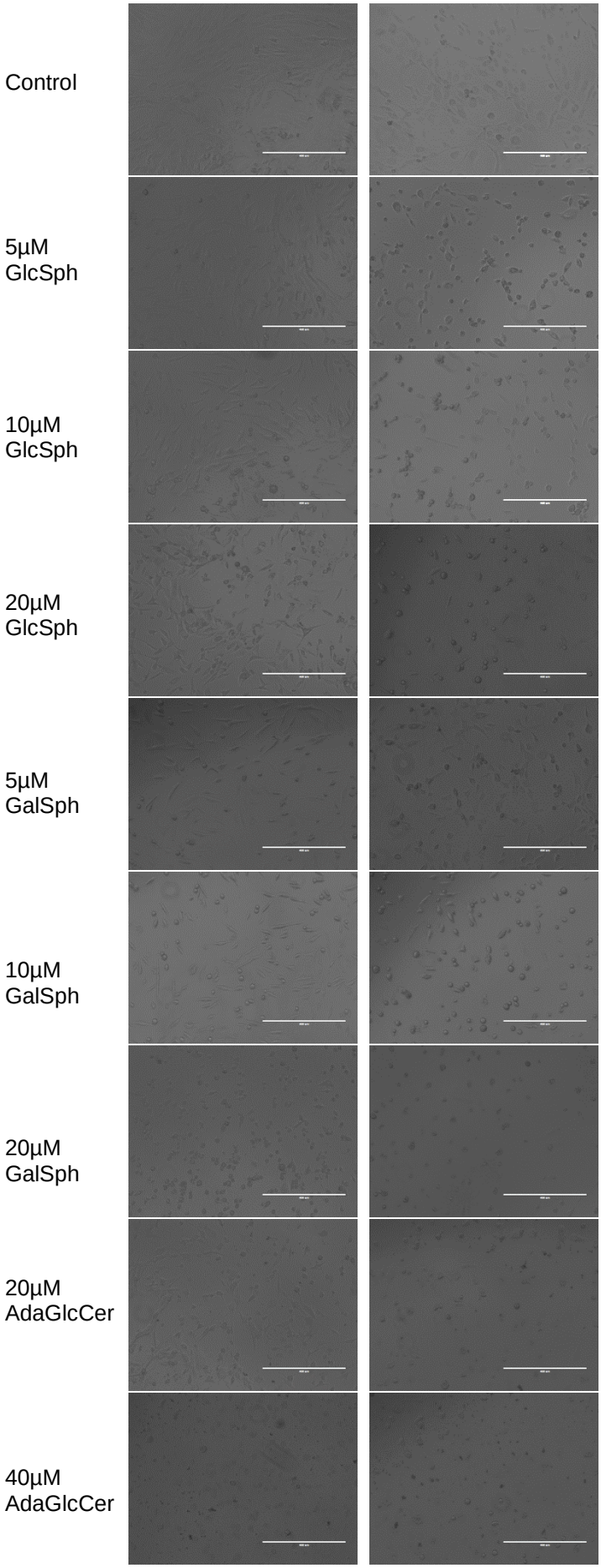

Figure 12 Apparent apoptotic effects of sphingo-lipids on fibroblasts

Healthy cells shown on the right, NPCD on the left

Inhibiting mitochondrial cholesterol import

Given that the mitochondrial defect in NPCD had proved refractory to manipulation of sphingolipid levels and that, as discussed in chapter 1, mitochondrial cholesterol import is necessary for all cells so that Cyp27A1 and related enzymes can produce LXR ligands, mitochondrial cholesterol overload was reconsidered as the source of the metabolic defect in NPCD cells. The details of cholesterol import to mitochondria have yet to be worked out, but the broad outline is known (reviewed[629,630]) and the proteins involved shown in Figure 13. (The drugs used in this section are shown in Figure S3 and the concentrations and solvents in Table S1.)

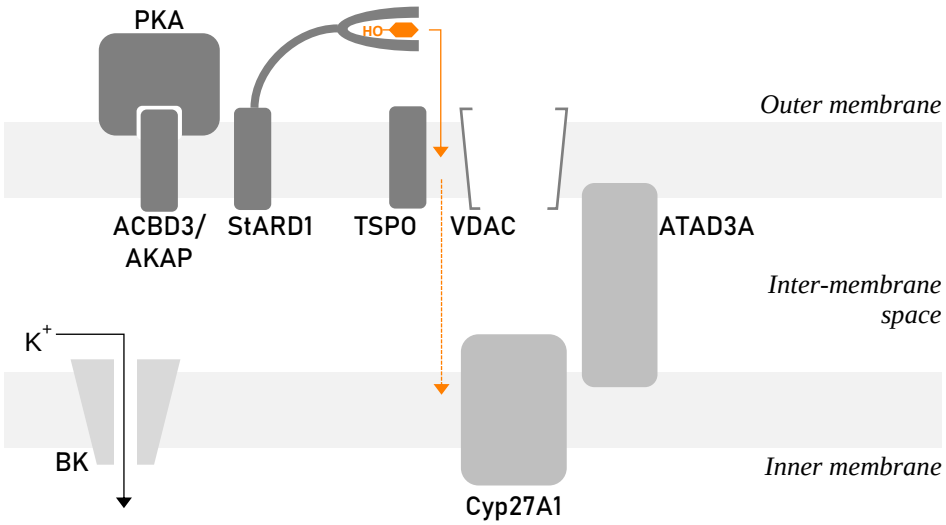

Figure 13 Working model for cholesterol import to mitochondria The functions of these proteins (if any) in cholesterol import have yet to be completely defined; see text for details.

About ATAD3A very little is known, though this protein may act to tether the outer and inner membranes[631] thereby facilitating cholesterol transport to the inner membrane where Cyp27A1 is believed to reside.

StARD1 is thought to transport cholesterol from the outer to the inner membrane though this protein's exact location and mode of action are both unclear. 21-acetoxy pregnenolone (21-AcP) has been identified as an inhibitor of StARD1[632] (given the close structural similarity of the StAR proteins 21-AcP may also act off-target to block StARD3-mediated lipid transport to the mitochondrial outer membrane). Incubation with this agent at its IC_{50} of 10μM did not alter ATP levels in either healthy or disease cells (Figure 14). Thus the concentration was increased to 40μM and cells treated for either 4 or 24 hours. At the longer time point this yielded a small increase in ATP levels in disease cells (79±4% of untreated healthy to 86±1%,

Figure 14) but a similar change in healthy cells (100 to 110±2%) questions whether this is through an impact on pathology or is a more general phenomenon.

StARD1 requires activation by PKA to achieve full capacity[633] and anchoring proteins (either ACBD3 or AKAP) for this cytosolic enzyme have been found in protein assemblies implicated in cholesterol import[629] (Figure 13). Therefore it is possible that a PKA inhibitor (H89 was chosen as being reasonably selective[162]) might reduce any cholesterol-induced mitochondrial toxicity. Indeed H89 at a concentration of 200nM (2.2x IC_{50} for PKA[162]) yielded an improvement of ATP production from 79±4% of untreated healthy to 89±1%; a corresponding increase was not seen in healthy cells (Figure 14).

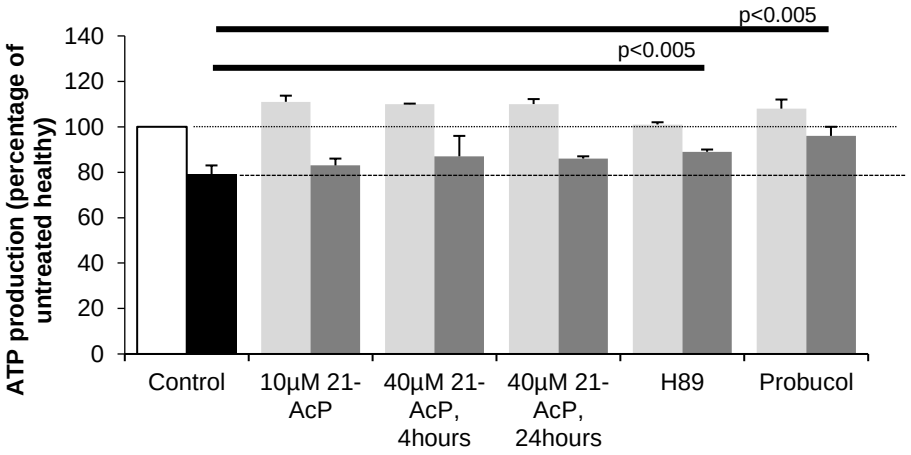

Figure 14 Attempted correction of impaired ATP production in NPC1-deficient cells by pharmacological manipulation of cholesterol transport proteins Inhibition of PKA by H89 and ABCA1 by probucol gave increased ATP production in NPC1-deficient fibroblasts but not in healthy cells (mean±SD of at least 2 independent experiments conducted in triplicate). White bars represent untreated healthy cells, black bars untreated disease cells; light grey bars represent treated healthy cells, dark grey treated disease.

Blocking cholesterol handling proteins results in modest improvements in respiratory function.

The success of both 21-AcP and H89 could be seen as supporting the cholesterol hypothesis of mitochondrial toxicity; as a control probucol, an inhibitor of cell-surface cholesterol exporter ABCA1[634] which would not be expected to increase mitochondrial function was also tried. Surprisingly this agent at its recommended concentration of 10µM[634] also gave an improvement in ATP production from 79±4% of untreated healthy to 96±4% (Figure 14) and a smaller enhancement (100 to 108±4%) in healthy cells suggesting that the influence of cellular cholesterol balance on energy metabolism is not simple.

Perhaps a surprising member of the cholesterol import machinery[629,630] is the voltage dependent anion channel (VDAC), an ATP release channel of the outer

mitochondrial membrane[635] (Figure 13). An NMR study identified cholesterol binding sites on the β-barrel pore;[636] MD simulations confirmed binding of cholesterol at these sites was stable and affected the structure of the protein though ion flux was found unchanged on lipid association.[637] (An alternative approach[638] to binding site discovery using photo-activatable cholesterol analogues arrived at different conclusions, predicting the lipid would bind anti-parallel to the membrane (see Chapter 2, Figure 6.) which seems less likely.) The computational work used a monomeric channel, which a later crystallographic study suggests may not be correct,[639] while a cholesterol derivative has been reported to affect the oligomerisation state of VDAC;[640] thus the effects of mitochondrial cholesterol on VDAC function remain to be clarified. Selective inhibitors of this channel have only just become avaialable[641] whilst activators are currently unknown rendering further study and potential correction of the role of VDAC in NPCD challenging.

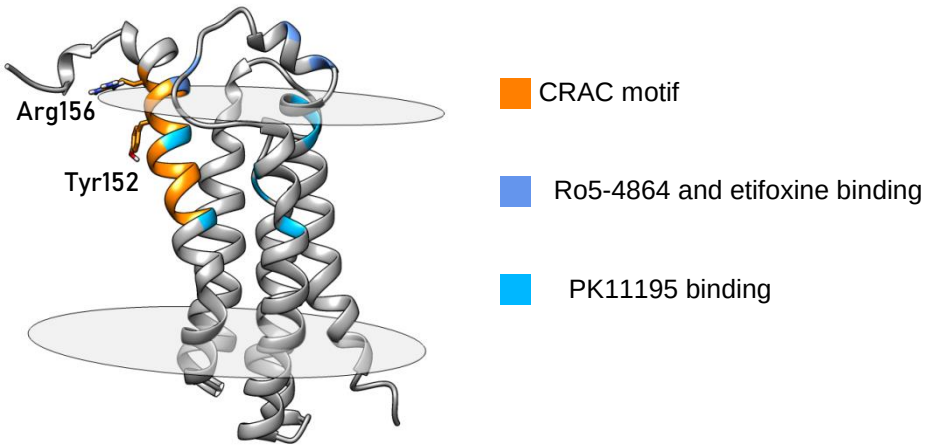

Figure 15 Binding sites on TSPO TSPO (grey) is embedded in the outer mitochondrial membrane (opaque disks); both reported ligand binding sites (blues overlap the CRAC cholesterol binding motif (orange, key residues shown). Structure taken from PDB 2no2.[642]

Translocator protein (TSPO) is a protein of the outer mitochondrial membrane which has been implicated in numerous CNS pathologies[643,644] including Alzheimer's.[645,646] It was initially named the peripheral benzodiazepine receptor (PBR); the updated nomenclature was adopted to reflect the evolving view that this protein transports substrates into the mitochondrion, a view that nonetheless remains controversial.[647] (For this reason there have been some attempts to hijack the acronym to mean tryptophan-rich sensory protein.) However there is a growing body of work that finds this protein involved in mitochondrial cholesterol import.[629,630] TSPO was in fact the first protein identified with a CRAC motif.[296] Chapter 2 expressed some skepticism regarding the general usefulness of such motifs for predicting lipid

binding sites, but in this case cholesterol binding to TSPO was unambiguously demonstrated at the predicted region.[648,649] (Given this binding motif lies on the surface of the protein the proposal that cholesterol import uses TSPO as a channel[650] is rather unlikely; molecular docking showed there is probably insufficient space for this without significant rearrangement of the protein's 3D structure (data not shown).) Since then various TSPO ligands have been shown to provoke cholesterol efflux in retinal epithelial cells,[651,652] macrophages[653] and astrocytes and fibroblasts.[654] Thus if mitochondrial dysfunction in NPCD is the result of cholesterol-induced toxicity then TSPO is a target worth investigating. This approach is also advocated by the implication of TSPO in mitochondrial calcium homeostasis and energy production.[655,656]

Previous work has identified two ligand binding sites on TSPO, both of which overlap with the CRAC motif (Figure 15). Thus mutagenesis experiments suggest benzodiazepine Ro5-4864 binds at an exposed site[657] while PK11195 binds at a site within the membrane by analogy with the crystal structure of a bacterial equivalent.[658] Etifoxine is found to bind at the same site as Ro5-4864 but with a higher potency than its binding inherently merits due to the phenomenon of slow-offset kinetics.[659] Incubation with the recommended concentrations[660] of these 3 drugs for 4 hours did not produce any changes in ATP levels in either healthy or disease fibroblasts (data not shown). Extending the incubation to 24 hours did not alter this picture for 1nM PK11195 (Figure 16A) though increasing the concentration to 100nM did enhance ATP production (data not shown). 24 hour incubation with 1μM Ro5-4864 produced a small increase in ATP (79±4% of untreated healthy to 86±3%, Figure 16A) but a similar increase could be observed in healthy cells (100 to 109±6%) suggesting this treatment may not genuinely be disease modifying. (Increasing the concentration of Ro5-4864 to 10μM did not further increase ATP production in disease cells, data not shown.) In contrast, use of 20μM etifoxine for 24 hours increased ATP production in NPC1-deficient cells from 79±4% of untreated healthy to 93±3% (Figure 16A) but only a negligible increase in healthy cells (100 to 105±5%). Given that cholesterol off-load is seen with TSPO ligands in a variety of cell types[651–654] and that sphingosine probably won't bind TSPO (at least not at the cholesterol binding site) due to electrostatic repulsion between the protonated head group and Arg156, this result argues in favour of cholesterol as the toxic lipid in NPCD and against sphingosine. This is consistent with the docking/MD studies of StARD3 reported above (Figures 5-9).

The positive results seen with etifoxine, probucol and H89 raises the question of whether combinations of these drugs could enhance ATP production further.

Unfortunately this was not found to be the case - co-incubation with etifoxine and inhibitors of either PKA or ABCA1 failed to increase mitochondrial function above the levels seen with etifoxine alone (Figure 16B).

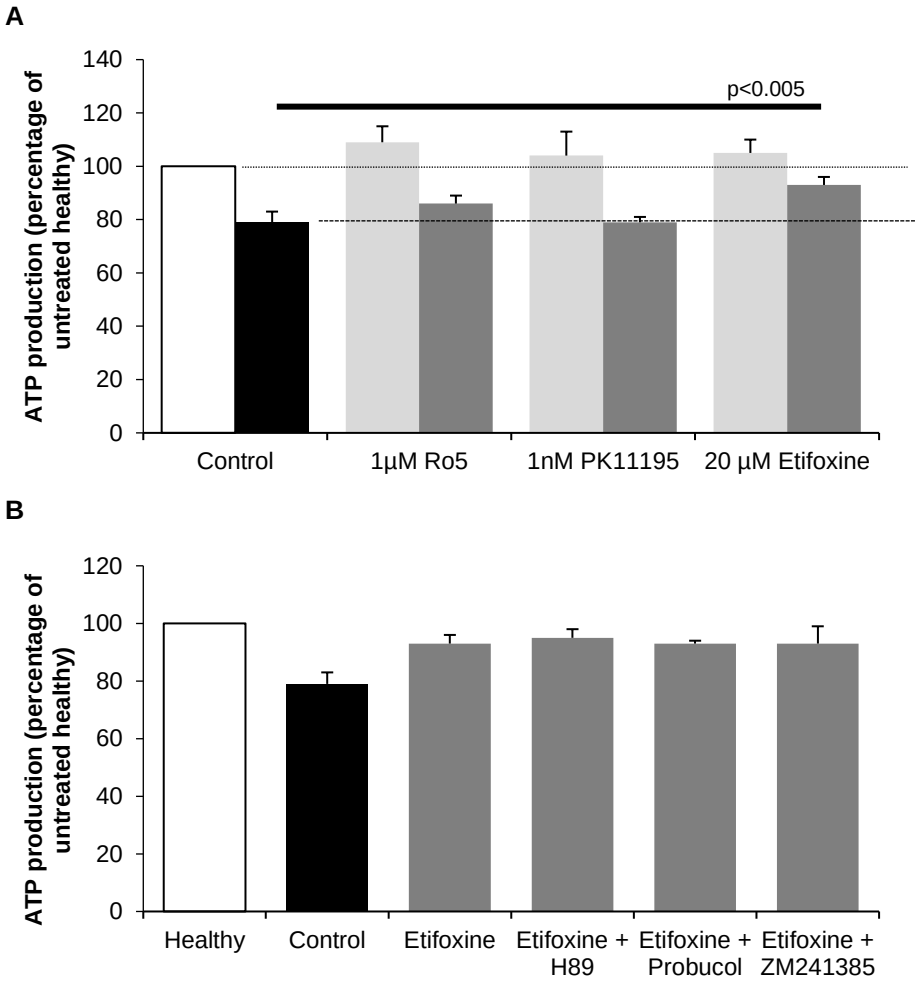

Figure 16 Attempted correction of impaired ATP production in NPC1-deficient cells by TSPO ligands (**A**) Of the TSPO ligands tested only etifoxine produces an increase in ATP production in disease but not healthy cells. (**B**) The response to etifoxine is neither blocked nor augmented selected other agents. Both charts show mean±SD (or SEM where appropriate) of at least 2 independent experiments conducted in triplicate. White bars represent untreated healthy cells, black bars untreated disease cells; light grey bars represent treated healthy cells, dark grey treated disease.

Any of these agents may be operating at their expected targets but not by the predicted pathways or indeed off-target. This is difficult to clarify pharmacologically for PKA and ABCA1 as selective kinase inhibition is a notoriously difficult task[162] and the ABC proteins are designed to bind a broad range of substrates. Off-target pharmacology of etifoxine is easier to elucidate. This compound binds TSPO at the same binding site as the benzodiazepine Ro5-4864[659] (Figure 15) and structurally mimics this class of compounds (Figure S3). Benzodiazepines have been suggested to affect $A_{2A}R$ binding sites[661] while $A_{2A}R$ agonists have been reported to correct mitochondrial errors in NPCD cells[55,234] thus it is plausible that etifoxine could be

acting off-target at $A_{2A}R$. However co-incubation with etifoxine and 500nM $A_{2A}R$ antagonist ZM241385[55,234] did not suppress the ATP enhancement seen with etifoxine alone (Figure 16B) allowing the conclusion that this agent is not mediating its effects through $A_{2A}R$ agonism.

Some ligands of TSPO result in increased ATP production. This probably does not occur through a mitochondrial pathway.

The question of off-target effects was further investigated by measuring oxygen consumption in NPC1-deficient fibroblasts treated with etifoxine. No increase in this parameter was observed whether or not respiratory complexes were fed with substrates (Figure 17). This suggests that the enhancements in ATP production found above arose from etifoxine acting through a non-mitochondrial pathway and that this drug is therefore unlikely to correct any cholesterol-induced damage to mitochondria. Whilst disappointing this is consistent with recent work suggesting that off-target effects of TSPO ligands are not uncommon.[662]

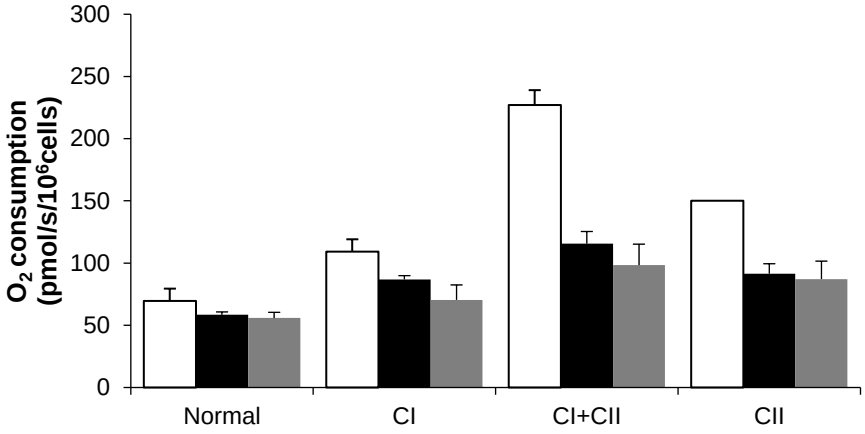

Figure 17 Etifoxine does not increase oxygen consumption in NPC1-deficient fibroblasts Oxygen consumption is unchanged after 24 hour incubation with etifoxine under all conditions tested (mean±SEM, n=3-4). White bars represent healthy cells and black bars disease; grey bars represent treated disease cells.

Do TSPO ligands affect lysosomes?

While both mitochondrial and lysosomal dysfunction are widely recognised features of neurodegenerative disorders they have only recently started to be connected; the emerging links are bidirectional. Thus knockout of lysosomal K^+ channel TMEM175 (implicated in Parkinson's disease[84,457]) results in not only lysosomal abnormalities but also reduced cellular oxygen consumption,[85] while knockout of a mitochondrial transcription factor leads to increased endolysosomal pH and storage of sphingolipids.[663] A genetic deficiency in mitochondrial complex I led to reduced expression of lysosomal proteins LAMP1 and cathepsin D a key protease[664] while knockdown of a complex III component affects lysosomal calcium.[665] Similar links

emerge from attempts at treatment. Thus supplying ubiquinone (see Figure 1) to model cells of the LSD Gaucher disease corrected not just mitochondrial abnormalities but also endosomal proliferation.[519] Most relevantly for the current study, compensation for mitochondrial errors in NPCD mice led to corrected sphingolipid storage in brain, though not in liver.[172] Thus the wider application of TSPO ligands was considered worth investigating despite the failure of GBA2 inhibition to correct respiratory errors in NPCD (Figure 10) when it had succeeded at the lysosome (Chapter 3).

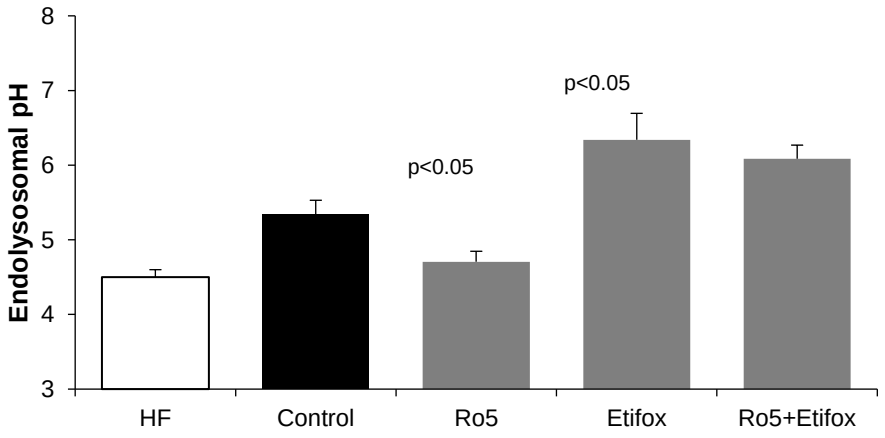

Figure 18 Effect of TSPO ligands on endolysosomal pH in NPC1-deficient cells 1μM Ro5-4864 significantly reduces endolysosomal pH will 20μM etifoxine increases it (results shown as mean ± SEM, n=3-5 export for Ro5-4864 + etifoxine mean ± SD, n=2).

Surprisingly, TSPO ligands reduce endolysosomal pH in NPCD cells.

Elevated endolysosomal pH was found to be corrected in NPC1-deficient fibroblasts treated with Ro5-4864 for 24 hours (Figure 18) just as it had been on GBA2 inhibition. Perhaps equally importantly etifoxine, which binds at the same site as Ro5-4864,[659] produced a significant increase in pH and blocked the effect of Ro5-4864. (This antagonism may be the result of using a higher concentration of etifoxine.) Thus the effects of synthetic modulators of a relatively small mitochondrial protein of unclear function[647] extend beyond its organelle of residence to reactivate enervated lysosomes.

Open questions and future work

Will my head split - or will it see? I see half - I only see half.

G K Chesterton

The Innocence of Father Brown

Several lines of evidence presented in this chapter support the working hypothesis[138,171,181,186] that cholesterol is responsible for mitochondrial dysfunction in NPCD. Sphingolipid manipulations failed to affect respiratory function in either control or disease cells (Figures 9 and 10) with the exception of excess sphingosine and its congener (Figures 3 and 4) for which a viable pathway to the mitochondrion could not be identified (Figures 7 and 8). Conversely pharmacological inhibition of mitochondrial cholesterol import increased ATP production in disease cells (Figure 13) consistent with the previous identification of an NPC1-independent transport pathway for this lipid from lysosomes to mitochondria.[185] Whilst the question of mitochondrial cholesterol loading can only finally be settled by lipidomic analysis of a clean and complete mitochondrial fraction[180] from NPCD and control cells there are some easier experiments that could offer partial insight. Filipin is a natural product which forms a fluorescent complex with cholesterol. NPCD cells would therefore be expected to show increased filipin staining co-localised with a mitochondrial label[186] such as a fluorescently tagged antibody or MitoTracker green (which stains mitochondria in a $\Delta\Psi$-independent manner). Fluorescent cholesterol analogues are another possibility but the tag can sometimes affect lipid-protein interactions (eg[666]) which may mean that results obtained with such compounds do not reflect biological reality. The assumption that this mechanism is correct also suggests further experiments aimed at therapy. If cholesterol transport to mitochondria is NPC2-dependent as suggested[185] then knockdown of NPC2 in NPC1-deficient cells may correct the respiratory defects. Combining effective drug treatments (eg H89 with 21-AcP) may lead to greater improvements than the already successful monotherapies (Figure 13).

The cholesterol hypothesis is, however, questioned by the failure of TSPO ligands to correct mitochondrial dysfunction (Figures 15 and 16) when they have previously provoked cholesterol off-load in a variety of cell types.[651–654] Assaying these compounds for cholesterol efflux or accumulation in lipid droplets might illuminate this apparent difficulty;[652,654] asking whether the effect changes on knockdown of cell surface cholesterol exporters such as ABCA1 would add another layer of detail.

The presence of the BK channel at the inner mitochondrial membrane may explain cholesterol-induced toxicity

This work has not attempted to address the reasons for the putative toxicity of cholesterol at mitochondria. To the hypotheses tentatively advanced thus far[172,175] we may add the recent discovery of the BK channel at the inner mitochondrial membrane (reviewed[667,668]), including that of fibroblasts,[669] and the coupling of this channel to the respiratory chain.[670] We encountered this channel on the lysosome in chapter 2 together with the extensive evidence of its impaired function in the presence of excess cholesterol.[372–375] Thus if NPC1-deficient cells overload their mitochondria with cholesterol that is transported to the inner membrane then the flow of K^+ out[667] of the inter-membrane space and into the matrix (Figure 12) will be impaired. This will affect the voltage across the inner membrane making export of protons across it harder and thereby leading to reduced fATPase activity, reduced oxygen consumption and reduced ATP synthesis as observed. Consistently, BK openers inhibit ROS production.[671] It would thus be interesting to test the effect of BK channel activators on mitochondrial function in NPCD. Endolysosomal pH is another parameter worth investigating as BK is also localised to lysosomes[369,370] and channel agonism has corrected the endocytic defects in this disease.[384] Some BK channel openers are cytotoxic[672] so it is important to choose agents from this class that do not exhibit this property.

The opposite effects of Ro5-4864 and etifoxine on endolysosomal pH (Figure 17) suggest they are mediated through the same protein. It might be considered surprising that ligation of a protein in the mitochondrion could affect such a fundamental property of the lysosomes, but is consistent with the growing evidence cited above of bidirectional links between these organelles. The alternative explanation is that both compounds affect a currently unknown, possibly lysosomal, target. This issue can be investigated by testing whether the effects persist on genetic knockdown of TSPO. As noted above (Figure 12) TSPO is part of a multi-protein complex with PKA. PKA is reported to activate the CFTR chloride channel[235] which may have a role in lysosomal acidification.[236] The intermediacy of these two proteins could be tested by incubating cells with combinations of etifoxine, H89 (to inhibit PKA)[162] and $CFTR_{inh}172$ (to inhibit CFTR).[573] Any effects could be confirmed by genetic knockdown of the relevant protein.

Chapter 2 showed that AMP-DNJ corrected not only lysosomal acidification but also mistargeting of an endocytic marker. It will therefore be interesting to find out if TSPO ligands have the same effect, and if they can correct the endolysosomal volume defect that AMP-DNJ left unchanged (Chapter 3, Figure 4).

Materials and methods

General

For general methods and details of cells used see chapter 3.

ATP production assay

Cells were placed in a white cell-culture treated 96-well plate (Corning 3610) at a density of 6000 cells per well and incubated overnight. Medium was removed, cells washed with 100µL sterile PBS per well and 100µL fresh media containing drugs or sphingolipids added at concentrations shown in Table S1. Three wells were used for each treatment. The plate was incubated for 4 or 24 hours. After this time 100µL of the Promega Cell-Titer Glo reagent (catalogue number: G7570) which had been thawed in the dark for at least two hours was added. The plate was gently shaken for 2 minutes and allowed to stand for a further 10 minutes before measuring the luminescence at 560nm using a GloMax plate reader.

As per the manufacturer's recommendation each plate also contained 3 wells each of 100µL aqueous ATP solution at concentrations of 10^{-5}, 10^{-6} and 10^{-7} M. Adding 100µL Glo reagent to these invariably gave luminescence readings linearly correlated with concentration with $r^2 > 0.95$.

Oxygen consumption assay

Cells were either treated or untreated depending on the experiment. Approximately 10^6 cells were harvested, counted and centrifuged (1500rpm, 5 minutes) the pellet resuspended in 2mL MiR05 buffer (see below) and placed in the OxyGraph machine (oroboros.at/?Oxygraph). The cells were allowed to come to equilibrium (indicated by stabilised oxygen consumption) before drugs and substrates were added as per Table S2. After each addition oxygen consumption was allowed to stabilise before a reading was taken.

MiR05 buffer:[593] to 100mL ddH_2O was added lactobionic acid (35.83g, Acros 167111), the solution adjusted to pH 7 with aqueous KOH solution and diluted to 200mL with ddH_2O. 120mL of this was added to 500mL ddH_2O containing EGTA (190mg, Sigma E3889, fc 0.5mM), anhydrous $MgCl_2$ (286mg, Sigma M8266, fc 3mM), taurine (2.502g, Sigma T0625, fc 20mM), $KH_2PO_4.7H_2O$ (2.622g, fc 10mM), HEPES (4.77g, Sigma H3375 fc 20mM), sucrose (37.65g, fc 110mM) and BSA (1g). The volume was adjusted to 1L with ddH_2O and the pH adjusted to 7.1 using aqueous KOH solution; lactobionic acid fc 60mM. Buffer was split into 50mL aliquots and stored at -20°C until needed when an aliquot was thawed and subsequently stored at 4°C.

Docking

100 or 200 conformers of neutral and protonated sphingosine were generated as a single sdf file using Frog2.[623] This file was submitted to the ROSIE-Rosetta ligand docking protocol[311,312] with a starting position of CZ2 of Trp404 of StARD3 (PDB: 5i9j;[360] QMEAN score 0.91, see Chapter 2 Table S1 for output). 1000 structures were generated; all other settings were defaults. Results were triaged

by interface energy score and total energy score followed by more detailed assessment of the structure of the most favourable as described in the main text.

Molecular dynamics

This was performed as described in chapter 2 except for the use of neutral sphingosine which was parameterised using CgenFF[320,673] giving very few adverse penalty scores (Figure S1); the calculated values for charges and angles behind all of these were considered acceptable on close inspection so the parameter file was used without modification.

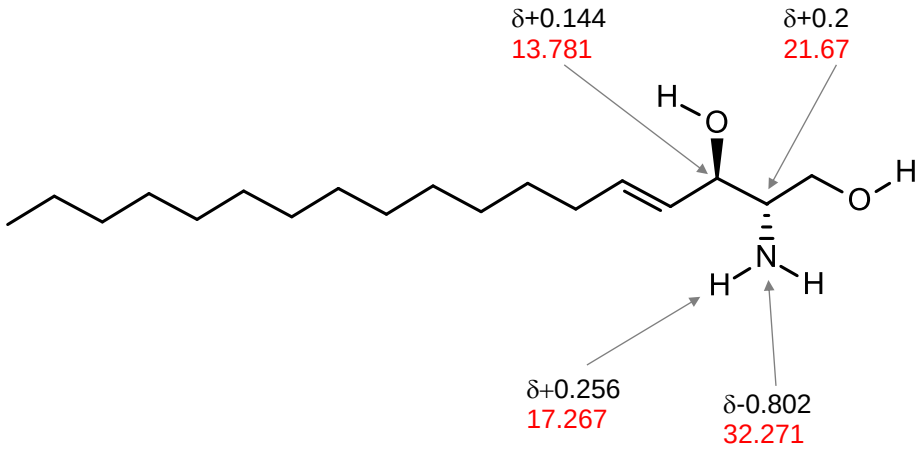

Figure 19 CGenFF penalty scores for unprotonated sphingosine For details see text

Table S1 Drugs used in the ATP production assay

All solutions and dilutions were made with DMSO. Solutions were stored at -20°C.

Drug	Mode of action	Supplier, Catalogue number	Initial concen-tration	Dilution	Volume added to (media volume)	Final concen-tration	Ref
Myriocin	SPT inhibitor	Sigma M1177	2mg/mL	-	10µL (5mL)	10µM	
Fumonisin B_1	Cer synthase inhibitor	Cayman 62580	5.4mg/mL	-	10µL (5mL)	15µM	[589]
(D)-PDMP	GCS inhibitor	Matreya 1756	2.1mg/mL	-	10µL (5mL)	10µM	[518]
(L)-PDMP		Matreya 1749	2.1mg/mL	-	10µL (5mL)	10µM	
PPMP	GCS inhibitor	Cayman 17236	10mg/mL	-	3.8µL (5mL)	15µM	
CBE	GBA1 inhibitor	Cayman 15216	4mg/mL	-	10µL (5mL)	50µM	[518]
AMP-DNJ	GBA2 inhibitor	See footnote f	1mg/mL	1:250	10µL (5mL)	20nM [a]	[523,588]
GlcSph		Sigma 43659	4.6mg/mL	-	10µL (5mL)	20µM [a]	[518]
GalSph		Sigma D9256	4.6mg/mL	-	10µL (5mL)	20µM [a]	
AdaGlcCer	GlcCer mimic	Matreya 1945	12.7mg/mL	-	10µL (5mL)	40µM [a]	[627]
21-AcP	StARD1 blocker	Sigma A3750	1.9mg/mL	-	10µL (5mL)	10µM	[632]
21-AcP	StARD1 blocker	Sigma A3750	7.5mg/mL	-	10µL (5mL)	40µM	
Ro5-4864	TSPO ligand	Sigma C5174	1.6mg/mL	1:10 [b]	10µL (5mL)	1µM	
Etifoxine	TSPO ligand	Sigma SML0272	3mg/mL	-	10µL (5mL)	20µM	[660]
PK11195	TSPO ligand	Sigma CO424	1.8mg/mL	1:100	10µL (5mL)	100nM	
Probucol	ABCA1 blocker	MP Biomedicals 156271	2.6mg/mL	-	10µL (5mL)	10µM	[634]
H89	PKA inhibitor	Tocris 2910	8mg/mL	1:100	10µL (5mL)	300nM (2.2x IC_{50})	[162]
ZM241385	$A_{2A}R$ antagonist	Tocris 1036	2.4mg/mL	1:28	10µL (5mL)	500nM	[55]
ATP	Assay standard	Sigma A26209	5.6mg/mL	1:1000	-	10^{-5}M	

[a] Lower concentrations were achieved by using a reduced amount of drug solution and normalising the volume with DMSO.

[b] Stored as single use aliquots.

Table S2 Drugs used in the O_2 consumption assay

Substances were Solutions were divided into aliquots; the working aliquot was stored at 4°C, the remainder were stored at -20°C until needed.

Drug	**Mode of action**	**Supplier, Catalogue number**	**Concen-tration**	**Solvent**	**Volume added to 2mL MiR05**	**Final concen-tration**
Digitonin	Cell perme-abiliser	Sigma D141	10mg/mL	DMSO	1µL	4µM
(L)-malic acid	Complex I substrate	Sigma M1000	107mg/mL	Water	5µL	2mM
(L)-glutamic acid	Complex I substrate	Sigma G1626	374mg/mL	Water	10µL	10mM
ADP	fATPase substrate	Sigma A5285	245mg/mL	Water	5µL	1.2mM
Succinic acid	Complex II substrate	Sigma S2378	270mg/mL	Water	20µL	10mM
Rotenone	Complex I inhibitor	Sigma R8875	0.059mg/mL	Ethanol	1µL	0.05µM
Oligomycin	fATPase inhibitor	Sigma O4876	4mg/mL	Ethanol	1µL	2.5µM

Figure S1 Chemical structures of sphingolipids used to treat cells

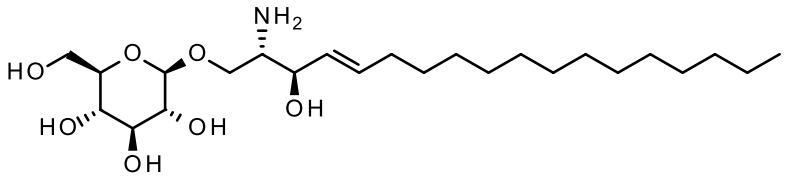

GlcSph

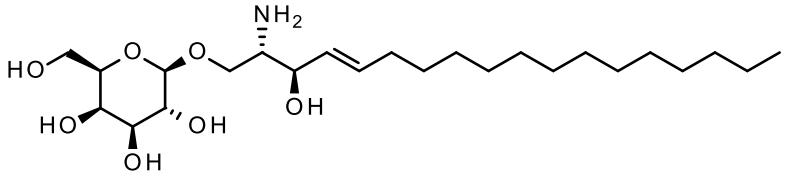

GalSph

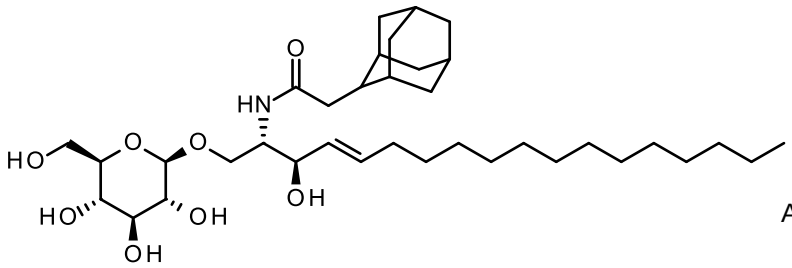

AdaGlcCer

Figure S2 Chemical structures of drugs affecting sphingolipid metabolism

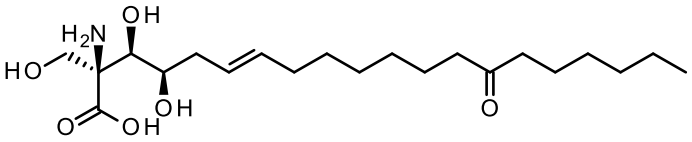

Myriocin

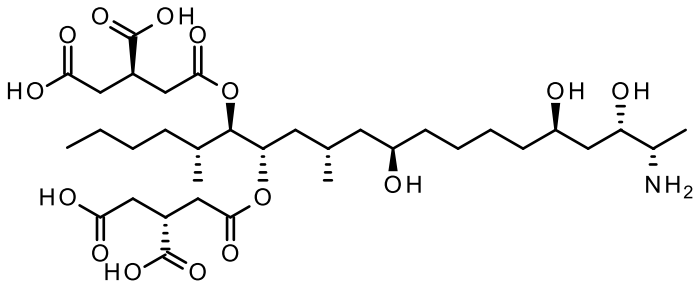

FumonisinB $_1$

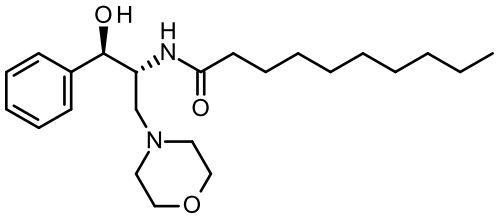

(D)-PDMP

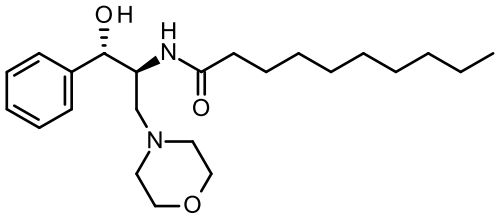

(L)-PDMP

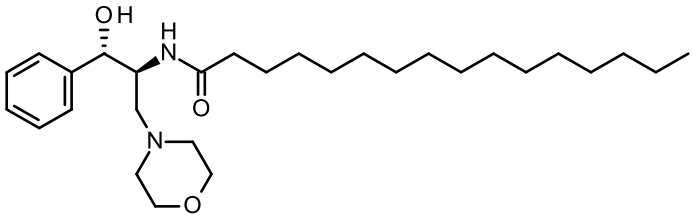

+ enantiomer
PPMP

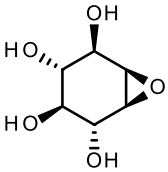

Conduritol-β-epoxide

Figure S3 Chemical structures of other drugs used in this chapter

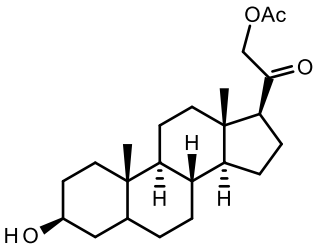

21-AcP

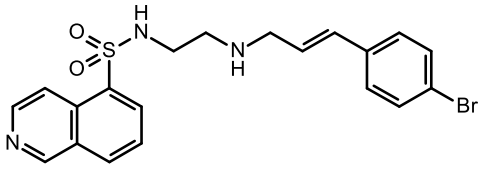

H89

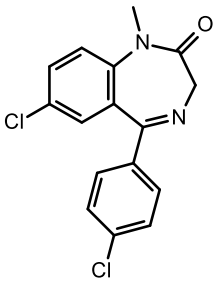

Ro5-4864

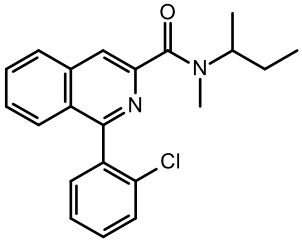

PK11195

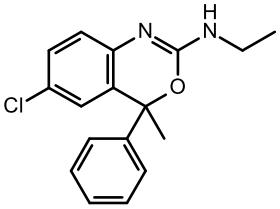

Etifoxine

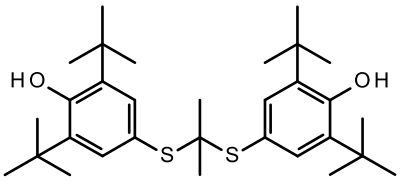

Probucol

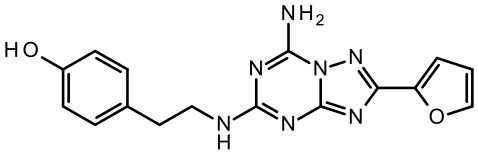

ZM241385

5

Integration

Chapter 1 introduced the cellular manifestations of Niemann-Pick type C disease as originating with mutations in a protein of late endosomes and lysosomes and with pathology not limited to those organelles but rather spreading to ER, mitochondria and nucleus. This widespread dysfunction calls for an integrated approach which was not possible at the start of this work as links between different aspects of the disease were largely unclear. This chapter attempts to connect the various disease aspects studied here with very recent work and so to articulate such a synthesis asking also how it illuminates future treatment approaches.

Summary of findings

The accumulation of cholesterol in the late endolysosomes (LELs) of NPCD cells triggers the secondary storage of other lipids. Chapter 2 used computational tools to suggest that one of these lipids, sphingosine, might accumulate because it is a substrate for the NPC proteins. This chapter also examined how other lipids might interact with proteins key to the functions of LELs and found numerous lipid-protein interactions with likely negative functional consequences. The implication of this is that successful treatment of NPCD probably requires a reduction in LEL cholesterol; how that can be achieved clinically is currently unclear.

Chapter 3 examined inhibition of GBA2, the only approved treatment of NPCD available at this time; it found that the treatment restores key endocytic functions included LEL pH. This effectiveness was postulated to arise because GBA2 is upregulated in NPCD for unknown reasons; inhibition restores normal function, in particular enriching the depleted pool of glucosylceramide on the cytosolic face of membranes and so, perhaps, activating vATPase. GBA2 inhibition was found ineffective in some related disease but provisionally useful in others.

Chapter 4 studied respiratory dysfunction in NPCD and found that it was not corrected by GBA2 inhibition, perhaps explaining why such a treatment approach is only partially clinically effective. The idea that sphingolipid manipulations more generally could correct respiratory defects in NPCD was not upheld by experiment. While the support it offered was only qualified, this chapter did not contradict the widely held, though unproved, hypothesis that cholesterol overload poisons mitochondria.

More recent work

And you see it all, and you've worked it out
And you see it all, and you want to shout

REM
Aftermath

Since the completion of the work contained in this thesis two papers have been published that offer significant insight into the disease process. The first of these[674] showed that cholesterol transfer occurs at ER-endosome contact sites and that NPC1-deficiency results in a reduction in these contacts and a corresponding increase in endosome contacts with mitochondria. In principle this potentially explains almost every aspect of the disease. If there are fewer contacts between endosomes and the ER then there will be a reduction in cholesterol at the ER causing, indirectly, the translocation of SREBP to the nucleus and increases in genes related to cholesterol synthesis and uptake (Chapter 1, Figure 2). However, communication between LELs and ER is bidirectional as the ER is the source of the Ca^{2+} required for endolysosomal calcium refilling.[52,56] Adequate LEL calcium is necessary for correct endocytosis (Chapter 1, Figure 1), functional autophagy,[93] lysosomal genetic regulation via calcineurin and TFEB (Chapter 1, Figure 2) and possibly correct lysosomal acidification. Reduced endosome-ER contacts therefore impair all of these processes. In exact contrast, increased endosome-mitochondria contacts will likely overload the respiratory centre with cholesterol, postulated to be toxic to its normal function. Seen in these terms it is quite possible that defective NPC1 protein leads not to reduced cholesterol export but to its misdirection away from the ER and to the mitochondria. If mitochondria have a lower capacity for processing cholesterol than does the ER, then congestion will result leading ultimately to lysosomal storage of cholesterol. Thus this study[674] found that some disease manifestations could be corrected by forcing an endosome-ER tether, which adds to the already extensive list of means noted in Chapter 1 for normalising cholesterol export from lysosomes of NPC1-deficient cells.[41,216,217,264,266–268]

The second paper[675] studied yeast NPC1 orthologue ncr1 which it showed was responsible for the export of ergosterol from the vacuole. Structural work showed the NTD in a conformation not previously observed for NPC1, but correctly oriented to deliver a sterol to a site intermediate between NTD and SSD; ergosterol was found in this site in the crystal (Figure 1). This 'tunnel' site is formed from the MLD and CTD (Chapter 2, Figure 7) and so is consistent with other work[338] suggesting the CTD is necessary for cholesterol export (it does not necessarily contradict another

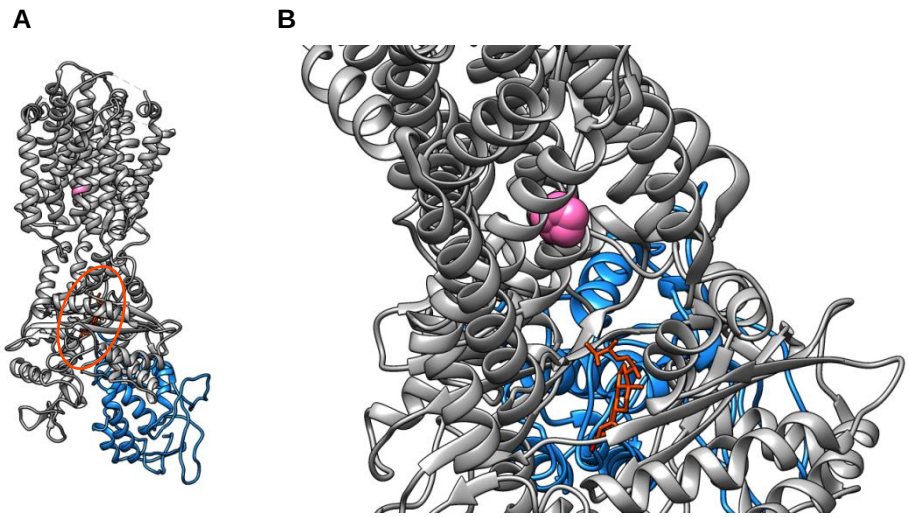

Figure 1 Two views of *S. cerevisiae* ncr1 (PDB: 6r4l) (**A**) Full length protein showing the NTD (blue), the ergosterol molecule (orange, ringed) in the tunnel binding site and Pro622 (pink) the yeast equivalent of Pro691 to mark the SSD. (**B**) There appears to be nothing obstructing the movement of ergosterol (orange) from the tunnel binding site where it was found in the crystal to the SSD marked by Pro622 (pink).

study[339] arguing that cholesterol export requires dimerisation of NPC1). The idea expressed in Chapter 2 that the relay mechanism of cholesterol export is a way of getting the lipid through the highly polar glycocalyx that lines the inside of the lysosomal limiting membrane is very much supported by this new study. Very recent work established LIMP-2 as an alternative lysosomal cholesterol exporter which appears to have a similar hydrophobic tunnel.[676] The structure of ncr1 (PDB: 6r4l) suggests that the questions raised in Chapter 2 about the function of the non-SSD TMHs present in NPC1 are not entirely appropriate. The small luminal loops of NPC1 are likely to be necessary to hold the MLD and CTD in place, the function of the TMHs is to secure the loops. Figure 2 shows an updated version of the cholesterol export narrative introduced in Chapter 2 Figure 7.

Thus NPC2 binds to the MLD of NPC1 (Figure 2, ❶) and delivers cholesterol to the NTD (Figure 2, ❷) before rearrangement of the protein allows transfer to the tunnel site (Figure 2, ❸). From here there are at least two possibilities. A larger rearrangement may open a channel through the middle of NPC1 allowing cholesterol to traverse the protein (Figure 2, ❹) and presumably be collected by a cytosolic carrier. This has previously been suggested by analogy with a similar protein[460] and also on computational grounds,[346] though Chapter 2 noted serious reservations about the latter study deriving from the likely inaccuracy of the protein structure used. If cholesterol follows this pathway in the manner shown (rather than rotating inside the protein) then it will emerge tail-first from NPC1 and therefore probably enter

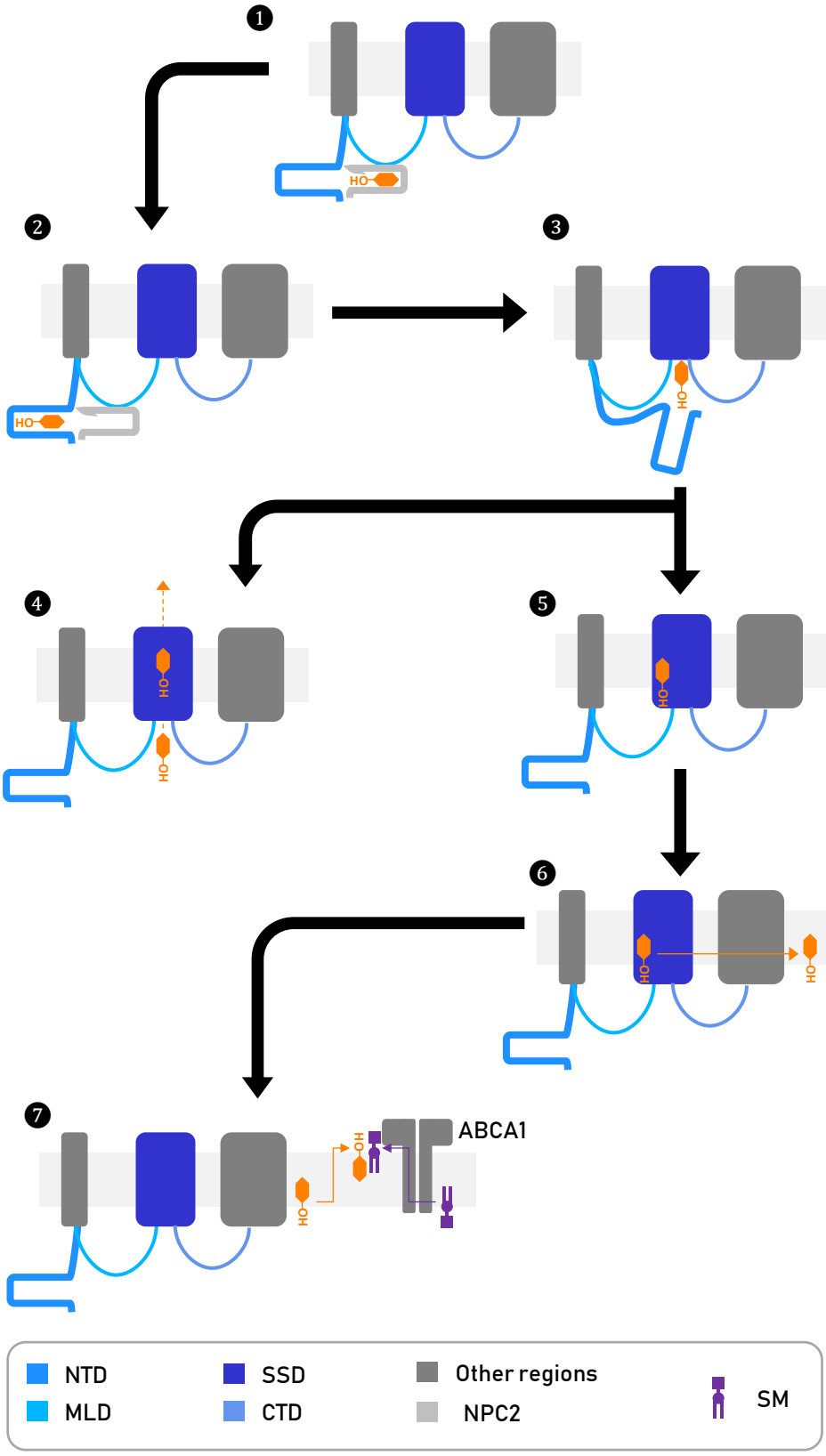

Figure 2 Cartoon of cholesterol export by the NPC system NPC1 co-operates with NPC2 and possibly ABCA1 to export cholesterol from the lysosome. For details see text.

the lipid-binding cavity of any cytosolic carrier protein tail first. This imposes constraints on the identity of that protein - it almost certainly cannot be a StAR (see Chapter 4) and perhaps cannot be an Aster, despite the reported interaction of a member of this family with NPC1,[674] as they appear to bind cholesterol with the same geometry as the StAR proteins.[677] It could be ORP5 though conflicting results have been reported on NPC1-ORP5 interaction.[109,674] (Depending on just how much conformational flexibility NPC1 has this alternative opens the possibility that the protein may export molecules larger than cholesterol, such as glucosylceramide, though the issue of how such lipids are transported to NPC1 when they are too large for NPC2 is a problem.) The second possibility (Figure 2, ❺) is that cholesterol moves from the tunnel site to the SSD (the binding sites appear to be aligned correctly to allow this, Figure 1B) where it would likely bind approximately as calculated in Chapter 2 before diffusing away from the protein and into the membrane (Figure 2, ❻). On this model the completion of cholesterol export is regulated by ABCA1 which, it is largely unappreciated, localises to endosomes[678] as well as the cell membrane. Furthermore, detailed investigations suggest that ABCA1 is not, as is usually assumed, a cholesterol transporter; rather cholesterol movement is a secondary effect resulting from the ability of ABCA1 to translocate ('flip') other lipids, particularly sphingomyelin (SM).[129,678,679] Consistently, cholesterol distribution in membranes was recently found to be dependent on SM molecules with a rather specific chain length.[680] Thus we may hypothesise that endosomal ABCA1 flips SM and cholesterol follows (Figure 2, ❼) driven by the energetically favourable interactions[276] between the two. This might also explain why ATP production increases on blocking ABCA1 with probucol (Chapter 4, Figure 13). Tentatively, this also offers another alternative mode of action for AMP-DNJ. If ABCA1 flips GlcCer as well as sphingomyelin, and if cholesterol can follow GlcCer as much as sphingomyelin (both reasonable assumptions but currently untested) then GlcCer on the cytosolic face of the lysosomal membrane can regulate post-NPC1 cholesterol transport. It follows that increasing this pool of lipid with AMP-DNJ will increase cholesterol export with the consequent relief of lysosomal pathology as found in Chapter 3.

This narrative still leaves some questions unanswered. Figure 2 omits the putative cytosolic facing binding site for cholesterol and the possible collection of the lipid from there by StARD3 (Chapter 2, Figures 8 and 12) as these currently lack direct validation from *in vitro* lab experiments. It is worth noting that endosome mitochondria contacts were found to be dependent on StARD3[674] so further investigations may support this as a third route of cholesterol export. Perhaps more

significantly for the work reported here the issue of sphingosine (Sph) is unresolved. The accumulation of Sph in lysosomes of cells deficient in NPC1[54,114,347] suggests either that this is a secondary effect of cholesterol storage or that Sph can use the same export machinery as cholesterol. Chapter 2 favoured the second hypothesis but designing an experiment to distinguish these two potential mechanisms will be hard. In any case the pathological consequences of sphingosine accumulation are currently unclear. Perhaps most importantly the reasons for the aberrant contact site populations[674] discussed above have not yet been clarified. It is currently no more than speculation to think that this contact site error can be explained, by some unknown mechanism, by the role of the MLD and CTD in forming the tunnel binding site, though the regulation of lysosomal proteins[461] (including cathepsin D) by this part of NPC1 might be the beginnings of a coherent story.

The contact site findings also offer us a new way of thinking about pharmacological treatment. If the principle defect in NPCD is endolysosomes contacting the wrong organelle then the task of therapy is to reduce those contacts and re-establish correct ones. This suggests that AMP-DNJ is only partially successful because, though it has benefits for the lysosome (Chapter 3, Figure 4), it does not sufficiently disrupt lysosome-mitochondria contacts. Such contact disruption may be achieved by first identifying the proteins involved – early studies have identified rab7 in human cells[71] and the Vam6-Vps39 pair in yeast[614] (see also[681]) – and then asking how to disturb their interactions with partner proteins. Whether such a tactic would be enough to provoke the endolysosome into re-establishing contacts with the ER is unclear. While the claim to see all of NPC biology is certainly premature and possibly wildly optimistic it is also true that further studies along these lines may lead both to successful treatment and to solving the mystery of NPC1.

References

(1) Vanier, M. T.; Millat, G. Niemann-Pick Disease Type C. *Clin. Genet.* **2003**, *64* (4), 269–281. https://doi.org/147

(2) Vanier, M. T. Niemann-Pick Disease Type C. *Orphanet J. Rare Dis.* **2010**, *5* (1), 16. https://doi.org/10.1186/1750-1172-5-16".

(3) Karten, B.; Peake, K. B.; Vance, J. E. Mechanisms and Consequences of Impaired Lipid Trafficking in Niemann–Pick Type C1-Deficient Mammalian Cells. *Biochim. Biophys. Acta - Mol. Cell Biol. Lipids* **2009**, *1791* (7), 659–670. https://doi.org///dx.doi.org/10.1016/j.bbalip.2009.01.025.

(4) Carstea, E. D.; Morris, J. A.; Coleman, K. G.; Loftus, S. K.; Zhang, D.; Cummings, C.; Gu, J.; Rosenfeld, M. A.; Pavan, W. J.; Krizman, D. B.; et al. Niemann-Pick C1 Disease Gene: Homology to Mediators of Cholesterol Homeostasis. *Science.* **1997**, *277* (5323), 228–231. https://doi.org/10.1126/science.277.5323.228.

(5) Loftus, S. K.; Morris, J. A.; Carstea, E. D.; Gu, J. Z.; Cummings, C.; Brown, A.; Ellison, J.; Ohno, K.; Rosenfeld, M. A.; Tagle, D. A.; et al. Murine Model of Niemann-Pick C Disease: Mutation in a Cholesterol Homeostasis Gene. *Science* **1997**, *277* (5323), 232–235.

(6) Davies, J. P.; Chen, F. W.; Ioannou, Y. A. Transmembrane Molecular Pump Activity of Niemann-Pick C1 Protein. *Science.* **2000**, *290* (5500), 2295.

(7) Kaufmann, A. M.; Krise, J. P. Niemann-Pick C1 Functions in Regulating Lysosomal Amine Content. *J. Biol. Chem.* **2008**, *283* (36), 24584–24593. https://doi.org/10.1074/jbc.M803715200.

(8) Malathi, K.; Higaki, K.; Tinkelenberg, A. H.; Balderes, D. A.; Almanzar-Paramio, D.; Wilcox, L. J.; Erdeniz, N.; Redican, F.; Padamsee, M.; Liu, Y.; et al. Mutagenesis of the Putative Sterol-Sensing Domain of Yeast Niemann Pick C–related Protein Reveals a Primordial Role in Subcellular Sphingolipid Distribution. *J. Cell Biol.* **2004**, *164* (4), 547–556. https://doi.org/10.1083/jcb.200310046.

(9) Fineran, P.; Lloyd-Evans, E.; Lack, N. A.; Platt, N.; Davis, L. C.; Morgan, A. J.; Höglinger, D.; Tatituri, R. V. V.; Clark, S.; Williams, I. M.; et al. Pathogenic Mycobacteria Achieve Cellular Persistence by Inhibiting the Niemann-Pick Type C Disease Cellular Pathway. *Wellcome Open Res.* **2017**, *1*, 18. https://doi.org/10.12688/wellcomeopenres.10036.1.

(10) Millard, E. E.; Gale, S. E.; Dudley, N.; Zhang, J.; Schaffer, J. E.; Ory, D. S. The Sterol-Sensing Domain of the Niemann-Pick C1 (NPC1) Protein Regulates Trafficking of Low Density Lipoprotein Cholesterol. *J. Biol. Chem.* **2005**, *280* (31), 28581–28590. https://doi.org/10.1074/jbc.M414024200.

(11) Ohgami, N.; Ko, D. C.; Thomas, M.; Scott, M. P.; Chang, C. C. Y.; Chang, T.-Y. Binding between the Niemann–Pick C1 Protein and a Photoactivatable Cholesterol Analog Requires a Functional Sterol-Sensing Domain. *Proc. Natl. Acad. Sci.* **2004**, *101* (34), 12473–12478. https://doi.org/10.1073/pnas.0405255101.

(12) Naureckiene, S.; Sleat, D. E.; Lackland, H.; Fensom, A.; Vanier, M. T.; Wattiaux, R.; Jadot, M.; Lobel, P. Identification of HE1 as the Second Gene of Niemann-Pick C Disease. *Science* **2000**, *290* (5500), 2298–2301. https://doi.org/10.1126/science.290.5500.2298.

(13) Ko, D. C.; Binkley, J.; Sidow, A.; Scott, M. P. The Integrity of a Cholesterol-Binding Pocket in Niemann–Pick C2 Protein Is Necessary to Control Lysosome Cholesterol Levels. *Proc. Natl. Acad. Sci.* **2003**, *100* (5), 2518–2525. https://doi.org/10.1073/pnas.0530027100.

(14) Friedland, N.; Liou, H.-L.; Lobel, P.; Stock, A. M. Structure of a Cholesterol-Binding Protein Deficient in Niemann–Pick Type C2 Disease. *Proc. Natl. Acad. Sci.* **2003**, *100* (5), 2512–2517. https://doi.org/10.1073/pnas.0437840100.

(15) Xu, S.; Benoff, B.; Liou, H. L.; Lobel, P.; Stock, A. M. Structural Basis of Sterol Binding by NPC2, a Lysosomal Protein Deficient in Niemann-Pick Type C2 Disease. *J. Biol. Chem.* **2007**, *282* (32), 23525–23531. https://doi.org/10.1074/jbc.M703848200.

(16) Infante, R. E.; Radhakrishnan, A.; Abi-Mosleh, L.; Kinch, L. N.; Wang, M. L.; Grishin, N. V; Goldstein, J. L.; Brown, M. S. Purified NPC1 Protein: II. Localization of Sterol Binding to a 240-Amino Acid Soluble Luminal Loop. *J. Biol. Chem.* **2008**, *283* (2), 1064–1075. https://doi.org/10.1074/jbc.M707944200.

(17) Subramanian, K.; Balch, W. E. NPC1/NPC2 Function as a Tag Team Duo to Mobilize Cholesterol. *Proc. Natl. Acad. Sci.* **2008**, *105* (40), 15223–15224.

https://doi.org/10.1073/pnas.0808256105.
(18) Infante, R. E.; Wang, M. L.; Radhakrishnan, A.; Kwon, H. J.; Brown, M. S.; Goldstein, J. L. NPC2 Facilitates Bidirectional Transfer of Cholesterol between NPC1 and Lipid Bilayers, a Step in Cholesterol Egress from Lysosomes. *Proc. Natl. Acad. Sci.* **2008**, *105* (40), 15287–15292. https://doi.org/10.1073/pnas.0807328105.
(19) Berzina, Z.; Solanko, L. M.; Mehadi, A. S.; Jensen, M. L. V.; Lund, F. W.; Modzel, M.; Szomek, M.; Solanko, K. A.; Dupont, A.; Nielsen, G. K.; et al. Niemann-Pick C2 Protein Regulates Sterol Transport between Plasma Membrane and Late Endosomes in Human Fibroblasts. *Chem. Phys. Lipids* **2018**, *213*, 48–61. https://doi.org/10.1016/j.chemphyslip.2018.03.006.
(20) Gustavsson, J.; Parpal, S.; Karlsson, M.; Ramsing, C.; Thorn, H.; Borg, M.; Lindroth, M.; Peterson, K. H.; Magnusson, K. E.; Strâlfors, P. Localization of the Insulin Receptor in Caveolae of Adipocyte Plasma Membrane. *FASEB J.* **1999**, *13* (14), 1961–1971. https://doi.org/10.1096/fasebj.13.14.1961.
(21) Lakshminarayan, R.; Wunder, C.; Becken, U.; Howes, M. T.; Benzing, C.; Arumugam, S.; Sales, S.; Ariotti, N.; Chambon, V.; Lamaze, C.; et al. Galectin-3 Drives Glycosphingolipid-Dependent Biogenesis of Clathrin-Independent Carriers. *Nat. Cell Biol.* **2014**, *16* (6), 592–603. https://doi.org/10.1038/ncb2970.
(22) Shen, D.; Wang, X.; Xu, H. Pairing Phosphoinositides with Calcium Ions in Endolysosomal Dynamics. *BioEssays* **2011**, *33* (6), 448–457. https://doi.org/10.1002/bies.201000152.
(23) Li, X.; Garrity, A. G.; Xu, H. Regulation of Membrane Trafficking by Signalling on Endosomal and Lysosomal Membranes. *J. Physiol.* **2013**, *591* (18), 4389–4401. https://doi.org/10.1113/jphysiol.2013.258301.
(24) Rocha, N.; Kuijl, C.; van der Kant, R.; Janssen, L.; Houben, D.; Janssen, H.; Zwart, W.; Neefjes, J. Cholesterol Sensor ORP1L Contacts the ER Protein VAP to Control Rab7–RILP–p150Glued and Late Endosome Positioning. *J. Cell Biol.* **2009**, *185* (7), 1209–1225. https://doi.org/10.1083/jcb.200811005.
(25) Chen, H.; Yang, J.; Low, P. S.; Cheng, J.-X. Cholesterol Level Regulates Endosome Motility via Rab Proteins. *Biophys. J.* **2008**, *94* (4), 1508–1520. https://doi.org///dx.doi.org/10.1529/biophysj.106.099366.
(26) Lebrand, C.; Corti, M.; Goodson, H.; Cosson, P.; Cavalli, V.; Mayran, N.; Fauré, J.; Gruenberg, J. Late Endosome Motility Depends on Lipids via the Small GTPase Rab7. *EMBO J.* **2002**, *21* (6), 1289–1300. https://doi.org/10.1093/emboj/21.6.1289.
(27) Mayran, N.; Parton, R. G.; Gruenberg, J. Annexin II Regulates Multivesicular Endosome Biogenesis in the Degradation Pathway of Animal Cells. *EMBO J.* **2003**, *22* (13), 3242–3253. https://doi.org/10.1093/emboj/cdg321.
(28) Morel, E.; Gruenberg, J. Annexin A2 Binding to Endosomes and Functions in Endosomal Transport Are Regulated by Tyrosine 23 Phosphorylation. *J. Biol. Chem.* **2009**, *284* (3), 1604–1611. https://doi.org/10.1074/jbc.M806499200.
(29) Grill, D.; Matos, A. L. L.; de Vries, W. C.; Kudruk, S.; Heflik, M.; Dörner, W.; Mootz, H. D.; Jan Ravoo, B.; Galla, H.-J.; Gerke, V. Bridging of Membrane Surfaces by Annexin A2. *Sci. Rep.* **2018**, *8* (1), 14662. https://doi.org/10.1038/s41598-018-33044-3.
(30) Luzio, J. P.; Pryor, P. R.; Bright, N. A. Lysosomes: Fusion and Function. *Nat. Rev. Mol. Cell Biol.* **2007**, *8* (8), 622–632.
(31) Pryor, P. R.; Mullock, B. M.; Bright, N. A.; Gray, S. R.; Luzio, J. P. The Role of Intraorganellar Ca2+In Late Endosome–Lysosome Heterotypic Fusion and in the Reformation of Lysosomes from Hybrid Organelles. *J. Cell Biol.* **2000**, *149* (5), 1053–1062. https://doi.org/10.1083/jcb.149.5.1053.
(32) Ward, D. M.; Pevsner, J.; Scullion, M. A.; Vaughn, M.; Kaplan, J. Syntaxin 7 and VAMP-7 Are SolubleN-Ethylmaleimide–sensitive Factor Attachment Protein Receptors Required for Late Endosome–Lysosome and Homotypic Lysosome Fusion in Alveolar Macrophages. *Mol. Biol. Cell* **2000**, *11* (7), 2327–2333. https://doi.org/10.1091/mbc.11.7.2327.
(33) Pryor, P. R.; Mullock, B. M.; Bright, N. A.; Lindsay, M. R.; Gray, S. R.; Richardson, S. C. W.; Stewart, A.; James, D. E.; Piper, R. C.; Luzio, J. P. Combinatorial SNARE Complexes with VAMP7 or VAMP8 Define Different Late Endocytic Fusion Events. *EMBO Rep.* **2004**, *5* (6), 590–595. https://doi.org/10.1038/sj.embor.7400150.
(34) Mullock, B. M.; Smith, C. W.; Ihrke, G.; Bright, N. A.; Lindsay, M.; Parkinson, E. J.;

Brooks, D. A.; Parton, R. G.; James, D. E.; Luzio, J. P.; et al. Syntaxin 7 Is Localized to Late Endosome Compartments, Associates with Vamp 8, and Is Required for Late Endosome–Lysosome Fusion. *Mol. Biol. Cell* **2000**, *11* (9), 3137–3153. https://doi.org/10.1091/mbc.11.9.3137.

(35) Xiong, J.; Zhu, M. X. Regulation of Lysosomal Ion Homeostasis by Channels and Transporters. *Sci. China Life Sci.* **2016**, *59* (8), 777–791. https://doi.org/10.1007/s11427-016-5090-x.

(36) Forgac, M. Vacuolar ATPases: Rotary Proton Pumps in Physiology and Pathophysiology. *Nat. Rev. Mol. Cell Biol.* **2007**, *8* (11), 917–929.

(37) Baravalle, G.; Schober, D.; Huber, M.; Bayer, N.; Murphy, R. F.; Fuchs, R. Transferrin Recycling and Dextran Transport to Lysosomes Is Differentially Affected by Bafilomycin, Nocodazole, and Low Temperature. *Cell Tissue Res.* **2005**, *320* (1), 99–113. https://doi.org/10.1007/s00441-004-1060-x.

(38) van Weert, A. W.; Dunn, K. W.; Gueze, H. J.; Maxfield, F. R.; Stoorvogel, W. Transport from Late Endosomes to Lysosomes, but Not Sorting of Integral Membrane Proteins in Endosomes, Depends on the Vacuolar Proton Pump. *J. Cell Biol.* **1995**, *130* (4), 821–834. https://doi.org/10.1083/jcb.130.4.821.

(39) Neufeld, E. B.; Wastney, M.; Patel, S.; Suresh, S.; Cooney, A. M.; Dwyer, N. K.; Roff, C. F.; Ohno, K.; Morris, J. A.; Carstea, E. D.; et al. The Niemann-Pick C1 Protein Resides in a Vesicular Compartment Linked to Retrograde Transport of Multiple Lysosomal Cargo. *J. Biol. Chem.* **1999**, *274* (14), 9627–9635. https://doi.org/10.1074/jbc.274.14.9627.

(40) Choudhury, A.; Sharma, D. K.; Marks, D. L.; Pagano, R. E. Elevated Endosomal Cholesterol Levels in Niemann-Pick Cells Inhibit Rab4 and Perturb Membrane Recycling. *Mol. Biol. Cell* **2004**, *15* (10), 4500–4511. https://doi.org/10.1091/mbc.E04-05-0432.

(41) Choudhury, A.; Dominguez, M.; Puri, V.; Sharma, D. K.; Narita, K.; Wheatley, C. L.; Marks, D. L.; Pagano, R. E. Rab Proteins Mediate Golgi Transport of Caveola-Internalized Glycosphingolipids and Correct Lipid Trafficking in Niemann-Pick C Cells. *J. Clin. Invest.* **2002**, *109* (12), 1541–1550. https://doi.org/10.1172/JCI0215420.

(42) Pipalia, N. H.; Hao, M.; Mukherjee, S.; Maxfield, F. R. Sterol, Protein and Lipid Trafficking in Chinese Hamster Ovary Cells with Niemann-Pick Type C1 Defect. *Traffic* **2007**, *8* (2), 130–141. https://doi.org/10.1111/j.1600-0854.2006.00513.x.

(43) Tharkeshwar, A. K.; Trekker, J.; Vermeire, W.; Pauwels, J.; Sannerud, R.; Priestman, D. A.; Te Vruchte, D.; Vints, K.; Baatsen, P.; Decuypere, J.-P.; et al. A Novel Approach to Analyze Lysosomal Dysfunctions through Subcellular Proteomics and Lipidomics: The Case of NPC1 Deficiency. *Sci. Rep.* **2017**, *7*, 41408. https://doi.org/10.1038/srep41408.

(44) Kaufmann, A. M.; Goldman, S. D. B.; Krise, J. P. A Fluorescence Resonance Energy Transfer-Based Approach for Investigating Late Endosome–lysosome Retrograde Fusion Events. *Anal. Biochem.* **2009**, *386* (1), 91–97. https://doi.org/10.1016/J.AB.2008.11.036.

(45) Liscum, L. Niemann-Pick Type C Mutations Cause Lipid Traffic Jam. *Traffic*. **2000**, pp 218–225. https://doi.org/10.1034/j.1600-0854.2000.010304.x.

(46) Levitan, I.; Singh, D.; Rosenhouse-Dantsker, A. Cholesterol Binding to Ion Channels. *Front. Physiol.* **2014**, *5*, 65. https://doi.org/10.3389/fphys.2014.00065.

(47) Epand, R. M. Cholesterol and the Interaction of Proteins with Membrane Domains. *Prog. Lipid Res.* **2006**, *45* (4), 279–294. https://doi.org///dx.doi.org/10.1016/j.plipres.2006.02.001.

(48) Vihervaara, T.; Uronen, R.-L.; Wohlfahrt, G.; Björkhem, I.; Ikonen, E.; Olkkonen, V. M. Sterol Binding by OSBP-Related Protein 1L Regulates Late Endosome Motility and Function. *Cell. Mol. Life Sci.* **2011**, *68* (3), 537–551. https://doi.org/10.1007/s00018-010-0470-z.

(49) Zhang, M.; Dwyer, N. K.; Love, D. C.; Cooney, A.; Comly, M.; Neufeld, E.; Pentchev, P. G.; Blanchette-Mackie, E. J.; Hanover, J. A. Cessation of Rapid Late Endosomal Tubulovesicular Trafficking in Niemann–Pick Type C1 Disease. *Proc. Natl. Acad. Sci.* **2001**, *98* (8), 4466–4471. https://doi.org/10.1073/pnas.081070898.

(50) Takahashi, M.; Kobayashi, T. Cholesterol Regulation of Rab-Mediated Sphingolipid Endocytosis. *Glycoconj. J.* **2009**, *26* (6), 705–710. https://doi.org/10.1007/s10719-008-9191-z.

(51) Ko, D. C.; Gordon, M. D.; Jin, J. Y.; Scott, M. P. Dynamic Movements of Organelles Containing Niemann-Pick C1 Protein: NPC1 Involvement in Late Endocytic Events. *Mol.*

Biol. Cell **2001**, *12* (3), 601–614. https://doi.org/10.1091/mbc.12.3.601.
(52) Gerasimenko, J. V; Tepikin, A. V; Petersen, O. H.; Gerasimenko, O. V. Calcium Uptake via Endocytosis with Rapid Release from Acidifying Endosomes. *Curr. Biol.* **1998**, *8* (24), 1335–1338.
(53) Xu, M.; Liu, K.; Swaroop, M.; Porter, F. D.; Sidhu, R.; Finkes, S.; Ory, D. S.; Marugan, J. J.; Xiao, J.; Southall, N.; et al. D-Tocopherol Reduces Lipid Accumulation in Niemann-Pick Type C1 and Wolman Cholesterol Storage Disorders. *J. Biol. Chem.* **2012**, *287* (47), 39349–39360. https://doi.org/10.1074/jbc.M112.357707.
(54) Lloyd-Evans, E.; Morgan, A. J.; He, X.; Smith, D. A.; Elliot-Smith, E.; Sillence, D. J.; Churchill, G. C.; Schuchman, E. H.; Galione, A.; Platt, F. M. Niemann-Pick Disease Type C1 Is a Sphingosine Storage Disease That Causes Deregulation of Lysosomal Calcium. *Nat. Med.* **2008**, *14*, 1247–1255.
(55) Visentin, S.; De Nuccio, C.; Bernardo, A.; Pepponi, R.; Ferrante, A.; Minghetti, L.; Popoli, P. The Stimulation of Adenosine A2A Receptors Ameliorates the Pathological Phenotype of Fibroblasts from Niemann-Pick Type C Patients. *J. Neurosci.* **2013**, *33* (39), 15388–15393. https://doi.org/10.1523/JNEUROSCI.0558-13.2013.
(56) Garrity, A. G.; Wang, W.; Collier, C. M. D.; Levey, S. A.; Gao, Q.; Xu, H. The Endoplasmic Reticulum, Not the PH Gradient, Drives Calcium Refilling of Lysosomes. *Elife* **2016**, *5*, e15887. https://doi.org/10.7554/eLife.15887.
(57) Harder, T.; Kellner, R.; Parton, R. G.; Gruenberg, J. Specific Release of Membrane-Bound Annexin II and Cortical Cytoskeletal Elements by Sequestration of Membrane Cholesterol. *Mol. Biol. Cell* **1997**, *8* (3), 533–545. https://doi.org/10.1091/mbc.8.3.533.
(58) Domon, M. M.; Matar, G.; Strzelecka-Kiliszek, A.; Bandorowicz-Pikula, J.; Pikula, S.; Besson, F. Interaction of Annexin A6 with Cholesterol Rich Membranes Is PH-Dependent and Mediated by the Sterol OH. *J. Colloid Interface Sci.* **2010**, *346* (2), 436–441. https://doi.org///dx.doi.org/10.1016/j.jcis.2010.03.015.
(59) de Diego, I.; Schwartz, F.; Siegfried, H.; Dauterstedt, P.; Heeren, J.; Beisiegel, U.; Enrich, C.; Grewal, T. Cholesterol Modulates the Membrane Binding and Intracellular Distribution of Annexin 6. *J. Biol. Chem.* **2002**, *277* (35), 32187–32194. https://doi.org/10.1074/jbc.M205499200.
(60) Domon, M. M.; Besson, F.; Bandorowicz-Pikula, J.; Pikula, S. Annexin A6 Is Recruited into Lipid Rafts of Niemann–Pick Type C Disease Fibroblasts in a Ca2+-Dependent Manner. *Biochem. Biophys. Res. Commun.* **2011**, *405* (2), 192–196. https://doi.org///dx.doi.org/10.1016/j.bbrc.2010.12.138.
(61) Te Vruchte, D.; Lloyd-Evans, E.; Veldman, R. J.; Neville, D. C. A.; Dwek, R. A.; Platt, F. M.; Van Blitterswijk, W. J.; Sillences, D. J. Accumulation of Glycosphingolipids in Niemann-Pick C Disease Disrupts Endosomal Transport. *J. Biol. Chem.* **2004**, *279* (25), 26167–26175. https://doi.org/10.1074/jbc.M311591200.
(62) Yu, H.; Wakim, B.; Li, M.; Halligan, B.; Tint, G. S.; Patel, S. B. Quantifying Raft Proteins in Neonatal Mouse Brain by "tube-Gel" Protein Digestion Label-Free Shotgun Proteomics. *Proteome Sci.* **2007**, *5*, 17. https://doi.org/10.1186/1477-5956-5-17.
(63) Enrich, C.; Rentero, C.; Hierro, A.; Grewal, T. Role of Cholesterol in SNARE-Mediated Trafficking on Intracellular Membranes. *J. Cell Sci.* **2015**, *128* (6), 1071–1081. https://doi.org/10.1242/jcs.164459.
(64) Gu, M.-X.; Fu, Y.; Sun, X.-L.; Ding, Y.-Z.; Li, C.-H.; Pang, W.; Pan, S.; Zhu, Y. Proteomic Analysis of Endothelial Lipid Rafts Reveals a Novel Role of Statins in Antioxidation. *J. Proteome Res.* **2012**, *11* (4), 2365–2373. https://doi.org/10.1021/pr300098f.
(65) Fraldi, A.; Annunziata, F.; Lombardi, A.; Kaiser, H.-J.; Medina, D. L.; Spampanato, C.; Fedele, A. O.; Polishchuk, R.; Sorrentino, N. C.; Simons, K.; et al. Lysosomal Fusion and SNARE Function Are Impaired by Cholesterol Accumulation in Lysosomal Storage Disorders. *EMBO J.* **2010**, *29*, 3607–3620. https://doi.org/10.1038/emboj.2010.237.
(66) Xu, S.; Zhou, S.; Xia, D.; Xia, J.; Chen, G.; Duan, S.; Luo, J. Defects of Synaptic Vesicle Turnover at Excitatory and Inhibitory Synapses in Niemann-Pick C1-Deficient Neurons. *Neuroscience* **2010**, *167* (3), 608–620. https://doi.org/10.1016/j.neuroscience.2010.02.033.
(67) Guerra, F.; Bucci, C. Multiple Roles of the Small GTPase Rab7. *Cells* **2016**, *5* (3), 34. https://doi.org/10.3390/cells5030034.
(68) Zhang, M.; Chen, L.; Wang, S.; Wang, T. Rab7: Roles in Membrane Trafficking and

Disease. *Biosci. Rep.* **2009**, *29* (3), 193–209. https://doi.org/10.1042/BSR20090032.
(69) Gutierrez, M. G.; Munafó, D. B.; Berón, W.; Colombo, M. I. Rab7 Is Required for the Normal Progression of the Autophagic Pathway in Mammalian Cells. *J. Cell Sci.* **2004**, *117* (13), 2687–2697. https://doi.org/10.1242/jcs.01114.
(70) Ganley, I. G.; Wong, P.-M.; Gammoh, N.; Jiang, X. Distinct Autophagosomal-Lysosomal Fusion Mechanism Revealed by Thapsigargin-Induced Autophagy Arrest. *Mol. Cell* **2011**, *42* (6), 731–743. https://doi.org///dx.doi.org/10.1016/j.molcel.2011.04.024.
(71) Wong, Y. C.; Ysselstein, D.; Krainc, D. Mitochondria–lysosome Contacts Regulate Mitochondrial Fission via RAB7 GTP Hydrolysis. *Nature* **2018**, *554*, 382–386.
(72) Chakraborty, K.; Leung, K.; Krishnan, Y. High Lumenal Chloride in the Lysosome Is Critical for Lysosome Function. *Elife* **2017**, *6*, e28862. https://doi.org/10.7554/eLife.28862.
(73) Bach, G.; Chen, C.-S.; Pagano, R. E. Elevated Lysosomal PH in Mucolipidosis Type IV Cells. *Clin. Chim. Acta* **1999**, *280* (1–2), 173–179. https://doi.org///dx.doi.org/10.1016/S0009-8981(98)00183-1.
(74) Elrick, M. J.; Yu, T.; Chung, C.; Lieberman, A. P. Impaired Proteolysis Underlies Autophagic Dysfunction in Niemann–Pick Type C Disease. *Hum. Mol. Genet.* **2012**, *21* (22), 4876–4887. https://doi.org/10.1093/hmg/dds324.
(75) Ishida, Y.; Nayak, S.; Mindell, J. A.; Grabe, M. A Model of Lysosomal PH Regulation. *J. Gen. Physiol.* **2013**, *141* (6), 705–720. https://doi.org/10.1085/jgp.201210930.
(76) Cang, C.; Aranda, K.; Seo, Y.; Gasnier, B.; Ren, D. TMEM175 Is an Organelle K+ Channel Regulating Lysosomal Function. *Cell* **2015**, *162* (5), 1101–1112. https://doi.org///dx.doi.org/10.1016/j.cell.2015.08.002.
(77) Mindell, J. A. Lysosomal Acidification Mechanisms. *Annu. Rev. Physiol.* **2012**, *74* (1), 69–86. https://doi.org/10.1146/annurev-physiol-012110-142317.
(78) Koivusalo, M.; Steinberg, B. E.; Mason, D.; Grinstein, S. In Situ Measurement of the Electrical Potential across the Lysosomal Membrane Using FRET. *Traffic* **2011**, *12* (8), 972–982. https://doi.org/10.1111/j.1600-0854.2011.01215.x.
(79) DiCiccio, J. E.; Steinberg, B. E. Lysosomal PH and Analysis of the Counter Ion Pathways That Support Acidification. *J. Gen. Physiol.* **2011**, *137* (4), 385–390. https://doi.org/10.1085/jgp.201110596.
(80) Sun, M. Mucolipidosis Type IV Is Caused by Mutations in a Gene Encoding a Novel Transient Receptor Potential Channel. *Hum. Mol. Genet.* **2000**, *9* (17), 2471–2478. https://doi.org/10.1093/hmg/9.17.2471.
(81) Poët, M.; Kornak, U.; Schweizer, M.; Zdebik, A. A.; Scheel, O.; Hoelter, S.; Wurst, W.; Schmitt, A.; Fuhrmann, J. C.; Planells-Cases, R.; et al. Lysosomal Storage Disease upon Disruption of the Neuronal Chloride Transport Protein ClC-6. *Proc. Natl. Acad. Sci.* **2006**, *103* (37), 13854–13859. https://doi.org/10.1073/pnas.0606137103.
(82) Pressey, S. N. R.; O'Donnell, K. J.; Stauber, T.; Fuhrmann, J. C.; Tyynelä, J.; Jentsch, T. J.; Cooper, J. D. Distinct Neuropathologic Phenotypes After Disrupting the Chloride Transport Proteins ClC-6 or ClC-7/Ostm1. *J. Neuropathol. Exp. Neurol.* **2010**, *69* (12), 1228–1246. https://doi.org/10.1097/NEN.0b013e3181ffe742.
(83) Kasper, D.; Planells-Cases, R.; Fuhrmann, J. C.; Scheel, O.; Zeitz, O.; Ruether, K.; Schmitt, A.; Poët, M.; Steinfeld, R.; Schweizer, M.; et al. Loss of the Chloride Channel ClC-7 Leads to Lysosomal Storage Disease and Neurodegeneration. *EMBO J.* **2005**, *24* (5), 1079–1091. https://doi.org/10.1038/sj.emboj.7600576.
(84) Lill, C. M.; Hansen, J.; Olsen, J. H.; Binder, H.; Ritz, B.; Bertram, L. Impact of Parkinson's Disease Risk Loci on Age at Onset. *Mov. Disord.* **2015**, *30* (6), 847–850. https://doi.org/10.1002/mds.26237.
(85) Jinn, S.; Drolet, R. E.; Cramer, P. E.; Wong, A. H.-K.; Toolan, D. M.; Gretzula, C. A.; Voleti, B.; Vassileva, G.; Disa, J.; Tadin-Strapps, M.; et al. TMEM175 Deficiency Impairs Lysosomal and Mitochondrial Function and Increases α-Synuclein Aggregation. *Proc. Natl. Acad. Sci.* **2017**, *114* (9), 2389–2394. https://doi.org/10.1073/pnas.1616332114.
(86) Zolov, S. N.; Bridges, D.; Zhang, Y.; Lee, W.-W.; Riehle, E.; Verma, R.; Lenk, G. M.; Converso-Baran, K.; Weide, T.; Albin, R. L.; et al. In Vivo, Pikfyve Generates PI(3,5)P2, Which Serves as Both a Signaling Lipid and the Major Precursor for PI5P. *Proc. Natl. Acad. Sci.* **2012**, *109* (43), 17472–17477. https://doi.org/10.1073/pnas.1203106109.
(87) Isobe, Y.; Nigorikawa, K.; Tsurumi, G.; Takemasu, S.; Takasuga, S.; Kofuji, S.; Hazeki, K.

PIKfyve Accelerates Phagosome Acidification through Activation of TRPML1 While Arrests Aberrant Vacuolation Independent of the Ca 2+ Channel. *J. Biochem.* **2019**, *165* (1), 75–84. https://doi.org/10.1093/jb/mvy084.
(88) Xie, Z.; Nair, U.; Klionsky, D. J.; Riezman, H. Atg8 Controls Phagophore Expansion during Autophagosome Formation. *Mol. Biol. Cell* **2008**, *19* (8), 3290–3298. https://doi.org/10.1091/mbc.e07-12-1292.
(89) Kawai, A.; Uchiyama, H.; Takano, S.; Nakamura, N.; Ohkuma, S. Autophagosome-Lysosome Fusion Depends on the PH in Acidic Compartments in CHO Cells. *Autophagy* **2007**, *3* (2), 154–157.
(90) Koga, H.; Kaushik, S.; Cuervo, A. M. Altered Lipid Content Inhibits Autophagic Vesicular Fusion. *FASEB J.* **2010**, *24* (8), 3052–3065. https://doi.org/10.1096/fj.09-144519.
(91) Aldrich, L. N.; Kuo, S.-Y.; Castoreno, A. B.; Goel, G.; Kuballa, P.; Rees, M. G.; Seashore-Ludlow, B.; Cheah, J. H.; Latorre, I. J.; Schreiber, S. L.; et al. Discovery of a Small-Molecule Probe for V-ATPase Function. *J. Am. Chem. Soc.* **2015**, *137* (16), 5563–5568. https://doi.org/10.1021/jacs.5b02150.
(92) Wijdeven, R. H.; Janssen, H.; Nahidiazar, L.; Janssen, L.; Jalink, K.; Berlin, I.; Neefjes, J. Cholesterol and ORP1L-Mediated ER Contact Sites Control Autophagosome Transport and Fusion with the Endocytic Pathway. *Nat. Commun.* **2016**, *7* (1), 11808. https://doi.org/10.1038/ncomms11808.
(93) Zhang, X.; Cheng, X.; Yu, L.; Yang, J.; Calvo, R.; Patnaik, S.; Hu, X.; Gao, Q.; Yang, M.; Lawas, M.; et al. MCOLN1 Is a ROS Sensor in Lysosomes That Regulates Autophagy. *Nat. Commun.* **2016**, *7*, 12109. https://doi.org/10.1038/ncomms12109.
(94) Itakura, E.; Kishi-Itakura, C.; Mizushima, N. The Hairpin-Type Tail-Anchored SNARE Syntaxin 17 Targets to Autophagosomes for Fusion with Endosomes/Lysosomes. *Cell* **2012**, *151* (6), 1256–1269. https://doi.org/10.1016/j.cell.2012.11.001.
(95) Furuta, N.; Fujita, N.; Noda, T.; Yoshimori, T.; Amano, A. Combinational Soluble N-Ethylmaleimide-Sensitive Factor Attachment Protein Receptor Proteins VAMP8 and Vti1b Mediate Fusion of Antimicrobial and Canonical Autophagosomes with Lysosomes. *Mol. Biol. Cell* **2010**, *21* (6), 1001–1010. https://doi.org/10.1091/mbc.E09-08-0693.
(96) Fader, C. M.; Sánchez, D. G.; Mestre, M. B.; Colombo, M. I. TI-VAMP/VAMP7 and VAMP3/Cellubrevin: Two v-SNARE Proteins Involved in Specific Steps of the Autophagy/Multivesicular Body Pathways. *Biochim. Biophys. Acta - Mol. Cell Res.* **2009**, *1793* (12), 1901–1916. https://doi.org///dx.doi.org/10.1016/j.bbamcr.2009.09.011.
(97) Ko, D. C.; Milenkovic, L.; Beier, S. M.; Manuel, H.; Buchanan, J.; Scott, M. P. Cell-Autonomous Death of Cerebellar Purkinje Neurons with Autophagy in Niemann-Pick Type C Disease. *PLOS Genet.* **2005**, *1* (1), e7.
(98) Pacheco, C. D.; Kunkel, R.; Lieberman, A. P. Autophagy in Niemann–Pick C Disease Is Dependent upon Beclin-1 and Responsive to Lipid Trafficking Defects. *Hum. Mol. Genet.* **2007**, *16* (12), 1495–1503. https://doi.org/10.1093/hmg/ddm100.
(99) Sarkar, S.; Carroll, B.; Buganim, Y.; Maetzel, D.; Ng, A. H. M.; Cassady, J. P.; Cohen, M. A.; Chakraborty, S.; Wang, H.; Spooner, E.; et al. Impaired Autophagy in the Lipid-Storage Disorder Niemann-Pick Type C1 Disease. *Cell Rep.* **2013**, *5* (5), 1302–1315. https://doi.org///dx.doi.org/10.1016/j.celrep.2013.10.042.
(100) Ordonez, M. P.; Roberts, E. A.; Kidwell, C. U.; Yuan, S. H.; Plaisted, W. C.; Goldstein, L. S. B. Disruption and Therapeutic Rescue of Autophagy in a Human Neuronal Model of Niemann Pick Type C1. *Hum. Mol. Genet.* **2012**, *21* (12), 2651–2662. https://doi.org/10.1093/hmg/dds090.
(101) Lie, P. P. Y.; Nixon, R. A. Lysosome Trafficking and Signaling in Health and Neurodegenerative Diseases. *Neurobiology of Disease*. **2019**, pp 94–105. https://doi.org/10.1016/j.nbd.2018.05.015.
(102) Pfisterer, S. G.; Peränen, J.; Ikonen, E. LDL–cholesterol Transport to the Endoplasmic Reticulum. *Curr. Opin. Lipidol.* **2016**, *27* (3), 282–287. https://doi.org/10.1097/MOL.0000000000000292.
(103) Raiborg, C.; Wenzel, E. M.; Stenmark, H. ER-Endosome Contact Sites: Molecular Compositions and Functions. *EMBO J.* **2015**, *34* (14), 1848–1858. https://doi.org/10.15252/embj.201591481.
(104) van der Kant, R.; Neefjes, J. Small Regulators, Major Consequences – Ca2+ and Cholesterol

at the Endosome–ER Interface. *J. Cell Sci.* **2014**, *127* (5), 929–938. https://doi.org/10.1242/jcs.137539.
(105) Ikonen, E. Mechanisms of Cellular Cholesterol Compartmentalization: Recent Insights. *Curr. Opin. Cell Biol.* **2018**, *53*, 77–83. https://doi.org/10.1016/J.CEB.2018.06.002.
(106) Du, X.; Kazim, A. S.; Dawes, I. W.; Brown, A. J.; Yang, H. The AAA ATPase VPS4/SKD1 Regulates Endosomal Cholesterol Trafficking Independently of ESCRT-III. *Traffic* **2013**, *14* (1), 107–119. https://doi.org/10.1111/tra.12015.
(107) Bishop, N.; Woodman, P. ATPase-Defective Mammalian VPS4 Localizes to Aberrant Endosomes and Impairs Cholesterol Trafficking. *Mol. Biol. Cell* **2000**, *11* (1), 227–239. https://doi.org/10.1091/mbc.11.1.227.
(108) Frolov, A.; Zielinski, S. E.; Crowley, J. R.; Dudley-Rucker, N.; Schaffer, J. E.; Ory, D. S. NPC1 and NPC2 Regulate Cellular Cholesterol Homeostasis through Generation of Low Density Lipoprotein Cholesterol-Derived Oxysterols. *J. Biol. Chem.* **2003**, *278* (28), 25517–25525. https://doi.org/10.1074/jbc.M302588200.
(109) Du, X.; Kumar, J.; Ferguson, C.; Schulz, T. A.; Ong, Y. S.; Hong, W.; Prinz, W. A.; Parton, R. G.; Brown, A. J.; Yang, H. A Role for Oxysterol-Binding Protein–related Protein 5 in Endosomal Cholesterol Trafficking. *J. Cell Biol.* **2011**, *192* (1), 121–135. https://doi.org/10.1083/jcb.201004142.
(110) Garver, W. S.; Krishnan, K.; Gallagos, J. R.; Michikawa, M.; Francis, G. A.; Heidenreich, R. A. Niemann-Pick C1 Protein Regulates Cholesterol Transport to the Trans-Golgi Network and Plasma Membrane Caveolae. *J. Lipid Res.* **2002**, *43* (4), 579–589.
(111) Brown, M. S.; Goldstein, J. L. Sterol Regulatory Element Binding Proteins (SREBPs): Controllers of Lipid Synthesis and Cellular Uptake. *Nutr. Rev.* **1998**, *56* (SUPPL.1), S1–S3. https://doi.org/10.1111/j.1753-4887.1998.tb01680.x.
(112) Liscum, L.; Faust, J. R. The Intracellular Transport of Low Density Lipoprotein-Derived Cholesterol Is Inhibited in Chinese Hamster Ovary Cells Cultured with 3-Beta-[2-(Diethylamino)Ethoxy]Androst-5-En-17-One. *J. Biol. Chem.* **1989**, *264* (20), 11796–11806.
(113) Reddy, J. V; Ganley, I. G.; Pfeffer, S. R. Clues to Neuro-Degeneration in Niemann-Pick Type C Disease from Global Gene Expression Profiling. *PLoS One* **2006**, *1*, e19.
(114) Höglinger, D.; Haberkant, P.; Aguilera-Romero, A.; Riezman, H.; Porter, F. D.; Platt, F. M.; Galione, A.; Schultz, C. Intracellular Sphingosine Releases Calcium from Lysosomes. *Elife* **2015**, *4*, e10616. https://doi.org/10.7554/eLife.10616.
(115) Shen, D.; Wang, X.; Li, X.; Zhang, X.; Yao, Z.; Dibble, S.; Dong, X.; Yu, T.; Lieberman, A. P.; Showalter, H. D.; et al. Lipid Storage Disorders Block Lysosomal Trafficking by Inhibiting a TRP Channel and Lysosomal Calcium Release. *Nat. Commun.* **2012**, *3*, 731.
(116) Medina, D. L.; Di Paola, S.; Peluso, I.; Armani, A.; De Stefani, D.; Venditti, R.; Montefusco, S.; Scotto-Rosato, A.; Prezioso, C.; Forrester, A.; et al. Lysosomal Calcium Signalling Regulates Autophagy through Calcineurin and TFEB. *Nat. Cell Biol.* **2015**, *17* (3), 288–299. https://doi.org/10.1038/ncb3114.
(117) Napolitano, G.; Ballabio, A. TFEB at a Glance. *J. Cell Sci.* **2016**, *129* (13), 2475–2481. https://doi.org/10.1242/jcs.146365.
(118) Sardiello, M.; Palmieri, M.; di Ronza, A.; Medina, D. L.; Valenza, M.; Gennarino, V. A.; Di Malta, C.; Donaudy, F.; Embrione, V.; Polishchuk, R. S.; et al. A Gene Network Regulating Lysosomal Biogenesis and Function. *Science* **2009**, *325* (5939), 473–477. https://doi.org/10.1126/science.1174447.
(119) Palmieri, M.; Impey, S.; Kang, H.; di Ronza, A.; Pelz, C.; Sardiello, M.; Ballabio, A. Characterization of the CLEAR Network Reveals an Integrated Control of Cellular Clearance Pathways. *Hum. Mol. Genet.* **2011**, *20* (19), 3852–3866. https://doi.org/10.1093/hmg/ddr306.
(120) Settembre, C.; Di Malta, C.; Polito, V. A.; Garcia Arencibia, M.; Vetrini, F.; Erdin, S.; Erdin, S. U.; Huynh, T.; Medina, D.; Colella, P.; et al. TFEB Links Autophagy to Lysosomal Biogenesis. *Science* **2011**, *332* (6036), 1429–1433. https://doi.org/10.1126/science.1204592.
(121) Medina, D. L.; Fraldi, A.; Bouche, V.; Annunziata, F.; Mansueto, G.; Spampanato, C.; Puri, C.; Pignata, A.; Martina, J. A.; Sardiello, M.; et al. Transcriptional Activation of Lysosomal Exocytosis Promotes Cellular Clearance. *Dev. Cell* **2011**, *21* (3), 421–430. https://doi.org///dx.doi.org/10.1016/j.devcel.2011.07.016.
(122) Sawamura, N.; Gong, J.-S.; Garver, W. S.; Heidenreich, R. A.; Ninomiya, H.; Ohno, K.;

Yanagisawa, K.; Michikawa, M. Site-Specific Phosphorylation of Tau Accompanied by Activation of Mitogen-Activated Protein Kinase (MAPK) in Brains of Niemann-Pick Type C Mice. *J. Biol. Chem.* **2001**, *276* (13), 10314–10319. https://doi.org/10.1074/jbc.M009733200.

(123) Sawamura, N.; Gong, J.-S.; Chang, T.-Y.; Yanagisawa, K.; Michikawa, M. Promotion of Tau Phosphorylation by MAP Kinase Erk1/2 Is Accompanied by Reduced Cholesterol Level in Detergent-Insoluble Membrane Fraction in Niemann-Pick C1-Deficient Cells. *J. Neurochem.* **2003**, *84* (5), 1086–1096.

(124) Nada, S.; Hondo, A.; Kasai, A.; Koike, M.; Saito, K.; Uchiyama, Y.; Okada, M. The Novel Lipid Raft Adaptor P18 Controls Endosome Dynamics by Anchoring the MEK-ERK Pathway to Late Endosomes. *EMBO J.* **2009**, *28* (5), 477–489. https://doi.org/10.1038/emboj.2008.308.

(125) Castellano, B. M.; Thelen, A. M.; Moldavski, O.; Feltes, M.; van der Welle, R. E. N.; Mydock-McGrane, L.; Jiang, X.; van Eijkeren, R. J.; Davis, O. B.; Louie, S. M.; et al. Lysosomal Cholesterol Activates MTORC1 via an SLC38A9-Niemann-Pick C1 Signaling Complex. *Science* **2017**, *355* (6331), 1306–1311. https://doi.org/10.1126/science.aag1417.

(126) Xu, J.; Dang, Y.; Ren, Y. R.; Liu, J. O. Cholesterol Trafficking Is Required for MTOR Activation in Endothelial Cells. *Proc. Natl. Acad. Sci.* **2010**, *107* (10), 4764–4769. https://doi.org/10.1073/pnas.0910872107.

(127) Lin, L. L.; Wartmann, M.; Lin, A. Y.; Knopf, J. L.; Seth, A.; Davis, R. J. CPLA2 Is Phosphorylated and Activated by MAP Kinase. *Cell* **1993**, *72* (2), 269–278. https://doi.org/10.1016/0092-8674(93)90666-E.

(128) Zhou, L.; Choi, H. Y.; Li, W. P.; Xu, F.; Herz, J. LRP1 Controls CPLA2 Phosphorylation, ABCA1 Expression and Cellular Cholesterol Export. *PLoS One* **2009**, *4* (8), e6853. https://doi.org/10.1371/journal.pone.0006853.

(129) Choi, H. Y.; Karten, B.; Chan, T.; Vance, J. E.; Greer, W. L.; Heidenreich, R. A.; Garver, W. S.; Francis, G. A. Impaired ABCA1-Dependent Lipid Efflux and Hypoalphalipoproteinemia in Human Niemann-Pick Type C Disease. *J. Biol. Chem.* **2003**, *278* (35), 32569–32577. https://doi.org/10.1074/jbc.M304553200.

(130) Wang, M.-D.; Franklin, V.; Sundaram, M.; Kiss, R. S.; Ho, K.; Gallant, M.; Marcel, Y. L. Differential Regulation of ATP Binding Cassette Protein A1 Expression and ApoA-I Lipidation by Niemann-Pick Type C1 in Murine Hepatocytes and Macrophages. *J. Biol. Chem.* **2007**, *282* (31), 22525–22533. https://doi.org/10.1074/jbc.M700326200.

(131) Chung, C.; Puthanveetil, P.; Ory, D. S.; Lieberman, A. P. Genetic and Pharmacological Evidence Implicates Cathepsins in Niemann-Pick C Cerebellar Degeneration. *Hum. Mol. Genet.* **2016**, *25* (7), 1434–1446. https://doi.org/10.1093/hmg/ddw025.

(132) Gabande-Rodriguez, E.; Boya, P.; Labrador, V.; Dotti, C. G.; Ledesma, M. D. High Sphingomyelin Levels Induce Lysosomal Damage and Autophagy Dysfunction in Niemann Pick Disease Type A. *Cell Death Differ.* **2014**, *21* (6), 864–875.

(133) Amritraj, A.; Wang, Y.; Revett, T. J.; Vergote, D.; Westaway, D.; Kar, S. Role of Cathepsin D in U18666A-Induced Neuronal Cell Death: Potential Implication in Niemann-Pick Type C Disease Pathogenesis. *J. Biol. Chem.* **2013**, *288* (5), 3136–3152. https://doi.org/10.1074/jbc.M112.412460.

(134) Kosicek, M.; Gudelj, I.; Horvatic, A.; Jovic, T.; Vuckovic, F.; Lauc, G.; Hecimovic, S. N-Glycome of the Lysosomal Glycocalyx Is Altered in Niemann-Pick Type C Disease (NPC) Model Cells. *Mol. Cell. Proteomics* **2018**, *17* (4), 631–642. https://doi.org/10.1074/mcp.RA117.000129.

(135) Cirman, T.; Orešić, K.; Mazovec, G. D.; Turk, V.; Reed, J. C.; Myers, R. M.; Salvesen, G. S.; Turk, B. Selective Disruption of Lysosomes in HeLa Cells Triggers Apoptosis Mediated by Cleavage of Bid by Multiple Papain-like Lysosomal Cathepsins. *J. Biol. Chem.* **2004**, *279* (5), 3578–3587. https://doi.org/10.1074/jbc.M308347200.

(136) Koh, C. H. V.; Whiteman, M.; Li, Q.-X.; Halliwell, B.; Jenner, A. M.; Wong, B. S.; Laughton, K. M.; Wenk, M.; Masters, C. L.; Beart, P. M.; et al. Chronic Exposure to U18666A Is Associated with Oxidative Stress in Cultured Murine Cortical Neurons. *J. Neurochem.* **2006**, *98* (4), 1278–1289. https://doi.org/10.1111/j.1471-4159.2006.03958.x.

(137) Klein, A.; Maldonado, C.; Vargas, L. M.; Gonzalez, M.; Robledo, F.; Perez de Arce, K.; Munoz, F. J.; Hetz, C.; Alvarez, A. R.; Zanlungo, S. Oxidative Stress Activates the C-

Abl/P73 Proapoptotic Pathway in Niemann-Pick Type C Neurons. *Neurobiol. Dis.* **2011**, *41* (1), 209–218. https://doi.org/10.1016/j.nbd.2010.09.008.
(138) Kennedy, B. E.; Madreiter, C. T.; Vishnu, N.; Malli, R.; Graier, W. F.; Karten, B. Adaptations of Energy Metabolism Associated with Increased Levels of Mitochondrial Cholesterol in Niemann-Pick Type C1-Deficient Cells. *J. Biol. Chem.* **2014**, *289* (23), 16278–16289. https://doi.org/10.1074/jbc.M114.559914.
(139) Fu, R.; Yanjanin, N. M.; Bianconi, S.; Pavan, W. J.; Porter, F. D. Oxidative Stress in Niemann–Pick Disease, Type C. *Mol. Genet. Metab.* **2010**, *101* (2–3), 214–218. https://doi.org///doi.org/10.1016/j.ymgme.2010.06.018.
(140) Ribas, G. S.; Pires, R.; Coelho, J. C.; Rodrigues, D.; Mescka, C. P.; Vanzin, C. S.; Biancini, G. B.; Negretto, G.; Wayhs, C. A. Y.; Wajner, M.; et al. Oxidative Stress in Niemann-Pick Type C Patients: A Protective Role of N-Butyl-Deoxynojirimycin Therapy. *Int. J. Dev. Neurosci.* **2012**, *30* (6), 439–444. https://doi.org/10.1016/J.IJDEVNEU.2012.07.002.
(141) Alvarez, A. R.; Sandoval, P. C.; Leal, N. R.; Castro, P. U.; Kosik, K. S. Activation of the Neuronal C-Abl Tyrosine Kinase by Amyloid-β-Peptide and Reactive Oxygen Species. *Neurobiol. Dis.* **2004**, *17* (2), 326–336. https://doi.org/10.1016/j.nbd.2004.06.007.
(142) Sun, X.; Majumder, P.; Shioya, H.; Wu, F.; Kumar, S.; Weichselbaum, R.; Kharbanda, S.; Kufe, D. Activation of the Cytoplasmic C-Abl Tyrosine Kinase by Reactive Oxygen Species. *J. Biol. Chem.* **2000**, *275* (23), 17237–17240. https://doi.org/10.1074/jbc.C000099200.
(143) Ito, Y.; Pandey, P.; Mishra, N. C.; Kumar, S.; Narula, N.; Kharbanda, S.; Saxena, S. P.; Kufe, D. Targeting of the C-Abl Tyrosine Kinase to Mitochondria in Endoplasmic Reticulum Stress-Induced Apoptosis. *Mol. Cell. Biol.* **2001**, *21* (18), 6233–6242. https://doi.org/10.1128/MCB.21.18.6233.
(144) Huang, Z.; Hou, Q.; Cheung, N. S.; Li, Q.-T. Neuronal Cell Death Caused by Inhibition of Intracellular Cholesterol Trafficking Is Caspase Dependent and Associated with Activation of the Mitochondrial Apoptosis Pathway. *J. Neurochem.* **2006**, *97* (1), 280–291. https://doi.org/10.1111/j.1471-4159.2006.03733.x.
(145) Cai, J.; Yang, J.; Jones, D. P. Mitochondrial Control of Apoptosis: The Role of Cytochrome C. *Biochim. Biophys. Acta - Bioenerg.* **1998**, *1366* (1–2), 139–149. https://doi.org/10.1016/S0005-2728(98)00109-1.
(146) Wu, Y.-P.; Mizukami, H.; Matsuda, J.; Saito, Y.; Proia, R. L.; Suzuki, K. Apoptosis Accompanied by Up-Regulation of TNF-α Death Pathway Genes in the Brain of Niemann–Pick Type C Disease. *Mol. Genet. Metab.* **2005**, *84* (1), 9–17. https://doi.org///dx.doi.org/10.1016/j.ymgme.2004.08.017.
(147) Alvarez, A. R.; Klein, A.; Castro, J.; Cancino, G. I.; Amigo, J.; Mosqueira, M.; Vargas, L. M.; Yevenes, L. F.; Bronfman, F. C.; Zanlungo, S. Imatinib Therapy Blocks Cerebellar Apoptosis and Improves Neurological Symptoms in a Mouse Model of Niemann-Pick Type C Disease. *FASEB J.* **2008**, *22* (10), 3617–3627. https://doi.org/10.1096/fj.07-102715.
(148) Vincent, M.; Sayre, N. L.; Graham, M. J.; Crooke, R. M.; Shealy, D. J.; Liscum, L. Evaluation of an Anti-Tumor Necrosis Factor Therapeutic in a Mouse Model of Niemann-Pick C Liver Disease. *PLoS One* **2010**, *5* (9), e12941.
(149) Sabio, G.; Davis, R. J. TNF and MAP Kinase Signalling Pathways. *Semin. Immunol.* **2014**, *26* (3), 237–245. https://doi.org/10.1016/J.SMIM.2014.02.009.
(150) Hunter, T.; Ling, N.; Cooper, J. A. Protein Kinase C Phosphorylation of the EGF Receptor at a Threonine Residue Close to the Cytoplasmic Face of the Plasma Membrane. *Nature* **1984**, *311* (5985), 480–483. https://doi.org/10.1038/311480a0.
(151) Livneh, E.; Dull, T. J.; Berent, E.; Prywes, R.; Ullrich, A.; Schlessinger, J. Release of a Phorbol Ester-Induced Mitogenic Block by Mutation at Thr-654 of the Epidermal Growth Factor Receptor. *Mol. Cell. Biol.* **2015**, *8* (6), 2302–2308. https://doi.org/10.1128/mcb.8.6.2302.
(152) Hannun, Y. A.; Bell, R. M. Lysosphingolipids Inhibit Protein Kinase C: Implications for the Sphingolipidoses. *Science* **1987**, *235* (4789), 670–674. https://doi.org/10.1126/science.3101176.
(153) Rodriguez-Lafrasse, C.; Rousson, R.; Valla, S.; Antignac, P.; Pierre, L.; Vanier, M. T. Modulation of Protein Kinase C by Endogenous Sphingosine: Inhibition of Phorbol Dibutyrate Binding in Niemann-Pick C Fibroblasts. *Biochem J* **1997**, *325*, 787.
(154) Bazzi, M. D.; Nelsestuen, G. L. Mechanism of Protein Kinase C Inhibition by Sphingosine.

Biochem. Biophys. Res. Commun. **1987**, *146* (1), 203–207. https://doi.org/10.1016/0006-291X(87)90711-X.

(155) Edsall, L. C.; Van Brocklyn, J. R.; Cuvillier, O.; Kleuser, B.; Spiegel, S. N,N-Dimethylsphingosine Is a Potent Competitive Inhibitor of Sphingosine Kinase but Not of Protein Kinase C: Modulation of Cellular Levels of Sphingosine 1-Phosphate and Ceramide. *Biochemistry* **1998**, *37* (37), 12892–12898. https://doi.org/10.1021/bi980744d.

(156) Orito, A.; Kumanogoh, H.; Yasaka, K.; Sokawa, J.; Hidaka, H.; Sokawa, Y.; Maekawa, S. Calcium-Dependent Association of Annexin VI, Protein Kinase Cα, and Neurocalcinα on the Raft Fraction Derived from the Synaptic Plasma Membrane of Rat Brain. *J. Neurosci. Res.* **2001**, *64* (3), 235–241. https://doi.org/10.1002/jnr.1071.

(157) Mattsson, N.; Zetterberg, H.; Bianconi, S.; Yanjanin, N. M.; Fu, R.; Månsson, J.-E. E.; Porter, F. D.; Blennow, K. γ-Secretase-Dependent Amyloid-β Is Increased in Niemann-Pick Type C: A Cross-Sectional Study. *Neurology* **2011**, *76* (4), 366–372. https://doi.org/10.1212/WNL.0b013e318208f4ab.

(158) Auer, I. A.; Schmidt, M. L.; Lee, V. M. Y.; Curry, B.; Suzuki, K.; Shin, R.-W.; Pentchev, P. G.; Carstea, E. D.; Trojanowski, J. Q. Paired Helical Filament Tau (PHFtau) in Niemann-Pick Type C Disease Is Similar to PHFtau in Alzheimer's Disease. *Acta Neuropathol.* **1995**, *90* (6), 547–551. https://doi.org/10.1007/BF00318566.

(159) Bu, B.; Li, J.; Davies, P.; Vincent, I. Deregulation of Cdk5, Hyperphosphorylation, and Cytoskeletal Pathology in the Niemann–Pick Type C Murine Model. *J. Neurosci.* **2002**, *22* (15), 6515–6525.

(160) Zhang, M.; Li, J.; Chakrabarty, P.; Bu, B.; Vincent, I. Cyclin-Dependent Kinase Inhibitors Attenuate Protein Hyperphosphorylation, Cytoskeletal Lesion Formation, and Motor Defects in Niemann-Pick Type C Mice. *Am. J. Pathol.* **2004**, *165* (3), 843–853. https://doi.org///dx.doi.org/10.1016/S0002-9440(10)63347-0.

(161) Zhang, M.; Hallows, J. L.; Wang, X.; Bu, B.; Wang, W.; Vincent, I. Mitogen-Activated Protein Kinase Activity May Not Be Necessary for the Neuropathology of Niemann-Pick Type C Mice. *J. Neurochem.* **2008**, *107* (3), 814–822. https://doi.org/10.1111/j.1471-4159.2008.05657.x.

(162) Davies, S. P.; Reddy, H.; Caivano, M.; Cohen, P. Specificity and Mechanism of Action of Some Commonly Used Protein Kinase Inhibitors. *Biochem. J.* **2000**, *351* (Pt 1), 95–105.

(163) Gaulton, A.; Hersey, A.; Nowotka, M.; Bento, A. P.; Chambers, J.; Mendez, D.; Mutowo, P.; Atkinson, F.; Bellis, L. J.; Cibrián-Uhalte, E.; et al. The ChEMBL Database in 2017. *Nucleic Acids Res.* **2017**, *45* (D1), D945–D954. https://doi.org/10.1093/nar/gkw1074.

(164) Hallows, J. L.; Iosif, R. E.; Biasell, R. D.; Vincent, I. P35/P25 Is Not Essential for Tau and Cytoskeletal Pathology or Neuronal Loss in Niemann–Pick Type C Disease. *J. Neurosci.* **2006**, *26* (10), 2738 LP-2744. https://doi.org/10.1523/JNEUROSCI.4834-05.2006.

(165) Tamari, F.; Chen, F. W.; Li, C.; Chaudhari, J.; Ioannou, Y. A. PKC Activation in Niemann Pick C1 Cells Restores Subcellular Cholesterol Transport. *PLoS One* **2013**, *8* (8), e74169. https://doi.org/10.1371/journal.pone.0074169.

(166) Peter, F.; Rost, S.; Rolfs, A.; Frech, M. J. Activation of PKC Triggers Rescue of NPC1 Patient Specific IPSC Derived Glial Cells from Gliosis. *Orphanet J. Rare Dis.* **2017**, *12* (1), 145. https://doi.org/10.1186/s13023-017-0697-y.

(167) Walter, M.; Davies, J. P.; Ioannou, Y. A. Telomerase Immortalization Upregulates Rab9 Expression and Restores LDL Cholesterol Egress from Niemann-Pick C1 Late Endosomes. *J. Lipid Res.* **2003**, *44* (2), 243–253. https://doi.org/10.1194/jlr.M200230-JLR200.

(168) Walter, M.; Chen, F. W.; Tamari, F.; Wang, R.; Ioannou, Y. A. Endosomal Lipid Accumulation in NPC1 Leads to Inhibition of PKC, Hypophosphorylation of Vimentin and Rab9 Entrapment. *Biol. Cell* **2009**, *101* (3), 141–153. https://doi.org/10.1042/BC20070171.

(169) Nanda, A.; Gukovskaya, A.; Tseng, J.; Grinstein, S. Activation of Vacuolar-Type Proton Pumps by Protein Kinase C. Role in Neutrophil PH Regulation. *J. Biol. Chem.* **1992**, *267* (32), 22740–22746.

(170) Zhou, X.-B.; Wulfsen, I.; Utku, E.; Sausbier, U.; Sausbier, M.; Wieland, T.; Ruth, P.; Korth, M. Dual Role of Protein Kinase C on BK Channel Regulation. *Proc. Natl. Acad. Sci.* **2010**, *107* (17), 8005–8010. https://doi.org/10.1073/pnas.0912029107.

(171) Yu, W.; Gong, J.-S.; Ko, M.; Garver, W. S.; Yanagisawa, K.; Michikawa, M. Altered Cholesterol Metabolism in Niemann-Pick Type C1 Mouse Brains Affects Mitochondrial

Function. *J. Biol. Chem.* **2005**, *280* (12), 11731–11739. https://doi.org/10.1074/jbc.M412898200.
(172) Torres, S.; Matías, N.; Baulies, A.; Nuñez, S.; Alarcon-Vila, C.; Martinez, L.; Nuño, N.; Fernandez, A.; Caballeria, J.; Levade, T.; et al. *Mitochondrial GSH Replenishment as a Potential Therapeutic Approach for Niemann Pick Type C Disease*; Elsevier, **2017**; Vol. 11, pp 60–72. https://doi.org///doi.org/10.1016/j.redox.2016.11.010.
(173) Domínguez-Pérez, M.; Simoni-Nieves, A.; Rosales, P.; Nuño-Lámbarri, N.; Rosas-Lemus, M.; Souza, V.; Miranda, R. U.; Bucio, L.; Uribe Carvajal, S.; Marquardt, J. U.; et al. Cholesterol Burden in the Liver Induces Mitochondrial Dynamic Changes and Resistance to Apoptosis. *J. Cell. Physiol.* **2019**, *234* (5), 7213–7223. https://doi.org/10.1002/jcp.27474.
(174) Asalla, S.; Girada, S. B.; Kuna, R. S.; Chowdhury, D.; Kandagatla, B.; Oruganti, S.; Bhadra, U.; Bhadra, M. P.; Kalivendi, S. V.; Rao, S. P.; et al. Restoring Mitochondrial Function: A Small Molecule-Mediated Approach to Enhance Glucose Stimulated Insulin Secretion in Cholesterol Accumulated Pancreatic Beta Cells. *Sci. Rep.* **2016**, *6*, 27513.
(175) Solsona-Vilarrasa, E.; Fucho, R.; Torres, S.; Nuñez, S.; Nuño-Lámbarri, N.; Enrich, C.; García-Ruiz, C.; Fernández-Checa, J. C. Cholesterol Enrichment in Liver Mitochondria Impairs Oxidative Phosphorylation and Disrupts the Assembly of Respiratory Supercomplexes. *Redox Biol.* **2019**, *24*, 101214. https://doi.org/10.1016/j.redox.2019.101214.
(176) Allen, A. M.; Taylor, J. M. W.; Graham, A. Mitochondrial (Dys)Function and Regulation of Macrophage Cholesterol Efflux. *Clin. Sci.* **2013**, *124* (8), 509–515. https://doi.org/10.1042/CS20120358.
(177) Vivas, O.; Tiscione, S. A.; Dixon, R. E.; Ory, D. S.; Dickson, E. J. Niemann-Pick Type C Disease Reveals a Link between Lysosomal Cholesterol and PtdIns(4,5)P 2 That Regulates Neuronal Excitability. *Cell Rep.* **2019**, *27* (9), 2636–2648.e4. https://doi.org/10.1016/j.celrep.2019.04.099.
(178) Zeng, L.; Liao, H.; Liu, Y.; Lee, T. S.; Zhu, M.; Wang, X.; Stemerman, M. B.; Zhu, Y.; Shyy, J. Y.-J. Sterol-Responsive Element-Binding Protein (SREBP) 2 down-Regulates ATP-Binding Cassette Transporter A1 in Vascular Endothelial Cells: A Novel Role of SREBP in Regulating Cholesterol Metabolism. *J. Biol. Chem.* **2004**, *279* (47), 48801–48807. https://doi.org/10.1074/jbc.M407817200.
(179) Wong, J.; Quinn, C. M.; Brown, A. J. SREBP-2 Positively Regulates Transcription of the Cholesterol Efflux Gene, ABCA1, by Generating Oxysterol Ligands for LXR. *Biochem. J.* **2006**, *400* (3), 485–491. https://doi.org/10.1042/BJ20060914.
(180) Kappler, L.; Li, J.; Häring, H. U.; Weigert, C.; Lehmann, R.; Xu, G.; Hoene, M. Purity Matters: A Workflow for the Valid High-Resolution Lipid Profiling of Mitochondria from Cell Culture Samples. *Sci. Rep.* **2016**, *6* (1), 21107. https://doi.org/10.1038/srep21107.
(181) Charman, M.; Kennedy, B. E.; Osborne, N.; Karten, B. MLN64 Mediates Egress of Cholesterol from Endosomes to Mitochondria in the Absence of Functional Niemann-Pick Type C1 Protein. *J. Lipid Res.* **2010**, *51* (5), 1023–1034. https://doi.org/10.1194/jlr.M002345.
(182) Balboa, E.; Castro, J.; Pinochet, M. J.; Cancino, G. I.; Matías, N.; José Sáez, P.; Martínez, A.; Álvarez, A. R.; Garcia-Ruiz, C.; Fernandez-Checa, J. C.; et al. MLN64 Induces Mitochondrial Dysfunction Associated with Increased Mitochondrial Cholesterol Content. *Redox Biol.* **2017**, *12*, 274–284. https://doi.org/10.1016/j.redox.2017.02.024.
(183) Ziolkowski, W.; Szkatula, M.; Nurczyk, A.; Wakabayashi, T.; Kaczor, J. J.; Olek, R. A.; Knap, N.; Antosiewicz, J.; Wieckowski, M. R.; Wozniak, M. *Methyl-Beta-Cyclodextrin Induces Mitochondrial Cholesterol Depletion and Alters the Mitochondrial Structure and Bioenergetics*; FEBS Letters, **2010**; Vol. 584, pp 4606–4610. https://doi.org///doi.org/10.1016/j.febslet.2010.10.023.
(184) Garver, W. S.; Krishnan, K.; Gallagos, J. R.; Michikawa, M.; Francis, G. A.; Heidenreich, R. A. Niemann-Pick C1 Protein Regulates Cholesterol Transport to the Trans-Golgi Network and Plasma Membrane Caveolae. *J. Lipid Res.* **2002**, *43* (4), 579–589.
(185) Kennedy, B. E.; Charman, M.; Karten, B. Niemann-Pick Type C2 Protein Contributes to the Transport of Endosomal Cholesterol to Mitochondria without Interacting with NPC1. *J. Lipid Res.* **2012**, *53* (12), 2632–2642. https://doi.org/10.1194/jlr.M029942
(186) Balboa, E.; Castro, J.; Pinochet, M.-J.; Cancino, G. I.; Matías, N.; José Sáez, P.; Martínez,

A.; Álvarez, A. R.; Garcia-Ruiz, C.; Fernandez-Checa, J. C.; et al. MLN64 Induces Mitochondrial Dysfunction Associated with Increased Mitochondrial Cholesterol Content. *Redox Biol.* **2017**, *12*, 274–284. https://doi.org/10.1016/J.REDOX.2017.02.024.

(187) Rone, M. B.; Fan, J.; Papadopoulos, V. Cholesterol Transport in Steroid Biosynthesis: Role of Protein-Protein Interactions and Implications in Disease States. *Biochimica et Biophysica Acta - Molecular and Cell Biology of Lipids*. **2009**, pp 646–658. https://doi.org/10.1016/j.bbalip.2009.03.001.

(188) Sandhoff, R.; Sandhoff, K. Emerging Concepts of Ganglioside Metabolism. *FEBS Letters*. 2018, pp 3835–3864. https://doi.org/10.1002/1873-3468.13114.

(189) Tidhar, R.; Futerman, A. H. The Complexity of Sphingolipid Biosynthesis in the Endoplasmic Reticulum. *Biochim. Biophys. Acta - Mol. Cell Res.* **2013**, *1833* (11), 2511–2518. https://doi.org///dx.doi.org/10.1016/j.bbamcr.2013.04.010.

(190) Giussani, P.; Colleoni, T.; Brioschi, L.; Bassi, R.; Hanada, K.; Tettamanti, G.; Riboni, L.; Viani, P. Ceramide Traffic in C6 Glioma Cells: Evidence for CERT-Dependent and Independent Transport from ER to the Golgi Apparatus. *Biochim. Biophys. Acta - Mol. Cell Biol. Lipids* **2008**, *1781* (1–2), 40–51. https://doi.org///dx.doi.org/10.1016/j.bbalip.2007.11.002.

(191) Futerman, A. H.; Pagano, R. E. Determination of the Intracellular Sites and Topology of Glucosylceramide Synthesis in Rat Liver. *Biochem. J.* **1991**, *280* (2), 295–302. https://doi.org/10.1042/bj2800295.

(192) Jeckel, D.; Karrenbauer, A.; Burger, K. N.; van Meer, G.; Wieland, F. Glucosylceramide Is Synthesized at the Cytosolic Surface of Various Golgi Subfractions. *J. Cell Biol.* **1992**, *117* (2), 259–267. https://doi.org/10.1083/jcb.117.2.259.

(193) D'Angelo, G.; Uemura, T.; Chuang, C. C.; Polishchuk, E.; Santoro, M.; Ohvo-Rekilä, H.; Sato, T.; Di Tullio, G.; Varriale, A.; D'Auria, S.; et al. Vesicular and Non-Vesicular Transport Feed Distinct Glycosylation Pathways in the Golgi. *Nature* **2013**, *501* (7465), 116–120. https://doi.org/10.1038/nature12423.

(194) Halter, D.; Neumann, S.; van Dijk, S. M.; Wolthoorn, J.; de Mazière, A. M.; Vieira, O. V; Mattjus, P.; Klumperman, J.; van Meer, G.; Sprong, H. Pre- and Post-Golgi Translocation of Glucosylceramide in Glycosphingolipid Synthesis. *J. Cell Biol.* **2007**, *179* (1), 101–115. https://doi.org/10.1083/jcb.200704091.

(195) Gillard, B. K.; Clement, R. G.; Marcus, D. M. Variations among Cell Lines in the Synthesis of Sphingolipids in de Novo and Recycling Pathways. *Glycobiology* **1998**, *8* (9), 885–890.

(196) Tamargo, R. J.; Velayati, A.; Goldin, E.; Sidransky, E. The Role of Saposin C in Gaucher Disease. *Mol. Genet. Metab.* **2012**, *106* (3), 257–263. https://doi.org///dx.doi.org/10.1016/j.ymgme.2012.04.024.

(197) van Meer, G.; Voelker, D. R.; Feigenson, G. W. Membrane Lipids: Where They Are and How They Behave. *Nat. Rev. Mol. Cell Biol.* **2008**, *9* (2), 112–124.

(198) Mattjus, P. Glycolipid Transfer Proteins and Membrane Interaction. *Biochimica et Biophysica Acta - Biomembranes*. Elsevier 2009, pp 267–272. https://doi.org/10.1016/j.bbamem.**2008**.10.003.

(199) Munkacsi, A. B.; Chen, F. W.; Brinkman, M. A.; Higaki, K.; Gutiérrez, G. D.; Chaudhari, J.; Layer, J. V; Tong, A.; Bard, M.; Boone, C.; et al. An "Exacerbate-Reverse" Strategy in Yeast Identifies Histone Deacetylase Inhibition as a Correction for Cholesterol and Sphingolipid Transport Defects in Human Niemann-Pick Type C Disease. *J. Biol. Chem.* **2011**, *286* (27), 23842–23851. https://doi.org/10.1074/jbc.M111.227645.

(200) Contreras, P. S.; Gonzalez-Zuñiga, M.; González-Hódar, L.; Yáñez, M. J.; Dulcey, A.; Marugan, J.; Seto, E.; Alvarez, A. R.; Zanlungo, S. Neuronal Gene Repression in Niemann-Pick Type C Models Is Mediated by the c-Abl/HDAC2 Signaling Pathway. *Biochim. Biophys. Acta - Gene Regul. Mech.* **2016**, *1859* (2), 269–279. https://doi.org/10.1016/j.bbagrm.2015.11.006.

(201) Pipalia, N. H.; Cosner, C. C.; Huang, A.; Chatterjee, A.; Bourbon, P.; Farley, N.; Helquist, P.; Wiest, O.; Maxfield, F. R. Histone Deacetylase Inhibitor Treatment Dramatically Reduces Cholesterol Accumulation in Niemann-Pick Type C1 Mutant Human Fibroblasts. *Proc. Natl. Acad. Sci.* **2011**, *108* (14), 5620–5625. https://doi.org/10.1073/pnas.1014890108.

(202) Pipalia, N. H.; Subramanian, K.; Mao, S.; Ralph, H.; Hutt, D. M.; Scott, S. M.; Balch, W. E.; Maxfield, F. R. Histone Deacetylase Inhibitors Correct the Cholesterol Storage Defect in

Most Niemann-Pick C1 Mutant Cells. *J. Lipid Res.* **2017**, *58* (4), 695–708. https://doi.org/10.1194/jlr.m072140.
(203) Pugach, E. K.; Feltes, M.; Kaufman, R. J.; Ory, D. S.; Bang, A. G. High-Content Screen for Modifiers of Niemann-Pick Type C Disease in Patient Cells. *Hum. Mol. Genet.* **2018**, *27* (12), 2101–2112. https://doi.org/10.1093/hmg/ddy117.
(204) Alam, M. S.; Cooper, B.; Farris, J. D.; Haldar, K. Tolerance of Chronic HDACi Treatment for Neurological, Visceral and Lung Niemann-Pick Type C Disease in Mice. *Sci. Rep.* **2018**, *8* (1), 3875. https://doi.org/10.1038/s41598-018-22162-7.
(205) Nakasone, N.; Nakamura, Y. S.; Higaki, K.; Oumi, N.; Ohno, K.; Ninomiya, H. Endoplasmic Reticulum-Associated Degradation of Niemann-Pick C1: Evidence for the Role of Heat Shock Proteins and Identification of Lysine Residues That Accept Ubiquitin. *J. Biol. Chem.* **2014**, *289* (28), 19714–19725. https://doi.org/10.1074/jbc.M114.549915.
(206) Gelsthorpe, M. E.; Baumann, N.; Millard, E.; Gale, S. E.; Langmade, S. J.; Schaffer, J. E.; Ory, D. S. Niemann-Pick Type C1 I1061T Mutant Encodes a Functional Protein That Is Selected for Endoplasmic Reticulum-Associated Degradation Due to Protein Misfolding. *J. Biol. Chem.* **2008**, *283* (13), 8229–8236. https://doi.org/10.1074/jbc.M708735200.
(207) Ohgane, K.; Karaki, F.; Noguchi-Yachide, T.; Dodo, K.; Hashimoto, Y. Structure–activity Relationships of Oxysterol-Derived Pharmacological Chaperones for Niemann–Pick Type C1 Protein. *Bioorg. Med. Chem. Lett.* **2014**, *24* (15), 3480–3485. https://doi.org///dx.doi.org/10.1016/j.bmcl.2014.05.064.
(208) Ohgane, K.; Karaki, F.; Dodo, K.; Hashimoto, Y. Discovery of Oxysterol-Derived Pharmacological Chaperones for NPC1: Implication for the Existence of Second Sterol-Binding Site. *Chem. Biol.* **2013**, *20* (3), 391–402. https://doi.org///dx.doi.org/10.1016/j.chembiol.2013.02.009.
(209) Yu, T.; Chung, C.; Shen, D.; Xu, H.; Lieberman, A. P. Ryanodine Receptor Antagonists Adapt NPC1 Proteostasis to Ameliorate Lipid Storage in Niemann–Pick Type C Disease Fibroblasts. *Hum. Mol. Genet.* **2012**, *21* (14), 3205–3214. https://doi.org/10.1093/hmg/dds145.
(210) Liou, B.; Peng, Y.; Li, R.; Inskeep, V.; Zhang, W.; Quinn, B.; Dasgupta, N.; Blackwood, R.; Setchell, K. D. R.; Fleming, S.; et al. Modulating Ryanodine Receptors with Dantrolene Attenuates Neuronopathic Phenotype in Gaucher Disease Mice. *Hum. Mol. Genet.* **2016**, *25* (23), 5126–5141. https://doi.org/10.1093/hmg/ddw322.
(211) Patterson, M. C.; Di Bisceglie, A. M.; Higgins, J. J.; Abel, R. B.; Schiffmann, R.; Parker, C. C.; Argoff, C. E.; Grewal, R. P.; Yu, K.; Pentchev, P. G.; et al. The Effect of Cholesterol-Lowering Agents on Hepatic and Plasma Cholesterol in Niemann-Pick Disease Type C. *Neurology* **1993**, *43* (1 Part 1), 61. https://doi.org/10.1212/WNL.43.1_Part_1.61.
(212) Erickson, R. P.; Garver, W. S.; Camargo, F.; Hossian, G. S.; Heidenreich, R. A. Pharmacological and Genetic Modifications of Somatic Cholesterol Do Not Substantially Alter the Course of CNS Disease in Niemann-Pick C Mice. *J. Inherit. Metab. Dis.* **2000**, *23*, 54–62. https://doi.org/1005650930330.
(213) Beheregaray, A. P. C.; Souza, F. T. S.; Coelho, J. C. Effect of a Peroxysomal Proliferator Agent on Intracellular Cholesterol Accumulation in Cultured Fibroblasts from Niemann-Pick Type C Disease Patients. *Clin. Chim. Acta* **2003**, *336* (1–2), 137–142. https://doi.org/10.1016/S0009-8981(03)00341-3.
(214) Yu, D.; Swaroop, M.; Wang, M.; Baxa, U.; Yang, R.; Yan, Y.; Coksaygan, T.; DeTolla, L.; Marugan, J. J.; Austin, C. P.; et al. Niemann–Pick Disease Type C: Induced Pluripotent Stem Cell–Derived Neuronal Cells for Modeling Neural Disease and Evaluating Drug Efficacy. *J. Biomol. Screen.* **2014**, *19* (8), 1164–1173. https://doi.org/10.1177/1087057114537378.
(215) Yang, F.; Feng, X.; Rolfs, A.; Luo, J. Lovastatin Promotes Myelin Formation in NPC1 Mutant Oligodendrocytes. *J. Neurol. Sci.* **2018**, *386*, 56–63. https://doi.org/10.1016/j.jns.2018.01.015.
(216) Boadu, E.; Choi, H. Y.; Lee, D. W. K.; Waddington, E. I.; Chan, T.; Asztalos, B.; Vance, J. E.; Chan, A.; Castro, G.; Francis, G. A. Correction of Apolipoprotein A-I-Mediated Lipid Efflux and High Density Lipoprotein Particle Formation in Human Niemann-Pick Type C Disease Fibroblasts. *J. Biol. Chem.* **2006**, *281* (48), 37081–37090. https://doi.org/10.1074/jbc.M606890200.
(217) Boadu, E.; Nelson, R. C.; Francis, G. A. ABCA1-Dependent Mobilization of Lysosomal

Cholesterol Requires Functional Niemann-Pick C2 but Not Niemann-Pick C1 Protein. *Biochim. Biophys. Acta - Mol. Cell Biol. Lipids* **2012**, *1821* (3), 396–404. https://doi.org/10.1016/j.bbalip.2011.11.013.

(218) Repa, J. J.; Li, H.; Frank-Cannon, T. C.; Valasek, M. A.; Turley, S. D.; Tansey, M. G.; Dietschy, J. M. Liver X Receptor Activation Enhances Cholesterol Loss from the Brain, Decreases Neuroinflammation, and Increases Survival of the NPC1 Mouse. *J. Neurosci.* **2007**, *27* (52), 14470–14480. https://doi.org/10.1523/JNEUROSCI.4823-07.2007.

(219) Chen, F. W.; Li, C.; Ioannou, Y. A. Cyclodextrin Induces Calcium-Dependent Lysosomal Exocytosis. *PLoS One* **2010**, *5* (11), e15054.

(220) Rosenbaum, A. I.; Zhang, G.; Warren, J. D.; Maxfield, F. R. Endocytosis of Beta-Cyclodextrins Is Responsible for Cholesterol Reduction in Niemann-Pick Type C Mutant Cells. *Proc. Natl. Acad. Sci.* **2010**, *107* (12), 5477–5482. https://doi.org/10.1073/pnas.0914309107.

(221) Vacca, F.; Vossio, S.; Mercier, V.; Moreau, D.; Johnson, S.; Scott, C. C.; Montoya, J. P.; Moniatte, M.; Gruenberg, J. Cyclodextrin Triggers MCOLN1-Dependent Endo-Lysosome Secretion in Niemann-Pick Type C Cells. *J. Lipid Res.* **2019**, *60* (4), 832–843. https://doi.org/10.1194/jlr.m089979.

(222) Abi-Mosleh, L.; Infante, R. E.; Radhakrishnan, A.; Goldstein, J. L.; Brown, M. S. Cyclodextrin Overcomes Deficient Lysosome-to-Endoplasmic Reticulum Transport of Cholesterol in Niemann-Pick Type C Cells. *Proc. Natl. Acad. Sci.* **2009**, *106* (46), 19316–19321. https://doi.org/10.1073/pnas.0910916106.

(223) Liu, B.; Turley, S. D.; Burns, D. K.; Miller, A. M.; Repa, J. J.; Dietschy, J. M. Reversal of Defective Lysosomal Transport in NPC Disease Ameliorates Liver Dysfunction and Neurodegeneration in the Npc1−/− Mouse. *Proc. Natl. Acad. Sci.* **2009**, *106* (7), 2377 LP-2382.

(224) Dai, S.; Dulcey, A. E.; Hu, X.; Wassif, C. A.; Porter, F. D.; Austin, C. P.; Ory, D. S.; Marugan, J.; Zheng, W. Methyl-β-Cyclodextrin Restores Impaired Autophagy Flux in Niemann-Pick C1-Deficient Cells through Activation of AMPK. *Autophagy* **2017**, *13* (8), 1435–1451. https://doi.org/10.1080/15548627.2017.1329081.

(225) Young, M. M.; Takahashi, Y.; Fox, T. E.; Yun, J. K.; Kester, M.; Wang, H. G. Sphingosine Kinase 1 Cooperates with Autophagy to Maintain Endocytic Membrane Trafficking. *Cell Rep.* **2016**, *17* (6), 1532–1545. https://doi.org/10.1016/j.celrep.2016.10.019.

(226) Lima, S.; Milstien, S.; Spiegel, S. Sphingosine and Sphingosine Kinase 1 Involvement in Endocytic Membrane Trafficking. *J. Biol. Chem.* **2017**, *292* (8), 3074–3088. https://doi.org/10.1074/jbc.M116.762377.

(227) Davidson, C. D.; Ali, N. F.; Micsenyi, M. C.; Stephney, G.; Renault, S.; Dobrenis, K.; Ory, D. S.; Vanier, M. T.; Walkley, S. U. Chronic Cyclodextrin Treatment of Murine Niemann-Pick C Disease Ameliorates Neuronal Cholesterol and Glycosphingolipid Storage and Disease Progression. *PLoS One* **2009**, *4*, e6951.

(228) Ramirez, C. M.; Liu, B.; Taylor, A. M.; Repa, J. J.; Burns, D. K.; Weinberg, A. G.; Turley, S. D.; Dietschy, J. M. Weekly Cyclodextrin Administration Normalizes Cholesterol Metabolism in Nearly Every Organ of the Niemann-Pick Type C1 Mouse and Markedly Prolongs Life. *Pediatr. Res.* **2010**, *68*, 309–315.

(229) Calias, P. 2-Hydroxypropyl-Beta-Cyclodextrins and the Blood-Brain Barrier: Considerations for Niemann-Pick Disease Type C1. *Curr. Pharm. Des.* **2017**, *23* (40), 6231–6238. https://doi.org/10.2174/1381612823666171019164220.

(230) Ory, D. S.; Ottinger, E. A.; Farhat, N. Y.; King, K. A.; Jiang, X.; Weissfeld, L.; Berry-Kravis, E.; Davidson, C. D.; Bianconi, S.; Keener, L. A.; et al. Intrathecal 2-ß-Hydroxypropylcyclodextrin Decreases Neurological Disease Progression in Niemann-Pick Disease, Type C1: A Non-Randomised, Open-Label, Phase 1-2 Trial. *Lancet* **2017**, *390* (10104), 1758–1768. https://doi.org/10.1016/S0140-6736(17)31465-4.

(231) Berry-Kravis, E.; Chin, J.; Hoffmann, A.; Winston, A.; Stoner, R.; LaGorio, L.; Friedmann, K.; Hernandez, M.; Ory, D. S.; Porter, F. D.; et al. Long-Term Treatment of Niemann-Pick Type C1 Disease With Intrathecal 2-Hydroxypropyl-β-Cyclodextrin. *Pediatr. Neurol.* **2018**, *80*, 24–34. https://doi.org/10.1016/j.pediatrneurol.2017.12.014.

(232) Williams, I. M.; Wallom, K.-L.; Smith, D. A.; Al Eisa, N.; Smith, C.; Platt, F. M. Improved Neuroprotection Using Miglustat, Curcumin and Ibuprofen as a Triple Combination Therapy

in Niemann–Pick Disease Type C1 Mice. *Neurobiol. Dis.* **2014**, *67*, 9–17. https://doi.org///dx.doi.org/10.1016/j.nbd.2014.03.001.
(233) Borbon, I. A.; Hillman, Z.; Duran Jr., E.; Kiela, P. R.; Frautschy, S. A.; Erickson, R. P. Lack of Efficacy of Curcumin on Neurodegeneration in the Mouse Model of Niemann–Pick C1. *Pharmacol. Biochem. Behav.* **2012**, *101* (1), 125–131. https://doi.org///dx.doi.org/10.1016/j.pbb.2011.12.009.
(234) Ferrante, A.; De Nuccio, C.; Pepponi, R.; Visentin, S.; Martire, A.; Bernardo, A.; Minghetti, L.; Popoli, P. Stimulation of Adenosine A2A Receptors Reduces Intracellular Cholesterol Accumulation and Rescues Mitochondrial Abnormalities in Human Neural Cell Models of Niemann-Pick C1. *Neuropharmacology* **2016**, *103*, 155–162. https://doi.org/10.1016/j.neuropharm.2015.11.022.
(235) Chang, X. B.; Tabcharani, J. A.; Hou, Y. X.; Jensen, T. J.; Kartner, N.; Alon, N.; Hanrahan, J. W.; Riordan, J. R. Protein Kinase A (PKA) Still Activates CFTR Chloride Channel after Mutagenesis of All 10 PKA Consensus Phosphorylation Sites. *J. Biol. Chem.* **1993**, *268* (15), 11304–11311.
(236) Folts, C. J.; Scott-Hewitt, N.; Pröschel, C.; Mayer-Pröschel, M.; Noble, M. Lysosomal Re-Acidification Prevents Lysosphingolipid-Induced Lysosomal Impairment and Cellular Toxicity. *PLOS Biol.* **2016**, *14* (12), e1002583.
(237) Bingham, T. C.; Fisher, E. A.; Parathath, S.; Reiss, A. B.; Chan, E. S.; Cronstein, B. N. A2A Adenosine Receptor Stimulation Decreases Foam Cell Formation by Enhancing ABCA1-Dependent Cholesterol Efflux. *J. Leukoc. Biol.* **2010**, *87* (4), 683–690. https://doi.org/10.1189/jlb.0709513.
(238) Ferrante, A.; Pezzola, A.; Matteucci, A.; Di Biase, A.; Attorri, L.; Armida, M.; Martire, A.; Chern, Y.; Popoli, P. The Adenosine A2Areceptor Agonist T1–11 Ameliorates Neurovisceral Symptoms and Extends the Lifespan of a Mouse Model of Niemann-Pick Type C Disease. *Neurobiol. Dis.* **2018**, *110*, 1–11. https://doi.org/10.1016/j.nbd.2017.10.013.
(239) Yévenes, L. F.; Klein, A.; Castro, J. F.; Marín, T.; Leal, N.; Leighton, F.; Alvarez, A. R.; Zanlungo, S. Lysosomal Vitamin E Accumulation in Niemann–Pick Type C Disease. *Biochim. Biophys. Acta - Mol. Basis Dis.* **2012**, *1822* (2), 150–160. https://doi.org/10.1016/J.BBADIS.2011.11.009.
(240) Ulatowski, L.; Parker, R.; Davidson, C.; Yanjanin, N.; Kelley, T. J.; Corey, D.; Atkinson, J.; Porter, F.; Arai, H.; Walkley, S. U.; et al. Altered Vitamin E Status in Niemann-Pick Type C Disease. *J. Lipid Res.* **2011**, *52* (7), 1400–1410. https://doi.org/10.1194/jlr.M015560.
(241) Marín, T.; Contreras, P.; Castro, J. F.; Chamorro, D.; Balboa, E.; Bosch-Morató, M.; Muñoz, F. J.; Alvarez, A. R.; Zanlungo, S. Vitamin E Dietary Supplementation Improves Neurological Symptoms and Decreases C-Abl/P73 Activation in Niemann-Pick C Mice. *Nutrients* **2014**, *6* (8), 3000–3017. https://doi.org/10.3390/nu6083000.
(242) Zervas, M.; Somers, K. L.; Thrall, M. A.; Walkley, S. U. Critical Role for Glycosphingolipids in Niemann-Pick Disease Type C. *Curr. Biol.* **2001**, *11* (16), 1283–1287. https://doi.org///dx.doi.org/10.1016/S0960-9822(01)00396-7.
(243) Lachmann, R. H.; te Vruchte, D.; Lloyd-Evans, E.; Reinkensmeier, G.; Sillence, D. J.; Fernandez-Guillen, L.; Dwek, R. A.; Butters, T. D.; Cox, T. M.; Platt, F. M. Treatment with Miglustat Reverses the Lipid-Trafficking Defect in Niemann–Pick Disease Type C. *Neurobiol. Dis.* **2004**, *16* (3), 654–658. https://doi.org///dx.doi.org/10.1016/j.nbd.2004.05.002.
(244) Patterson, M. C.; Vecchio, D.; Prady, H.; Abel, L.; Wraith, J. E. Miglustat for Treatment of Niemann-Pick C Disease: A Randomised Controlled Study. *Lancet Neurol.* **2007**, *6* (9), 765–772. https://doi.org///dx.doi.org/10.1016/S1474-4422(07)70194-1.
(245) Pineda, M.; Wraith, J. E.; Mengel, E.; Sedel, F.; Hwu, W. L.; Rohrbach, M.; Bembi, B.; Walterfang, M.; Korenke, G. C.; Marquardt, T.; et al. Miglustat in Patients with Niemann-Pick Disease Type C (NP-C): A Multicenter Observational Retrospective Cohort Study. *Mol. Genet. Metab.* **2009**, *98* (3), 243–249. https://doi.org/10.1016/j.ymgme.2009.07.003.
(246) Pineda, M.; Juríčková, K.; Karimzadeh, P.; Kolnikova, M.; Malinova, V.; Insua, J. L.; Velten, C.; Kolb, S. A. Disease Characteristics, Prognosis and Miglustat Treatment Effects on Disease Progression in Patients with Niemann-Pick Disease Type C: An International, Multicenter, Retrospective Chart Review. *Orphanet Journal of Rare Diseases*, **2019**, *14*(1) 32. https://doi.org/10.1186/s13023-019-0996-6.

(247) Nietupski, J. B.; Pacheco, J. J.; Chuang, W.-L.; Maratea, K.; Li, L.; Foley, J.; Ashe, K. M.; Cooper, C. G. F.; Aerts, J. M. F. G.; Copeland, D. P.; et al. Iminosugar-Based Inhibitors of Glucosylceramide Synthase Prolong Survival but Paradoxically Increase Brain Glucosylceramide Levels in Niemann–Pick C Mice. *Mol. Genet. Metab.* **2012**, *105* (4), 621–628. https://doi.org///dx.doi.org/10.1016/j.ymgme.2012.01.020.

(248) Ridley, C. M.; Thur, K. E.; Shanahan, J.; Thillaiappan, N. B.; Shen, A.; Uhl, K.; Walden, C. M.; Rahim, A. A.; Waddington, S. N.; Platt, F. M.; et al. β-Glucosidase 2 (GBA2) Activity and Imino Sugar Pharmacology. *J. Biol. Chem.* **2013**, *288* (36), 26052–26066. https://doi.org/10.1074/jbc.M113.463562.

(249) Overkleeft, H. S.; Renkema, G. H.; Neele, J.; Vianello, P.; Hung, I. O.; Strijland, A.; van der Burg, A. M.; Koomen, G.-J.; Pandit, U. K.; Aerts, J. M. F. G. Generation of Specific Deoxynojirimycin-Type Inhibitors of the Non-Lysosomal Glucosylceramidase. *J. Biol. Chem.* **1998**, *273* (41), 26522–26527. https://doi.org/10.1074/jbc.273.41.26522.

(250) Marques, A. R. A.; Aten, J.; Ottenhoff, R.; van Roomen, C. P. A. A.; Herrera Moro, D.; Claessen, N.; Vinueza Veloz, M. F.; Zhou, K.; Lin, Z.; Mirzaian, M.; et al. Reducing GBA2 Activity Ameliorates Neuropathology in Niemann-Pick Type C Mice. *PLoS One* **2015**, *10* (8), e0135889.

(251) Liu, Y.; Wu, Y.-P.; Wada, R.; Neufeld, E. B.; Mullin, K. A.; Howard, A. C.; Pentchev, P. G.; Vanier, M. T.; Suzuki, K.; Proia, R. L. Alleviation of Neuronal Ganglioside Storage Does Not Improve the Clinical Course of the Niemann–Pick C Disease Mouse. *Hum. Mol. Genet.* **2000**, *9* (7), 1087–1092. https://doi.org/10.1093/hmg/9.7.1087.

(252) Lee, H.; Jong, K. L.; Yong, C. B.; Song, H. Y.; Okino, N.; Schuchman, E. H.; Yamashita, T.; Bae, J.; and Hee, K. J. Inhibition of GM3 Synthase Attenuates Neuropathology of Niemann-Pick Disease Type C by Affecting Sphingolipid Metabolism. *Mol. Cells* **2014**, *37* (2), 161–171.

(253) Burke, D. G.; Rahim, A. A.; Waddington, S. N.; Karlsson, S.; Enquist, I.; Bhatia, K.; Mehta, A.; Vellodi, A.; Heales, S. Increased Glucocerebrosidase (GBA) 2 Activity in GBA1 Deficient Mice Brains and in Gaucher Leucocytes. *J. Inherit. Metab. Dis.* **2013**, *36* (5), 869–872. https://doi.org/10.1007/s10545-012-9561-3.

(254) Chevallier, J.; Chamoun, Z.; Jiang, G.; Prestwich, G.; Sakai, N.; Matile, S.; Parton, R. G.; Gruenberg, J. Lysobisphosphatidic Acid Controls Endosomal Cholesterol Levels. *J. Biol. Chem.* **2008**, *283* (41), 27871–27880. https://doi.org/10.1074/jbc.M801463200.

(255) Kobayashi, T.; Beuchat, M.-H.; Lindsay, M.; Frias, S.; Palmiter, R. D.; Sakuraba, H.; Parton, R. G.; Gruenberg, J. Late Endosomal Membranes Rich in Lysobisphosphatidic Acid Regulate Cholesterol Transport. *Nat. Cell Biol.* **1999**, *1* (2), 113–118.

(256) Reagan, J. W.; Hubbert, M. L.; Shelness, G. S. Posttranslational Regulation of Acid Sphingomyelinase in Niemann-Pick Type C1 Fibroblasts and Free Cholesterol-Enriched Chinese Hamster Ovary Cells. *J. Biol. Chem.* **2000**, *275* (48), 38104–38110. https://doi.org/10.1074/jbc.M005296200.

(257) Tamura, H.; Takahashi, T.; Ban, N.; Torisu, H.; Ninomiya, H.; Takada, G.; Inagaki, N. Niemann–Pick Type C Disease: Novel NPC1 Mutations and Characterization of the Concomitant Acid Sphingomyelinase Deficiency. *Mol. Genet. Metab.* **2006**, *87* (2), 113–121. https://doi.org///dx.doi.org/10.1016/j.ymgme.2005.07.025.

(258) Kirkegaard, T.; Roth, A. G.; Petersen, N. H. T.; Mahalka, A. K.; Olsen, O. D.; Moilanen, I.; Zylicz, A.; Knudsen, J.; Sandhoff, K.; Arenz, C.; et al. Hsp70 Stabilizes Lysosomes and Reverts Niemann-Pick Disease-Associated Lysosomal Pathology. *Nature* **2010**, *463* (7280), 549–553. https://doi.org/10.1038/nature08710.

(259) Kirkegaard, T.; Gray, J.; Priestman, D. A.; Wallom, K. L.; Atkins, J.; Olsen, O. D.; Klein, A.; Drndarski, S.; Petersen, N. H. T.; Ingemann, L.; et al. Heat Shock Protein-Based Therapy as a Potential Candidate for Treating the Sphingolipidoses. *Sci. Transl. Med.* **2016**, *8* (355), 355ra118-355ra118. https://doi.org/10.1126/scitranslmed.aad9823.

(260) Puri, V.; Jefferson, J. R.; Singh, R. D.; Wheatley, C. L.; Marks, D. L.; Pagano, R. E. Sphingolipid Storage Induces Accumulation of Intracellular Cholesterol by Stimulating SREBP-1 Cleavage. *J. Biol. Chem.* **2003**, *278*, 20961–20970.

(261) Abdul-Hammed, M.; Breiden, B.; Adebayo, M. A.; Babalola, J. O.; Schwarzmann, G.; Sandhoff, K. Role of Endosomal Membrane Lipids and NPC2 in Cholesterol Transfer and Membrane Fusion. *J. Lipid Res.* **2010**, *51* (7), 1747–1760.

https://doi.org/10.1194/jlr.m003822.
(262) Enkavi, G.; Mikkolainen, H.; Güngör, B.; Ikonen, E.; Vattulainen, I. Concerted Regulation of NPC2 Binding to Endosomal/Lysosomal Membranes by Bis(Monoacylglycero)Phosphate and Sphingomyelin. *PLoS Comput. Biol.* **2017**, *13* (10), e1005831. https://doi.org/10.1371/journal.pcbi.1005831.
(263) Gallala, H. D.; Breiden, B.; Sandhoff, K. Regulation of the NPC2 Protein-Mediated Cholesterol Trafficking by Membrane Lipids. *J. Neurochem.* **2011**, *116* (5), 702–707. https://doi.org/10.1111/j.1471-4159.2010.07014.x.
(264) Devlin, C.; Pipalia, N. H.; Liao, X.; Schuchman, E. H.; Maxfield, F. R.; Tabas, I. Improvement in Lipid and Protein Trafficking in Niemann-Pick C1 Cells by Correction of a Secondary Enzyme Defect. *Traffic* **2010**, *11* (5), 601–615. https://doi.org/10.1111/j.1600-0854.2010.01046.x.
(265) Moreau, D.; Vacca, F.; Vossio, S.; Scott, C.; Colaco, A.; Paz Montoya, J.; Ferguson, C.; Damme, M.; Moniatte, M.; Parton, R. G.; et al. Drug-induced Increase in Lysobisphosphatidic Acid Reduces the Cholesterol Overload in Niemann–Pick Type C Cells and Mice. *EMBO Rep.* **2019**, *20* (7), e47055. https://doi.org/10.15252/embr.201847055.
(266) Cianciola, N. L.; Carlin, C. R. Adenovirus RID-α Activates an Autonomous Cholesterol Regulatory Mechanism That Rescues Defects Linked to Niemann-Pick Disease Type C. *J. Cell Biol.* **2009**, *187* (4), 537–552. https://doi.org/10.1083/jcb.200903039.
(267) Cianciola, N. L.; Greene, D. J.; Morton, R. E.; Carlin, C. R. Adenovirus RID Uncovers a Novel Pathway Requiring ORP1L for Lipid Droplet Formation Independent of NPC1. *Mol. Biol. Cell* **2013**, *24* (21), 3309–3325. https://doi.org/10.1091/mbc.e12-10-0760.
(268) Li, J.; Deffieu, M. S.; Lee, P. L.; Saha, P.; Pfeffer, S. R. Glycosylation Inhibition Reduces Cholesterol Accumulation in NPC1 Protein-Deficient Cells. *Proc. Natl. Acad. Sci.* **2015**, *112* (48), 14876–14881. https://doi.org/10.1073/pnas.1520490112.
(269) Morozov, A. V.; Kortemme, T. Potential Functions for Hydrogen Bonds in Protein Structure Prediction and Design. *Adv. Protein Chem.* **2005**, *72*, 1–38. https://doi.org/10.1016/S0065-3233(05)72001-5.
(270) Milovanovic, D.; Honigmann, A.; Koike, S.; Göttfert, F.; Pähler, G.; Junius, M.; Müllar, S.; Diederichsen, U.; Janshoff, A.; Grubmüller, H.; et al. Hydrophobic Mismatch Sorts SNARE Proteins into Distinct Membrane Domains. *Nat. Commun. 2015 6* **2015**, *6*, 5984. https://doi.org/10.1038/ncomms6984.
(271) Contreras, F.-X.; Ernst, A. M.; Haberkant, P.; Bjorkholm, P.; Lindahl, E.; Gonen, B.; Tischer, C.; Elofsson, A.; von Heijne, G.; Thiele, C.; et al. Molecular Recognition of a Single Sphingolipid Species by a Protein's Transmembrane Domain. *Nature* **2012**, *481* (7382), 525–529.
(272) Grouleff, J.; Irudayam, S. J.; Skeby, K. K.; Schiøtt, B. The Influence of Cholesterol on Membrane Protein Structure, Function, and Dynamics Studied by Molecular Dynamics Simulations. *Biochim. Biophys. Acta - Biomembr.* **2015**, *1848* (9), 1783–1795. https://doi.org///dx.doi.org/10.1016/j.bbamem.2015.03.029.
(273) Huang, J.; Feigenson, G. W. A Microscopic Interaction Model of Maximum Solubility of Cholesterol in Lipid Bilayers. *Biophys. J.* **1999**, *76* (4), 2142–2157. https://doi.org/10.1016/S0006-3495(99)77369-8.
(274) Ingólfsson, H. I.; Arnarez, C.; Periole, X.; Marrink, S. J. Computational 'Microscopy' of Cellular Membranes. *J. Cell Sci.* **2016**. https://doi.org/10.1242/jcs.176040.
(275) Bennett, W. F. D.; Tieleman, D. P. Molecular Simulation of Rapid Translocation of Cholesterol, Diacylglycerol, and Ceramide in Model Raft and Nonraft Membranes. *J. Lipid Res.* **2012**, *53* (3), 421–429. https://doi.org/10.1194/jlr.M022491.
(276) Engberg, O.; Yasuda, T.; Hautala, V.; Matsumori, N.; Nyholm, T. K. M.; Murata, M.; Slotte, J. P. Lipid Interactions and Organization in Complex Bilayer Membranes. *Biophys. J.* **2016**, *110* (7), 1563–1573. https://doi.org/10.1016/j.bpj.2015.12.043.
(277) Brown, D. A.; London, E. Functions of Lipid Rafts in Biolgoical Membranes. *Annu. Rev. Cell Dev. Biol.* **1998**, *14* (1), 111–136. https://doi.org/10.1146/annurev.cellbio.14.1.111.
(278) Brown, D. A.; London, E. Structure and Function of Sphingolipid- and Cholesterol-Rich Membrane Rafts. *J. Biol. Chem.* **2000**, *275* (23), 17221–17224. https://doi.org/10.1074/jbc.R000005200.
(279) Lingwood, D.; Simons, K. Lipid Rafts as a Membrane-Organizing Principle. *Science.* **2010**,

327 (5961), 46–50. https://doi.org/327/5961/46
(280) Sillence, D. J. New Insights into Glycosphingolipid Functions--Storage, Lipid Rafts, and Translocators. *Int. Rev. Cytol.* **2007**, *262*, 151–189. https://doi.org/S0074-7696(07)62003-8
(281) Kinoshita, M.; Suzuki, K. G. N.; Matsumori, N.; Takada, M.; Ano, H.; Morigaki, K.; Abe, M.; Makino, A.; Kobayashi, T.; Hirosawa, K. M.; et al. Raft-Based Sphingomyelin Interactions Revealed by New Fluorescent Sphingomyelin Analogs. *J. Cell Biol.* **2017**, *216* (4), 1183–1204. https://doi.org/10.1083/jcb.201607086.
(282) Koushik, A. B.; Powell, R. R.; Temesvari, L. A. Localization of Phosphatidylinositol 4,5-Bisphosphate to Lipid Rafts and Uroids in the Human Protozoan Parasite Entamoeba Histolytica. *Infect. Immun.* **2013**, *81* (6), 2145–2155. https://doi.org/10.1128/IAI.00040-13.
(283) Bacia, K.; Schuette, C. G.; Kahya, N.; Jahn, R.; Schwille, P. SNAREs Prefer Liquid-Disordered over "Raft" (Liquid-Ordered) Domains When Reconstituted into Giant Unilamellar Vesicles. *J. Biol. Chem.* **2004**, *279* (36), 37951–37955. https://doi.org/10.1074/jbc.M407020200.
(284) Jiang, Z.; Redfern, R. E.; Isler, Y.; Ross, A. H.; Gericke, A. Cholesterol Stabilizes Fluid Phosphoinositide Domains. *Chem. Phys. Lipids* **2014**, *182*, 52–61. https://doi.org///doi.org/10.1016/j.chemphyslip.2014.02.003.
(285) Picas, L.; Gaits-Iacovoni, F.; Goud, B. The Emerging Role of Phosphoinositide Clustering in Intracellular Trafficking and Signal Transduction [Version 1; Referees: 4 Approved]. *F1000Research* **2016**, *5* (422). https://doi.org/10.12688/f1000research.7537.1.
(286) Drücker, P.; Pejic, M.; Grill, D.; Galla, H. J.; Gerke, V. Cooperative Binding of Annexin A2 to Cholesterol- and Phosphatidylinositol-4,5-Bisphosphate-Containing Bilayers. *Biophys. J.* **2014**, *107* (9), 2070–2081. https://doi.org/10.1016/j.bpj.2014.08.027.
(287) Leung, K. F.; Baron, R.; Seabra, M. C. Thematic Review Series: Lipid Posttranslational Modifications. Geranylgeranylation of Rab GTPases. *J. Lipid Res.* **2006**, *47* (3), 467–475. https://doi.org/10.1194/jlr.r500017-jlr200.
(288) Singer, S. J.; Nicolson, G. L. The Fluid Mosaic Model of the Structure of Cell Membranes. *Science* **1972**, *175* (4023), 720 LP-731. https://doi.org/10.1126/science.175.4023.720.
(289) Rosenhouse-Dantsker, A. Insights Into the Molecular Requirements for Cholesterol Binding to Ion Channels. *Current Topics in Membranes*. **2017**. *80* 187-208 https://doi.org///dx.doi.org/10.1016/bs.ctm.2017.05.003.
(290) Lucero, H. A.; Robbins, P. W. Lipid Rafts–protein Association and the Regulation of Protein Activity. *Arch. Biochem. Biophys.* **2004**, *426* (2), 208–224. https://doi.org///dx.doi.org/10.1016/j.abb.2004.03.020.
(291) Richens, J. L.; Lane, J. S.; Bramble, J. P.; O'Shea, P. The Electrical Interplay between Proteins and Lipids in Membranes. *Biochim. Biophys. Acta - Biomembr.* **2015**, *1848* (9), 1828–1836. https://doi.org///dx.doi.org/10.1016/j.bbamem.2015.03.017.
(292) Lee, A. G. Lipid–protein Interactions in Biological Membranes: A Structural Perspective. *Biochim. Biophys. Acta - Biomembr.* **2003**, *1612* (1), 1–40. https://doi.org///dx.doi.org/10.1016/S0005-2736(03)00056-7.
(293) Luckey, M. *Membrane Structural Biology*; Cambridge University Press: Cambridge, 2008. https://doi.org/10.1017/CBO9780511811098.
(294) Wheeler, S.; Schmid, R.; Sillence, D. J.; Wheeler, S.; Schmid, R.; Sillence, D. J. Lipid–Protein Interactions in Niemann–Pick Type C Disease: Insights from Molecular Modeling. *Int. J. Mol. Sci.* **2019**, *20* (3), 717. https://doi.org/10.3390/IJMS20030717.
(295) Fantini, J.; Barrantes, F. J. How Cholesterol Interacts with Membrane Proteins: An Exploration of Cholesterol-Binding Sites Including CRAC, CARC and Tilted Domains. *Front. Physiol.* **2013**, *4* (31). https://doi.org/10.3389/fphys.2013.00031.
(296) Li, H.; Papadopoulos, V. Peripheral-Type Benzodiazepine Receptor Function in Cholesterol Transport. Identification of a Putative Cholesterol Recognition/Interaction Amino Acid Sequence and Consensus Pattern. *Endocrinology* **1998**, *139* (12), 4991–4997. https://doi.org/10.1210/endo.139.12.6390.
(297) Palmer, M. Cholesterol and the Activity of Bacterial Toxins. *FEMS Microbiology Letters*. 2004, pp 281–289. https://doi.org/10.1016/j.femsle.2004.07.059.
(298) Baier, C. J.; Fantini, J.; Barrantes, F. J. Disclosure of Cholesterol Recognition Motifs in Transmembrane Domains of the Human Nicotinic Acetylcholine Receptor. *Sci. Rep.* **2011**, *1*, 69. https://doi.org/10.1038/srep00069.

(299) Björkholm, P.; Ernst, A. M.; Hacke, M.; Wieland, F.; Brügger, B.; von Heijne, G. Identification of Novel Sphingolipid-Binding Motifs in Mammalian Membrane Proteins. *Biochim. Biophys. Acta - Biomembr.* **2014**, *1838* (8), 2066–2070. https://doi.org///dx.doi.org/10.1016/j.bbamem.2014.04.026.
(300) Ramachandran, G. N.; Ramakrishnan, C.; Sasisekharan, V. Stereochemistry of Polypeptide Chain Configurations. *J. Mol. Biol.* **1963**, *7* (1), 95–99. https://doi.org/10.1016/S0022-2836(63)80023-6.
(301) Blow, D. *Outline of Crystallography for Biologists*; Oxford University Press: Oxford, 2002.
(302) Wlodawer, A.; Minor, W.; Dauter, Z.; Jaskolski, M. Protein Crystallography for Non-Crystallographers, or How to Get the Best (but Not More) from Published Macromolecular Structures. *FEBS J.* **2008**, *275* (1), 1–21. https://doi.org/10.1111/j.1742-4658.2007.06178.x.
(303) Rost, B. Twilight Zone of Protein Sequence Alignments. *Protein Eng.* **1999**, *12* (2), 85–94. https://doi.org/10.1093/protein/12.2.85.
(304) Arnold, K.; Bordoli, L.; Kopp, J.; Schwede, T. The SWISS-MODEL Workspace: A Web-Based Environment for Protein Structure Homology Modelling. *Bioinformatics* **2006**, *22* (2), 195–201. https://doi.org/bti770 (305) Kelley, L. A.; Mezulis, S.; Yates, C. M.; Wass, M. N.; Sternberg, M. J. E. The Phyre2 Web Portal for Protein Modeling, Prediction and Analysis. *Nat.Protocols* **2015**, *10* (6), 845–858.
(306) Benkert, P.; Biasini, M.; Schwede, T. Toward the Estimation of the Absolute Quality of Individual Protein Structure Models. *Bioinformatics* **2011**, *27* (3), 343–350. https://doi.org/btq662
(307) Studer, G.; Biasini, M.; Schwede, T. Assessing the Local Structural Quality of Transmembrane Protein Models Using Statistical Potentials (QMEANBrane). *Bioinformatics* **2014**, *30* (17), i505–i511.
(308) Lomize, M. A.; Pogozheva, I. D.; Joo, H.; Mosberg, H. I.; Lomize, A. L. OPM Database and PPM Web Server: Resources for Positioning of Proteins in Membranes. *Nucleic Acids Res.* **2012**, *40* (Database issue), D370-6. https://doi.org/10.1093/nar/gkr703.
(309) Morris, G. M.; Huey, R.; Lindstrom, W.; Sanner, M. F.; Belew, R. K.; Goodsell, D. S.; Olson, A. J. AutoDock4 and AutoDockTools4: Automated Docking with Selective Receptor Flexibility. *J.Comput.Chem.* **2009**, *30* (16), 2785–2791. https://doi.org/10.1002/jcc.21256.
(310) Sanner, M. F. Python: A Programming Language for Software Integration and Development. *J. Mol. Graph. Model.* **1999**, *17* (1), 57–61.
(311) Combs, S. A.; DeLuca, S. L. S. H. S. L.; DeLuca, S. L. S. H. S. L.; Lemmon, G. H.; Nannemann, D. P.; Nguyen, E. D.; Willis, J. R.; Sheehan, J. H.; Meiler, J. Small-Molecule Ligand Docking into Comparative Models with Rosetta. *Nat.Protocols* **2013**, *8* (7), 1277–1298.
(312) Lyskov, S.; Chou, F.-C.; Conchuir, S. Ó.; Der, B. S.; Drew, K.; Kuroda, D.; Xu, J.; Weitzner, B. D.; Renfrew, P. D.; Sripakdeevong, P.; et al. Serverification of Molecular Modeling Applications: The Rosetta Online Server That Includes Everyone (ROSIE). *PLoS One* **2013**, *8* (5), e63906.
(313) DeLuca, S.; Khar, K.; Meiler, J. Fully Flexible Docking of Medium Sized Ligand Libraries with RosettaLigand. *PLoS One* **2015**, *10* (7), e0132508.
(314) De Colibus, L.; Wang, X.; Spyrou, J. A. B.; Kelly, J.; Ren, J.; Grimes, J.; Puerstinger, G.; Stonehouse, N.; Walter, T. S.; Hu, Z.; et al. More-Powerful Virus Inhibitors from Structure-Based Analysis of HEV71 Capsid-Binding Molecules. *Nat. Struct. Mol. Biol.* **2014**, *21* (3), 282–288. https://doi.org/10.1038/nsmb.2769.
(315) Kothiwale, S.; Mendenhall, J. L.; Meiler, J. BCL::Conf: Small Molecule Conformational Sampling Using a Knowledge Based Rotamer Library. *J. Cheminform.* **2015**, *7* (1), 47. https://doi.org/10.1186/s13321-015-0095-1.
(316) Jorgensen, W. L.; Chandrasekhar, J.; Madura, J. D.; Impey, R. W.; Klein, M. L. Comparison of Simple Potential Functions for Simulating Liquid Water. *J. Chem. Phys.* **1983**, *79* (2), 926–935. https://doi.org/10.1063/1.445869.
(317) Huang, J.; Rauscher, S.; Nawrocki, G.; Ran, T.; Feig, M.; De Groot, B. L.; Grubmüller, H.; MacKerell, A. D. CHARMM36m: An Improved Force Field for Folded and Intrinsically Disordered Proteins. *Nat. Methods* **2016**, *14* (1), 71–73. https://doi.org/10.1038/nmeth.4067.
(318) Lim, J. B.; Rogaski, B.; Klauda, J. B. Update of the Cholesterol Force Field Parameters in

CHARMM. *J. Phys. Chem. B* **2012**, *116* (1), 203–210. https://doi.org/10.1021/jp207925m.
(319) Wang, Z.; Min, X.; Xiao, S.-H.; Johnstone, S.; Romanow, W.; Meininger, D.; Xu, H.; Liu, J.; Dai, J.; An, S.; et al. Molecular Basis of Sphingosine Kinase 1 Substrate Recognition and Catalysis. *Structure* **2013**, *21* (5), 798–809. https://doi.org/10.1016/j.str.2013.02.025.
(320) Vanommeslaeghe, K.; MacKerell, A. D. Automation of the CHARMM General Force Field (CGenFF) I: Bond Perception and Atom Typing. *J. Chem. Inf. Model.* **2012**, *52* (12), 3144–3154. https://doi.org/10.1021/ci300363c.
(321) Bilgin, M.; Nylandsted, J.; Jäättelä, M.; Maeda, K. Quantitative Profiling of Lysosomal Lipidome by Shotgun Lipidomics; Humana Press, New York, NY, **2017**; pp 19–34. https://doi.org/10.1007/978-1-4939-6934-0_2.
(322) Phillips, J. C.; Braun, R.; Wang, W.; Gumbart, J.; Tajkhorshid, E.; Villa, E.; Chipot, C.; Skeel, R. D.; Kalé, L.; Schulten, K. Scalable Molecular Dynamics with NAMD. *J. Comput. Chem.* **2005**, *26* (16), 1781–1802. https://doi.org/10.1002/jcc.20289.
(323) Ribeiro, J. V.; Bernardi, R. C.; Rudack, T.; Stone, J. E.; Phillips, J. C.; Freddolino, P. L.; Schulten, K. QwikMD - Integrative Molecular Dynamics Toolkit for Novices and Experts. *Sci. Rep.* **2016**, *6* (1), 26536. https://doi.org/10.1038/srep26536.
(324) Humphrey, W.; Dalke, A.; Schulten, K. VMD: Visual Molecular Dynamics. *J. Mol. Graph.* **1996**, *14* (1), 33–38. https://doi.org/10.1016/0263-7855(96)00018-5.
(325) Khelashvili, G.; Pabst, G.; Harries, D. Cholesterol Orientation and Tilt Modulus in DMPC Bilayers. *J. Phys. Chem. B* **2010**, *114* (22), 7524–7534. https://doi.org/10.1021/jp101889k.
(326) Glaser, F.; Pupko, T.; Paz, I.; Bell, R. E.; Bechor-Shental, D.; Martz, E.; Ben-Tal, N. ConSurf: Identification of Functional Regions in Proteins by Surface-Mapping of Phylogenetic Information. *Bioinformatics* **2003**, *19* (1), 163–164. https://doi.org/10.1093/bioinformatics/19.1.163.
(327) Ashkenazy, H.; Abadi, S.; Martz, E.; Chay, O.; Mayrose, I.; Pupko, T.; Ben-Tal, N. ConSurf 2016: An Improved Methodology to Estimate and Visualize Evolutionary Conservation in Macromolecules. *Nucleic Acids Res.* **2016**, *44* (W1), W344–W350. https://doi.org/10.1093/nar/gkw408.
(328) Roversi, P.; Johnson, S.; Preston, S. G.; Nunn, M. A.; Paesen, G. C.; Austyn, J. M.; Nuttall, P. A.; Lea, S. M. Structural Basis of Cholesterol Binding by a Novel Clade of Dendritic Cell Modulators from Ticks. *Sci. Rep.* **2017**, *7* (1), 16057. https://doi.org/10.1038/s41598-017-16413-2.
(329) Wüstner, D.; Solanko, K. How Cholesterol Interacts with Proteins and Lipids during Its Intracellular Transport. *Biochimica et Biophysica Acta - Biomembranes*. Elsevier September 1, **2015**, pp 1908–1926. https://doi.org/10.1016/j.bbamem.2015.05.010.
(330) Kwon, H. J.; Abi-Mosleh, L.; Wang, M. L.; Deisenhofer, J.; Goldstein, J. L.; Brown, M. S.; Infante, R. E. Structure of N-Terminal Domain of NPC1 Reveals Distinct Subdomains for Binding and Transfer of Cholesterol. *Cell* **2009**, *137* (7), 1213–1224. https://doi.org/10.1016/j.cell.2009.03.049.
(331) Li, X.; Wang, J.; Coutavas, E.; Shi, H.; Hao, Q.; Blobel, G. Structure of Human Niemann–Pick C1 Protein. *Proc. Natl. Acad. Sci.* **2016**, *113* (29), 8212–8217. https://doi.org/10.1073/pnas.1607795113.
(332) Hulce, J. J.; Cognetta, A. B.; Niphakis, M. J.; Tully, S. E.; Cravatt, B. F. Proteome-Wide Mapping of Cholesterol-Interacting Proteins in Mammalian Cells. *Nat Meth* **2013**, *10* (3), 259–264.
(333) Deffieu, M. S.; Pfeffer, S. R. Niemann–Pick Type C 1 Function Requires Lumenal Domain Residues That Mediate Cholesterol-Dependent NPC2 Binding. *Proc. Natl. Acad. Sci.* **2011**, *108* (47), 18932–18936. https://doi.org/10.1073/pnas.1110439108.
(334) Li, X.; Saha, P.; Li, J.; Blobel, G.; Pfeffer, S. R. Clues to the Mechanism of Cholesterol Transfer from the Structure of NPC1 Middle Lumenal Domain Bound to NPC2. *Proc. Natl. Acad. Sci.* **2016**, *113* (36), 10079–10084. https://doi.org/10.1073/pnas.1611956113.
(335) Gong, X.; Qian, H.; Zhou, X.; Wu, J.; Wan, T.; Cao, P.; Huang, W.; Zhao, X.; Wang, X.; Wang, P.; et al. Structural Insights into the Niemann-Pick C1 (NPC1)-Mediated Cholesterol Transfer and Ebola Infection. *Cell* **2016**, *165* (6), 1467–1478. https://doi.org/10.1016/j.cell.2016.05.022.
(336) Wang, M. L.; Motamed, M.; Infante, R. E.; Abi-Mosleh, L.; Kwon, H. J.; Brown, M. S.; Goldstein, J. L. Identification of Surface Residues on Niemann-Pick C2 Essential for

Hydrophobic Handoff of Cholesterol to NPC1 in Lysosomes. *Cell Metab.* **2010**, *12* (2), 166–173. https://doi.org///dx.doi.org/10.1016/j.cmet.2010.05.016.
(337) Hodošček, M.; Elghobashi-Meinhardt, N. Simulations of NPC1(NTD):NPC2 Protein Complex Reveal Cholesterol Transfer Pathways. *Int. J. Mol. Sci.* **2018**, *19* (9), 2623. https://doi.org/10.3390/ijms19092623.
(338) Li, X.; Lu, F.; Trinh, M. N.; Schmiege, P.; Seemann, J.; Wang, J.; Blobel, G. 3.3 Å Structure of Niemann–Pick C1 Protein Reveals Insights into the Function of the C-Terminal Luminal Domain in Cholesterol Transport. *Proc. Natl. Acad. Sci.* **2017**, *114* (34), 9116–9121. https://doi.org/10.1073/pnas.1711716114.
(339) Trinh, M. N.; Brown, M. S.; Seemann, J.; Goldstein, J. L.; Lu, F. Lysosomal Cholesterol Export Reconstituted from Fragments of Niemann-Pick C1. *Elife* **2018**, *7*. https://doi.org/10.7554/eLife.38564.
(340) Cheruku, S. R.; Xu, Z.; Dutia, R.; Lobel, P.; Storch, J. Mechanism of Cholesterol Transfer from the Niemann-Pick Type C2 Protein to Model Membranes Supports a Role in Lysosomal Cholesterol Transport. *J. Biol. Chem.* **2006**, *281* (42), 31594–31604. https://doi.org/10.1074/jbc.M602765200.
(341) McCauliff, L. A.; Xu, Z.; Li, R.; Kodukula, S.; Ko, D. C.; Scott, M. P.; Kahn, P. C.; Storch, J. Multiple Surface Regions on the Niemann-Pick C2 Protein Facilitate Intracellular Cholesterol Transport. *J. Biol. Chem.* **2015**, *290* (45), 27321–27331. https://doi.org/10.1074/jbc.M115.667469.
(342) Schulze, H.; Kolter, T.; Sandhoff, K. Principles of Lysosomal Membrane Degradation: Cellular Topology and Biochemistry of Lysosomal Lipid Degradation. *Biochim. Biophys. Acta - Mol. Cell Res.* **2009**, *1793* (4), 674–683. https://doi.org///dx.doi.org/10.1016/j.bbamcr.2008.09.020.
(343) Steck, T.; Lange, Y. How Slow Is the Transbilayer Diffusion (Flip-Flop) of Cholesterol? *Biophys. J.* **2012** *102* (4), 945–946. https://doi.org/10.1016/j.bpj.2011.10.059.
(344) Di Scala, C.; Fantini, J.; Yahi, N.; Barrantes, F. J.; Chahinian, H. Anandamide Revisited: How Cholesterol and Ceramides Control Receptor-Dependent and Receptor-Independent Signal Transmission Pathways of a Lipid Neurotransmitter. *Biomolecules* **2018**, *8* (2). https://doi.org/10.3390/biom8020031.
(345) Fantini, J.; Di Scala, C.; Evans, L. S.; Williamson, P. T. F.; Barrantes, F. J. A Mirror Code for Protein-Cholesterol Interactions in the Two Leaflets of Biological Membranes. *Sci. Rep.* **2016**, *6*, 21907. https://doi.org/10.1038/srep21907.
(346) Elghobashi-Meinhardt, N. Computational Tools Unravel Putative Sterol Binding Sites in the Lysosomal NPC1 Protein. *J. Chem. Inf. Model.* **2019**, *59* (5), 2432–2441. https://doi.org/10.1021/acs.jcim.9b00186.
(347) Höglinger, D.; Nadler, A.; Haberkant, P.; Kirkpatrick, J.; Schifferer, M.; Stein, F.; Hauke, S.; Porter, F. D.; Schultz, C. Trifunctional Lipid Probes for Comprehensive Studies of Single Lipid Species in Living Cells. *Proc. Natl. Acad. Sci.* **2017**, *114* (7), 1566–1571. https://doi.org/10.1073/pnas.1611096114.
(348) Sasaki, H.; Arai, H.; Cocco, M. J.; White, S. H. PH Dependence of Sphingosine Aggregation. *Biophys. J.* **2009**, *96* (7), 2727–2733. https://doi.org/10.1016/j.bpj.2008.12.3926.
(349) López-García, F.; Micol, V.; Villalaín, J.; Gómez-Fernández, J. C. Interaction of Sphingosine and Stearylamine with Phosphatidylserine as Studied by DSC and NMR. *BBA - Biomembr.* **1993**, *1153* (1), 1–8. https://doi.org/10.1016/0005-2736(93)90269-6.
(350) Poongavanam, V.; Kongsted, J.; Wüstner, D. Computational Analysis of Sterol Ligand Specificity of the Niemann Pick C2 Protein. *Biochemistry* **2016**, *55* (36), 5165–5179. https://doi.org/10.1021/acs.biochem.6b00217.
(351) Humphrey, W.; Dalke, A.; Schulten, K. VMD: Visual Molecular Dynamics. *J. Mol. Graph.* **1996**, *14* (1), 33–38. https://doi.org/10.1016/0263-7855(96)00018-5.
(352) Di Pasquale, E.; Chahinian, H.; Sanchez, P.; Fantini, J. The Insertion and Transport of Anandamide in Synthetic Lipid Membranes Are Both Cholesterol-Dependent. *PLoS One* **2009**, *4* (3), e4989. https://doi.org/10.1371/journal.pone.0004989.
(353) Garmy, N.; Taïeb, N.; Yahi, N.; Fantini, J. Interaction of Cholesterol with Sphingosine: Physicochemical Characterization and Impact on Intestinal Absorption. *J. Lipid Res.* **2005**, *46* (1), 36–45. https://doi.org/10.1194/jlr.M400199-JLR200.

(354) Bartz, F.; Kern, L.; Erz, D.; Zhu, M.; Gilbert, D.; Meinhof, T.; Wirkner, U.; Erfle, H.; Muckenthaler, M.; Pepperkok, R.; et al. Identification of Cholesterol-Regulating Genes by Targeted RNAi Screening. *Cell Metab.* **2009**, *10* (1), 63–75. https://doi.org/10.1016/j.cmet.2009.05.009.
(355) Li, J.; Pfeffer, S. R. Lysosomal Membrane Glycoproteins Bind Cholesterol and Contribute to Lysosomal Cholesterol Export. *Elife* **2016**, *5*, e21635. https://doi.org/10.7554/elife.21635.
(356) Lange, Y.; D'Alessandro, J. S. Characterization of Mechanisms for Transfer of Cholesterol between Human Erythrocytes and Plasma. *Biochemistry* **1977**, *16* (20), 4339–4343. https://doi.org/10.1021/bi00639a002.
(357) Clark, B. J. The Mammalian START Domain Protein Family in Lipid Transport in Health and Disease. *J. Endocrinol.* **2012**, *212* (3), 257–275. https://doi.org/10.1530/JOE-11-0313.
(358) Luo, J.; Jiang, L.-Y.; Yang, H.; Song, B.-L. Intracellular Cholesterol Transport by Sterol Transfer Proteins at Membrane Contact Sites. *Trends Biochem. Sci.* **2019**, *44* (3), 273–292. https://doi.org/10.1016/J.TIBS.2018.10.001.
(359) Murcia, M.; Faraldo-Gomez, J. D.; Maxfield, F. R.; Roux, B. Modeling the Structure of the StART Domains of MLN64 and StAR Proteins in Complex with Cholesterol. *J. Lipid Res.* **2006**, *47* (12), 2614–2630. https://doi.org/M600232-JLR200.
(360) Horvath, M. P.; George, E. W.; Tran, Q. T.; Baumgardner, K.; Zharov, G.; Lee, S.; Sharifzadeh, H.; Shihab, S.; Mattinson, T.; Li, B.; et al. Structure of the Lutein-Binding Domain of Human StARD3 at 1.74Å Resolution and Model of a Complex with Lutein. *Acta Crystallogr. Sect. F* **2016**, *72* (8), 609–618. https://doi.org/10.1107/S2053230X16010694.
(361) Chaudhury, S.; Berrondo, M.; Weitzner, B. D.; Muthu, P.; Bergman, H.; Gray, J. J. Benchmarking and Analysis of Protein Docking Performance in Rosetta v3.2. *PLoS One* **2011**, *6* (8), e22477. https://doi.org/10.1371/journal.pone.0022477.
(362) Šali, A.; Blundell, T. L. Comparative Protein Modelling by Satisfaction of Spatial Restraints. *J. Mol. Biol.* **1993**, *234* (3), 779–815. https://doi.org/10.1006/JMBI.1993.1626.
(363) Pettersen, E. F.; Goddard, T. D.; Huang, C. C.; Couch, G. S.; Greenblatt, D. M.; Meng, E. C.; Ferrin, T. E. UCSF Chimera - A Visualization System for Exploratory Research and Analysis. *J. Comput. Chem.* **2004**, *25* (13), 1605–1612. https://doi.org/10.1002/jcc.20084.
(364) Von Filseck, J. M.; Čopič, A.; Delfosse, V.; Vanni, S.; Jackson, C. L.; Bourguet, W.; Drin, G. Phosphatidylserine Transport by ORP/Osh Proteins Is Driven by Phosphatidylinositol 4-Phosphate. *Science* **2015**, *349* (6246), 432–436. https://doi.org/10.1126/science.aab1346.
(365) von Filseck, J. M.; Vanni, S.; Mesmin, B.; Antonny, B.; Drin, G. A Phosphatidylinositol-4-Phosphate Powered Exchange Mechanism to Create a Lipid Gradient between Membranes. *Nat. Commun.* **2015**, *6*, 6671.
(366) Ghai, R.; Du, X.; Wang, H.; Dong, J.; Ferguson, C.; Brown, A. J.; Parton, R. G.; Wu, J. W.; Yang, H. ORP5 and ORP8 Bind Phosphatidylinositol-4, 5-Biphosphate (PtdIns(4,5)P 2) and Regulate Its Level at the Plasma Membrane. *Nat. Commun.* **2017**, *8* (1), 757. https://doi.org/10.1038/s41467-017-00861-5.
(367) Rogaski, B.; Klauda, J. B. Membrane-Binding Mechanism of a Peripheral Membrane Protein through Microsecond Molecular Dynamics Simulations. *J. Mol. Biol.* **2012**, *423* (5), 847–861. https://doi.org/10.1016/j.jmb.2012.08.015.
(368) Alpy, F.; Rousseau, A.; Schwab, Y.; Legueux, F.; Stoll, I.; Wendling, C.; Spiegelhalter, C.; Kessler, P.; Mathelin, C.; Rio, M.-C.; et al. STARD3 or STARD3NL and VAP Form a Novel Molecular Tether between Late Endosomes and the ER. *J. Cell Sci.* **2013**, *126* (23), 5500 LP-5512. https://doi.org/10.1242/jcs.139295.
(369) Wang, W.; Zhang, X.; Gao, Q.; Lawas, M.; Yu, L.; Cheng, X.; Gu, M.; Sahoo, N.; Li, X.; Li, P.; et al. A Voltage-Dependent K+channel in the Lysosome Is Required for Refilling Lysosomal Ca2+stores. *J. Cell Biol.* **2017**, *216* (6), 1715–1730. https://doi.org/10.1083/jcb.201612123.
(370) Cao, Q.; Zhong, X. Z.; Zou, Y.; Zhang, Z.; Toro, L.; Dong, X.-P. BK Channels Alleviate Lysosomal Storage Diseases by Providing Positive Feedback Regulation of Lysosomal Ca2+ Release. *Dev. Cell* **2015**, *33* (4), 427–441. https://doi.org///dx.doi.org/10.1016/j.devcel.2015.04.010.
(371) Tao, X.; Hite, R. K.; MacKinnon, R. Cryo-EM Structure of the Open High-Conductance Ca2+-Activated K+ Channel. *Nature* **2017**, *541* (7635), 46–51.
(372) Yuan, C.; O'Connell, R. J.; Feinberg-Zadek, P. L.; Johnston, L. J.; Treistman, S. N. Bilayer

Thickness Modulates the Conductance of the BK Channel in Model Membranes. *Biophys. J.* **2004**, *86* (6), 3620–3633. https://doi.org///dx.doi.org/10.1529/biophysj.103.029678.
(373) Lam, R. S.; Shaw, A. R.; Duszyk, M. Membrane Cholesterol Content Modulates Activation of BK Channels in Colonic Epithelia. *Biochim. Biophys. Acta - Biomembr.* **2004**, *1667* (2), 241–248. https://doi.org///dx.doi.org/10.1016/j.bbamem.2004.11.004.
(374) Yuan, C.; O'Connell, R. J.; Jacob, R. F.; Mason, R. P.; Treistman, S. N. Regulation of the Gating of BKCa Channel by Lipid Bilayer Thickness. *J. Biol. Chem.* **2007**, *282* (10), 7276–7286. https://doi.org/10.1074/jbc.M607593200.
(375) Purcell, E. K.; Liu, L.; Thomas, P. V; Duncan, R. K. Cholesterol Influences Voltage-Gated Calcium Channels and BK-Type Potassium Channels in Auditory Hair Cells. *PLoS One* **2011**, *6* (10), e26289.
(376) Bukiya, A. N.; Belani, J. D.; Rychnovsky, S.; Dopico, A. M. Specificity of Cholesterol and Analogs to Modulate BK Channels Points to Direct Sterol–channel Protein Interactions. *J. Gen. Physiol.* **2010**, *137* (1), 93–110. https://doi.org/10.1085/jgp.201010519.
(377) Yuan, C.; Chen, M.; Covey, D. F.; Johnston, L. J.; Treistman, S. N. Cholesterol Tuning of BK Ethanol Response Is Enantioselective, and Is a Function of Accompanying Lipids. *PLoS One* **2011**, *6* (11), e27572.
(378) Singh, A. K.; McMillan, J.; Bukiya, A. N.; Burton, B.; Parrill, A. L.; Dopico, A. M. Multiple Cholesterol Recognition/Interaction Amino Acid Consensus (CRAC) Motifs in Cytosolic C Tail of Slo1 Subunit Determine Cholesterol Sensitivity of Ca2+- and Voltage-Gated K+ (BK) Channels. *J. Biol. Chem.* **2012**, *287* (24), 20509–20521. https://doi.org/10.1074/jbc.M112.356261.
(379) Hite, R. K.; Tao, X.; MacKinnon, R. Structural Basis for Gating the High-Conductance Ca2+-Activated K+ Channel. *Nature* **2017**, *541* (7635), 52–57.
(380) Hanson, M. A.; Cherezov, V.; Griffith, M. T.; Roth, C. B.; Jaakola, V.-P.; Chien, E. Y. T.; Velasquez, J.; Kuhn, P.; Stevens, R. C. A Specific Cholesterol Binding Site Is Established by the 2.8 Å Structure of the Human B2-Adrenergic Receptor. *Structure*. **2008**, pp 897–905. https://doi.org///doi.org/10.1016/j.str.2008.05.001.
(381) Zhu, M. X. A Well-Known Potassium Channel Plays a Critical Role in Lysosomes. *J. Cell Biol.* **2017**. https://doi.org/10.1083/jcb.201704017.
(382) Bukiya, A. N.; Vaithianathan, T.; Toro, L.; Dopico, A. M. Channel B2–4 Subunits Fail to Substitute for B1 in Sensitizing BK Channels to Lithocholate. *Biochem. Biophys. Res. Commun.* **2009**, *390* (3), 995–1000. https://doi.org///doi.org/10.1016/j.bbrc.2009.10.091.
(383) Wallner, M.; Meera, P.; Toro, L. Determinant for β-Subunit Regulation in High-Conductance Voltage-Activated and Ca2+-Sensitive K+ Channels: An Additional Transmembrane Region at the N Terminus. *Proc. Natl. Acad. Sci.* **1996**, *93* (25), 14922–14927.
(384) Zhong, X. Z.; Sun, X.; Cao, Q.; Dong, G.; Schiffmann, R.; Dong, X. P. BK Channel Agonist Represents a Potential Therapeutic Approach for Lysosomal Storage Diseases. *Sci. Rep.* **2016**, *6* (1), 33684. https://doi.org/10.1038/srep33684.
(385) Wang, W.; Zhang, X.; Gao, Q.; Lawas, M.; Yu, L.; Cheng, X.; Gu, M.; Sahoo, N.; Li, X.; Li, P.; et al. A Voltage-Dependent K+ Channel in the Lysosome Is Required for Refilling Lysosomal Ca2+ Stores. *J. Cell Biol.* **2017**, *216* (6), 1715.
(386) Li, M.; Zhang, W. K.; Benvin, N. M.; Zhou, X.; Su, D.; Li, H.; Wang, S.; Michailidis, I. E.; Tong, L.; Li, X.; et al. Structural Basis of Dual Ca 2+ /PH Regulation of the Endolysosomal TRPML1 Channel. *Nat. Struct. Mol. Biol.* **2017**, *24* (3), 205–213. https://doi.org/10.1038/nsmb.3362.
(387) Li, G.; Huang, D.; Hong, J.; Bhat, O. M.; Yuan, X.; Li, P.-L. Control of Lysosomal TRPML1 Channel Activity and Exosome Release by Acid Ceramidase in Mouse Podocytes. *Am. J. Physiol. Physiol.* **2019**, *317* (3), C481–C491. https://doi.org/10.1152/ajpcell.00150.2019.
(388) Schmiege, P.; Fine, M.; Blobel, G.; Li, X. Human TRPML1 Channel Structures in Open and Closed Conformations. *Nature* **2017**, *550*, 366.
(389) Fine, M.; Schmiege, P.; Li, X. Structural Basis for PtdInsP2-Mediated Human TRPML1 Regulation. *Nat. Commun.* **2018**, *9* (1), 4192. https://doi.org/10.1038/s41467-018-06493-7.
(390) Hirschi, M.; Herzik Jr, M. A.; Wie, J.; Suo, Y.; Borschel, W. F.; Ren, D.; Lander, G. C.; Lee, S.-Y. Cryo-Electron Microscopy Structure of the Lysosomal Calcium-Permeable Channel TRPML3. *Nature* **2017**, *550*, 411.

(391) Pryor, P. R.; Reimann, F.; Gribble, F. M.; Luzio, J. P. Mucolipin-1 Is a Lysosomal Membrane Protein Required for Intracellular Lactosylceramide Traffic. *Traffic* **2006**, *7* (10), 1388–1398. https://doi.org/10.1111/j.1600-0854.2006.00475.x.
(392) Venkatachalam, K.; Kiselyov, K. TRPML1-Dependent Processes as Therapeutic Targets. In *TRP Channels as Therapeutic Targets: From Basic Science to Clinical Use*; Academic Press, 2015; pp 469–482. https://doi.org/10.1016/B978-0-12-420024-1.00025-4.
(393) Vergarajauregui, S.; Connelly, P. S.; Daniels, M. P.; Puertollano, R. Autophagic Dysfunction in Mucolipidosis Type IV Patients. *Hum. Mol. Genet.* **2008**, *17* (17), 2723–2737.
(394) Ward, C.; Martinez-Lopez, N.; Otten, E. G.; Carroll, B.; Maetzel, D.; Singh, R.; Sarkar, S.; Korolchuk, V. I. Autophagy, Lipophagy and Lysosomal Lipid Storage Disorders. *Biochim. Biophys. Acta - Mol. Cell Biol. Lipids* **2016**, *1861* (4), 269–284. https://doi.org///dx.doi.org/10.1016/j.bbalip.2016.01.006.
(395) Harvald, E. B.; Olsen, A. S. B.; Faergeman, N. J. Autophagy in the Light of Sphingolipid Metabolism. *Apoptosis* **2015**, *20* (5), 658–670. https://doi.org/10.1007/s10495-015-1108-2.
(396) Ruas, M.; Rietdorf, K.; Arredouani, A.; Davis, L. C.; Lloyd-Evans, E.; Koegel, H.; Funnell, T. M.; Morgan, A. J.; Ward, J. A.; Watanabe, K.; et al. Purified TPC Isoforms Form NAADP Receptors with Distinct Roles for Ca2+ Signaling and Endolysosomal Trafficking. *Curr. Biol.* **2010**, *20* (8), 703–709. https://doi.org///dx.doi.org/10.1016/j.cub.2010.02.049.
(397) Lin, P.-H.; Duann, P.; Komazaki, S.; Park, K. H.; Li, H.; Sun, M.; Sermersheim, M.; Gumpper, K.; Parrington, J.; Galione, A.; et al. Lysosomal Two-Pore Channel Subtype 2 (TPC2) Regulates Skeletal Muscle Autophagic Signaling. *J. Biol. Chem.* **2015**, *290* (6), 3377–3389. https://doi.org/10.1074/jbc.M114.608471.
(398) Cao, Q.; Zhong, X. Z.; Zou, Y.; Murrell-Lagnado, R.; Zhu, M. X.; Dong, X.-P. Calcium Release through P2X4 Activates Calmodulin to Promote Endolysosomal Membrane Fusion. *J. Cell Biol.* **2015**, *209* (6), 879–894. https://doi.org/10.1083/jcb.201409071.
(399) Tian, X.; Gala, U.; Zhang, Y.; Shang, W.; Nagarkar Jaiswal, S.; di Ronza, A.; Jaiswal, M.; Yamamoto, S.; Sandoval, H.; Duraine, L.; et al. A Voltage-Gated Calcium Channel Regulates Lysosomal Fusion with Endosomes and Autophagosomes and Is Required for Neuronal Homeostasis. *PLOS Biol.* **2015**, *13* (3), e1002103.
(400) Moreau, K.; Ghislat, G.; Hochfeld, W.; Renna, M.; Zavodszky, E.; Runwal, G.; Puri, C.; Lee, S.; Siddiqi, F.; Menzies, F. M.; et al. Transcriptional Regulation of Annexin A2 Promotes Starvation-Induced Autophagy. *Nat. Commun.* **2015**, *6* (1), 8045. https://doi.org/10.1038/ncomms9045.
(401) Gokhale, N. A.; Abraham, A.; Digman, M. A.; Gratton, E.; Cho, W. Phosphoinositide Specificity of and Mechanism of Lipid Domain Formation by Annexin A2-P11 Heterotetramer. *J. Biol. Chem.* **2005**, *280* (52), 42831–42840. https://doi.org/10.1074/jbc.M508129200.
(402) Rescher, U.; Ruhe, D.; Ludwig, C.; Zobiack, N.; Gerke, V. Annexin 2 Is a Phosphatidylinositol (4,5)-Bisphosphate Binding Protein Recruited to Actin Assembly Sites at Cellular Membranes. *J. Cell Sci.* **2004**, *117* (16), 3473–3480. https://doi.org/10.1242/jcs.01208.
(403) Ross, M.; Gerke, V.; Steinem, C. Membrane Composition Affects the Reversibility of Annexin A2t Binding to Solid Supported Membranes: A QCM Study. *Biochemistry* **2003**, *42* (10), 3131–3141. https://doi.org/10.1021/bi027069z.
(404) Drücker, P.; Pejic, M.; Galla, H.-J.; Gerke, V. Lipid Segregation and Membrane Budding Induced by the Peripheral Membrane Binding Protein Annexin A2. *J. Biol. Chem.* **2013**, *288* (34), 24764–24776. https://doi.org/10.1074/jbc.M113.474023.
(405) Shao, C.; Zhang, F.; Kemp, M. M.; Linhardt, R. J.; Waisman, D. M.; Head, J. F.; Seaton, B. A. Crystallographic Analysis of Calcium-Dependent Heparin Binding to Annexin A2. *J. Biol. Chem.* **2006**, *281* (42), 31689–31695. https://doi.org/10.1074/jbc.M604502200.
(406) Rosengarth, A.; Luecke, H. Annexin A2 Does It Induce Membrane Aggregation by a New Multimeric State of the Protein? *Annexins* **2004**, *1* (2), e34–e41.
(407) Ionescu, C.-M.; Sehnal, D.; Falginella, F. L.; Pant, P.; Pravda, L.; Bouchal, T.; Svobodová Vařeková, R.; Geidl, S.; Koča, J. AtomicChargeCalculator: Interactive Web-Based Calculation of Atomic Charges in Large Biomolecular Complexes and Drug-like Molecules. *J. Cheminform.* **2015**, *7* (1), 50. https://doi.org/10.1186/s13321-015-0099-x.
(408) Illien, F.; Piao, H.-R.; Coué, M.; di Marco, C.; Ayala-Sanmartin, J. Lipid Organization

Regulates Annexin A2 Ca2 +-Sensitivity for Membrane Bridging and Its Modulator Effects on Membrane Fluidity. *Biochim. Biophys. Acta - Biomembr.* **2012**, *1818* (11), 2892–2900. https://doi.org///dx.doi.org/10.1016/j.bbamem.2012.07.012.

(409) Hakobyan, D.; Gerke, V.; Heuer, A. Modeling of Annexin A2—Membrane Interactions by Molecular Dynamics Simulations. *PLoS One* **2017**, *12* (9), e0185440. https://doi.org/10.1371/journal.pone.0185440.

(410) Goebeler, V.; Poeter, M.; Zeuschner, D.; Gerke, V.; Rescher, U. Annexin A8 Regulates Late Endosome Organization and Function. *Mol. Biol. Cell* **2008**, *19* (12), 5267–5278. https://doi.org/10.1091/mbc.e08-04-0383.

(411) Heitzig, N.; Kühnl, A.; Grill, D.; Ludewig, K.; Schloer, S.; Galla, H. J.; Grewal, T.; Gerke, V.; Rescher, U. Cooperative Binding Promotes Demand-Driven Recruitment of AnxA8 to Cholesterol-Containing Membranes. *Biochim. Biophys. Acta - Mol. Cell Biol. Lipids* **2018**, *1863* (4), 349–358. https://doi.org/10.1016/j.bbalip.2018.01.001.

(412) Goebeler, V.; Ruhe, D.; Gerke, V.; Rescher, U. Annexin A8 Displays Unique Phospholipid and F-Actin Binding Properties. *FEBS Lett.* **2006**, *580* (10), 2430–2434. https://doi.org/10.1016/j.febslet.2006.03.076.

(413) Réty, S.; Sopková-De Oliveira Santos, J.; Dreyfuss, L.; Blondeau, K.; Hofbauerová, K.; Raguénès-Nicol, C.; Kerboeuf, D.; Renouard, M.; Russo-Marie, F.; Lewit-Bentley, A. The Crystal Structure of Annexin A8 Is Similar to That of Annexin A3. *J. Mol. Biol.* **2005**, *345* (5), 1131–1139. https://doi.org/10.1016/j.jmb.2004.11.015.

(414) Voges, D.; Berendes, R.; Burger, A.; Demange, P.; Baumeister, W.; Huber, R. Three-Dimensional Structure of Membrane-Bound Annexin V. *Journal of Molecular Biology*. 1994, pp 199–213. https://doi.org///dx.doi.org/10.1006/jmbi.1994.1281.

(415) Murray, D. H.; Tamm, L. K. Molecular Mechanism of Cholesterol- and Polyphosphoinositide-Mediated Syntaxin Clustering. *Biochemistry* **2011**, *50* (42), 9014–9022. https://doi.org/10.1021/bi201307u.

(416) Murray, D. H.; Tamm, L. K. Clustering of Syntaxin-1A in Model Membranes Is Modulated by Phosphatidylinositol 4,5-Bisphosphate and Cholesterol. *Biochemistry* **2009**, *48* (21), 4617–4625. https://doi.org/10.1021/bi9003217.

(417) Khelashvili, G.; Galli, A.; Weinstein, H. Phosphatidylinositol 4,5-Biphosphate (PIP(2)) Lipids Regulate the Phosphorylation of Syntaxin N-Terminus by Modulating Both Its Position and Local Structure. *Biochemistry* **2012**, *51* (39), 7685–7698. https://doi.org/10.1021/bi300833z.

(418) Singer-Lahat, D.; Barak-Broner, N.; Sheinin, A.; Greitzer-Antes, D.; Michaelevski, I.; Lotan, I. The Dual Function of the Polybasic Juxtamembrane Region of Syntaxin 1A in Clamping Spontaneous Release and Stimulating Ca2+-Triggered Release in Neuroendocrine Cells. *J. Neurosci.* **2018**, *38* (1), 220–231. https://doi.org/10.1523/JNEUROSCI.1541-17.2017.

(419) Williams, D.; Vicôgne, J.; Zaitseva, I.; McLaughlin, S.; Pessin, J. E. Evidence That Electrostatic Interactions between Vesicle-Associated Membrane Protein 2 and Acidic Phospholipids May Modulate the Fusion of Transport Vesicles with the Plasma Membrane. *Mol. Biol. Cell* **2009**, *20* (23), 4910–4919. https://doi.org/10.1091/mbc.E09-04-0284.

(420) Stein, A.; Weber, G.; Wahl, M. C.; Jahn, R. Helical Extension of the Neuronal SNARE Complex into the Membrane. *Nature* **2009**, *460* (7254), 525–528. https://doi.org/10.1038/nature08156.

(421) Takáts, S.; Nagy, P.; Varga, Á.; Pircs, K.; Kárpáti, M.; Varga, K.; Kovács, A. L.; Hegedűs, K.; Juhász, G. Autophagosomal Syntaxin17-Dependent Lysosomal Degradation Maintains Neuronal Function in Drosophila. *J. Cell Biol.* **2013**, *201* (4), 531–539. https://doi.org/10.1083/jcb.201211160.

(422) Lizarbe, A. M.; Barrasa, I. J.; Olmo, N.; Gavilanes, F.; Turnay, J. Annexin-Phospholipid Interactions. Functional Implications. *International Journal of Molecular Sciences*. **2013**. *14* (2) 2652-2683 https://doi.org/10.3390/ijms14022652.

(423) Freye-Minks, C.; Kretsinger, R. H.; Creutz, C. E. Structural and Dynamic Changes in Human Annexin VI Induced by a Phosphorylation-Mimicking Mutation, T356D,. *Biochemistry* **2003**, *42* (3), 620–630. https://doi.org/10.1021/bi026742h.

(424) Kawasaki, H.; Avila-Sakar, A.; Creutz, C. E.; Kretsinger, R. H. The Crystal Structure of Annexin VI Indicates Relative Rotation of the Two Lobes upon Membrane Binding. *Biochimica et Biophysica Acta (BBA) - Molecular Cell Research*. **1996**, pp 277–282. https://doi.org///dx.doi.org/10.1016/0167-4889(96)00100-0.

(425) Avila-Sakar, A. J.; Kretsinger, R. H.; Creutz, C. E. Membrane-Bound 3D Structures Reveal the Intrinsic Flexibility of Annexin VI. *Journal of Structural Biology*. **2000**, pp 54–62. https://doi.org///dx.doi.org/10.1006/jsbi.2000.4246.
(426) Buzhynskyy, N.; Golczak, M.; Lai-Kee-Him, J.; Lambert, O.; Tessier, B.; Gounou, C.; Bérat, R.; Simon, A.; Granier, T.; Chevalier, J.-M.; et al. Annexin-A6 Presents Two Modes of Association with Phospholipid Membranes. A Combined QCM-D, AFM and Cryo-TEM Study. *J. Struct. Biol.* **2009**, *168* (1), 107–116. https://doi.org///dx.doi.org/10.1016/j.jsb.2009.03.007.
(427) Bianchi, R.; Giambanco, I.; Ceccarelli, P.; Pula, G.; Donato, R. Membrane-Bound Annexin V Isoforms (CaBP33 and CaBP37) and Annexin VI in Bovine Tissues Behave like Integral Membrane Proteins. *FEBS Lett.* **1992**, *296* (2), 158–162. https://doi.org/10.1016/0014-5793(92)80369-R.
(428) Kirilenko, A.; Pikula, S.; Bandorowicz-Pikula, J. Effects of Mutagenesis of W343 in Human Annexin A6 Isoform 1 on Its Interaction with GTP: Nucleotide-Induced Oligomer Formation and Ion Channel Activity. *Biochemistry* **2006**, *45* (15), 4965–4973. https://doi.org/10.1021/bi051629n.
(429) Catimel, B.; Schieber, C.; Condron, M.; Patsiouras, H.; Connolly, L.; Catimel, J.; Nice, E. C.; Burgess, A. W.; Holmes, A. B. The PI(3,5)P2 and PI(4,5)P2 Interactomes. *J. Proteome Res.* **2008**, *7* (12), 5295–5313. https://doi.org/10.1021/pr800540h.
(430) Zacharias, D. A.; Violin, J. D.; Newton, A. C.; Tsien, R. Y. Partitioning of Lipid-Modified Monomeric GFPs into Membrane Microdomains of Live Cells. *Science.* **2002**, *296* (5569), 913–916. https://doi.org/10.1126/science.1068539.
(431) Wu, M.; Wang, T.; Loh, E.; Hong, W.; Song, H. Structural Basis for Recruitment of RILP by Small GTPase Rab7. *EMBO J.* **2005**, *24* (8), 1491 LP-1501. https://doi.org/10.1038/sj.emboj.7600643.
(432) McCray, B. A.; Skordalakes, E.; Taylor, J. P. Disease Mutations in Rab7 Result in Unregulated Nucleotide Exchange and Inappropriate Activation. *Hum. Mol. Genet.* **2010**, *19* (6), 1033–1047. https://doi.org/10.1093/hmg/ddp567.
(433) Rak, A.; Pylypenko, O.; Niculae, A.; Pyatkov, K.; Goody, R. S.; Alexandrov, K. Structure of the Rab7:REP-1 Complex: Insights into the Mechanism of Rab Prenylation and Choroideremia Disease. *Cell* **2004**, *117* (6), 749–760. https://doi.org/10.1016/J.CELL.2004.05.017.
(434) Ganley, I. G.; Pfeffer, S. R. Cholesterol Accumulation Sequesters Rab9 and Disrupts Late Endosome Function in NPC1-Deficient Cells. *J. Biol. Chem.* **2006**, *281* (26), 17890–17899. https://doi.org/10.1074/jbc.M601679200.
(435) Kaptzan, T.; West, S. A.; Holicky, E. L.; Wheatley, C. L.; Marks, D. L.; Wang, T.; Peake, K. B.; Vance, J.; Walkley, S. U.; Pagano, R. E. Development of a Rab9 Transgenic Mouse and Its Ability to Increase the Lifespan of a Murine Model of Niemann-Pick Type C Disease. *Am. J. Pathol.* **2009**, *174* (1), 14–20. https://doi.org///dx.doi.org/10.2353/ajpath.2009.080660.
(436) Chen, L.; DiGiammarino, E.; Zhou, X. E.; Wang, Y.; Toh, D.; Hodge, T. W.; Meehan, E. J. High Resolution Crystal Structure of Human Rab9 GTPase. *J. Biol. Chem.* **2004**, *279* (38), 40204–40208. https://doi.org/10.1074/jbc.m407114200.
(437) Ignoul, S.; Simaels, J.; Hermans, D.; Annaert, W.; Eggermont, J. Human ClC-6 Is a Late Endosomal Glycoprotein That Associates with Detergent-Resistant Lipid Domains. *PLoS One* **2007**, *2*, e474.
(438) Graves, A. R.; Curran, P. K.; Smith, C. L.; Mindell, J. A. The Cl-/H+ Antiporter ClC-7 Is the Primary Chloride Permeation Pathway in Lysosomes. *Nature* **2008**, *453* (7196), 788–792. https://doi.org/10.1038/nature06907.
(439) Hara-Chikuma, M.; Yang, B.; Sonawane, N. D.; Sasaki, S.; Uchida, S.; Verkman, A. S. ClC-3 Chloride Channels Facilitate Endosomal Acidification and Chloride Accumulation. *J. Biol. Chem.* **2005**, *280* (2), 1241–1247. https://doi.org/10.1074/jbc.M407030200.
(440) Hinzpeter, A.; Fritsch, J.; Borot, F.; Trudel, S.; Vieu, D.-L.; Brouillard, F.; Baudouin-Legros, M.; Clain, J.; Edelman, A.; Ollero, M. Membrane Cholesterol Content Modulates ClC-2 Gating and Sensitivity to Oxidative Stress. *J. Biol. Chem.* **2007**, *282* (4), 2423–2432. https://doi.org/10.1074/jbc.M608251200.
(441) Leung, K. H.; Chakraborty, K.; Saminathan, A.; Krishnan, Y. A DNA Nanomachine

Chemically Resolves Lysosomes in Live Cells. *Nature Nanotechnology*. **2018**, pp 176–183. https://doi.org/10.1038/s41565-018-0318-5.
(442) Steinberg, B. E.; Huynh, K. K.; Brodovitch, A.; Jabs, S.; Stauber, T.; Jentsch, T. J.; Grinstein, S. A Cation Counterflux Supports Lysosomal Acidification. *J. Cell Biol.* **2010**, *189* (7), 1171–1186. https://doi.org/10.1083/jcb.200911083.
(443) Park, E.; Campbell, E. B.; MacKinnon, R. Structure of a CLC Chloride Ion Channel by Cryo-Electron Microscopy. *Nature* **2017**, *541* (7638), 500–505.
(444) Wang, K.; Preisler, S. S.; Zhang, L.; Cui, Y.; Missel, J. W.; Grønberg, C.; Gotfryd, K.; Lindahl, E.; Andersson, M.; Calloe, K.; et al. Structure of the Human ClC-1 Chloride Channel. *PLOS Biol.* **2019**, *17* (4), e3000218. https://doi.org/10.1371/journal.pbio.3000218.
(445) Morgan, A. J.; Galione, A. Two-Pore Channels (TPCs): Current Controversies. *BioEssays* **2014**, *36* (2), 173–183. https://doi.org/10.1002/bies.201300118.
(446) Wang, X.; Zhang, X.; Dong, X.; Samie, M.; Li, X.; Cheng, X.; Goschka, A.; Shen, D.; Zhou, Y.; Harlow, J.; et al. TPC Proteins Are Phosphoinositide- Activated Sodium-Selective Ion Channels in Endosomes and Lysosomes. *Cell* **2012**, *151* (2), 372–383. https://doi.org///dx.doi.org/10.1016/j.cell.2012.08.036.
(447) Pitt, S. J.; Lam, A. K. M.; Rietdorf, K.; Galione, A.; Sitsapesan, R. Reconstituted Human TPC1 Is a Proton-Permeable Ion Channel and Is Activated by NAADP or Ca2+. *Sci. Signal.* **2014**, *7* (326), ra46. https://doi.org/10.1126/scisignal.2004854.
(448) Brailoiu, E.; Churamani, D.; Cai, X.; Schrlau, M. G.; Brailoiu, G. C.; Gao, X.; Hooper, R.; Boulware, M. J.; Dun, N. J.; Marchant, J. S.; et al. Essential Requirement for Two-Pore Channel 1 in NAADP-Mediated Calcium Signaling. *J. Cell Biol.* **2009**, *186* (2), 201–209. https://doi.org/10.1083/jcb.200904073.
(449) Kilpatrick, B. S.; Yates, E.; Grimm, C.; Schapira, A. H.; Patel, S. Endo-Lysosomal TRP Mucolipin-1 Channels Trigger Global ER Ca2+ Release and Ca2+ Influx. *J. Cell Sci.* **2016**, *129* (20), 3859–3867. https://doi.org/10.1242/jcs.190322.
(450) Rivero-Ríos, P.; Fernández, B.; Madero-Pérez, J.; Lozano, M. R.; Hilfiker, S. Two-Pore Channels and Parkinson's Disease: Where's the Link? *Messenger* **2016**, *5* (1–2), 67–75. https://doi.org/10.1166/msr.2016.1051.
(451) She, J.; Zeng, W.; Guo, J.; Chen, Q.; Bai, X.; Jiang, Y. Structural Mechanisms of Phospholipid Activation of the Human TPC2 Channel. *Elife* **2019**, *8*, e45222. https://doi.org/10.7554/elife.45222.
(452) Kintzer, A. F.; Stroud, R. M. Structure, Inhibition and Regulation of Two-Pore Channel TPC1 from Arabidopsis Thaliana. *Nature* **2016**, *531* (7593), 258–264.
(453) Schröder, B.; Wrocklage, C.; Hasilik, A.; Saftig, P. Molecular Characterisation of "transmembrane Protein 192" (TMEM192), a Novel Protein of the Lysosomal Membrane. *Biol. Chem.* **2010**, *391* (6), 695–704. https://doi.org/10.1515/BC.2010.062.
(454) Liu, Z.; Lv, Y. J.; Song, Y. P.; Li, X. H.; Du, Y. N.; Wang, C. H.; Hu, L. K. Lysosomal Membrane Protein TMEM192 Deficiency Triggers Crosstalk between Autophagy and Apoptosis in HepG2 Hepatoma Cells. *Oncol. Rep.* **2012**, *28* (3), 985–991. https://doi.org/10.3892/or.2012.1881.
(455) Nguyen, T. L.; Schneppenheim, J.; Rudnik, S.; Lüllmann-Rauch, R.; Bernreuther, C.; Hermans-Borgmeyer, I.; Glatzel, M.; Saftig, P.; Schröder, B. Functional Characterization of the Lysosomal Membrane Protein TMEM192 in Mice. *Oncotarget* **2017**, *8* (27), 43635–43652. https://doi.org/10.18632/oncotarget.17514.
(456) Finn, R. D.; Attwood, T. K.; Babbitt, P. C.; Bateman, A.; Bork, P.; Bridge, A. J.; Chang, H.-Y.; Dosztányi, Z.; El-Gebali, S.; Fraser, M.; et al. InterPro in 2017—beyond Protein Family and Domain Annotations. *Nucleic Acids Res.* **2016**, *45* (D1), D199. https://doi.org/10.1093/nar/gkw1107.
(457) Blauwendraat, C.; Heilbron, K.; Vallerga, C. L.; Bandres-Ciga, S.; von Coelln, R.; Pihlstrøm, L.; Simón-Sánchez, J.; Schulte, C.; Sharma, M.; Krohn, L.; et al. Parkinson's Disease Age at Onset Genome-Wide Association Study: Defining Heritability, Genetic Loci, and α-Synuclein Mechanisms. *Mov. Disord.* **2019**, *34* (6), 866–875. https://doi.org/10.1002/mds.27659.
(458) Lee, C.; Guo, J.; Zeng, W.; Kim, S.; She, J.; Cang, C.; Ren, D.; Jiang, Y. The Lysosomal Potassium Channel TMEM175 Adopts a Novel Tetrameric Architecture. *Nature* **2017**, *547*, 472.

(459) Estiu, G.; Khatri, N.; Wiest, O. Computational Studies of the Cholesterol Transport between NPC2 and the N-Terminal Domain of NPC1 (NPC1(NTD)). *Biochemistry* **2013**, *52* (39), 6879–6891. https://doi.org/10.1021/bi4005478.
(460) Pfeffer, S. R. NPC Intracellular Cholesterol Transporter 1 (NPC1)-Mediated Cholesterol Export from Lysosomes. *J. Biol. Chem.* **2019**, *294* (5), 1706–1709. https://doi.org/10.1074/jbc.TM118.004165.
(461) Macías-Vidal, J.; Guerrero-Hernández, M.; Estanyol, J. M.; Aguado, C.; Knecht, E.; Coll, M. J.; Bachs, O. Identification of Lysosomal Npc1-Binding Proteins: Cathepsin D Activity Is Regulated by NPC1. *Proteomics* **2016**, *16* (1), 150–158. https://doi.org/10.1002/pmic.201500110.
(462) Enrich, C.; Rentero, C.; de Muga, S. V.; Reverter, M.; Mulay, V.; Wood, P.; Koese, M.; Grewal, T. Annexin A6—Linking Ca2+ Signaling with Cholesterol Transport. *Biochim. Biophys. Acta - Mol. Cell Res.* **2011**, *1813* (5), 935–947. https://doi.org///dx.doi.org/10.1016/j.bbamcr.2010.09.015.
(463) Huang, X.; Sun, S.; Wang, X.; Fan, F.; Zhou, Q.; Lu, S.; Cao, Y.; Wang, Q. W.; Dong, M. Q.; Yao, J.; et al. Mechanistic Insights into the SNARE Complex Disassembly. *Sci. Adv.* **2019**, *5* (4), eaau8164. https://doi.org/10.1126/sciadv.aau8164.
(464) Bykhovskaia, M. Molecular Dynamics Simulations of the SNARE Complex. In *Methods in Molecular Biology*; Humana Press, New York, NY, **2019**; Vol. 1860, pp 3–13. https://doi.org/10.1007/978-1-4939-8760-3_1.
(465) Sievers, F.; Wilm, A.; Dineen, D.; Gibson, T. J.; Karplus, K.; Li, W.; Lopez, R.; McWilliam, H.; Remmert, M.; Söding, J.; et al. Fast, Scalable Generation of High-quality Protein Multiple Sequence Alignments Using Clustal Omega. *Mol. Syst. Biol.* **2011**, *7* (1).
(466) Waterhouse, A. M.; Procter, J. B.; Martin, D. M. A.; Clamp, M.; Barton, G. J. Jalview Version 2—a Multiple Sequence Alignment Editor and Analysis Workbench. *Bioinformatics* **2009**, *25* (9), 1189–1191.
(467) Irwin, J. J.; Sterling, T.; Mysinger, M. M.; Bolstad, E. S.; Coleman, R. G. ZINC: A Free Tool to Discover Chemistry for Biology. *Journal of Chemical Information and Modeling*. American Chemical Society July 23, **2012**, pp 1757–1768. https://doi.org/10.1021/ci3001277.
(468) Wang, H.; Shi, Y.; Song, J.; Qi, J.; Lu, G.; Yan, J.; Gao, G. F. Ebola Viral Glycoprotein Bound to Its Endosomal Receptor Niemann-Pick C1. *Cell* **2016**, *164* (1–2), 258–268. https://doi.org/10.1016/j.cell.2015.12.044.
(469) Zhao, Y.; Ren, J.; Harlos, K.; Stuart, D. I. Structure of Glycosylated NPC1 Luminal Domain C Reveals Insights into NPC2 and Ebola Virus Interactions. *FEBS Lett.* **2016**, *590* (5), 605–612. https://doi.org/10.1002/1873-3468.12089.
(470) Brett, C. L.; Kallay, L.; Hua, Z.; Green, R.; Chyou, A.; Zhang, Y.; Graham, T. R.; Donowitz, M.; Rao, R. Genome-Wide Analysis Reveals the Vacuolar PH-Stat of Saccharomyces Cerevisiae. *PLoS One* **2011**, *6* (3), e17619.
(471) Wheeler, S.; Haberkant, P.; Bhardwaj, M.; Tongue, P.; Ferraz, M. J.; Halter, D.; Sprong, H.; Schmid, R.; Aerts, J. M. F. G.; Sullo, N.; et al. Cytosolic Glucosylceramide Regulates Endolysosomal Function in Niemann-Pick Type C Disease. *Neurobiol. Dis.* **2019**, *127*, 242–252. https://doi.org/10.1016/j.nbd.2019.03.005.
(472) Wang, R.; Hosaka, M.; Han, L.; Yokota-Hashimoto, H.; Suda, M.; Mitsushima, D.; Torii, S.; Takeuchi, T. Molecular Probes for Sensing the Cholesterol Composition of Subcellular Organelle Membranes. *Biochim. Biophys. Acta* **2006**, *1761* (10), 1169–1181. https://doi.org/S1388-1981(06)00234-4.
(473) Duvvuri, M.; Gong, Y.; Chatterji, D.; Krise, J. P. Weak Base Permeability Characteristics Influence the Intracellular Sequestration Site in the Multidrug-Resistant Human Leukemic Cell Line HL-60. *J. Biol. Chem.* **2004**, *279* (31), 32367–32372. https://doi.org/10.1074/jbc.M400735200.
(474) Shoemaker, C. J.; Schornberg, K. L.; Delos, S. E.; Scully, C.; Pajouhesh, H.; Olinger, G. G.; Johansen, L. M.; White, J. M. Multiple Cationic Amphiphiles Induce a Niemann-Pick C Phenotype and Inhibit Ebola Virus Entry and Infection. *PLoS One* **2013**, *8*, e56265.
(475) Lafourcade, C.; Sobo, K.; Kieffer-Jaquinod, S.; Garin, J.; van der Goot, F. G. Regulation of the V-ATPase along the Endocytic Pathway Occurs through Reversible Subunit Association and Membrane Localization. *PLoS One* **2008**, *3* (7), e2758.

https://doi.org/10.1371/journal.pone.0002758.
(476) Simons, K.; Gruenberg, J. Jamming the Endosomal System: Lipid Rafts and Lysosomal Storage Diseases. *Trends Cell Biol.* **2000**, *10* (11), 459–462. https://doi.org/10.1016/S0962-8924(00)01847-X.
(477) Johnson, D. E.; Ostrowski, P.; Jaumouillé, V.; Grinstein, S. The Position of Lysosomes within the Cell Determines Their Luminal PH. *J. Cell Biol.* **2016**, *212* (6), 677–692. https://doi.org/10.1083/jcb.201507112.
(478) Cheng, X. T.; Xie, Y. X.; Zhou, B.; Huang, N.; Farfel-Becker, T.; Sheng, Z. H. Characterization of LAMP1-Labeled Nondegradative Lysosomal and Endocytic Compartments in Neurons. *J. Cell Biol.* **2018**, *217* (9), 3127–3139. https://doi.org/10.1083/jcb.201711083.
(479) Surana, S.; Bhat, J. M.; Koushika, S. P.; Krishnan, Y. An Autonomous DNA Nanomachine Maps Spatiotemporal PH Changes in a Multicellular Living Organism. *Nat. Commun.* **2011**, *2* (1), 340. https://doi.org/10.1038/ncomms1340.
(480) Diwu, Z.; Chen, C.-S.; Zhang, C.; Klaubert, D. H.; Haugland, R. P. A Novel Acidotropic PH Indicator and Its Potential Application in Labeling Acidic Organelles of Live Cells. *Chem. Biol.* **1999**, *6* (7), 411–418. https://doi.org///dx.doi.org/10.1016/S1074-5521(99)80059-3.
(481) Guha, S.; Coffey, E. E.; Lu, W.; Lim, J. C.; Beckel, J. M.; Laties, A. M.; Boesze-Battaglia, K.; Mitchell, C. H. Approaches for Detecting Lysosomal Alkalinization and Impaired Degradation in Fresh and Cultured RPE Cells: Evidence for a Role in Retinal Degenerations. *Exp. Eye Res.* **2014**, *126*, 68–76. https://doi.org///dx.doi.org/10.1016/j.exer.2014.05.013.
(482) Lu, F.; Liang, Q.; Abi-Mosleh, L.; Das, A.; De Brabander K., J.; Goldstein, J. L.; Brown, M. S. Identification of NPC1 as the Target of U18666A, an Inhibitor of Lysosomal Cholesterol Export and Ebola Infection. *Elife* **2015**, *4*, e12177. https://doi.org/10.7554/eLife.12177.
(483) Funk, R. S.; Krise, J. P. Cationic Amphiphilic Drugs Cause a Marked Expansion of Apparent Lysosomal Volume: Implications for an Intracellular Distribution-Based Drug Interaction. *Mol. Pharm.* **2012**, *9* (5), 1384–1395. https://doi.org/10.1021/mp200641e.
(484) Lu, S.; Sung, T.; Lin, N.; Abraham, R. T.; Jessen, B. A. Lysosomal Adaptation: How Cells Respond to Lysosomotropic Compounds. *PLoS One* **2017**, *12* (3), e0173771. https://doi.org/10.1371/journal.pone.0173771.
(485) Incardona, J. P.; Gaffield, W.; Lange, Y.; Cooney, A.; Pentchev, P. G.; Liu, S.; Watson, J. A.; Kapur, R. P.; Roelink, H. Cyclopamine Inhibition of Sonic Hedgehog Signal Transduction Is Not Mediated through Effects on Cholesterol Transport. *Dev. Biol.* **2000**, *224* (2), 440–452. https://doi.org///dx.doi.org/10.1006/dbio.2000.9775.
(486) Cenedella, R. J.; Sexton, P. S.; Krishnan, K.; Covey, D. F. Comparison of Effects of U18666A and Enantiomeric U18666A on Sterol Synthesis and Induction of Apoptosis. *Lipids* **2005**, *40*, 635. https://doi.org/10.1007/s11745-005-1426-9.
(487) Cenedella, R. J. Cholesterol Synthesis Inhibitor U18666A and the Role of Sterol Metabolism and Trafficking in Numerous Pathophysiological Processes. *Lipids* **2009**, *44* (6), 477–487. https://doi.org/10.1007/s11745-009-3305-7.
(488) te Vruchte, D.; Wallom, K. L.; Platt, F. M. Measuring Relative Lysosomal Volume for Monitoring Lysosomal Storage Diseases. *Methods Cell Biol.* **2015**, *126*, 331–347. https://doi.org/10.1016/bs.mcb.2014.10.027.
(489) Otomo, T.; Higaki, K.; Nanba, E.; Ozono, K.; Sakai, N. Lysosomal Storage Causes Cellular Dysfunction in Mucolipidosis II Skin Fibroblasts. *J. Biol. Chem.* **2011**, *286* (40), 35283–35290. https://doi.org/10.1074/jbc.M111.267930.
(490) Coffey, E. E.; Beckel, J. M.; Laties, A. M.; Mitchell, C. H. Lysosomal Alkalization and Dysfunction in Human Fibroblasts with the Alzheimer's Disease-Linked Presenilin 1 A246E Mutation Can Be Reversed with CAMP. *Neuroscience* **2014**, *263*, 111–124. https://doi.org/10.1016/j.neuroscience.2014.01.001.
(491) Xu, M.; Liu, K.; Swaroop, M.; Sun, W.; Dehdashti, S. J.; McKew, J. C.; Zheng, W. A Phenotypic Compound Screening Assay for Lysosomal Storage Diseases. *J. Biomol. Screen.* **2014**, *19* (1), 168–175. https://doi.org/10.1177/1087057113501197.
(492) te Vruchte, D.; Speak, A. O.; Wallom, K. L.; Al Eisa, N.; Smith, D. A.; Hendriksz, C. J.; Simmons, L.; Lachmann, R. H.; Cousins, A.; Hartung, R.; et al. Relative Acidic Compartment Volume as a Lysosomal Storage Disorder-Associated Biomarker. *J. Clin. Invest.* **2014**, *124* (3), 1320–1328. https://doi.org/10.1172/JCI72835.

(493) Yoshinaka, K.; Kumanogoh, H.; Nakamura, S.; Maekawa, S. Identification of V-ATPase as a Major Component in the Raft Fraction Prepared from the Synaptic Plasma Membrane and the Synaptic Vesicle of Rat Brain. *Neurosci. Lett.* **2004**, *363* (2), 168–172. https://doi.org///dx.doi.org/10.1016/j.neulet.2004.04.002.
(494) Jia, J.; Lamer, S.; Schümann, M.; Schmidt, M. R.; Krause, E.; Haucke, V. Quantitative Proteomics Analysis of Detergent-Resistant Membranes from Chemical Synapses: Evidence for Cholesterol as Spatial Organizer of Synaptic Vesicle Cycling. *Mol. Cell. Proteomics* **2006**, *5* (11), 2060–2071. https://doi.org/10.1074/mcp.M600161-MCP200.
(495) Möbius, W.; van Donselaar, E.; Ohno-Iwashita, Y.; Shimada, Y.; Heijnen, H. F. G.; Slot, J. W.; Geuze, H. J. Recycling Compartments and the Internal Vesicles of Multivesicular Bodies Harbor Most of the Cholesterol Found in the Endocytic Pathway. *Traffic* **2003**, *4* (4), 222–231. https://doi.org/10.1034/j.1600-0854.2003.00072.x.
(496) Mazhab-Jafari, M.; Rohou, A.; Schmidt, C.; Bueler, S. A.; Benlekbir, S.; Robinson, C. V; Rubinstein, J. L. Atomic Model for the Membrane-Embedded VO Motor of a Eukaryotic V-ATPase. *Nature* **2016**, *539* (7627), 118–122.
(497) Huss, M.; Ingenhorst, G.; König, S.; Gaßel, M.; Dröse, S.; Zeeck, A.; Altendorf, K.; Wieczorek, H. Concanamycin A, the Specific Inhibitor of V-ATPases, Binds to the Vo Subunit C. *J. Biol. Chem.* **2002**, *277* (43), 40544–40548. https://doi.org/10.1074/jbc.M207345200.
(498) Bowman, B. J.; McCall, M. E.; Baertsch, R.; Bowman, E. J. A Model for the Proteolipid Ring and Bafilomycin/Concanamycin-Binding Site in the Vacuolar ATPase of Neurospora Crassa. *J. Biol. Chem.* **2006**, *281* (42), 31885–31893. https://doi.org/10.1074/jbc.M605532200.
(499) Bockelmann, S.; Menche, D.; Rudolph, S.; Bender, T.; Grond, S.; von Zezschwitz, P.; Muench, S. P.; Wieczorek, H.; Huss, M. Archazolid A Binds to the Equatorial Region of the C-Ring of the Vacuolar H+-ATPase. *J. Biol. Chem.* **2010**, *285* (49), 38304–38314. https://doi.org/10.1074/jbc.M110.137539.
(500) Whyteside, G.; Meek, P. J.; Ball, S. K.; Dixon, N.; Finbow, M. E.; Kee, T. P.; Findlay, J. B. C.; Harrison, M. A. Concanamycin and Indolyl Pentadieneamide Inhibitors of the Vacuolar H+-ATPase Bind with High Affinity to the Purified Proteolipid Subunit of the Membrane Domain. *Biochemistry* **2005**, *44* (45), 15024–15031. https://doi.org/10.1021/bi051529h.
(501) Muench, S. P.; Rawson, S.; Eyraud, V.; Delmas, A. F.; Da Silva, P.; Phillips, C.; Trinick, J.; Harrison, M. A.; Gressent, F.; Huss, M. PA1b Inhibitor Binding to Subunits c and e of the Vacuolar ATPase Reveals Its Insecticidal Mechanism. *J. Biol. Chem.* **2014**, *289* (23), 16399–16408. https://doi.org/10.1074/jbc.M113.541250.
(502) Xie, X.-S.; Padron, D.; Liao, X.; Wang, J.; Roth, M. G.; De Brabander, J. K. Salicylihalamide A Inhibits the V0 Sector of the V-ATPase through a Mechanism Distinct from Bafilomycin A1. *J. Biol. Chem.* **2004**, *279* (19), 19755–19763. https://doi.org/10.1074/jbc.M313796200.
(503) Osteresch, C.; Bender, T.; Grond, S.; von Zezschwitz, P.; Kunze, B.; Jansen, R.; Huss, M.; Wieczorek, H. The Binding Site of the V-ATPase Inhibitor Apicularen Is in the Vicinity of Those for Bafilomycin and Archazolid. *J. Biol. Chem.* **2012**, *287* (38), 31866–31876. https://doi.org/10.1074/jbc.M112.372169.
(504) Murata, T.; Yamato, I.; Kakinuma, Y.; Leslie, A. G. W.; Walker, J. E. Structure of the Rotor of the V-Type Na+-ATPase from Enterococcus Hirae. *Science.* **2005**, *308* (5722), 654–659. https://doi.org/10.1126/science.1110064.
(505) Dreisigacker, S.; Latek, D.; Bockelmann, S.; Huss, M.; Wieczorek, H.; Filipek, S.; Gohlke, H.; Menche, D.; Carlomagno, T. Understanding the Inhibitory Effect of Highly Potent and Selective Archazolides Binding to the Vacuolar ATPase. *J. Chem. Inf. Model.* **2012**, *52* (8), 2265–2272. https://doi.org/10.1021/ci300242d.
(506) Gu, X.; Gupta, V.; Yang, Y.; Zhu, J. Y.; Carlson, E. J.; Kingsley, C.; Tash, J. S.; Schönbrunn, E.; Hawkinson, J.; Georg, G. I. Structure–Activity Studies of N-Butyl-1-Deoxynojirimycin (NB-DNJ) Analogues: Discovery of Potent and Selective Aminocyclopentitol Inhibitors of GBA1 and GBA2. *ChemMedChem* **2017**, *12* (23), 1977–1984. https://doi.org/10.1002/cmdc.201700558.
(507) Edwards, M. P.; Price, D. A. *Role of Physicochemical Properties and Ligand Lipophilicity Efficiency in Addressing Drug Safety Risks*; Academic Press, **2010**; Vol. 45. https://doi.org/10.1016/S0065-7743(10)45023-X.

(508) Hopkins, A. L.; Keseru, G. M.; Leeson, P. D.; Rees, D. C.; Reynolds, C. H. The Role of Ligand Efficiency Metrics in Drug Discovery. *Nat Rev Drug Discov* **2014**, *13* (2), 105–121.
(509) Nakagome, I.; Kato, A.; Yamaotsu, N.; Yoshida, T.; Ozawa, S.; Adachi, I.; Hirono, S.; Nakagome, I.; Kato, A.; Yamaotsu, N.; et al. Design of a New α-1-C-Alkyl-DAB Derivative Acting as a Pharmacological Chaperone for β-Glucocerebrosidase Using Ligand Docking and Molecular Dynamics Simulation. *Molecules* **2018**, *23* (10), 2683. https://doi.org/10.3390/molecules23102683.
(510) Kuo, C. L.; van Meel, E.; Kytidou, K.; Kallemeijn, W. W.; Witte, M.; Overkleeft, H. S.; Artola, M. E.; Aerts, J. M. Activity-Based Probes for Glycosidases: Profiling and Other Applications. In *Methods in Enzymology*; Academic Press, **2018**; Vol. 598, pp 217–235. https://doi.org/10.1016/bs.mie.2017.06.039.
(511) Aerts, J. M. F. G.; Sa Miranda, M. C.; Brouwer-Kelder, E. M.; Van Weely, S.; Barranger, J. A.; Tager, J. M. Conditions Affecting the Activity of Glucocerebrosidase Purified Fom Spleens of Control Subjects and Patients with Type 1 Gaucher Disease. *Biochim. Biophys. Acta - Protein Struct. Mol. Enzymol.* **1990**, *1041* (1), 55–63. https://doi.org/10.1016/0167-4838(90)90122-V.
(512) Caputo, A. T.; Alonzi, D. S.; Marti, L.; Reca, I.-B.; Kiappes, J. L.; Struwe, W. B.; Cross, A.; Basu, S.; Lowe, E. D.; Darlot, B.; et al. Structures of Mammalian ER α-Glucosidase II Capture the Binding Modes of Broad-Spectrum Iminosugar Antivirals. *Proc. Natl. Acad. Sci.* **2016**, *113* (32), E4630-8. https://doi.org/10.1073/pnas.1604463113.
(513) Kiappes, J. L.; Hill, M. L.; Alonzi, D. S.; Miller, J. L.; Iwaki, R.; Sayce, A. C.; Caputo, A. T.; Kato, A.; Zitzmann, N. ToP-DNJ, a Selective Inhibitor of Endoplasmic Reticulum α-Glucosidase II Exhibiting Antiflaviviral Activity. *ACS Chem. Biol.* **2018**, *13* (1), 60–65. https://doi.org/10.1021/acschembio.7b00870.
(514) Shen, W.; Henry, A. G.; Paumier, K. L.; Li, L.; Mou, K.; Dunlop, J.; Berger, Z.; Hirst, W. D. Inhibition of Glucosylceramide Synthase Stimulates Autophagy Flux in Neurons. *J. Neurochem.* **2014**, *129* (5), 884–894. https://doi.org/10.1111/jnc.12672.
(515) van der Poel, S.; Wolthoorn, J.; van den Heuvel, D.; Egmond, M.; Groux-Degroote, S.; Neumann, S.; Gerritsen, H.; van Meer, G.; Sprong, H. Hyperacidification of Trans-Golgi Network and Endo/Lysosomes in Melanocytes by Glucosylceramide-Dependent V-ATPase Activity. *Traffic* **2011**, *12* (11), 1634–1647. https://doi.org/10.1111/j.1600-0854.2011.01263.x.
(516) Yamaguchi, M.; Kasamo, K. Modulation in the Activity of Purified Tonoplast H+-ATPase by Tonoplast Glycolipids Prepared from Cultured Rice (Oryza Sativa L. Var. Boro) Cells. *Plant Cell Physiol.* **2001**, *42* (5), 516–523. https://doi.org/10.1093/pcp/pce064.
(517) Zhu, H.; Shen, H.; Sewell, A. K.; Kniazeva, M.; Han, M. A Novel Sphingolipid-TORC1 Pathway Critically Promotes Postembryonic Development in Caenorhabditis Elegans. *Elife* **2013**, *2:e00429.*, e00429. https://doi.org/10.7554/eLife.00429.
(518) Sillence, D. J. Glucosylceramide Modulates Endolysosomal PH in Gaucher Disease. *Mol. Genet. Metab.* **2013**, *109* (2), 194–200. https://doi.org///dx.doi.org/10.1016/j.ymgme.2013.03.015.
(519) De La Mata, M.; Cotán, D.; Oropesa-Ávila, M.; Villanueva-Paz, M.; De Lavera, I.; Álvarez-Córdoba, M.; Luzón-Hidalgo, R.; Suárez-Rivero, J. M.; Tiscornia, G.; Sánchez-Alcázar, J. A. Coenzyme Q10 Partially Restores Pathological Alterations in a Macrophage Model of Gaucher Disease. *Orphanet J. Rare Dis.* **2017**, *12* (1), 1–15. https://doi.org/10.1186/s13023-017-0574-8.
(520) Magalhaes, J.; Gegg, M. E.; Migdalska-Richards, A.; Doherty, M. K.; Whitfield, P. D.; Schapira, A. H. V. Autophagic Lysosome Reformation Dysfunction in Glucocerebrosidase Deficient Cells: Relevance to Parkinson Disease. *Hum. Mol. Genet.* **2015**, *25* (16), 3432–3445. https://doi.org/10.1093/hmg/ddw185.
(521) Bourdenx, M.; Daniel, J.; Genin, E.; Soria, F. N.; Blanchard-Desce, M.; Bezard, E.; Dehay, B. Nanoparticles Restore Lysosomal Acidification Defects: Implications for Parkinson and Other Lysosomal-Related Diseases. *Autophagy* **2016**, *12* (3), 472–483. https://doi.org/10.1080/15548627.2015.1136769.
(522) Dekker, N.; Voorn-Brouwer, T.; Verhoek, M.; Wennekes, T.; Narayan, R. S.; Speijer, D.; Hollak, C. E. M.; Overkleeft, H. S.; Boot, R. G.; Aerts, J. M. F. G. The Cytosolic β-Glucosidase GBA3 Does Not Influence Type 1 Gaucher Disease Manifestation. *Blood Cells,*

Mol. Dis. **2011**, *46* (1), 19–26. https://doi.org///dx.doi.org/10.1016/j.bcmd.2010.07.009.
(523) Marques, A. R. A.; Mirzaian, M.; Akiyama, H.; Wisse, P.; Ferraz, M. J.; Gaspar, P.; Ghauharali-van der Vlugt, K.; Meijer, R.; Giraldo, P.; Alfonso, P.; et al. Glucosylated Cholesterol in Mammalian Cells and Tissues: Formation and Degradation by Multiple Cellular β-Glucosidases. *J. Lipid Res.* **2016**, *57* (3), 451–463. https://doi.org/10.1194/jlr.m064923.
(524) Sillence, D. J.; Puri, V.; Marks, D. L.; Butters, T. D.; Dwek, R. A.; Pagano, R. E.; Platt, F. M. Glucosylceramide Modulates Membrane Traffic along the Endocytic Pathway. *J. Lipid Res.* **2002**, *43* (11), 1837–1845. https://doi.org/10.1194/jlr.M200232-JLR200.
(525) Warnock, D. E.; Lutz, M. S.; Blackburn, W. A.; Young, W. W.; Baenziger, J. U. Transport of Newly Synthesized Glucosylceramide to the Plasma-Membrane by a Non-Golgi Pathway. *Proc. Natl. Acad. Sci.* **1994**, *91* (7), 2708–2712. https://doi.org/10.1073/pnas.91.7.2708.
(526) Zhang, Y.-Q.; Gamarra, S.; Garcia-Effron, G.; Park, S.; Perlin, D. S.; Rao, R. Requirement for Ergosterol in V-ATPase Function Underlies Antifungal Activity of Azole Drugs. *PLoS Pathog* **2010**, *6* (6), e1000939.
(527) Vasanthakumar, T.; Bueler, S. A.; Wu, D.; Beilsten-Edmands, V.; Robinson, C. V.; Rubinstein, J. L. Structural Comparison of the Vacuolar and Golgi V-ATPases from Saccharomyces Cerevisiae. *Proc. Natl. Acad. Sci.* **2019**, *116* (15), 7272–7277. https://doi.org/10.1073/pnas.1814818116.
(528) Saito, K.; Takakuwa, N.; Ohnishi, M.; Oda, Y. Presence of Glucosylceramide in Yeast and Its Relation to Alkali Tolerance of Yeast. *Appl. Microbiol. Biotechnol.* **2006**, *71* (4), 515–521. https://doi.org/10.1007/s00253-005-0187-3.
(529) Warnecke, D.; Heinz, E. Recently Discovered Functions of Glucosylceramides in Plants and Fungi. *Cell. Mol. Life Sci. C.* **2003**, *60* (5), 919–941. https://doi.org/10.1007/s00018-003-2243-4.
(530) Vaccaro, A. M.; Ciaffoni, F.; Tatti, M.; Salvioli, R.; Barca, A.; Tognozzi, D.; Scerch, C. PH-Dependent Conformational Properties of Saposins and Their Interactions with Phospholipid Membranes. *J. Biol. Chem.* **1995**, *270* (51), 30576–30580. https://doi.org/10.1074/jbc.270.51.30576.
(531) Schonauer, S.; Körschen, H. G.; Penno, A.; Rennhack, A.; Breiden, B.; Sandhoff, K.; Gutbrod, K.; Dörmann, P.; Raju, D. N.; Haberkant, P.; et al. Identification of a Feedback Loop Involving Beta-Glucosidase 2 and Its Product Sphingosine Sheds Light on the Molecular Mechanisms in Gaucher Disease. *J. Biol. Chem.* **2017**, *292* (15), 6177–6189. https://doi.org/10.1074/jbc.M116.762831.
(532) Goldman, S. D. B.; Krise, J. P. Niemann-Pick C1 Functions Independently of Niemann-Pick C2 in the Initial Stage of Retrograde Transport of Membrane-Impermeable Lysosomal Cargo. *J. Biol. Chem.* **2010**, *285* (7), 4983–4994. https://doi.org/10.1074/jbc.M109.037622.
(533) Li, H.; Kim, W. S.; Guillemin, G. J.; Hill, A. F.; Evin, G.; Garner, B. Modulation of Amyloid Precursor Protein Processing by Synthetic Ceramide Analogues. *Biochim. Biophys. Acta - Mol. Cell Biol. Lipids* **2010**, *1801* (8), 887–895. https://doi.org/10.1016/j.bbalip.2010.05.012.
(534) Stelzer, G.; Rosen, N.; Plaschkes, I.; Zimmerman, S.; Twik, M.; Fishilevich, S.; Stein, T. I.; Nudel, R.; Lieder, I.; Mazor, Y.; et al. The GeneCards Suite: From Gene Data Mining to Disease Genome Sequence Analyses. In *Current Protocols in Bioinformatics*; John Wiley & Sons, Inc.: Hoboken, NJ, USA, 2016; Vol. 54, p 1.30.1-1.30.33. https://doi.org/10.1002/cpbi.5.
(535) Hallett, P. J.; Huebecker, M.; Brekk, O. R.; Moloney, E. B.; Rocha, E. M.; Priestman, D. A.; Platt, F. M.; Isacson, O. Glycosphingolipid Levels and Glucocerebrosidase Activity Are Altered in Normal Aging of the Mouse Brain. *Neurobiol. Aging* **2018**, *67*, 189–200. https://doi.org/10.1016/J.NEUROBIOLAGING.2018.02.028.
(536) Santos-Lozano, A.; Sanchis-Gomar, F.; Fiuza-Luces, C.; Pareja-Galeano, H.; Garatachea, N.; Lucia, A.; García, D. V.; Gadea, G. N. Niemann-Pick Disease Treatment: A Systematic Review of Clinical Trials. *Ann. Transl. Med.* **2015**, *3* (22). https://doi.org/10.3978/j.issn.2305-5839.2015.12.04.
(537) Brady, R. O.; Kanfer, J. N.; Mock, M. B.; Fredrickson, D. S. The Metabolism of Sphingomyelin. II. Evidence of an Enzymatic Deficiency in Niemann-Pick Diseae. *Proc. Natl. Acad. Sci.* **1966**, *55* (2), 366–369. https://doi.org/10.1073/pnas.55.2.366.

(538) Scandroglio, F.; Venkata, J. K.; Loberto, N.; Prioni, S.; Schuchman, E. H.; Chigorno, V.; Prinetti, A.; Sonnino, S. Lipid Content of Brain, Brain Membrane Lipid Domains, and Neurons from Acid Sphingomyelinase Deficient Mice. *J. Neurochem.* **2008**, *107* (2), 329–338. https://doi.org/10.1111/j.1471-4159.2008.05591.x.
(539) Galvan, C.; Camoletto, P. G.; Cristofani, F.; Van Veldhoven, P. P.; Ledesma, M. D. Anomalous Surface Distribution of Glycosyl Phosphatidyl Inositol-Anchored Proteins in Neurons Lacking Acid Sphingomyelinase. *Mol. Biol. Cell* **2008**, *19* (2), 509–522. https://doi.org/10.1091/mbc.e07-05-0439.
(540) Camoletto, P. G.; Vara, H.; Morando, L.; Connell, E.; Marletto, F. P.; Giustetto, M.; Sassoè-Pognetto, M.; Van Veldhoven, P. P.; Ledesma, M. D. Synaptic Vesicle Docking: Sphingosine Regulates Syntaxin1 Interaction with Munc18. *PLoS One* **2009**, *4* (4), e5310. https://doi.org/10.1371/journal.pone.0005310.
(541) Leventhal, A. R.; Chen, W.; Tall, A. R.; Tabas, I. Acid Sphingomyelinase-Deficient Macrophages Have Defective Cholesterol Trafficking and Efflux. *J. Biol. Chem.* **2001**, *276* (48), 44976–44983. https://doi.org/10.1074/jbc.M106455200.
(542) McGovern, M. M.; Pohl-Worgall, T.; Deckelbaum, R. J.; Simpson, W.; Mendelson, D.; Desnick, R. J.; Schuchman, E. H.; Wasserstein, M. P. Lipid Abnormalities in Children with Types A and B Niemann Pick Disease. *J. Pediatr.* **2004**, *145* (1), 77–81. https://doi.org/10.1016/j.jpeds.2004.02.048.
(543) Wu, B. X.; Fan, J.; Boyer, N. P.; Jenkins, R. W.; Koutalos, Y.; Hannun, Y. A.; Crosson, C. E. Lack of Acid Sphingomyelinase Induces Age-Related Retinal Degeneration. *PLoS One* **2015**, *10* (7), e0133032. https://doi.org/10.1371/journal.pone.0133032.
(544) Rappaport, J.; Garnacho, C.; Muro, S. Clathrin-Mediated Endocytosis Is Impaired in Type A-B Niemann-Pick Disease Model Cells and Can Be Restored by ICAM-1-Mediated Enzyme Replacement. *Mol. Pharm.* **2014**, *11* (8), 2887–2895. https://doi.org/10.1021/mp500241y.
(545) Andrade, F.; Aldámiz-Echevarría, L.; Llarena, M.; Couce, M. L. Sanfilippo Syndrome: Overall Review. *Pediatr. Int.* **2015**, *57* (3), 331–338. https://doi.org/10.1111/ped.12636.
(546) LaPlante, J. M.; Falardeau, J.; Sun, M.; Kanazirska, M.; Brown, E. M.; Slaugenhaupt, S. A.; Vassilev, P. M. Identification and Characterization of the Single Channel Function of Human Mucolipin-1 Implicated in Mucolipidosis Type IV, a Disorder Affecting the Lysosomal Pathway. *FEBS Lett.* **2002**, *532* (1–2), 183–187. https://doi.org/10.1016/S0014-5793(02)03670-0.
(547) Chen, C.-C.; Keller, M.; Hess, M.; Schiffmann, R.; Urban, N.; Wolfgardt, A.; Schaefer, M.; Bracher, F.; Biel, M.; Wahl-Schott, C.; et al. A Small Molecule Restores Function to TRPML1 Mutant Isoforms Responsible for Mucolipidosis Type IV. *Nat. Commun.* **2014**, *5*, 4681.
(548) Guffon, N.; Bin-Dorel, S.; Decullier, E.; Paillet, C.; Guitton, J.; Fouilhoux, A. Evaluation of Miglustat Treatment in Patients with Type III Mucopolysaccharidosis: A Randomized, Double-Blind, Placebo-Controlled Study. *J. Pediatr.* **2011**, *159* (5), 838–844.e1. https://doi.org/10.1016/J.JPEDS.2011.04.040.
(549) Boudewyn, L. C.; Sikora, J.; Kuchar, L.; Ledvinova, J.; Grishchuk, Y.; Wang, S. L.; Dobrenis, K.; Walkley, S. U. N-Butyldeoxynojirimycin Delays Motor Deficits, Cerebellar Microgliosis, and Purkinje Cell Loss in a Mouse Model of Mucolipidosis Type IV. *Neurobiol. Dis.* **2017**, *105*, 257–270. https://doi.org/10.1016/j.nbd.2017.06.003.
(550) Suzuki, Y.; Suzuki, K. Krabbe's Globoid Cell Leukodystrophy: Deficiency of Galactocerebrosidase in Serum, Leukocytes, and Fibroblasts. *Science.* **1971**, *171* (3966), 73–75. https://doi.org/10.1126/science.171.3966.73.
(551) Ehtishamul, H.; Shailendra, G.; Inderjit, S.; K., S. A.; Haq, E.; Giri, S.; Singh, I.; Singh, A. K. Molecular Mechanism of Psychosine-induced Cell Death in Human Oligodendrocyte Cell Line. *J. Neurochem.* **2003**, *86* (6), 1428–1440. https://doi.org/doi:10.1046/j.1471-4159.2003.01941.x.
(552) Yamazaki, T.; Chang, T.-Y.; Haass, C.; Ihara, Y. Accumulation and Aggregation of Amyloid SS-Protein in Late Endosomes of Niemann-Pick Type C Cells. *J. Biol. Chem.* **2001**, *276* (6), 4454–4460. https://doi.org/10.1074/jbc.M009598200.
(553) Nixon, R. A. Amyloid Precursor Protein and Endosomal–lysosomal Dysfunction in Alzheimer's Disease: Inseparable Partners in a Multifactorial Disease. *FASEB J.* **2017**, *31* (7), 2729–2743. https://doi.org/10.1096/fj.201700359.

(554) Hao, L.; Ben-David, O.; Babb, S. M.; Futerman, A. H.; Cohen, B. M.; Buttner, E. A. Clozapine Modulates Glucosylceramide, Clears Aggregated Proteins, and Enhances ATG8/LC3 in Caenorhabditis Elegans. *Neuropsychopharmacology* **2017**, *42* (4), 951–962. https://doi.org/10.1038/npp.2016.230.
(555) Choi, Y.; Jeong, H. J.; Liu, Q. F.; Oh, S. T.; Koo, B.-S.; Kim, Y.; Chung, I.-W.; Kim, Y. S.; Jeon, S. Clozapine Improves Memory Impairment and Reduces Aβ Level in the Tg-APPswe/PS1dE9 Mouse Model of Alzheimer's Disease. *Mol. Neurobiol.* **2017**, *54* (1), 450–460. https://doi.org/10.1007/s12035-015-9636-x.
(556) Hui, L.; Soliman, M. L.; Geiger, N. H.; Miller, N. M.; Afghah, Z.; Lakpa, K. L.; Chen, X.; Geiger, J. D. Acidifying Endolysosomes Prevented Low-Density Lipoprotein-Induced Amyloidogenesis. *J. Alzheimer's Dis.* **2019**, *67* (1), 393–410. https://doi.org/10.3233/JAD-180941.
(557) Andrew, R. J.; Fisher, K.; Heesom, K. J.; Kellett, K. A. B.; Hooper, N. M. Quantitative Interaction Proteomics Reveals Differences in the Interactomes of Amyloid Precursor Protein Isoforms. *J. Neurochem.* **2019**, *149* (3), 399–412. https://doi.org/10.1111/jnc.14666.
(558) Noel, A.; Ingrand, S.; Barrier, L. Anti-Amyloidogenic Effects of Glycosphingolipid Synthesis Inhibitors Occur Independently of Ganglioside Alterations. *Mol. Cell. Neurosci.* **2016**, *75*, 63–70. https://doi.org/10.1016/j.mcn.2016.06.009.
(559) Noel, A.; Ingrand, S.; Barrier, L. Ganglioside and Related-Sphingolipid Profiles Are Altered in a Cellular Model of Alzheimer's Disease. *Biochimie* **2017**, *137*, 158–164. https://doi.org/10.1016/j.biochi.2017.03.019.
(560) Osenkowski, P.; Ye, W.; Wang, R.; Wolfe, M. S.; Selkoe, D. J. Direct and Potent Regulation of γ-Secretase by Its Lipid Microenvironment. *Journal of Biological Chemistry*. **2008**, pp 22529–22540. https://doi.org/10.1074/jbc.M801925200.
(561) Holmes, O.; Paturi, S.; Ye, W.; Wolfe, M. S.; Selkoe, D. J. Effects of Membrane Lipids on the Activity and Processivity of Purified Gamma-Secretase. *Biochemistry* **2012**, *51* (17), 3565–3575. https://doi.org/10.1021/bi300303g
(562) Kang, M. S.; Baek, S.-H.; Chun, Y. S.; Moore, A. Z.; Landman, N.; Berman, D.; Yang, H. O.; Morishima-Kawashima, M.; Osawa, S.; Funamoto, S.; et al. Modulation of Lipid Kinase PI4KIIalpha Activity and Lipid Raft Association of Presenilin 1 Underlies Gamma-Secretase Inhibition by Ginsenoside (20S)-Rg3. *J. Biol. Chem.* **2013**, *288* (29), 20868–20882. https://doi.org/10.1074/jbc.M112.445734.
(563) Hartley, S. L.; Handen, B. L.; Devenny, D.; Mihaila, I.; Hardison, R.; Lao, P. J.; Klunk, W. E.; Bulova, P.; Johnson, S. C.; Christian, B. T. Cognitive Decline and Brain Amyloid-β Accumulation across 3 Years in Adults with Down Syndrome. *Neurobiol. Aging* **2017**, *58*, 68–76. https://doi.org/10.1016/J.NEUROBIOLAGING.2017.05.019.
(564) Colacurcio, D. J.; Pensalfini, A.; Jiang, Y.; Nixon, R. A. Dysfunction of Autophagy and Endosomal-Lysosomal Pathways: Roles in Pathogenesis of Down Syndrome and Alzheimer's Disease. *Free Radical Biology and Medicine*. Pergamon January 1, **2018**, pp 40–51. https://doi.org/10.1016/j.freeradbiomed.2017.10.001.
(565) Ying, J.; Sato, Y.; Im, E.; Berg, M.; Bordi, M.; Darji, S.; Kumar, A.; Mohan, P. S.; Bandyopadhyay, U.; Diaz, A.; et al. Lysosomal Dysfunction in Down Syndrome Is APP-Dependent and Mediated by APP-BCTF (C99). *J. Neurosci.* **2019**, *39* (27), 0578-19. https://doi.org/10.1523/JNEUROSCI.0578-19.2019.
(566) Boot, R. G.; Verhoek, M.; Donker-Koopman, W.; Strijland, A.; van Marle, J.; Overkleeft, H. S.; Wennekes, T.; Aerts, J. M. F. G. Identification of the Non-Lysosomal Glucosylceramidase as ß-Glucosidase 2. *J. Biol. Chem.* **2007**, *282* (2), 1305–1312. https://doi.org/10.1074/jbc.M610544200.
(567) Aguisanda, F.; Yeh, C. D.; Chen, C. Z.; Li, R.; Beers, J.; Zou, J.; Thorne, N.; Zheng, W. Neural Stem Cells for Disease Modeling of Wolman Disease and Evaluation of Therapeutics. *Orphanet J. Rare Dis.* **2017**, *12* (1), 120. https://doi.org/10.1186/s13023-017-0670-9.
(568) Parmar, M.; Rawson, S.; Scarff, C. A.; Goldman, A.; Dafforn, T. R.; Muench, S. P.; Postis, V. L. G. Using a SMALP Platform to Determine a Sub-Nm Single Particle Cryo-EM Membrane Protein Structure. *Biochim. Biophys. Acta - Biomembr.* **2018**, *1860* (2), 378–383. https://doi.org/10.1016/j.bbamem.2017.10.005.
(569) Lee, S. C.; Knowles, T. J.; Postis, V. L. G.; Jamshad, M.; Parslow, R. A.; Lin, Y. P.;

Goldman, A.; Sridhar, P.; Overduin, M.; Muench, S. P.; et al. A Method for Detergent-Free Isolation of Membrane Proteins in Their Local Lipid Environment. *Nat. Protoc.* **2016**, *11* (7), 1149–1162. https://doi.org/10.1038/nprot.2016.070.

(570) Körschen, H. G.; Yildiz, Y.; Raju, D. N.; Schonauer, S.; Bönigk, W.; Jansen, V.; Kremmer, E.; Kaupp, U. B.; Wachten, D. The Non-Lysosomal ß-Glucosidase GBA2 Is a Non-Integral Membrane-Associated Protein at the Endoplasmic Reticulum (ER) and Golgi. *J. Biol. Chem.* **2013**, *288* (5), 3381–3393. https://doi.org/10.1074/jbc.M112.414714.

(571) Norez, C.; Noel, S.; Wilke, M.; Bijvelds, M.; Jorna, H.; Melin, P.; Dejonge, H.; Becq, F. Rescue of Functional DelF508-CFTR Channels in Cystic Fibrosis Epithelial Cells by the α-Glucosidase Inhibitor Miglustat. *FEBS Lett.* **2006**, *580* (8), 2081–2086. https://doi.org/10.1016/j.febslet.2006.03.010.

(572) Abu-Arish, A.; Pandzic, E.; Goepp, J.; Matthes, E.; Hanrahan, J. W.; Wiseman, P. W. Cholesterol Modulates CFTR Confinement in the Plasma Membrane of Primary Epithelial Cells. *Biophys. J.* **2015**, *109* (1), 85–94. https://doi.org/https://doi.org/10.1016/j.bpj.2015.04.042.

(573) Ma, T.; Thiagarajah, J. R.; Yang, H.; Sonawane, N. D.; Folli, C.; Galietta, L. J. V; Verkman, A. S. Thiazolidinone CFTR Inhibitor Identified by High-Throughput Screening Blocks Cholera Toxin-Induced Intestinal Fluid Secretion. *J. Clin. Invest.* **2002**, *110* (11), 1651–1658. https://doi.org/10.1172/JCI16112.

(574) Lloyd-Evans, E.; Pelled, D.; Riebeling, C.; Bodennec, J.; de-Morgan, A.; Waller, H.; Schiffmann, R.; Futerman, A. H. Glucosylceramide and Glucosylsphingosine Modulate Calcium Mobilization from Brain Microsomes via Different Mechanisms. *J. Biol. Chem.* **2003**, *278* (26), 23594–23599. https://doi.org/10.1074/jbc.M300212200.

(575) Nelson, K. M.; Dahlin, J. L.; Bisson, J.; Graham, J.; Pauli, G. F.; Walters, M. A. The Essential Medicinal Chemistry of Curcumin. *J. Med. Chem.* **2017**, *60* (5), 1620–1637. https://doi.org/10.1021/acs.jmedchem.6b00975.

(576) Aits, S.; Jäättelä, M.; Nylandsted, J. Methods for the Quantification of Lysosomal Membrane Permeabilization: A Hallmark of Lysosomal Cell Death. *Methods Cell Biol.* **2015**, *126*, 261–285. https://doi.org/10.1016/bs.mcb.2014.10.032.

(577) Soyombo, A. A.; Tjon-Kon-Sang, S.; Rbaibi, Y.; Bashllari, E.; Bisceglia, J.; Muallem, S.; Kiselyov, K. TRP-ML1 Regulates Lysosomal PH and Acidic Lysosomal Lipid Hydrolytic Activity. *J. Biol. Chem.* **2006**, *281* (11), 7294–7301. https://doi.org/10.1074/jbc.M508211200.

(578) Cunningham, M.; Tang, J. Purification and Properties of Cathepsin D from Porcine Spleen. *J. Biol. Chem.* **1976**, *251* (15), 4528–4536.

(579) Pohl, J.; Davinic, S.; Bláha, I.; Štrop, P.; Kostka, V. Chromophoric and Fluorophoric Peptide Substrates Cleaved through the Dipeptidyl Carboxypeptidase Activity of Cathepsin B. *Anal. Biochem.* **1987**, *165* (1), 96–101. https://doi.org/10.1016/0003-2697(87)90205-3.

(580) SenthilKumar, G.; Skiba, J. H.; Kimple, R. J. High-Throughput Quantitative Detection of Basal Autophagy and Autophagic Flux Using Image Cytometry. *Biotechniques* **2019**, *67* (2), 70–73. https://doi.org/10.2144/btn-2019-0044.

(581) Zaidi, M.; Li, J.; Keutzer, J.; Mistry, P. K.; Liu, J.; Jain, D.; New, M. I.; Stachnik, A.; Yuen, T.; Lu, P.; et al. Glucocerebrosidase 2 Gene Deletion Rescues Type 1 Gaucher Disease. *Proc. Natl. Acad. Sci.* **2014**, *111* (13), 4934–4939. https://doi.org/10.1073/pnas.1400768111.

(582) Williamson, C. D.; Wong, D. S.; Bozidis, P.; Zhang, A.; Colberg-Poley, A. M. Isolation of Endoplasmic Reticulum, Mitochondria, and Mitochondria-Associated Membrane and Detergent Resistant Membrane Fractions from Transfected Cells and from Human Cytomegalovirus-Infected Primary Fibroblasts. In *Current Protocols in Cell Biology*; John Wiley & Sons, Inc.: Hoboken, NJ, USA, **2015**; Vol. 68, p 3.27.1-3.27.33. https://doi.org/10.1002/0471143030.cb0327s68.

(583) Kobayashi, T. T.; Beuchat, M.-H.; Chevallier, J.; Makino, A.; Mayran, N.; Escola, J.-M.; Lebrand, C.; Cosson, P.; Kobayashi, T. T.; Gruenberg, J. Separation and Characterization of Late Endosomal Membrane Domains. *J. Biol. Chem.* **2002**, *277* (35), 32157–32164. https://doi.org/10.1074/jbc.M202838200.

(584) Sidransky, E.; Lopez, G. The Link between the GBA Gene and Parkinsonism. *Lancet Neurol.* **2012**, *11* (11), 986–998. https://doi.org///dx.doi.org/10.1016/S1474-4422(12)70190-

4.
(585) Hockey, L. N.; Kilpatrick, B. S.; Eden, E. R.; Lin-Moshier, Y.; Brailoiu, G. C.; Brailoiu, E.; Futter, C. E.; Schapira, A. H.; Marchant, J. S.; Patel, S. Dysregulation of Lysosomal Morphology by Pathogenic LRRK2 Is Corrected by TPC2 Inhibition. *J. Cell Sci.* **2015**, *128* (2), 232–238. https://doi.org/10.1242/jcs.164152.
(586) Dehay, B.; Ramirez, A.; Martinez-Vicente, M.; Perier, C.; Canron, M. H.; Doudnikoff, E.; Vital, A.; Vila, M.; Klein, C.; Bezard, E. Loss of P-Type ATPase ATP13A2/PARK9 Function Induces General Lysosomal Deficiency and Leads to Parkinson Disease Neurodegeneration. *Proc. Natl. Acad. Sci.* **2012**, *109* (24), 9611–9616. https://doi.org/10.1073/pnas.1112368109.
(587) Brodeur, G. M.; Green, A. A.; Hayes, F. A.; Williams, K. J.; Williams, D. L.; Tsiatis, A. A. Cytogenetic Features of Human Neuroblastomas and Cell Lines. *Cancer Res.* **1981**, *41*, 4678–4686.
(588) Dekker, N.; van Dussen, L.; Hollak, C. E. M.; Overkleeft, H.; Scheij, S.; Ghauharali, K.; van Breemen, M. elle J.; Ferraz, M. J.; Groener, J. E. M.; Maas, M.; et al. Elevated Plasma Glucosylsphingosine in Gaucher Disease: Relation to Phenotype, Storage Cell Markers, and Therapeutic Response. *Blood* **2011**, *118* (16), e127. https://doi.org/10.1182/blood-2011-05-352971.
(589) Puglielli, L.; Ellis, B. C.; Saunders, A. J.; Kovacs, D. M. Ceramide Stabilizes β-Site Amyloid Precursor Protein-Cleaving Enzyme 1 and Promotes Amyloid β-Peptide Biogenesis. *J. Biol. Chem.* **2003**, *278* (22), 19777–19783. https://doi.org/10.1074/jbc.M300466200.
(590) Mirzaian, M.; Wisse, P.; Ferraz, M. J.; Marques, A. R. A.; Gaspar, P.; Oussoren, S. V.; Kytidou, K.; Codée, J. D. C.; van der Marel, G.; Overkleeft, H. S.; et al. Simultaneous Quantitation of Sphingoid Bases by UPLC-ESI-MS/MS with Identical 13C-Encoded Internal Standards. *Clin. Chim. Acta* **2017**, *466*, 178–184. https://doi.org/10.1016/J.CCA.2017.01.014.
(591) Biasini, M.; Bienert, S.; Waterhouse, A.; Arnold, K.; Studer, G.; Schmidt, T.; Kiefer, F.; Cassarino, T. G.; Bertoni, M.; Bordoli, L.; et al. SWISS-MODEL: Modelling Protein Tertiary and Quaternary Structure Using Evolutionary Information. *Nucleic Acids Res.* **2014**, *42* (W1), W252–W258. https://doi.org/10.1093/nar/gku340.
(592) Guo, R.; Zong, S.; Wu, M.; Gu, J.; Yang, M. Architecture of Human Mitochondrial Respiratory Megacomplex I2III2IV2. *Cell* **2017**, *170* (6), 1247–1257.e12. https://doi.org/10.1016/j.cell.2017.07.050.
(593) Pesta, D.; Gnaiger, E. High-Resolution Respirometry: OXPHOS Protocols for Human Cells and Permeabilized Fibers from Small Biopsies of Human Muscle. *Methods Mol. Biol.* **2012**, *810*, 25–58. https://doi.org/10.1007/978-1-61779-382-0_3].
(594) Lucken-Ardjomande, S.; Montessuit, S.; Martinou, J. C. Bax Activation and Stress-Induced Apoptosis Delayed by the Accumulation of Cholesterol in Mitochondrial Membranes. *Cell Death Differ.* **2008**, *15* (3), 484–493. https://doi.org/10.1038/sj.cdd.4402280.
(595) Wos, M.; Szczepanowska, J.; Pikula, S.; Tylki-Szymanska, A.; Zablocki, K.; Bandorowicz-Pikula, J. Mitochondrial Dysfunction in Fibroblasts Derived from Patients with Niemann-Pick Type C Disease. *Arch. Biochem. Biophys.* **2016**, *593*, 50–59. https://doi.org///dx.doi.org/10.1016/j.abb.2016.02.012.
(596) Hassoun, S. M.; Lancel, S.; Petillot, P.; Decoster, B.; Favory, R.; Marchetti, P.; Neviere, R. Sphingosine Impairs Mitochondrial Function by Opening Permeability Transition Pore. *Mitochondrion* **2006**, *6* (3), 149–154. https://doi.org///doi.org/10.1016/j.mito.2006.05.001.
(597) Novgorodov, S. A.; Riley, C. L.; Yu, J.; Borg, K. T.; Hannun, Y. A.; Proia, R. L.; Kindy, M. S.; Gudz, T. I. Essential Roles of Neutral Ceramidase and Sphingosine in Mitochondrial Dysfunction Due to Traumatic Brain Injury. *J. Biol. Chem.* **2014**, *289* (19), 13142–13154. https://doi.org/10.1074/jbc.M113.530311.
(598) Strasberg, P. Cerebrosides and Psychosine Disrupt Mitochondrial Functions. *Biochem. Cell Biol.* **1986**, *64* (5), 485–489. https://doi.org/10.1139/o86-067.
(599) Osellame, L. D.; Rahim, A. A.; Hargreaves, I. P.; Gegg, M. E.; Richard-Londt, A.; Brandner, S.; Waddington, S. N.; Schapira, A. H. V; Duchen, M. R. Mitochondria and Quality Control Defects in a Mouse Model of Gaucher Disease—Links to Parkinson's Disease. *Cell Metab.* **2013**, *17* (6), 941–953. https://doi.org///dx.doi.org/10.1016/j.cmet.2013.04.014.
(600) Vilaça, R.; Barros, I.; Matmati, N.; Silva, E.; Martins, T.; Teixeira, V.; Hannun, Y. A.; Costa,

V. The Ceramide Activated Protein Phosphatase Sit4 Impairs Sphingolipid Dynamics, Mitochondrial Function and Lifespan in a Yeast Model of Niemann-Pick Type C1. *Biochim. Biophys. Acta - Mol. Basis Dis.* **2018**, *1864* (1), 79–88. https://doi.org/10.1016/J.BBADIS.2017.10.010.

(601) Vilaça, R.; Silva, E.; Nadais, A.; Teixeira, V.; Matmati, N.; Gaifem, J.; Hannun, Y. A.; Sá Miranda, M. C.; Costa, V. Sphingolipid Signalling Mediates Mitochondrial Dysfunctions and Reduced Chronological Lifespan in the Yeast Model of Niemann-Pick Type C1. *Mol. Microbiol.* **2014**, *91* (3), 438–451. https://doi.org/10.1111/mmi.12470.

(602) Vienken, H.; Mabrouki, N.; Grabau, K.; Claas, R. F.; Rudowski, A.; Schömel, N.; Pfeilschifter, J.; Lütjohann, D.; van Echten-Deckert, G.; Meyer, zu H. Characterization of Cholesterol Homeostasis in Sphingosine-1-Phosphate Lyase-Deficient Fibroblasts Reveals a Niemann-Pick Disease Type C-like Phenotype with Enhanced Lysosomal Ca2+ Storage. *Sci. Rep.* **2017**, *7*, 43575.

(603) Martín-Montañez, E.; Pavia, J.; Valverde, N.; Boraldi, F.; Lara, E.; Oliver, B.; Hurtado-Guerrero, I.; Fernandez, O.; Garcia-Fernandez, M. The S1P Mimetic Fingolimod Phosphate Regulates Mitochondrial Oxidative Stress in Neuronal Cells. *Free Radic. Biol. Med.* **2019**, *137*, 116–130. https://doi.org/10.1016/j.freeradbiomed.2019.04.022.

(604) Zigdon, H.; Kogot-Levin, A.; Park, J.-W.; Goldschmidt, R.; Kelly, S.; Merrill, A. H.; Scherz, A.; Pewzner-Jung, Y.; Saada, A.; Futerman, A. H. Ablation of Ceramide Synthase 2 Causes Chronic Oxidative Stress Due to Disruption of the Mitochondrial Respiratory Chain. *J. Biol. Chem.* **2013**, *288* (7), 4947–4956. https://doi.org/10.1074/jbc.M112.402719.

(605) Kiselyov, K.; Muallem, S. Mitochondrial Ca2+ Homeostasis in Lysosomal Storage Diseases. *Cell Calcium* **2008**, *44* (1), 103–111. https://doi.org///dx.doi.org/10.1016/j.ceca.2007.12.005.

(606) Wagner, N.; Stephan, M.; Hoglinger, D.; Nadler, A. A Click Cage: Organelle-Specific Uncaging of Lipid Messengers. *Angew. Chem. Int. Ed. Engl.* **2018**, *57* (40), 13339–13343. https://doi.org/10.1002/anie.201807497.

(607) Strub, G. M.; Paillard, M.; Liang, J.; Gomez, L.; Allegood, J. C.; Hait, N. C.; Maceyka, M.; Price, M. M.; Chen, Q.; Simpson, D. C.; et al. Sphingosine-1-Phosphate Produced by Sphingosine Kinase 2 in Mitochondria Interacts with Prohibitin 2 to Regulate Complex IV Assembly and Respiration. *FASEB J.* **2010**, *25* (2), 600–612. https://doi.org/10.1096/fj.10-167502.

(608) Cohen, G.; Kesler, N. Monoamine Oxidase and Mitochondrial Respiration. *J. Neurochem.* **1999**, *73* (6), 2310–2315. https://doi.org/10.1046/j.1471-4159.1999.0732310.x.

(609) Voccoli, V.; Tonazzini, I.; Signore, G.; Caleo, M.; Cecchini, M. Role of Extracellular Calcium and Mitochondrial Oxygen Species in Psychosine-Induced Oligodendrocyte Cell Death. *Cell Death &Amp; Dis.* **2014**, *5*, e1529.

(610) Annunziata, I.; Sano, R.; d'Azzo, A. Mitochondria-Associated ER Membranes (MAMs) and Lysosomal Storage Diseases. *Cell Death Dis.* **2018**, *9* (3), 328. https://doi.org/10.1038/s41419-017-0025-4.

(611) Hanada, K. Erratum: Lipid-Transfer Proteins Rectify Inter-Organelle Flux and Accurately Deliver Lipids at Membrane Contact Sites. *J. Lipid Res.* **2018**, *59* (10), 2034–2034. https://doi.org/10.1194/jlr.r085324err.

(612) Novgorodov, S. A.; Voltin, J. R.; Wang, W.; Tomlinson, S.; Riley, C. L.; Gudz, T. I. Acid Sphingomyelinase Deficiency Protects Mitochondria and Improves Function Recovery after Brain Injury. *J. Lipid Res.* **2019**, *60* (3), 609–623. https://doi.org/10.1194/jlr.m091132.

(613) Zhang, M.; Liu, P.; Dwyer, N. K.; Christenson, L. K.; Fujimoto, T.; Martinez, F.; Comly, M.; Hanover, J. A.; Joan Blanchette-Mackie, E.; Strauss, J. F. MLN64 Mediates Mobilization of Lysosomal Cholesterol to Steroidogenic Mitochondria. *J. Biol. Chem.* **2002**, *277* (36), 33300–33310. https://doi.org/10.1074/jbc.M200003200.

(614) Elbaz-Alon, Y.; Rosenfeld-Gur, E.; Shinder, V.; Futerman, A. H.; Geiger, T.; Schuldiner, M. A Dynamic Interface between Vacuoles and Mitochondria in Yeast. *Dev. Cell* **2014**, *30* (1), 95–102. https://doi.org/10.1016/j.devcel.2014.06.007.

(615) Lee, H. S.; Zhang, Y. BSP-SLIM: A Blind Low-Resolution Ligand-Protein Docking Approach Using Predicted Protein Structures. *Proteins Struct. Funct. Bioinforma.* **2012**, *80* (1), 93–110. https://doi.org/10.1002/prot.23165.

(616) Peters, C.; Tsirigos, K. D.; Shu, N.; Elofsson, A. Improved Topology Prediction Using the

Terminal Hydrophobic Helices Rule. *Bioinformatics* **2015**, *32* (8), 1158–1162. https://doi.org/10.1093/bioinformatics/btv709.
(617) Thorsell, A. G.; Lee, W. H.; Persson, C.; Siponen, M. I.; Nilsson, M.; Busam, R. D.; Kotenyova, T.; Schüler, H.; Lehtiö, L. Comparative Structural Analysis of Lipid Binding START Domains. *PLoS One* **2011**, *6* (6), e19521. https://doi.org/10.1371/journal.pone.0019521.
(618) Sluchanko, N. N.; Tugaeva, K. V.; Maksimov, E. G. Solution Structure of Human Steroidogenic Acute Regulatory Protein STARD1 Studied by Small-Angle X-Ray Scattering. *Biochem. Biophys. Res. Commun.* **2017**, *489* (4), 445–450. https://doi.org/10.1016/j.bbrc.2017.05.167.
(619) Iaea, D. B.; Dikiy, I.; Kiburu, I.; Eliezer, D.; Maxfield, F. R. STARD4 Membrane Interactions and Sterol Binding. *Biochemistry* **2015**, *54* (30), 4623–4636. https://doi.org/10.1021/acs.biochem.5b00618.
(620) Horenkamp, F. A.; Valverde, D. P.; Nunnari, J.; Reinisch, K. M. Molecular Basis for Sterol Transport by St ART -like Lipid Transfer Domains. *EMBO J.* **2018**, *37* (6). https://doi.org/10.15252/embj.201798002.
(621) Jentsch, J. A.; Kiburu, I.; Pandey, K.; Timme, M.; Ramlall, T.; Levkau, B.; Wu, J.; Eliezer, D.; Boudker, O.; Menon, A. K. Structural Basis of Sterol Binding and Transport by a Yeast StARkin Domain. *J. Biol. Chem.* **2018**, *293* (15), 5522–5531. https://doi.org/10.1074/jbc.RA118.001881.
(622) Tong, J.; Manik, M. K.; Im, Y. J. Structural Basis of Sterol Recognition and Nonvesicular Transport by Lipid Transfer Proteins Anchored at Membrane Contact Sites. *Proc. Natl. Acad. Sci.* **2018**, *115* (5), E856–E865. https://doi.org/10.1073/pnas.1719709115.
(623) Miteva, M. A.; Guyon, F.; Tuffery, P. Frog2: Efficient 3D Conformation Ensemble Generator for Small Compounds. *Nucleic Acids Res.* **2010**, *38* (Web Server issue), 622. https://doi.org/10.1093/nar/gkq325.
(624) Gudz, T. I.; Tserng, K. Y.; Hoppel, C. L. Direct Inhibition of Mitochondrial Respiratory Chain Complex III by Cell-Permeable Ceramide. *J. Biol. Chem.* **1997**, *272* (39), 24154–24158.
(625) Arrowsmith, C. H.; Audia, J. E.; Austin, C.; Baell, J.; Bennett, J.; Blagg, J.; Bountra, C.; Brennan, P. E.; Brown, P. J.; Bunnage, M. E.; et al. The Promise and Peril of Chemical Probes. *Nat. Chem. Biol.* **2015**, *11* (8), 536–541. https://doi.org/10.1038/nchembio.1867.
(626) Cleeter, M. W. J.; Chau, K.-Y.; Gluck, C.; Mehta, A.; Hughes, D. A.; Duchen, M.; Wood, N. W.; Hardy, J.; Mark Cooper, J.; Schapira, A. H. Glucocerebrosidase Inhibition Causes Mitochondrial Dysfunction and Free Radical Damage. *Neurochem. Int.* **2013**, *62* (1), 1–7. https://doi.org///dx.doi.org/10.1016/j.neuint.2012.10.010.
(627) Kamani, M.; Mylvaganam, M.; Tian, R.; Rigat, B.; Binnington, B.; Lingwood, C. Adamantyl Glycosphingolipids Provide a New Approach to the Selective Regulation of Cellular Glycosphingolipid Metabolism. *J. Biol. Chem.* **2011**, *286* (24), 21413–21426. https://doi.org/10.1074/jbc.M110.207670.
(628) Cho, K. H.; Kim, M. W.; Kim, S. U. Tissue Culture Model of Krabbe's Disease: Psychosine Cytotoxicity in Rat Oligodendrocyte Culture. *Dev. Neurosci.* **1997**, *19* (4), 321–327. https://doi.org/10.1159/000111228.
(629) Elustondo, P.; Martin, L. A.; Karten, B. Mitochondrial Cholesterol Import. *Biochim. Biophys. Acta* **2017**, *1862* (1), 90–101. https://doi.org/10.1016/j.bbalip.2016.08.012.
(630) Scharwey, M.; Tatsuta, T.; Langer, T. Mitochondrial Lipid Transport at a Glance. *J. Cell Sci.* **2013**, *126* (23), 5317–5323. https://doi.org/10.1242/jcs.134130.
(631) Gilquin, B.; Taillebourg, E.; Cherradi, N.; Hubstenberger, A.; Gay, O.; Merle, N.; Assard, N.; Fauvarque, M.-O.; Tomohiro, S.; Kuge, O.; et al. The AAA+ ATPase ATAD3A Controls Mitochondrial Dynamics at the Interface of the Inner and Outer Membranes. *Mol. Cell. Biol.* **2010**, *30* (8), 1984–1996. https://doi.org/10.1128/MCB.00007-10.
(632) Akula, N.; Midzak, A.; Lecanu, L.; Papadopoulos, V. Identification of Small-Molecule Inhibitors of the Steroidogenic Acute Regulatory Protein (STARD1) by Structure-Based Design. *Bioorganic Med. Chem. Lett.* **2012**, *22* (12), 4139–4143. https://doi.org/10.1016/j.bmcl.2012.04.058.
(633) Arakane, F.; King, S. R.; Du, Y.; Kallen, C. B.; Walsh, L. P.; Watari, H.; Stocco, D. M.; Strauss, J. F. Phosphorylation of Steroidogenic Acute Regulatory Protein (StAR) Modulates

Its Steroidogenic Activity. *J. Biol. Chem.* **1997**, *272* (51), 32656–32662. https://doi.org/10.1074/jbc.272.51.32656.
(634) Favari, E.; Zanotti, I.; Zimetti, F.; Ronda, N.; Bernini, F.; Rothblat, G. H. Probucol Inhibits ABCA1-Mediated Cellular Lipid Efflux. *Arterioscler. Thromb. Vasc. Biol.* **2004**, *24* (12), 2345–2350. https://doi.org/10.1161/01.ATV.0000148706.15947.8a.
(635) Rostovtseva, T. K.; Bezrukov, S. M. ATP Transport through a Single Mitochondrial Channel, VDAC, Studied by Current Fluctuation Analysis. *Biophys. J.* **1998**, *74* (5), 2365–2373.
(636) Hiller, S.; Garces, R. G.; Malia, T. J.; Orekhov, V. Y.; Colombini, M.; Wagner, G. Solution Structure of the Integral Human Membrane Protein VDAC-1 in Detergent Micelles. *Science* **2008**, *321* (5893), 1206–1210. https://doi.org/10.1126/science.1161302.
(637) Weiser, B. P.; Salari, R.; Eckenhoff, R. G.; Brannigan, G. Computational Investigation of Cholesterol Binding Sites on Mitochondrial VDAC. *J. Phys. Chem. B* **2014**, *118* (33), 9852–9860. https://doi.org/10.1021/jp504516a.
(638) Budelier, M. M.; Cheng, W. W. L.; Bergdoll, L.; Chen, Z.-W.; Janetka, J. W.; Abramson, J.; Krishnan, K.; Mydock-McGrane, L.; Covey, D. F.; Whitelegge, J. P.; et al. Photoaffinity Labeling with Cholesterol Analogues Precisely Maps a Cholesterol-Binding Site in Voltage-Dependent Anion Channel-1. *J. Biol. Chem.* **2017**, *292* (22), 9294–9304. https://doi.org/10.1074/jbc.M116.773069.
(639) Hosaka, T.; Okazaki, M.; Kimura-Someya, T.; Ishizuka-Katsura, Y.; Ito, K.; Yokoyama, S.; Dodo, K.; Sodeoka, M.; Shirouzu, M. Crystal Structural Characterization Reveals Novel Oligomeric Interactions of Human Voltage-Dependent Anion Channel 1. *Protein Sci.* **2017**, *26* (9), 1749–1758. https://doi.org/10.1002/pro.3211.
(640) Ferens, F. G.; Patel, T. R.; Oriss, G.; Court, D. A.; Stetefeld, J. A Cholesterol Analog Induces an Oligomeric Reorganization of VDAC. *Biophys. J.* **2019**, *116* (5), 847–859. https://doi.org/10.1016/j.bpj.2019.01.031.
(641) Unten, Y.; Murai, M.; Yamamoto, T.; Watanabe, A.; Ichimaru, N.; Aburaya, S.; Aoki, W.; Shinohara, Y.; Miyoshi, H. Pentenediol-Type Compounds Specifically Bind to Voltage-Dependent Anion Channel 1 in Saccharomyces Cerevisiae Mitochondria. *Biochemistry* **2019**, *58* (8), 1141–1154. https://doi.org/10.1021/acs.biochem.8b01209.
(642) Jaremko, M.; Jaremko, Ł.; Giller, K.; Becker, S.; Zweckstetter, M. Structural Integrity of the A147T Polymorph of Mammalian TSPO. *ChemBioChem* **2015**, *16* (10), 1483–1489. https://doi.org/10.1002/cbic.201500217.
(643) Kim, T. H.; Pae, A. N. Translocator Protein (TSPO) Ligands for the Diagnosis or Treatment of Neurodegenerative Diseases: A Patent Review (2010–2015; Part 1). *Expert Opinion on Therapeutic Patents*. Taylor & Francis November 1, **2016**, pp 1325–1351. https://doi.org/10.1080/13543776.2016.1230606.
(644) Guilarte, T. R. TSPO in Diverse CNS Pathologies and Psychiatric Disease: A Critical Review and a Way Forward. *Pharmacol. Ther.* **2019**, *194*, 44–58. https://doi.org/10.1016/J.PHARMTHERA.2018.09.003.
(645) Barron, A. M.; Garcia-Segura, L. M.; Caruso, D.; Jayaraman, A.; Lee, J.-W.; Melcangi, R. C.; Pike, C. J. Ligand for Translocator Protein Reverses Pathology in a Mouse Model of Alzheimer's Disease. *J. Neurosci.* **2013**, *33* (20), 8891–8897. https://doi.org/10.1523/JNEUROSCI.1350-13.2013.
(646) Christensen, A.; Pike, C. J. TSPO Ligand PK11195 Improves Alzheimer-Related Outcomes in Aged Female 3xTg-AD Mice. *Neurosci. Lett.* **2018**, *683*, 7–12. https://doi.org/10.1016/J.NEULET.2018.06.029.
(647) Selvaraj, V.; Stocco, D. M. The Changing Landscape in Translocator Protein (TSPO) Function. *Trends Endocrinol. Metab.* **2015**, *26* (7), 341–348. https://doi.org/10.1016/j.tem.2015.02.007.
(648) Jamin, N.; Neumann, J.-M.; Ostuni, M. A.; Vu, T. K. N.; Yao, Z.-X.; Murail, S.; Robert, J.-C.; Giatzakis, C.; Papadopoulos, V.; Lacapère, J.-J. Characterization of the Cholesterol Recognition Amino Acid Consensus Sequence of the Peripheral-Type Benzodiazepine Receptor. *Mol. Endocrinol.* **2004**, *19* (3), 588–594. https://doi.org/10.1210/me.2004-0308.
(649) Jaipuria, G.; Giller, K.; Leonov, A.; Becker, S.; Zweckstetter, M. Insights into Cholesterol/Membrane Protein Interactions Using Paramagnetic Solid-State NMR. *Chem. - A Eur. J.* **2018**, *24* (66), 17606–17611. https://doi.org/10.1002/chem.201804550.

(650) Rupprecht, R.; Papadopoulos, V.; Rammes, G.; Baghai, T. C.; Fan, J.; Akula, N.; Groyer, G.; Adams, D.; Schumacher, M. Translocator Protein (18 KDa) (TSPO) as a Therapeutic Target for Neurological and Psychiatric Disorders. *Nat. Rev. Drug Discov.* **2010**, *9* (12), 971–988. https://doi.org/10.1038/nrd3295.

(651) Biswas, L.; Zhou, X.; Dhillon, B.; Graham, A.; Shu, X. Retinal Pigment Epithelium Cholesterol Efflux Mediated by the 18 KDa Translocator Protein, TSPO, a Potential Target for Treating Age-Related Macular Degeneration. *Hum. Mol. Genet.* **2017**, *26* (22), 4327–4339. https://doi.org/10.1093/hmg/ddx319.

(652) Biswas, L.; Farhan, F.; Reilly, J.; Bartholomew, C.; Shu, X. TSPO Ligands Promote Cholesterol Efflux and Suppress Oxidative Stress and Inflammation in Choroidal Endothelial Cells. *Int. J. Mol. Sci.* **2018**, *19* (12), 3740. https://doi.org/10.3390/ijms19123740.

(653) Taylor, J. M. W.; Allen, A.-M.; Graham, A. Targeting Mitochondrial 18 KDa Translocator Protein (TSPO) Regulates Macrophage Cholesterol Efflux and Lipid Phenotype. *Clin. Sci.* **2014**, *127* (10), 603–613. https://doi.org/10.1042/CS20140047.

(654) Falchi, A. M.; Battetta, B.; Sanna, F.; Piludu, M.; Sogos, V.; Serra, M.; Melis, M.; Putzolu, M.; Diaz, G. Intracellular Cholesterol Changes Induced by Translocator Protein (18 KDa) TSPO/PBR Ligands. *Neuropharmacology* **2007**, *53* (2), 318–329. https://doi.org/10.1016/j.neuropharm.2007.05.016.

(655) Gatliff, J.; East, D. A.; Singh, A.; Alvarez, M. S.; Frison, M.; Matic, I.; Ferraina, C.; Sampson, N.; Turkheimer, F.; Campanella, M. A Role for TSPO in Mitochondrial Ca2+homeostasis and Redox Stress Signaling. *Cell Death Dis.* **2017**, *8* (6), e2896. https://doi.org/10.1038/cddis.2017.186.

(656) Milenkovic, V. M.; Slim, D.; Bader, S.; Koch, V.; Heinl, E.-S.; Alvarez-Carbonell, D.; Nothdurfter, C.; Rupprecht, R.; Wetzel, C. H. CRISPR-Cas9 Mediated TSPO Gene Knockout Alters Respiration and Cellular Metabolism in Human Primary Microglia Cells. *Int. J. Mol. Sci.* **2019**, *20* (13), 3359. https://doi.org/10.3390/ijms20133359.

(657) Farges, R.; Joseph-Liauzun, E.; Shire, D.; Caput, D.; Le Fur, G.; Ferrara, P. Site-Directed Mutagenesis of the Peripheral Benzodiazepine Receptor: Identification of Amino Acids Implicated in the Binding Site of Ro5-4864. *Mol. Pharmacol.* **1994**, *46* (6), 1160–1167.

(658) Guo, Y.; Kalathur, R. C.; Liu, Q.; Kloss, B.; Bruni, R.; Ginter, C.; Kloppmann, E.; Rost, B.; Hendrickson, W. A. Protein Structure. Structure and Activity of Tryptophan-Rich TSPO Proteins. *Science.* **2015**, *347* (6221), 551–555. https://doi.org/10.1126/science.aaa1534.

(659) Costa, B.; Cavallini, C.; Da Pozzo, E.; Taliani, S.; Da Settimo, F.; Martini, C. The Anxiolytic Etifoxine Binds to TSPO Ro5-4864 Binding Site with Long Residence Time Showing a High Neurosteroidogenic Activity. *ACS Chem. Neurosci.* **2017**, *8* (7), 1448–1454. https://doi.org/10.1021/acschemneuro.7b00027.

(660) Verleye, M.; Akwa, Y.; Liere, P.; Ladurelle, N.; Pianos, A.; Eychenne, B.; Schumacher, M.; Gillardin, J. M. The Anxiolytic Etifoxine Activates the Peripheral Benzodiazepine Receptor and Increases the Neurosteroid Levels in Rat Brain. *Pharmacol. Biochem. Behav.* **2005**, *82* (4), 712–720. https://doi.org/S0091-3057(05)00373-4.

(661) Snell, C. R.; Snell, P. H. Benzodiazepines Modulate the A2 Adenosine Binding Sites on 108CC15 Neuroblastoma X Glioma Hybrid Cells. *Br. J. Pharmacol.* **1984**, *83* (3), 791–798.

(662) Bader, S.; Wolf, L.; Milenkovic, V. M.; Gruber, M.; Nothdurfter, C.; Rupprecht, R.; Wetzel, C. H. Differential Effects of TSPO Ligands on Mitochondrial Function in Mouse Microglia Cells. *Psychoneuroendocrinology* **2019**, *106*, 65–76. https://doi.org/10.1016/j.psyneuen.2019.03.029.

(663) Baixauli, F.; Acín-Pérez, R.; Villarroya-Beltrí, C.; Mazzeo, C.; Nuñez-Andrade, N.; Gabandé-Rodriguez, E.; Ledesma, M. D.; Blázquez, A.; Martin, M. A.; Falcón-Pérez, J. M.; et al. Mitochondrial Respiration Controls Lysosomal Function during Inflammatory t Cell Responses. *Cell Metab.* **2015**, *22* (3), 485–498. https://doi.org/10.1016/j.cmet.2015.07.020.

(664) Fernández-Mosquera, L.; DIogo, C. V.; Yambire, K. F.; Santos, G. L.; Luna Sánchez, M.; Bénit, P.; Rustin, P.; Lopez, L. C.; Milosevic, I.; Raimundo, N. Acute and Chronic Mitochondrial Respiratory Chain Deficiency Differentially Regulate Lysosomal Biogenesis. *Sci. Rep.* **2017**, *7* (1), 45076. https://doi.org/10.1038/srep45076.

(665) Fernandez-Mosquera, L.; Yambire, K. F.; Couto, R.; Pereyra, L.; Pabis, K.; Ponsford, A. H.; Diogo, C. V.; Stagi, M.; Milosevic, I.; Raimundo, N. Mitochondrial Respiratory Chain Deficiency Inhibits Lysosomal Hydrolysis. *Autophagy* **2019**, *15* (9), 1572–1591.

https://doi.org/10.1080/15548627.2019.1586256.
(666) Liu, R.; Lu, P.; Chu, J. W. K.; Sharom, F. J. Characterization of Fluorescent Sterol Binding to Purified Human NPC1. *J. Biol. Chem.* **2009**, *284* (3), 1840–1852. https://doi.org/10.1074/jbc.M803741200.
(667) Laskowski, M.; Augustynek, B.; Kulawiak, B.; Koprowski, P.; Bednarczyk, P.; Jarmuszkiewicz, W.; Szewczyk, A. What Do We Not Know about Mitochondrial Potassium Channels? *Biochim. Biophys. Acta - Bioenerg.* **2016**, *1857* (8), 1247–1257. https://doi.org/10.1016/j.bbabio.2016.03.007.
(668) Balderas, E.; Zhang, J.; Stefani, E.; Toro, L. Mitochondrial BKCa Channel. *Frontiers in Physiology*. Frontiers March 31, 2015, p 104. https://doi.org/10.3389/fphys.2015.00104.
(669) Kicinska, A.; Augustynek, B.; Kulawiak, B.; Jarmuszkiewicz, W.; Szewczyk, A.; Bednarczyk, P. A Large-Conductance Calcium-Regulated K + Channel in Human Dermal Fibroblast Mitochondria. *Biochem. J.* **2016**, *473* (23), 4457–4471. https://doi.org/10.1042/BCJ20160732.
(670) Bednarczyk, P.; Wieckowski, M. R.; Broszkiewicz, M.; Skowronek, K.; Siemen, D.; Szewczyk, A. Putative Structural and Functional Coupling of the Mitochondrial BKCa Channel to the Respiratory Chain. *PLoS One* **2013**, *8* (6), e68125. https://doi.org/10.1371/journal.pone.0068125.
(671) Kulawiak, B.; Kudin, A. P.; Szewczyk, A.; Kunz, W. S. BK Channel Openers Inhibit ROS Production of Isolated Rat Brain Mitochondria. *Exp. Neurol.* **2008**, *212* (2), 543–547. https://doi.org/10.1016/j.expneurol.2008.05.004.
(672) Augustynek, B.; Koprowski, P.; Rotko, D.; Kunz, W. S.; Szewczyk, A.; Kulawiak, B. Mitochondrial BK Channel Openers CGS7181 and CGS7184 Exhibit Cytotoxic Properties. *Int. J. Mol. Sci.* **2018**, *19* (2), 353. https://doi.org/10.3390/ijms19020353.
(673) Vanommeslaeghe, K.; Raman, E. P.; MacKerell, A. D. Automation of the CHARMM General Force Field (CGenFF) II: Assignment of Bonded Parameters and Partial Atomic Charges. *J. Chem. Inf. Model.* **2012**, *52* (12), 3155–3168. https://doi.org/10.1021/ci3003649.
(674) Höglinger, D.; Thomas, B.; Elena, S. H.; Hartwig, P.; Colaco, A.; Newton, J.; Futter, C.; Spiegel, S.; Platt, F.; Eden, E. NPC1 Regulates ER Contacts with Endocytic Organelles to Mediate Cholesterol Egress. *Nat. Commun.* **2019**, *review* (1), 4276. https://doi.org/10.1038/nchembio.1496.
(675) Winkler, M. B. L., Kidmose R.T., Szomek M., Rawson S., Muench, S.P., Wüstner., D., Pedersen, B. P. Structural Insight into Eukaryotic Sterol Transport through Niemann-Pick Type C Proteins. *Cell*. September 19, 2019. https://doi.org/10.1016/J.CELL.2019.08.038.
(676) Heybrock, S.; Kanerva, K.; Meng, Y.; Ing, C.; Liang, A.; Xiong, Z.-J.; Weng, X.; Ah Kim, Y.; Collins, R.; Trimble, W.; et al. Lysosomal Integral Membrane Protein-2 (LIMP-2/SCARB2) Is Involved in Lysosomal Cholesterol Export. *Nat. Commun.* **2019**, *10* (1), 3521. https://doi.org/10.1038/s41467-019-11425-0.
(677) Sandhu, J.; Li, S.; Fairall, L.; Pfisterer, S. G.; Gurnett, J. E.; Xiao, X.; Weston, T. A.; Vashi, D.; Ferrari, A.; Orozco, J. L.; et al. Aster Proteins Facilitate Nonvesicular Plasma Membrane to ER Cholesterol Transport in Mammalian Cells. *Cell* **2018**, *175* (2), 514–529.e20. https://doi.org/10.1016/j.cell.2018.08.033.
(678) Quazi, F.; Molday, R. S. Differential Phospholipid Substrates and Directional Transport by ATP-Binding Cassette Proteins ABCA1, ABCA7, and ABCA4 and Disease-Causing Mutants. *J. Biol. Chem.* **2013**, *288* (48), 34414–34426. https://doi.org/10.1074/jbc.M113.508812.
(679) Reboul, E.; Dyka, F. M.; Quazi, F.; Molday, R. S. Cholesterol Transport via ABCA1: New Insights from Solid-Phase Binding Assay. *Biochimie* **2013**, *95* (4), 957–961. https://doi.org/10.1016/j.biochi.2012.11.009.
(680) Courtney, K. C.; Pezeshkian, W.; Raghupathy, R.; Zhang, C.; Darbyson, A.; Ipsen, J. H.; Ford, D. A.; Khandelia, H.; Presley, J. F.; Zha, X. C24 Sphingolipids Govern the Transbilayer Asymmetry of Cholesterol and Lateral Organization of Model and Live-Cell Plasma Membranes. *Cell Rep.* **2018**, *24* (4), 1037–1049. https://doi.org/10.1016/j.celrep.2018.06.104.
(681) Pols, M. S.; Ten Brink, C.; Gosavi, P.; Oorschot, V.; Klumperman, J. The HOPS Proteins HVps41 and HVps39 Are Required for Homotypic and Heterotypic Late Endosome Fusion.

Traffic **2013**, *14* (2), 219–232. https://doi.org/10.1111/tra.12027.
(682) Wennekes, T.; Lang, B.; Leeman, M.; Van Der Marel, G. A.; Smits, E.; Weber, M.; Van Wiltenburg, J.; Wolberg, M.; Aerts, J. M. F. G.; Overkleeft, H. S. Large-Scale Synthesis of the Glucosylceramide Synthase Inhibitor N-[5-(Adamantan-1-Yl-Methoxy)-Pentyl]-1-Deoxynojirimycin. *Org. Process Res. Dev.* **2008**, *12* (3), 414–423. https://doi.org/10.1021/op700295x.
(683) Holm, L.; Sander, C. Dali: A Network Tool for Protein Structure Comparison. *Trends Biochem. Sci.* **1995**, *20* (11), 478–480. https://doi.org/10.1016/S0968-0004(00)89105-7.
(684) Hasegawa, H.; Holm, L. Advances and Pitfalls of Protein Structural Alignment. *Current Opinion in Structural Biology*. Elsevier Current Trends June 1, 2009, pp 341–348. https://doi.org/10.1016/j.sbi.2009.04.003.